The role of obesity and insulin resistance in modulating immune cell function in cancer and liver disease

by

Megan Lee

A thesis submitted in partial fulfillment of the requirements for the degree of

Master of Science

in

Immunology

Department of Medical Microbiology and Immunology
University of Alberta

Abstract

Obesity and associated insulin resistance (IR) represent a significant global health burden, and predispose individuals to develop various diseases, including cancer and liver diseases. Heightened inflammation during obesity can on the one hand exacerbate liver inflammation, while on the other, dampen protective immune responses against tumours. However, the underlying mechanisms remain incompletely understood. My research aims to assess aspects of obesity and alterations in immune function within the context of cancer, focusing on how obesity and IR affects T cell-mediated anti-tumour responses. In addition, my research focuses on the role of Hippo signalling mediators Yes-associated protein (YAP) and Transcriptional co-activator with PDZ-binding motif (TAZ) activity in dendritic cells (DCs) in the development of IR and non-alcoholic fatty liver disease (NAFLD). In response to tension, DCs have enhanced pro-inflammatory function, but also upregulate the expression of TAZ. TAZ is involved in mechanosensing in non-immune cell types and has a homolog known as YAP, suggesting that DC mechanosensing and inflammatory function may involve YAP/TAZ signalling.

Here, I present my findings that diet-induced obesity accelerates tumour growth, which is associated with a decrease in tumour infiltrating lymphocytes. Intratumoural T cells in obese mice also exhibit reduced effector function, but similar levels of exhaustion compared to lean mice. To determine mechanistically how T cell anti-tumour immunity is impaired during obesity, I investigated the role of insulin signalling in T cells, as we found that T cells in obese mice are insulin resistant. To assess the role of insulin signalling in T cell-mediated anti-tumour immunity, I used a mouse model with insulin receptor (INSR)-specific ablation in T cells. Genetic insulin resistance in T cells dampens antigen-specific T cell-mediated immunity, which

is associated with decreased production of effector molecules, mirroring the observations in obese mice. Given that obesity imposes a similar phenotype, this supports the notion that obesity impairs T cell-mediated anti-tumour responses through inducing IR. This offers new insight into how obesity impairs immune responses in cancer, and provides implications for the potential of immunotherapies targeting immune cell metabolism against cancer.

I also report that YAP/TAZ in DCs, which we previously observed to be important for DCs' proinflammatory function, does not play a significant role in the pathogenesis of IR, NAFLD, and liver fibrosis in a high fat high sucrose model.

My findings highlight the complex signals that modulate immunity during obesity, which awaits further investigation for better understanding to ultimately develop therapeutics to improve health and blunt disease.

Preface

This thesis is composed of original work by Megan Lee. The introduction contains co-authored work published in Lee M et al. Mechanosensing in macrophages and dendritic cells in steady-state and disease. Front Cell Dev Biol. 2022 Nov 17;10:1044729.

The research project, of which this thesis is a part, received research ethics approval from the University of Alberta Research Ethics Board, Project Name “The impact of obesity and insulin resistance on immune function”, No. AUP00003251, approved August 6, 2019.

Acknowledgements

First and foremost, I am extremely grateful for my supervisors, Dr. Sue Tsai and Dr. Xavier Clemente-Casares, for their guidance and support throughout my Master's degree. Thank you for all of the time and dedication you have put into helping me throughout the past three years. You have both taught me an incredible breadth of knowledge, and have always provided feedback that has helped me grow both professionally and personally. Thank you for accepting me into your lab when times were uncertain in the pandemic, and for always being patient with me. Words cannot truly express how grateful I am to have had both of you as my mentors.

I would like to thank my committee members Dr. Troy Baldwin and Dr. Colin Anderson for their valuable input and constructive feedback. Thank you to my defense committee members Dr. Troy Baldwin, Dr. Colin Anderson, and Dr. Hanne Ostergaard. A special thank you to the Baldwin, Kane, and Ostergaard labs for providing me the opportunity to learn and present scientific knowledge in the joint lab meetings.

I am also grateful for all my friends and colleagues in the Tsai-Clemente lab. To Dr. Masoud Akbari, I am greatly appreciative for your technical support and assistance. To Kasia Dzierlega, you have been an incredible friend and colleague right from the beginning of my Master's program, and my graduate experience would not have been the same without you. To Aklima Akter, thank you for all of your kindness. Sharing an office space with you and Kasia has brought nothing but joy and laughter. Thank you to Derek Parker, Erin Strachan, Mengyi Zhu, Kevin Chu, as well as the newer members of our lab, for creating an amazing environment to work in. Thank you to the undergraduate students, especially to Lucy Lee for all of your help.

I would also like to thank my friends and family for being there for me throughout this experience. To my friends, thank you for all of your love, support, and encouragement. To name a few, a special thank you to Elanie, Hiulan, Erika, and my badminton friends including Laura and Serena. Although you cannot read this, thank you to my cat Maxie for always keeping me company through the late nights. To my parents, Daisy Ho and Francis Lee, and my brothers Jeremy and Zachary, thank you for your unconditional love and continuous encouragement. Thank you for always believing in me and supporting me in all of my endeavours.

Table of Contents

List of tables

List of figures

List of abbreviations

Abbreviation	Full Description
AKT	Ak strain transforming
AMPK	Adenosine monophosphate-activated protein kinase
APC	Antigen presenting cell
ATF4	Activating transcription factor 4
ATP	Adenosine trisphosphate
BAT	Brown adipose tissue
BMDC	Bone marrow-derived dendritic cell
BMI	Body mass index
Breg	Regulatory B cell
CCL	Chemokine (C-C motif) ligand
CCR7	C-C chemokine receptor 7
CD107α/LAMP-1	Lysosomal-associated membrane protein-1
CD11c	Alpha integrin X
CD206	Mannose receptor
CD62L	L-selectin
cDC	Conventional dendritic cell
CFSE	Carboxyfluorescein succinimidly ester
CLR	C-type lectin receptor
CTL	Cytotoxic T lymphocyte
DC	Dendritic cell
DIO	Diet-induced obesity
DKO	Double knockout
ECM	Extracellular matrix
ELISA	Enzyme-linked immunosorbent assay
EMSA	Electrophoretic mobility shift assay
ER	Endoplasmic reticulum
FFA	Free fatty acid
FLT3L	FMS-like tyrosine kinase 3 ligand
FOXP3	Forkhead box P3
GAPDH	Glyceraldehyde 3-phosphate dehydrogenase
GZMB	Granzyme B

HFD	High fat diet
HFHS	High fat high sucrose
HSC	Hepatic stellate cell
IBD	Inflammatory bowel disease
IFNγ	Interferon gamma
IKK	IκB kinase
IL	Interleukin
ILN	Inguinal lymph node
iNKT cell	Invariant natural killer T cell
INSR	Insulin receptor
IPGTT	Intraperitoneal glucose tolerance test
IR	Insulin resistance
IRS	Insulin receptor substrate
ITAM	Immunoreceptor tyrosine-based activation motif
ITT	Insulin tolerance test
JAK	Janus kinase
JNK	c-Jun N-termnal kinase
KC	Kupffer cell
KLRG1	Killer cell lectin-like receptor G1
KO	Knockout
kPa	Kilopascal
LAG-3	Lymphocyte activation gene-3
LAT	Large tumour suppressor
Lck	Lymphocyte-specific tyrosine kinase
LD	LIVE/DEAD
MAPK	Mitogen-activated protein kinase
MCP-1	Monocyte chemoattractant protein-1
MdM	Monocyte-derived macrophage
MFI	Mean fluorescence intensity
MHC	Major histocompatibility complex
MIP-2	Macrophage inflammatory protein-2
MOB1	Mps1-binder 1
moDC	Monocyte-derived dendritic cell
MST	Mammalian STE20-like kinase

NAFLD	Non-alcoholic fatty liver disease
NASH	Non-alcoholic steatohepatitis
NCD	Normal chow diet
NK cell	Natural killer cell
OT-I	Ovalbumin-specific $CD8^+$ TCR transgenic T cells
OVA	Ovalbumin
OXPHOS	Oxidative phosphorylation
PAK	p-21 activated kinase
PD-1	Programmed cell death protein 1
PD-L1	Programmed death-ligand 1
pDC	Plasmacytoid dendritic cell
PEG	Polyethylene glycol
PI3K	Phosphatidylinositol 3-kinase
PIEZO1	Piezo type mechanosensitive ion channel component 1
PIP_3	Phosphatidylinositol (3,4,5)-triphosphate
PKC	Protein kinase C
PMA	Phorbol 12-myristate 13-acetate
PMN	Polymorphonuclear leukocyte
PP2A	Protein phosphatase 2A
PPARγ	Peroxisome proliferator-activated receptor gamma
PRR	Pattern recognition receptor
PTEN	Phosphatase and tensin homolog
PTP1B	Protein tyrosine phosphatase 1B
Rac1	Rac family small GTPase 1
RhoA	Ras homolog family member A
RhoGAP	Rho GTPase-activating protein
S6K	S6 kinase
SAT	Subcutaneous adipose tissue
Ser	Serine
SLC2A1	Solute carrier family 2 member 1
SLC7A5	Solute carrier family 7 member 5
SOCS	Suppressor of cytokine signalling
STAT	Signal transducer and activator of transcription
SUN	Sad1-UNC-84
T-bet	T-box expressed in T cells

TAM	Tumour associated macrophage
TAZ	Transcriptional coactivator with PDZ-binding motif
TCR	T cell receptor
TEAD	Transcriptional enhanced associated domain
Tet	Tetramer
TGF	Transforming growth factor
Th	Type helper T cell
Thr	Threonine
TIL	Tumour infiltrating lymphocyte
TIM-3	T cell immunoglobulin and mucin domain-containing protein 3
TME	Tumour microenvironment
TNFα	Tumour necrosis factor alpha
Treg	Regulatory T cell
TRPV4	Transient receptor potential of vanilloid subtype 4
UTR	Untranslated region
VAT	Visceral adipose tissue
WAT	White adipose tissue
Wnt	Wingless/Integrated
WT	Wildtype
WWTR1	WW domain containing transcription regulator 1 (also known as TAZ)
YAP	Yes-associated protein
ZFP36L1	ZFP36 ring finger protein like 1

Chapter 1: Introduction

1.1 Obesity

Obesity is a major global health burden, affecting approximately 40% of the adult population worldwide[1]. It is characterized by an accumulation of abnormal or excessive fat, and develops when exceeding energy consumption overtakes energy expenditure from metabolic and physical activity, which results in positive energy balance[2]. Obesity is also typically defined by a body mass index (BMI) of >30, which is calculated by dividing an individual's body weight in kilograms by the square of their height in meters[3]. As a consequence of excessive or abnormal fat tissue accumulation which exceeds normal adipose tissue stores, fat gets deposited and accumulates as ectopic fat tissue, leading to increased risk for many diseases[2]. Obesity is linked to various complications, such as diabetes, cardiovascular disease, cancer, and nonalcoholic fatty liver disease (NAFLD). Obesity induces systemic perturbations in metabolism, leading to an increase of circulating free fatty acids (FFA) and amino acids, hyperinsulinemia and insulin resistance (IR), hyperglycemia, and alterations in adipokines compared to lean individuals[4]. Importantly, obesity can lead to a chronic, low-grade systemic inflammation that occurs in multiple organs and tissues through a complex interplay between adipose tissue, immune cells, and various signalling molecules[2].

1.1.1 Adipose tissue biology

Adipose tissue is a type of loose connective tissue that consists of lipid-filled cells, known as adipocytes, surrounded by collagen fibers, fibroblasts, blood vessels, and immune cells[5]. There are two types of adipose tissues with different functions: brown adipose tissue (BAT) and white adipose tissue (WAT). BAT is used for dissipating energy to generate heat, which is important in maintenance of body temperature[6]. BAT levels and activity are inversely correlated with BMI, and the loss of BAT activity is thought to be associated with increased levels of WAT[7]. In the context of obesity, WAT is the most relevant adipose tissue depot. WAT is critical for the storage of excess calories in the form of fat, which can be used by the body as an energy source during fasting or with increased energy expenditure[8]. In addition, WAT is involved in endocrine communication and insulin sensitivity[5]. WAT releases adipokines, which are bioactive molecules produced by adipose tissue that are involved in regulating a wide array

of processes such as appetite and satiety, inflammation and fat distribution[5]. WAT is further classified depending on its anatomical location: subcutaneous (beneath the skin; SAT) or visceral (lining internal organs; VAT). While both SAT and VAT are important and increased during obesity, particular attention has been focused on VAT due to its association with multiple pathologies[9]. In addition to adipocytes, VAT is composed of a stromal vascular fraction, which includes an extra-cellular matrix that holds together stem cells, fibroblasts, vascular endothelial cells, as well as immune cells[10].

1.1.2 Immune cell composition of visceral adipose tissue in homeostasis and obesity

VAT is not just an inert storage depot for excess energy, but rather has been recognized as an active organ that is involved in regulating physiological and pathological processes, including inflammation[11]. VAT is populated with a diverse array of innate and adaptive immune cells, which coordinate and regulate adipose tissue function (**Figure 1.1)**.

Under homeostatic conditions, innate immune cells such as macrophages and dendritic cells (DCs) generally exhibit an anti-inflammatory phenotype in VAT. Macrophages play an important role in inflammatory processes through the secretion of pro-inflammatory cytokines in response to pathogens or damaged tissue, but are also critical for maintaining homeostasis by clearing cellular debris and promoting tissue repair[12]. VAT is enriched in anti-inflammatory adipose tissue resident macrophages that exhibit increased expression of interleukin (IL)-10 and arginase, and maintain adipose tissue homeostasis through clearance of dead adipocytes[13, 14].

DCs are a heterogeneous population of antigen presenting cells (APCs) that are considered as the bridge between the innate and adaptive immune systems, as they play a role in priming T cells[15]. Two main populations of antigen presenting classical or conventional DCs (cDCs) are found in the VAT and promote a tolerogenic environment. In non-lymphoid tissues such as the VAT, cDC1s express CD103, an integrin involved in cell to cell or cell to matrix interactions, while cDC2s express CD11b, an integrin molecule that is involved in cell migration and adhesion[16]. cDC1s have enhanced cross-presentation abilities, and are crucial for the initiation of $CD8^+$ cytotoxic T cell responses and polarization of $CD4^+$ T cells into the T helper 1 (Th1) subset in the presence of immunogenic signals, emphasizing their importance during immune responses against intracellular pathogens[17]. cDC2s are more adept at presenting antigens

to $CD4^+$ T cells due to their increased expression of Major histocompatibility complex (MHC) II machinery, but can also cross-present at a decreased efficiency compared to cDC1[17]. cDC2s also demonstrate the ability to favour polarization towards Th2 or Th17 immune responses, suggesting a critical role during immune responses to extracellular pathogens[17]. Under homeostatic conditions in the VAT, there is activation of the Wnt (Wingless/Integrated)/β-catenin pathway in cDC1s which induces IL-10 production, while upregulation of the Peroxisome proliferator-activated receptor-γ (PPARγ) pathway in cDC2s suppresses their activation, promoting an anti-inflammatory and tolerogenic environment[18].

Eosinophils are also abundant in adipose tissue at steady-state. They are major producers of IL-4 and IL-13, which promotes the polarization and accumulation of more anti-inflammatory macrophages[19]. Adipose tissue in lean individuals exhibit an enrichment of invariant natural killer T (iNKT) cells, which are one of the subsets of innate-like T cells that possess innate-like mechanisms to rapidly respond to pathogens while also expressing antigen receptors similarly to T cells[20]. iNKT cells maintain adipose tissue homeostasis by secretion of IL-4 and IL-10, which promote anti-inflammatory macrophage polarization and maintenance of regulatory T cell (Treg) activity, respectively[21].

In terms of the adaptive immune system, both B and T cells at steady-state are found in VAT and are skewed towards anti-inflammatory subtypes. B cells play a critical role in the adaptive immune response through cytokine and antibody secretion, as well as in modulating the functions of other cells. The majority of B cells are broadly classified as B1 and B2 cells. B1 cells are primarily found in pleural and peritoneal cavities, while B2 cells are found in secondary lymphoid organs[22]. At steady state, the B cell compartment of VAT predominantly consists of B1 and regulatory B cells (Bregs), which produce IL-10 and can ameliorate inflammation[23]. T cells are another major component of the adaptive immune system, and can be categorized based on their expression of surface markers, composition of T cell receptors (TCR), and production of cytokines[24]. Conventional T cells have TCRs consisting of αβ chains, and are classified according to their expression of co-receptors CD4 or CD8. $CD4^+$ T cells can be further subdivided into various subsets based on expression of cytokines and lineage-specific master transcription factors, including interferon gamma (IFNγ)-producing T helper 1 (Th1) cells, IL-4

producing Th2 cells, IL-17-producing Th17 cells, and IL-10 producing Tregs[25]. Under homeostatic conditions, VAT is enriched in Tregs, which are characterized by their expression of the transcription factor Forkhead box P3 (FOXP3). Treg production of IL-10 helps promote the skewing of macrophages to a more anti-inflammatory phenotype in lean adipose tissue[26]. Th2 cells are also found in the VAT at steady-state, which help maintain a higher proportion of anti-inflammatory macrophages in an IL-4-dependent manner[27].

However, long-term caloric excess in obesity causes hypertrophy and endoplasmic reticulum (ER) stress in white adipocytes, resulting in the release of adipokines and chemoattractants that help activate and recruit both innate and adaptive immune cells such as pro-inflammatory macrophages, neutrophils, DCs, Th1 and Th17 $CD4^+$ T cells, $CD8^+$ T cells, and B cells to the VAT[27]. This is associated with a concomitant reduction in the proportion of anti-inflammatory macrophages, iNKT cells, eosinophils, and Tregs[27]. In obesity, one of the defining features of VAT inflammation is an increase in an accumulation of macrophages that surround dead or dying adipocytes in "crown-like structures", which are clusters of scavenging macrophages[28]. These pro-inflammatory macrophages express integrin alpha X (CD11c), a transmembrane protein involved in phagocytosis, and CD206, a C-type lectin that is important for endocytosis and phagocytosis[29]. Although CD206 has been predominantly described as a marker for more homeostatic and anti-inflammatory macrophages, $CD11c^+$ $CD206^+$ macrophages are abundant in obese VAT and express pro-inflammatory cytokines such as tumour necrosis factor alpha (TNFα)[27]. Neutrophils are normally found at a very low frequency inside the VAT at steady-state, comprising <1% of non-adipocyte cells[30]. During obesity, the frequency of neutrophils increase in VAT and exhibit increased production of elastase, a serine protease that promotes inflammation[30]. cDC populations are also expanded in VAT under obese conditions, which can induce differentiation of pro-inflammatory Th17 cells and promote macrophage infiltration[31]. Obesity also interferes with the Wnt/β-catenin and PPARγ pathways in cDC1s and cDC2s, abrogating the anti-inflammatory functions of cDCs normally observed at steady-state[18].

Generally, obesity induces an accumulation of total B cells and T cells in the VAT, which tend to exhibit pro-inflammatory phenotypes. B cells in VAT of obese mice secrete higher levels

of pro-inflammatory cytokines[32], and obesity induces an increase in dysfunctional Bregs[23]. $CD4^+$ T cells within the obese VAT have elevated production of IFNγ, indicating an increase in Th1 polarization[33]. IL-17 producing Th17 cells also accumulate in the VAT during obese states, which can induce the expression of chemokines that further promote immune cell infiltration[34]. $CD8^+$ T cells or cytotoxic T lymphocytes (CTLs) increase in the VAT during obesity and have enhanced ability to produce IFNγ[35]. CTLs in obese adipose tissue also produce higher levels of chemokines that contribute to the recruitment of macrophages into adipose tissue[35].

Altogether, increases in pro-inflammatory innate and adaptive immune cells in adipose tissue cause increased levels of inflammation and production of pro-inflammatory cytokines which can enter the bloodstream to cause systemic inflammation that occurs in multiple organs and tissues. Notably, alterations in the immune landscape during obesity and the resulting chronic inflammation is a major factor contributing to obesity-associated pathologies, including insulin resistance.

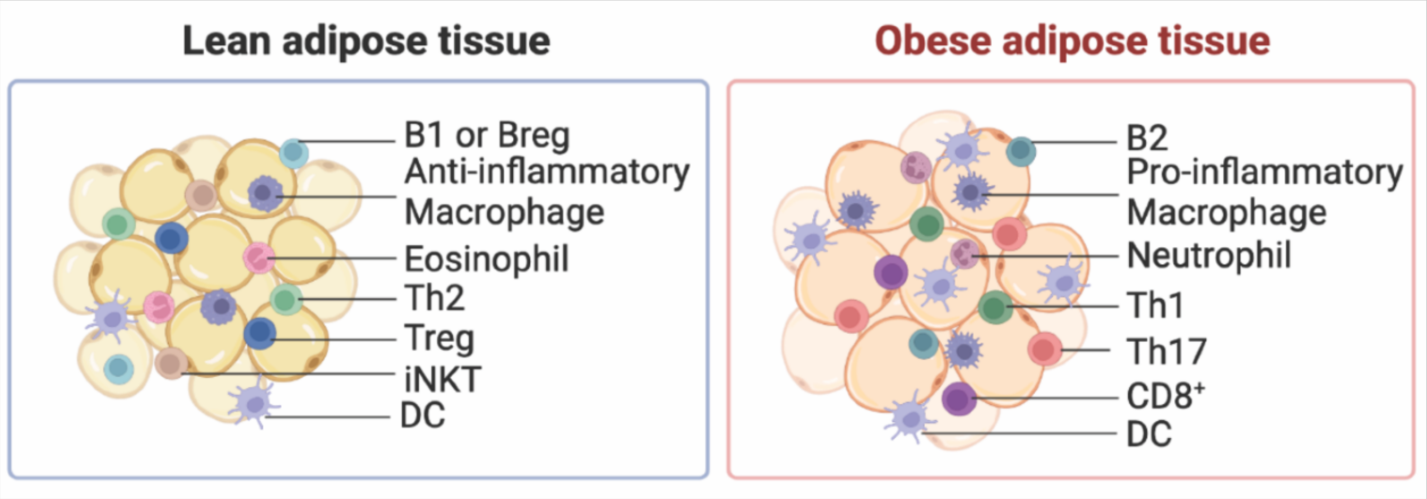

Figure 1.1 Comparison of immune cell composition in lean and obese adipose tissue. Lean adipose tissue contains regulatory immune cells that suppress proinflammatory immune cells, including B1 and Breg cells, anti-inflammatory macrophages, Treg cells, Th2 cells, iNKT cells, and eosinophils. There are also DCs in lean adipose tissue that have a more tolerogenic phenotype. In contrast, obese adipose tissue contains hypertrophic adipocytes that are surrounded by pro-inflammatory immune cells including B2 cells, pro-inflammatory macrophages, neutrophils, Th1 cells, Th17 cells, $CD8^+$ T cells, with increased levels of DCs. Drawn in BioRender.com.

1.2 Obesity and insulin resistance

1.2.1 Insulin signalling

Insulin is a hormone which gets secreted from β-cells in the pancreas in response to elevated blood glucose levels. Insulin plays important physiological roles including reducing blood glucose, but also controls the metabolism of carbohydrates, proteins, and lipids[36]. The major tissues targeted by insulin's effects on metabolism include the muscle, liver, and adipose tissue. In the muscle, insulin promotes glucose uptake and protein synthesis[37]. Insulin promotes glucose and fatty acid uptake and inhibits lipolysis in adipose tissue, and promotes glucose utilization, suppresses glucose production, and promotes triglyceride synthesis in the liver[36].

Insulin exerts its effects through its interaction with insulin receptors (INSR) (**Figure 1.2)**. INSR is a heterotetrameric transmembrane receptor that consists of two extracellular alpha subunits and two transmembrane beta subunits connected by disulfide bridges, and belongs to the class of receptor tyrosine kinases[38]. Upon binding of insulin to the extracellular alpha subunit, the INSR dimerizes which leads to activation of the tyrosine kinase domain of the intracellular portion of the beta subunit[39]. This causes self-phosphorylation of immunoreceptor tyrosine-based activation motifs (ITAM) on the beta subunit, and leads to the phosphorylation and activation of insulin receptor substrates (IRS)[39]. The two major substrates, IRS-1 and IRS-2, are linked to the activation of the phosphatidylinositol 3-kinase (PI3K)/Ak strain transforming (AKT) pathway, which is responsible for most of the metabolic actions of insulin, and to the Ras/mitogen-activated protein kinase (MAPK) pathway, which cooperates with the PI3K pathway to control cell proliferation[40]. In the AKT pathway, phosphorylated tyrosine sites on IRS-1 allows the binding of the lipid kinase PI3K, which synthesizes phosphatidylinositol (3,4,5)-triphosphate (PIP_3) at the plasma membrane[39]. This leads to the recruitment of 3-phosphoinositide-dependent kinase 1 (PDK1), which directly phosphorylates AKT at Threonine 308 (Thr308)[39]. A second phosphorylation on AKT occurs by mammalian target of rapamycin 2 (mTORC2) at Serine 473 (Ser473), leading to its full activation. Activation of AKT and its downstream signalling pathways leads to the promotion of glucose uptake, lipogenesis, glycogen synthesis, and repression of genes involved in gluconeogenesis[41].

Insulin activity also contains multiple points of regulation to prevent aberrant signalling that can lead to severe perturbations in metabolism. Insulin signalling can be attenuated by the action of several phosphatases. Phosphoprotein phosphatases, such as protein tyrosine phosphatase 1B (PTP1B) have been shown to dephosphorylate tyrosine residues on activated INSR and IRS proteins, thereby reducing their activity[42]. In addition, protein phosphatase 2A (PP2A) regulates the activities of many protein kinases involved in insulin action, including AKT, protein kinase C (PKC), and IκB kinase (IKK)[43]. Lipid phosphatases can also inhibit INSR signalling by regulating PIP_3 levels. Phosphatase and tensin homolog (PTEN) dephosphorylates PIP_3, which antagonizes PI3K signalling in cells[44]. Adaptor proteins, including proteins of the suppressor of cytokine signalling (SOCS) family, can inhibit INSR signalling either through inhibition of tyrosine kinase activity of INSR, competition for binding of IRS proteins to the receptor, or targeting IRS proteins to degradation[45].

INSR signalling is also modulated by serine phosphorylation of INSR and IRS substrates. Stress signals, including increased cytokines, fatty acids, mitochondrial dysfunction, and ER stress can activate multiple kinases, such as c-Jun amino-terminal kinase (JNK)[46], IKK[47], and PKCs[48]. Activation of these kinases causes inhibitory serine phosphorylation on INSR and IRS, thereby impairing insulin signalling. In addition, there is a negative feedback loop in insulin signalling, mediated by mTORC1. Activation of mTORC1 and S6 kinase (S6K) is downstream of insulin signalling and promotes cellular proliferation, but it also can inhibit insulin signalling by phosphorylating serine residues on IRS[49]. Overall, these regulatory pathways are critical for maintaining appropriate metabolic activity of cells. However, some of these inhibitory mechanisms can be overactivated during obese conditions and contribute to the development of IR.

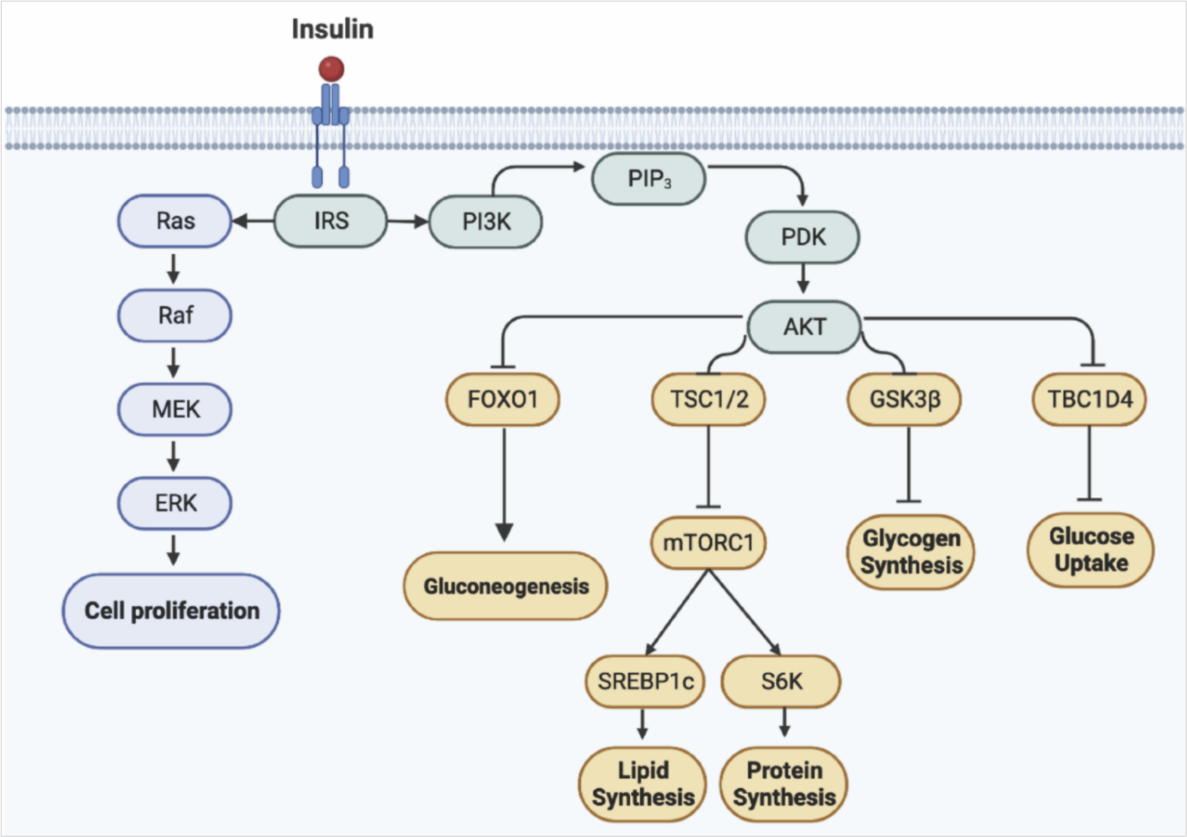

Figure 1.2 Condensed schematic of insulin/INSR signalling. The INSR signalling cascade is initiated by binding of insulin to INSR, triggering INSR dimerization, activation of its tyrosine kinase activity, and phosphorylation of IRS. Downstream signalling through the PI3K/AKT pathway promotes the expression of genes involved in lipid synthesis, protein synthesis, glycogen synthesis, and glucose uptake, while inhibiting gluconeogenesis. Signalling through the Ras/ERK pathway promotes cell proliferation. Abbreviations are as follows: IRS: insulin receptor substrate; PI3K: phosphatidylinositol 3-kinase; PIP_3: phosphatidylinositol (3,4,5)-triphosphate; PDK1: 3-phosphoinositide-dependent kinase 1; AKT: Ak strain transforming; FOXO1: forkhead box protein O1; TSC1/2: tuberous sclerosis complex 1/2; mTORC1: mammalian target of rapamycin 1; SREBP1c: sterol regulatory element-binding protein 1; S6K: S6 kinase; GSK3β: glycogen synthase kinase 3 beta; TBC1D4: TBC1 domain family member 4; Ras: rat sarcoma; Raf: rapidly accelerated fibrosarcoma; MEK: mitogen-activated protein kinase kinase ERK: extracellular signal-regulated kinase. Drawn on BioRender.com. Adapted from Haeusler et al.[39]

1.2.2 Development of obesity-associated insulin resistance

IR is a major metabolic feature of obesity. It is defined as an inadequate response to the physiological effects of circulating insulin to target tissues[36]. IR impairs glucose uptake, resulting in a compensatory increase in insulin production by β-cells and a state of elevated levels of circulating insulin, known as hyperinsulinemia. However, when β-cells are unable to compensate for decreased tissue insulin sensitivity, glucose homeostasis is dysregulated and type 2 diabetes develops[50]. Type 2 diabetes is perceived to be a polygenic disorder that develops due to interactions between environmental factors and a strong hereditary component[51]. IR and type 2 diabetes in obesity is a reflection of long-term nutrient excess, and develops through complex mechanisms that can involve fatty acid flux, mitochondrial stress, adipocyte-derived cytokines, and chronic tissue inflammation[50] (**Figure 1.3)**.

Obesity is also associated with dysfunctional lipid metabolism, which can impair insulin signalling. Elevated levels of circulating FFAs can activate inflammatory pathways via binding to pattern recognition receptors (PRRs). Saturated fatty acids can activate signalling in adipocytes and macrophages, inducing inflammation via activation of the NF-kB and JNK pathways[52]. Furthermore, fatty acids are able to induce the activation of JNK, IKK, and PKC, and thus leading to serine phosphorylation of IRS-1[50]. Accumulation of lipid derivatives, such as ceramides, can also negatively regulate insulin activity. Ceramides can induce IR via activation of JNK[53], and inhibit AKT activation by increasing the interaction between PP2A with AKT[54].

Mitochondrial stress is another factor that has been implicated in the development of obesity-associated IR. In an obese state, lipids induce mitochondrial overactivation by enhancing fatty acid beta-oxidation to enhance energy disposal. Consequently, large amounts of adenosine trisphosphate (ATP) are generated from fatty acid catabolism[55]. When ATP levels exceed the threshold, it can trigger a negative feedback pathway to attenuate substrate-induced mitochondrial function. Specifically, high levels of ATP are sensed by adenosine monophosphate-activated protein kinase (AMPK), leading to its inactivation and the subsequent reduction of insulin-induced glucose uptake to decrease ATP production[55]. Hyperinsulinemia can also further induce and sustain IR in obesity. As IR develops, glucose uptake into target tissues becomes impaired, resulting in a compensatory increase in insulin production and a state of

elevated levels of circulating insulin[56]. The insulin signalling pathway has a negative feedback loop to control the activity of insulin, which involves mTORC1 and S6K. Constant activation of mTORC1 and S6K downstream of insulin signalling can inhibit insulin signalling by phosphorylating serine residues on IRS[49].

One of the main mechanisms by which obesity fosters the development of IR is through inflammatory signals. With excess caloric intake during obesity, there is an increased demand for the storage of those calories, resulting in adipocytes becoming hypertrophic to accommodate for more storage of lipids. Eventually, these hypertrophic adipocytes become more stressed and begins to produce pro-inflammatory cytokines, which can signal through receptors to dampen insulin receptor signalling[57]. In addition, an increase in immune cells such as pro-inflammatory macrophages in adipose tissue enhances the levels of circulating inflammatory cytokines[57]. One cytokine that is implicated in the development of obesity-related IR is TNFα. TNFα acts through its p55 receptor to inhibit IRS-1 in the insulin signalling pathway[58]. TNFα signalling causes the activation of IKK and JNK pathways, which leads to IRS-1 inhibition. IKK can inhibit insulin signalling by phosphorylation of IRS-1 at multiple serine residues (Ser307, Ser270) in adipocytes, and thereby impairing signalling[49]. JNK can also mediate phosphorylation of IRS-1 at Ser307, which inhibits the insulin signalling pathway in response to TNFα[59]. In addition to TNFα, IFNγ and IL-6 are pro-inflammatory cytokines that are elevated under obese conditions and can impair insulin signalling. IFNγ signalling through the Janus kinase 1 (JAK1)/JAK2/Signal transducer and activator of transcription 1 (STAT1) pathway, and IL-6 activation of the STAT3 pathway can contribute to IR by modulating activation of SOCS proteins[60]. SOCS proteins can repress INSR tyrosine kinase activity, interrupt interaction of INSR with IRS proteins, and promote IRS degradation[45].

The role of adipose tissue DCs in mediating obesity-linked IR has been demonstrated by various models depleting DCs. Whole-body depletion of DCs using FMS-like tyrosine kinase 3 ligand knockout (*Flt3l*$^{-/-}$) mice, which is essential for DC development, was associated with decreased macrophage infiltration in adipose tissue and liver, and protected mice from obesity-induced IR[61]. C-C chemokine receptor type 7 knockout (*Ccr7*$^{-/-}$) mice have also been used to characterize DC function in obesity-associated inflammation, as CCR7 is necessary to direct

DCs to peripheral tissues[62]. HFD-fed *Ccr7*$^{-/-}$ mice did not exhibit DC accumulation in the VAT as normally observed during obesity. This was associated with protection from adipose tissue inflammation and IR[62], further implicating the importance of adipose tissue DCs in the pathogenesis of IR. DCs can also regulate obesity-associated inflammation through their antigen presenting capacity, particularly through interactions with T cells. T cells play a critical role in obesity-induced inflammation, as $CD8^+$ T cells produce TNFα and IFNγ, and Th1 and Th17 cells produce IFNγ and IL-17 respectively, which can enhance macrophage pro-inflammatory functions[63]. During obesity, the uptake of antigens or lipids by adipose tissue DCs leads to activation of the mitogen-activated protein kinase pathway (MAPK), causing increased MHC II expression and maturation. Through increased antigen presentation, adipose tissue DCs promote Th1 and Th17 subset proliferation, leading to increased production of IFNγ and IL-17 respectively, contributing to the pro-inflammatory environment[63]. In addition, there are alterations in tissue stiffness that could potentially modulate DC function. Increases in adipose tissue and liver stiffness can occur during obesity, as obese states induce increased extracellular matrix (ECM) and collagen fiber formation, causing fibrosis[64, 65]. Notably, previous work has demonstrated that increased environmental stiffness promotes DC inflammatory function[66]. However, the role of mechanical cues in modulating DC function in the pathogenesis of IR is unknown.

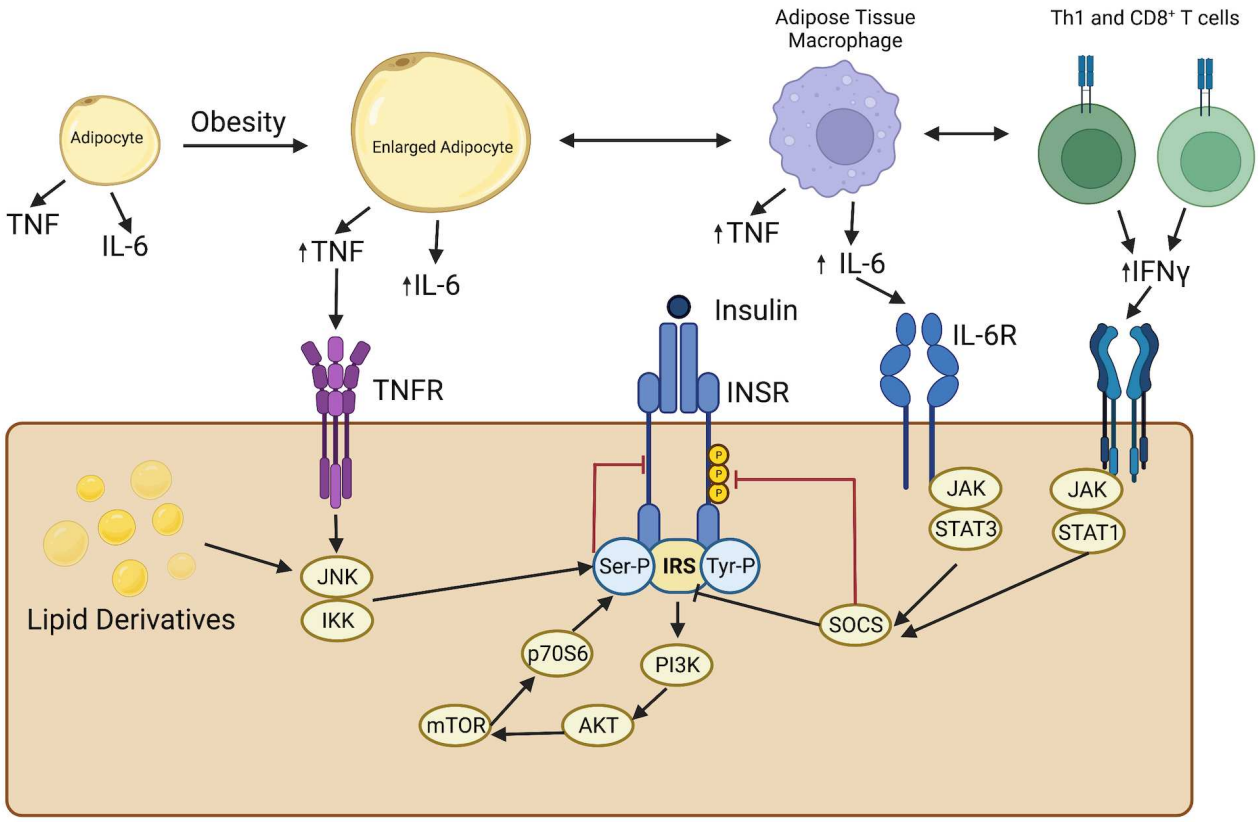

Figure 1.3 Mechanisms for obesity-associated insulin resistance.

Hypertrophic adipocytes during obesity become stressed and produce pro-inflammatory cytokines which can signal through receptors to dampen insulin receptor signalling, and promotes pro-inflammatory immune cell infiltration such as M1-like macrophages and Th1 and CD8+ T cells which enhance the levels of circulating inflammatory cytokines. Hyperactivation of mTOR from hyperinsulinemia results in serine phosphorylation of IRS-1 by p70S6 kinase. Serine phosphorylation of IRS can be promoted by JNK and IKK, which get activated by lipid derivatives or TNFR signalling. Increased SOCS activity downstream of IL-6 and IFNγ signalling inhibits INSR tyrosine kinase activity and interrupts interaction of INSR with IRS proteins. Abbreviations are as follows: TNF: tumour necrosis factor; IL-6: interleukin-6; IFNγ: interferon gamma; TNFR: tumour necrosis factor receptor; JNK: c-Jun N-termnal kinase; IKK: IκB kinase; INSR: insulin receptor; Ser: serine; Tyr: tyrosine; IRS: insulin receptor substrate; mTOR: mammalian target of rapamycin; AKT: Ak strain transforming; PI3K: phosphatidylinositol 3-kinase; SOCS: suppressor of cytokine signalling; JAK: Janus kinase; STAT: signal transducer and activator of transcription. Drawn on BioRender.com. Adapted from DeFronzo et al.[57]

1.3 DC Mechanotransduction in steady-state and disease

The following section is from the review article "Mechanosensing in macrophages and dendritic cells in steady-state and disease" published in Frontiers in Cell and Developmental Biology[67].

1.3.1 The role of mechanical stimuli in DCs

DCs are a heterogeneous population of APCs that are important for innate and adaptive responses to infection. As the most potent APCs, DCs help to stimulate antigen-specific T cell responses to eliminate foreign pathogens[68]. In addition to their immunogenic roles, they play a crucial role in maintaining immune tolerance to self-tissues[68]. Based on their transcriptional programming and functional characteristics, these professional APCs can be classified into monocyte-derived DCs (moDCs), cDC1, cDC2, and plasmacytoid DCs (pDCs)[69]. moDCs develop from monocytes in the circulation upon stimulation and are involved in inflammation and infection[70]. cDCs can recognize extracellular and intracellular pathogens and present peptides to $CD4^+$ and $CD8^+$ T cells[17]. pDCs are important for anti-viral responses and can produce large amounts of type I interferons[71]. DCs are exposed to a diverse array of mechanical environments. DCs originate in the bone marrow and migrate towards peripheral tissues through blood circulation, and can further travel from peripheral tissues towards lymph nodes through the lymphatic system[72]. How biochemical cues can influence DC maturation and function has been extensively studied[73, 74, 75], but recent studies have started to focus on the impact that biophysical stimuli have on DC activation[76, 77, 78], migration[77, 78], function[66, 79], and metabolism[66, 80] (**Figure 1.4)**.

1.3.1.1 Mechanical signals in DC activation

DCs can be activated directly by recognition of conserved pathogenic molecules via their pattern recognition receptors, and indirectly by inflammatory mediators produced by other cell types that have recognized foreign materials[81]. Activation of DCs will lead to the expression of appropriate 'maturation markers', including CD80, CD86, CD83, high levels of MHC I and II molecules, and CD40[81]. Studies have highlighted the impact that extracellular mechanical stimuli can play on the activation and expression of these maturation markers. The development and maturation of DCs are affected by extracellular pressure[76]. Specifically, the expression of activation markers (CD80, CD86, CD83, CD40) and MHC class II molecules is significantly upregulated on mature moDCs isolated from healthy human donors exposed to elevated pressure

in an airtight Lucite box[76]. Similarly, immature human moDCs showed a significant increase in the expression of CD80, CD86, CD83, and MHC class II molecules when maintained at elevated pressures[76]. Using a microfluidic channel to mimic inflammatory edema, murine bone marrow-derived DCs (BMDCs) exposed to higher shear stress show increased expression of the activation markers MHC class I and CD86 compared with DCs under static conditions[78]. In terms of static substrate stiffness effects on DCs, murine BMDCs grown on the stiffer hydrogels display significantly increased expression of CD80 and CD86 compared to those grown on more pliant hydrogels, with a trending increase in MHC class II molecules[66]. Consistently, CD83 and CD86 expression is significantly higher on moDCs cultured on higher stiffness substrates[77]. However, there are no significant differences in MHC class II molecule expression between human moDCs cultured on 2 kilopascal (kPa), 12 kPa, or 50 kPa substrates[77], suggesting that substrate stiffness may not play as significant of a role in influencing the expression of MHC class II molecules. In addition to pressure and substrate stiffness, DCs residing in the interior layers of the arterial wall experience transmural normal forces from blood flow strain arteries, which translates into a cyclic axial strain of the vessel wall layers[82]. Murine BMDCs cultured in vitro on ECM proteins (laminin, collagen, fibrinogen) that are exposed to cyclic strain increased expression of co-stimulatory molecules CD86 and CD40, and MHC class II molecules compared to BMDCs not exposed to any strain[79].

1.3.1.2 Impact of mechanical stimuli on the migration of DCs

The directed migration of DCs is essential during inflammatory responses, as they are professional APCs that transport antigens from the periphery to draining lymph nodes to help initiate adaptive immune responses[83]. The migration of mature DCs from peripheral tissues to lymph nodes is regulated by CCR7, which senses levels of chemokine (C-C motif) ligand 19 (CCL19) and CCL21, causing DCs to follow the concentration gradient leading towards lymphatic vessels[84]. CCR7 expression is lower on mature human moDCs conditioned on 12 kPa substrates compared to those on 2 and 50 kPa, which translates into a significantly lower level of CCL21-mediated migration[77]. Additionally, the formation of podosomes, which are important for DC adhesive and migratory behaviour, is significantly decreased in moDCs cultured on 12 kPa and 50 kPa compared to those conditioned on 2 kPa[77]. Although there is an increase in the proportion of DCs that migrate at 2 kPa, migration velocity is comparable between moDCs conditioned on the lower and higher substrate stiffnesses[77]. Similarly, murine BMDCs exposed

to differing levels of shear stress ranging from 0.2–0.6 dyne/cm^2 did not significantly differ in their migration speed[78]. However, increased shear stress potentiated their migratory abilities, as the BMDCs under higher shear stress followed more straightforward trajectories and demonstrated improved directness[78]. Therefore, these findings suggest that biomechanical cues may not affect DC migration velocity, but can impact the ability of DCs to migrate effectively.

1.3.1.3 Mechanical stimuli regulate DC effector function

Upon activation, DCs can perform immunogenic functions that are important for the clearance of pathogens, including the production and secretion of pro-inflammatory cytokines. When studying the effects of substrate stiffness on DC cytokine production, murine BMDCs that were cultured on higher substrate stiffnesses produced higher concentrations of TNF-α, IL-1α, IL-1β, IL-6, IL-12, monocyte chemoattractant protein-1 (MCP-1), and macrophage inflammatory protein-2 (MIP-2) in response to LPS stimulation[66]. Similarly, in response to pressure stimuli, the production of pro-inflammatory cytokines TNF-α, IL-6, and IFN-γ was significantly increased when the human moDCs were exposed to higher pressures[85]. Interestingly, the cytokine production of murine BMDCs under cyclic axial strain compared to non-stretched cells was similar[79], suggesting that only certain types of mechanical stimuli may regulate the production of cytokines by DCs.

In addition to cytokine production, another key function of DCs is to act as professional APCs. For the uptake of antigens, DCs express various types of pattern recognition receptors, including the class of C-type lectin receptors (CLRs), which recognize carbohydrate structures[86]. Substrate stiffness impacts the expression of CLRs on DCs, where human moDCs cultured on 2 kPa compared to 12 kPa substrates have 3-fold higher levels of CLRs, but the expression is intermediate on moDCs conditioned on 50 kPa gels[77]. This translates into functional differences, as moDCs conditioned on 2 kPa are more capable of C-type lectin-dependent antigen internalization and took up 1.5-2 fold more ovalbumin compared to those conditioned on 12 and 50 kPa[77]. Conversely, other studies have found that the phagocytic capability of murine BMDCs was enhanced when they were cultured on 50 kPa hydrogels compared to 2 kPa hydrogels[66].

Interactions between DCs and CD4$^+$ or CD8$^+$ T cells are also impacted by environmental mechanical cues. When examining the effects of cyclical axial strain, murine BMDCs under 3%

cyclical strain are more effective at inducing $CD4^+$ T cell proliferation[79]. Using an E.G7 tumour model, we showed that murine BMDCs grown on stiffer substrates and subsequently injected into tumour-implanted mice reduced the tumour growth rate compared to BMDCs grown on more pliant hydrogels[66]. The increased efficacy in tumour clearance in mice immunized with BMDCs grown on 50 kPa hydrogels was also associated with an increase in the frequency of effector memory T cells in the $CD4^+$ and $CD8^+$ T cells compartments[66]. Another study showed that T cells stimulated by murine BMDCs with increased cytoskeletal stiffness require a lower antigen concentration for activation than do T cells stimulated by BMDCs with softer cytoskeletal stiffness, indicating that DC cytoskeletal stiffness may promote T cell priming[87]. Altogether, this suggests that exposure to stiff extracellular matrices endows DCs with an enhanced ability to interact with and activate $CD4^+$ and $CD8^+$ T cells.

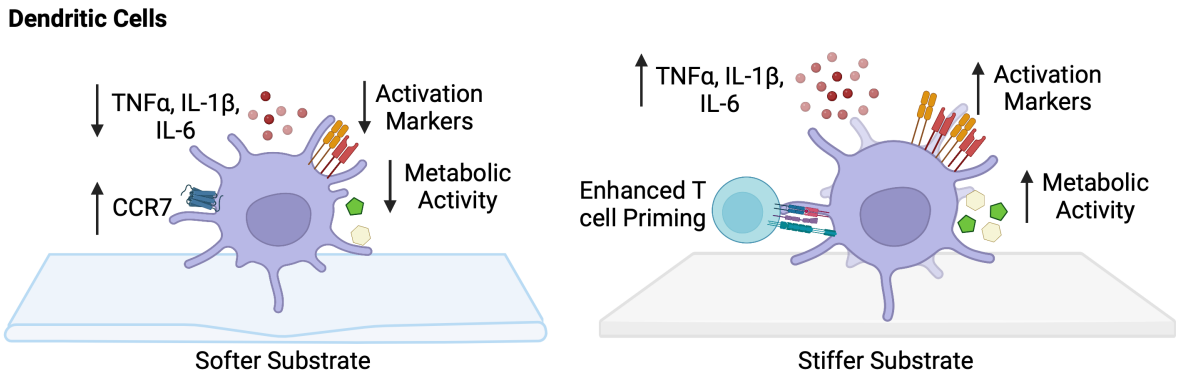

Figure 1.4 Impact of substrate stiffness on dendritic cells. DCs grown on softer substrates appear to have enhanced migratory capacity with increased expression of CCR7. There is a decreased ability to produce pro-inflammatory cytokines TNFα, IL-1β, and IL-6, and decrease in activation state. Metabolically, there is a decrease in glycolytic capacity. DCs cultured on stiffer substrates have greater ability to prime $CD4^+$ and $CD8^+$ T cells. They have increased capability to produce TNFα, IL-1β, and IL-6 and have an enhanced activation state with increased expression of CD80/86 and CD40. Metabolically, they have increased glycolytic capacity and express more intermediates of glycolysis. Abbreviations are as follows: CCR7: C-C chemokine receptor 7; TNFα: tumour necrosis factor alpha; IL-1β: interleukin-1 beta; IL-6: interleukin-6; Drawn in BioRender.com.

1.3.2 Mechanotransduction pathways in DCs

As mechanical stimuli impact macrophage and DC activation and function, it is important to understand the specific mechanosensing pathways used by DCs in these settings. In the following section, we discuss the molecular basis of mechanosensing including pathways that have been implicated including integrins, Hippo signalling mediators Yes-associated protein (YAP) and its homologue Transcriptional coactivator with PDZ-binding motif (TAZ), as well as mechanosensitive ion channels Transient Receptor Potential (TRP) of vanilloid subtype TRPV4 and Piezo Type Mechanosensitive Ion Channel Component 1 (PIEZO1) **(Figure 1.5)**.

1.3.2.1 Integrins and Rho GTPases

Cell adhesion molecules, such as integrins[88], can sense changes in the stiffness of the extracellular matrix (ECM). Broadly, alterations in ECM stiffness are detected and translated into signals that modulate the subcellular organization and fine structure of cytoskeletal components such as F-actin filaments[88]. In turn, this can regulate intracellular signalling pathways that ultimately impact cellular function. Integrins are adhesion receptors consisting of α and β subunits that participate in mechanotransduction. They bind to ECM and are important for bridging the extracellular environment with the intracellular cytoskeleton[89]. In addition, the activation state of integrins can be controlled by mechanosensitive ion channels such as Piezo1 through the modulation of intracellular calcium levels[90].

Regulators of the cytoskeletal network downstream of integrin signalling, including Rho GTPases, have been put forth as mediators connecting mechanical stimuli to DC function and homeostasis. Integrins act to retain cDC2s in blood-exposed regions of the spleen[91] and may participate in sensing shear stress. Ras homolog family member A (RhoA) has been ascribed a critical role in regulating DC homeostasis[92]. In the context of mechanosensing, RhoA and its associated Rho GTPase-activating protein (RhoGAP) regulate actin cytoskeleton rearrangement in response to mechanical forces[93], and also contributes to reciprocal activation of integrins through inside-out signalling[94]. In particular, the RhoGAP/RhoA/ROCK signalling pathway in DCs was found to be important in regulating directed migration of mature DCs to secondary lymphoid organs, as BMDCs that lacked effective RhoGAP signalling had exhibited significantly lower directness in response to CCL21 compared to BMDCs from wildtype mice[95].

Cytoskeletal rearrangements downstream of integrin signalling are also critical in processes such as immune synapse formation between DCs and T cells[96].

1.3.2.2 Mechanosensitive ion channels: PIEZO1

In addition to integrins, immune cells express mechanosensitive ion channels that modulate cellular activity through the gating of soluble ions. One family of ion channels that are found on the surface of immune cells are the Piezo proteins. PIEZO1 and PIEZO2 channels are found in most mammals and convert mechanical stimulation into biological signals[97]. These mechanosensitive channels respond to physical forces such as shear stress, which leads to changes in tension in the plasma membrane, causing them to open. PIEZO1 and PIEZO2 are permeable to monovalent cations including K^+ and Na^+, as well as divalent cations such as Ca^{2+} and Mg^{2+}[97]. Therefore, the opening of PIEZO channels results in the influx of cations and cell membrane depolarization, which can initiate intracellular Ca^{2+} signalling pathways that can impact the activation states of immune cells[98].

PIEZO1 has been implicated in bridging DC mechanosensation to function. DCs cultured on lower substrate stiffness conditions produced significantly lower levels of pro-inflammatory cytokines, but with the addition of PIEZO1 agonist Yoda-1, there was a marked upregulation of TNF-α and IL-6 production in the cell culture supernatants of BMDCs grown on softer substrate conditions[66]. PIEZO1 activation also led to a significant increase in the transcription of glycolytic genes, suggesting that PIEZO1 could also play a role in altering DCs metabolic state[66]. Additionally, mice with DC-specific deficiency of Piezo1 exhibited a moderately decreased anti-tumour response[66, 99], associated with an increase in the differentiation of Treg and decrease in the generation of Th1 cells[100]. Furthermore, PIEZO1 can potentiate integrin-mediated mechanosensing and adhesion. Activation of Piezo1 leads to the activation of Ca^{2+}-mediators Calpain and conventional PKCs, which in turn increases the activation of integrins[90]. Overall, these findings suggest that PIEZO1 could be important in DC function and metabolism.

1.3.2.3 Hippo signalling mediators: MST1/2 and YAP/TAZ

The Hippo signalling pathway is an evolutionarily conserved kinase cascade that is important for regulating cell survival, proliferation, and differentiation[101]. Upon activation, the core components of the pathway, mammalian STE20-like kinase 1 (MST1) and MST2, work

alongside the scaffold protein SAV1 to phosphorylate and activate large tumour suppressor 1 (LATS1) and LATS2 kinases[102]. In turn, LATS1/2 cooperate with the co-factor Mps1-binder 1 (MOB-1)[103] to phosphorylate key downstream mediators of the Hippo pathway, YAP[104] and its homologue TAZ[105]. Phosphorylation of YAP and TAZ prevents their translocation to the nucleus, as they are sequestered in the cytoplasm by 14.3.3 binding proteins or targeted for proteasomal degradation[104]. When the Hippo pathway is switched off, MST1/2 and LATS1/2 remain dephosphorylated, preventing the inhibition of YAP and TAZ[104, 105]. Thus, YAP and TAZ can translocate to the nucleus and bind to TEA domain (TEAD) transcription factors[106, 107]. The activity of YAP and TAZ can be regulated through mechanical inputs sensed by integrins. For example, the activation of YAP and TAZ by focal complex formation is linked to the activation of F-actin modulators such as GTPase Rac1 and its effector p-21 activated kinase (PAK), and Rho guanidine exchange factor β-PIX[108]. In turn, F-actin levels can modulate LATS1/2 kinase activity and consequently YAP and TAZ signalling[109] or can facilitate the nuclear entry of YAP and TAZ by directly impacting the mechanics of the nucleus through nesprin and Sad1-UNC-84 (SUN) complexes[110]. As a result, there is an upregulation of genes involved in metabolic programs such as glycolysis[111] and amino acid metabolism[112], cellular proliferation[113], and cell survival[114].

In macrophages, YAP/TAZ has been found to play a role in pro-reparative macrophage polarization within tumours[115, 116], and also during TGFβ1-induced fibrosis[117]. Also, the expression of YAP/TAZ is increased in macrophages with a pro-inflammatory phenotype. The activation of YAP enhances pro-inflammatory responses, while the genetic deletion of YAP and TAZ enhances reparative responses in macrophages[118]. In the setting of myocardial infarction, altered macrophage polarization leads to a reduction in cardiac fibrosis and hypertrophy and an improvement in overall cardiac function[118]. In the context of inflammatory bowel disease (IBD), YAP-deficient mice exhibited higher numbers of pro-resolving polarized macrophages in colonic tissue, which helped protect mice from IBD[119]. Concerning mechanical stiffness, adhesion of macrophages to soft hydrogels reduces inflammation when compared to adhesion on stiff materials, and is associated with reduced YAP expression and nuclear localization[120]. Furthermore, the depletion of YAP inhibits macrophage inflammation, whereas overexpression of active YAP increases inflammation, shown by differences in pro-inflammatory cytokine

secretion[120]. When cultured on various hydrogel materials (collagen, Matrigel, and polyethylene glycol (PEG)), macrophages secreted less TNF-α compared to cells on polystyrene controls[120]. Additionally, upstream modulators of YAP/TAZ in the Hippo signalling cascade, MST1/2, have been shown to play a role in regulating macrophage phenotypes. Specifically, mice with a specific deficiency of MST1/2 in macrophages displayed impaired post-myocardial infarction repair compared to wild-type mice[121]. Although these recent findings have shed light on the importance of YAP/TAZ signalling in mediating macrophage function and influencing their polarization and phenotype, the exact mechanism by which YAP/TAZ regulates these changes remains uncertain, as many upstream signals can regulate YAP/TAZ expression and activity[122].

Similarly, DCs can sense mechanical stimuli via YAP/TAZ, as transcriptomic analysis showed a marked upregulation of TAZ in the BMDCs grown on 50 kPa compared to 2 kPa, which was validated by RT-qPCR[66]. Additionally, the stiff substrate-induced production of TNF-α was abrogated when the BMDCs were cultured with verteporfin, an inhibitor of YAP/TAZ[66]. The Hippo signalling pathway was further implicated in DC mechanotransduction, as $CD8\alpha^+$ DCs had enrichment of kinases involved in Hippo signalling, including the phosphorylation of Mst1/2, Yap, and Lats1[123]. DC-specific deletion of *Mst1/2* disrupted the homeostasis and function of CD8α+ DCs and led to the impaired presentation of cognate peptides to prime $CD8^+$ T cells[123]. However, $CD8\alpha^-$ DCs deficient in Mst1/2 overall exhibited normal function[123], suggesting that the role of various mechanosensing pathways may differ for specific subtypes of DCs.

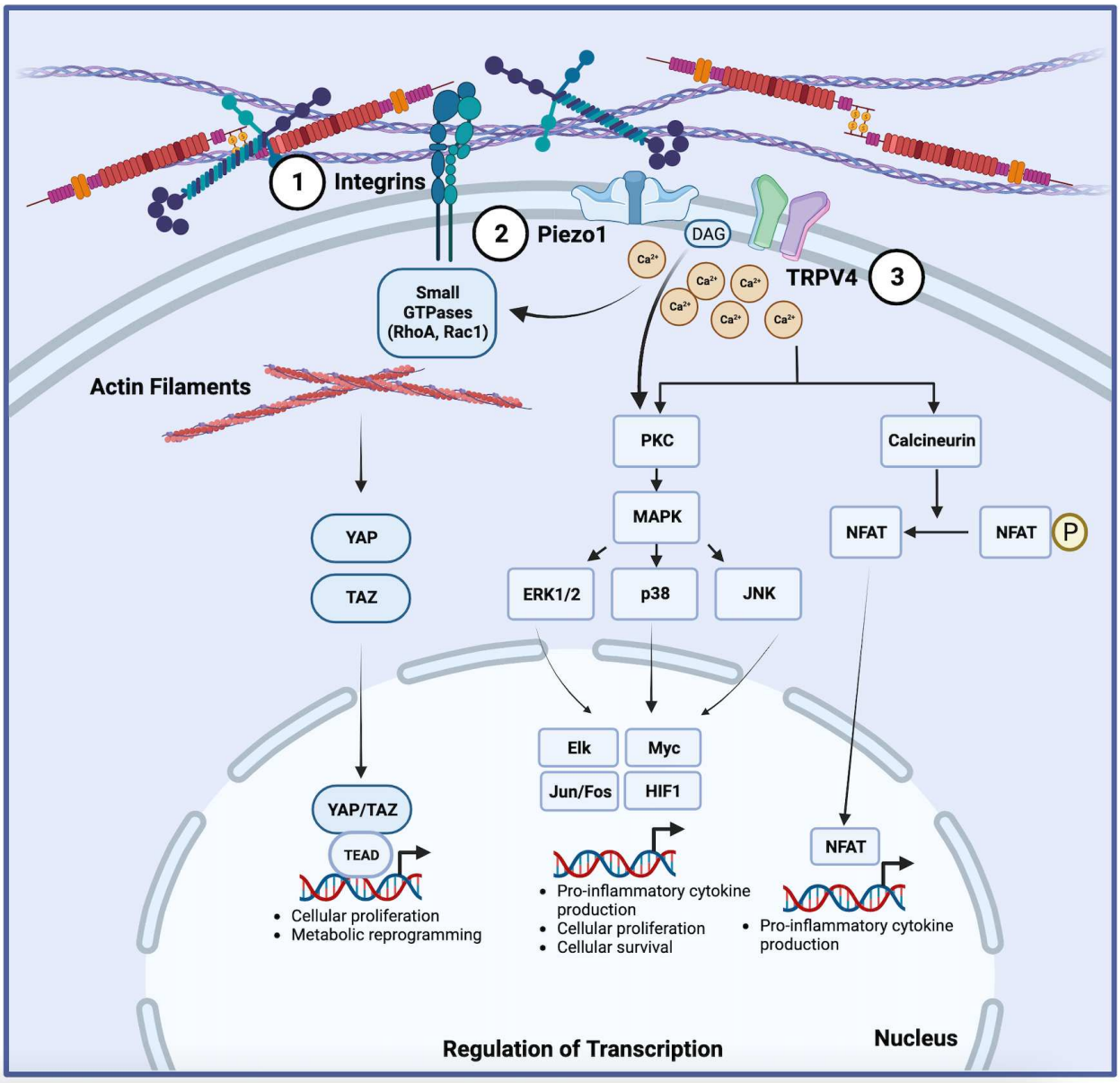

Figure 1.5 Proposed mechanotransduction pathways in DCs. Integrins can sense extracellular matrix stiffness changes, which can translate into activation of small GTPases and subsequent modification of the subcellular organization and structure of F-actin filaments. This is linked to activation of the Hippo signalling pathway by increasing YAP/TAZ activation, leading to the upregulation of genes involved in glycolysis, amino acid metabolism, cellular proliferation and cell survival. Mechanosensitive ion channels are expressed in DCs, including Piezo1 and TRPV4. Physical forces change the tension in the plasma membrane of cells, causing the ion channels to open. Piezo1 and TRPV4 opening allows the entry of extracellular Ca^{2+} ions into the cells. The influx of Ca^{2+} ions can activate the PKC/MAPK pathway or calcineurin/NF-κB

pathway, leading to the upregulation of transcriptional programs that can increase cellular proliferation, differentiation, and inflammatory responses. Abbreviations are as follows: RhoA: Ras homolog family member A; Rac1: Rac family small GTPase 1; YAP: Yes-associated protein TAZ: Transcriptional coactivator with PDZ-binding motif; TEAD: transcriptional enhanced associated domain; Piezo1: Piezo type mechanosensitive ion channel component 1; TRPV4: transient receptor potential of vanilloid subtype 4; DAG: diacylglycerol; PKC: protein kinase C; MAPK: mitogen-activated protein kinase; ERK1/2: extracellular signal-regulated kinase 1/2; JNK: c-Jun N-terminal kinase; NFAT: nuclear factor of activated T cells; NF-κB: nuclear factor kappa B. Drawn in BioRender.com.

1.3.3 Mechanotransduction in macrophages and DCs during pathophysiological conditions

Given the accumulating evidence illustrating the importance of mechanical cues on immune function, it is crucial to understand their impact on immune cells under different conditions and diseases, as well as the mechanosensing pathways mediating these effects. This is especially important because the stiffness of tissues can undergo substantial biomechanical alterations and significantly increase during pathophysiological conditions. Numerous studies have shown that biophysical changes in tissues are correlated with disease progression[124]. Specifically, an increase in tissue stiffness has been associated with atherosclerosis[125, 126], cardiovascular disease[127], IBD[128], and liver disease[129].

In macrophages, deficiency in Mst1/2 worsens cardiac dysfunction after myocardial infarction, as mice lacking Mst1/2 in their macrophages exhibited a marked increase in left ventricular end-diastolic and end-systolic volume and decrease in ejection fraction and fractional shortening[121]. In addition, the pharmacological inhibition of YAP/TAZ dampened pro-inflammatory gene expression (IL-1β and IL-12β)[118]. Additionally, mice with macrophage-specific activation of YAP develop higher levels of cardiac fibrosis and reduced cardiac function following myocardial infarction, compared to wild-type control mice, suggesting that YAP activation in macrophages contributes to increased fibrosis and accumulation of ECM proteins, consequently leading to worsened outcomes following myocardial infarction[118].

In terms of IBD, the effective stiffness of resected bowel portions from patients is significantly higher than healthy controls, which was associated with increased expression of collagen type I genes[128]. In addition, large numbers of macrophages are present in colon samples from IBD patients, which can regulate the initiation and resolution of inflammation[130]. Recent studies have shed light on a role of YAP/TAZ and Mst1/2 in macrophages and DCs in the setting of bowel inflammation, such as during intestinal infections and IBD. YAP regulates macrophage polarization, and YAP deficiency in macrophages mitigates dextran sulfate sodium-induced colitis[119]. Mice lacking Mst1/2 expression in DCs that were infected with ovalbumin-expressing Listeria monocytogenes exhibited reduced $CD8^+$ T-cell responses[123], suggesting an important role for Mst1/2 in clearance of infections.

Recent studies suggest that YAP is a key regulator of macrophage function in the pathogenesis of liver disease. Increased activation of YAP in Kupffer cells (KC), which are liver resident macrophages, enhanced the production of pro-inflammatory cytokines and contribute to the development of non-alcoholic steatohepatitis (NASH)[131]. Mice that were deficient in YAP in macrophages/monocytes and fed on a high-fat diet (HFD) had lower levels of hepatic inflammation and improved liver function[131] compared to HFD-fed wild-type mice. Administration of verteporfin, which inhibits the activity of YAP by increasing levels of 14-3-3σ which sequesters YAP in the cytoplasm and targets it for degradation in the proteasome[132], to HFD-fed mice, helps to reduce liver inflammation and mitigate the pathogenesis of NASH[131]. Although these studies support the hypothesis that YAP in macrophages worsens the development of liver diseases, there remains a paucity of studies focusing on how mechanosensing pathways can alter DC function during liver diseases, as well as how other mechanotransduction pathways may be involved.

1.4 Obesity and Cancer

Cancer is the second leading cause of death worldwide, with approximately 19 million new cases and 10 million deaths annually[133]. Cancer is characterized by the accumulation of genetic alterations and loss of normal cellular regulatory processes[134]. This leads to the development of abnormal cells that divide uncontrollably and have the ability to infiltrate and destroy normal body tissue[134]. There are many different types of cancer, each with its own set of symptoms, causes, and treatments. If left untreated, cancer cells continue to divide and multiply and can invade nearby tissues and organs to cause further damage[134]. To prevent the progression of cancer and to eliminate cancerous cells, our body is equipped with defense mechanisms orchestrated by immune cells.

1.4.1 Cancer immune surveillance

The body has immune mechanisms to identify and eliminate cancerous cells in a process called immune surveillance. For an antitumour immune response to effectively kill cancer cells, a series of events involving T cell responses needs to be initiated and expanded. The T cell antitumour immune cycle is a process of self-proliferation and self-amplification, which connects innate immunity to adaptive immunity and results in antigen-specific T cell-mediated immune responses[135] (**Figure 1.6)**. Firstly, neoantigens created by oncogenesis will be released and

captured and processed by professional APCs, including DCs. This would have to be accompanied by immunogenic signals that would induce an immune response, such as proinflammatory cytokines and factors released by dying tumour cells. The activated DC will then migrate to the tumour-draining lymph node and present the captured antigens on MHC class I and II molecules to naive $CD8^+$ and $CD4^+$ T cells, respectively[135]. Under the action of costimulatory signals, including the interaction of B7-type CD80/86 receptors on DCs with CD28 on T cells, as well as inflammatory cytokines produced by DCs, it will lead to effective priming and activation of T cell responses against cancer-specific antigens[135]. The activated T cells will then travel to the malignant tissue through the bloodstream, followed by specific elimination of cancerous cells expressing the respective tumour-specific antigens[135].

Cytotoxic $CD8^+$ T cells or CTLs are major killers of pathogens and cancerous cells, while $CD4^+$ T cells play important roles in maintenance of the $CD8^+$ response and production of cytokines to enhance other immune responses. Activated $CD8^+$ T cells generate an immunological synapse after recognition of its cognate peptide-MHC complex on target cells by TCRs. Once the synapse is formed, CTLs can degranulate, releasing the contents of granules containing perforin and granzyme proteases. Perforin forms pores in the target cell membrane, allowing free influx and efflux of ions and polypeptides, and induces a repair response[136]. This also enables granzymes to access the target cell cytoplasm, where they can induce apoptosis through activation of caspase pathways, resulting in target cell death[136]. $CD8^+$ T cells also secrete pro-inflammatory cytokines such as IFNγ, which can induce apoptosis in tumours cells[137]. IFNγ can also indirectly kill tumour cells by activating surrounding immune cells. In addition to CTLs, $CD4^+$ T cells play a role in shaping the anti-tumour immune response. $CD4^+$ Th1 cells secrete high amounts of pro-inflammatory cytokines which can promote T cell priming and activation and CTL cytotoxicity, enhance the anti-tumoural activity of macrophages and NK cells, and increase the presentation of tumour antigens by DCs[138]. In addition, IFNγ production by $CD4^+$ T cells have been shown to eliminate tumours without $CD8^+$ T cell help, as adoptive transfer of $CD4^+$ T cells led to rejection of a fibrosarcoma 6132A-PRO tumour challenge in severe combined immunodeficient mice[139]. Overall, these T-cell mediated anti-tumour responses are critical, as the presence of tumour-infiltrating $CD8^+$ T cells and Th1 cytokines in tumours

correlates with favorable prognosis in terms of overall survival and disease-free survival in many malignancies[140].

However, there are also multiple immune-regulatory mechanisms that have evolved for cancerous cells to evade elimination. During immune homeostasis, a critical mechanism of peripheral tolerance is regulation of effector T cell responses via immune checkpoints to protect tissue from inflammatory damage. When exposed to chronic antigen stimulation, T cells enter a dysfunctional state called T cell exhaustion[141]. Exhausted T cells are characterized by a decrease in the expression of effector cytokines, but also an increase in expression of co-inhibitory receptors including Killer cell lectin-like receptor G1 (KLRG1), Programmed cell death protein 1 (PD-1), T cell immunoglobulin and mucin domain-containing protein 3 (TIM-3), and Lymphocyte activation gene 3 (LAG-3)[141, 142]. An increase in these co-inhibitory receptors and their interactions with their respective ligands lead to downregulation of TCR signalling, resulting in decreased T cell proliferation, cytokine production, and cytolytic function[143, 144, 145]. Cancer cells can further promote T cell exhaustion through the expression of ligands for inhibitory receptors, such as PD-L1 and PD-L2, which interact with PD-1 on T cells, leading to their deactivation and anergy[146].

Nutrient competition occurs between tumour cells and immune cells, which can influence their survival and function. Immune cells including T cells must acquire adequate nutrients to engage the metabolism that supports their function. For instance, glucose metabolism and glycolysis is important for optimal T cell effector function[147], and amino acids such as glutamine and tryptophan are critical for T cell activation, proliferation, and differentiation[148]. In the tumour microenvironment, tumour cells proliferate at a high rate, and thus rapidly consume large amounts of nutrients, which can starve other cells in their proximity[149]. Indeed, tumour cells can outcompete T cells for glucose in vitro, which consequently impairs T cell cytokine production[150]. High rates of glutaminolysis and tryptophan usage in tumour cells reduces levels of glutamine and tryptophan available for optimal effector function in T cells[151].

Cancer cells can also evade recognition by the downregulation of MHC class I molecules. Expression of tumour antigens is decreased on the surface of tumour cells, which prevents CTLs

from recognizing target antigens on tumour cells[152]. Tumour cells can attract regulatory immune cells, such as Tregs and tumour-associated macrophages to the tumour microenvironment (TME), through the production of immunosuppressive cytokines such as CCL2[153]. In addition to recruitment, cancer cells can polarize immune cells to an immunosuppressive or regulatory phenotype by production of cytokines such as colony stimulating factor (CSF)-1, transforming growth factor (TGF)-β, and IL-10[154], thereby impairing anti-tumour immune responses.

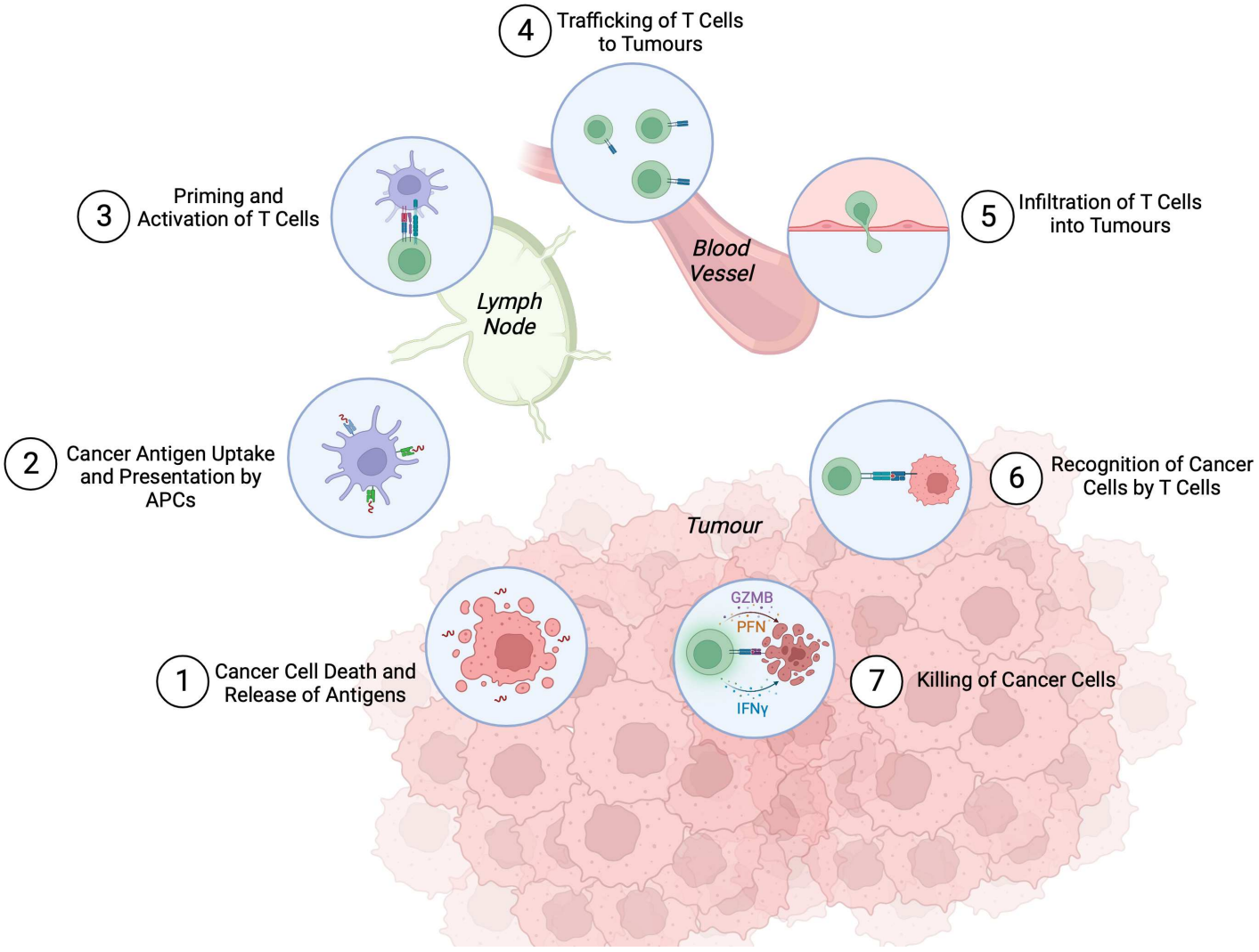

Figure 1.6 Major cancer immune surveillance mechanism mediated by APCs and T cells. For anticancer immune responses to have effective killing of cancer cells, a series of stepwise events need to be initiated and expanded iteratively. The cycle can be split into seven major steps, beginning with the release of antigens from the cancer cell, and ending with killing of cancer cells. Each step is described above, with the main cell types involved and anatomic location of the activity. Abbreviations are as follows: APC: antigen presenting cell; GZMB: granzyme B; PFN: perforin; IFNγ: interferon gamma. Drawn on BioRender.com. Adapted from Chen & Mellman[135].

1.4.2 Mechanistic links between obesity and cancer

Obesity is a major determinant of the increasing incidence and prevalence of cancer that could surpass smoking as a significant preventable cause against cancer[155]. Obesity is associated with an increased risk of 13 different types of cancers[155], increased diagnosis of cancer, cancer progression, worsened prognosis, and increased mortality[156, 157]. Therefore, it is critical to elucidate the underlying mechanisms by which obesity increases tumour burden.

There have been multiple mechanisms proposed linking obesity and increased cancer risk (**Figure 1.7)**. Obesity leads to chronic low grade inflammation, in which obese adipose tissue is infiltrated with pro-inflammatory cells such as pro-inflammatory macrophages, which can secrete high levels of pro-inflammatory cytokines such as TNF, IL-6, and IL-1. These cytokines can in turn promote JAK/STAT activation in cancerous cells, which enhances cell growth and can contribute to uncontrolled growth and carcinogenesis[158]. Growth hormones and adipokines that are elevated during obesity have mitogenic properties and can promote the proliferation of cells, which can result in cancer when growth is uncontrolled. For example, leptin, an adipokine that is involved in appetite regulation and is upregulated in obese conditions, can activate STAT3 signalling, which can upregulate expression of genes that enhance cell proliferation and survival[159].

Increase in lipid availability during obesity can have multiple protumourigenic effects. Although cancer cells rely predominantly on glucose and glutamine consumption as energy sources, they store high amounts of lipids in the form of lipid droplets[160]. Elevated lipid concentrations within cancer cells have been associated with cancer progression[160]. Cancer cells can utilize lipids to create energy by fatty acid oxidation, which has been shown to be critical for high rates of proliferation of cancer cells[161].

There is also evidence that lipids can inhibit anti-tumour responses by metabolically reprogramming immune cells. Lipids from an obese environment can suppress cancer immunosurveillance, affecting both innate and adaptive immune cells. Accumulation of oxidized lipids in DCs from the tumour microenvironment impairs cross presentation by inhibiting MHC translocation to the cell surface[162]. Lipid-loaded DCs cannot properly cross-present antigens and

activate T cells, which can impair CTL responses[162]. Obese individuals also have lower numbers of circulating NK cells, which is associated with increased cancer risk[163]. NK cells can normally recognize non-MHC expressing cancer cells, and release cytotoxic proteins such as perforin and granzymes that induce apoptosis in target cells[164]. However, lipids cause metabolic programming in NK cells that results in defects in cytokine secretion, cytotoxicity, and failure to form an immune synapse[165]. Obesity and lipid metabolism also promotes the differentiation of tumour associated macrophages (TAM), which can suppress anti-cancer T cell responses[166]. Macrophages in the TME can have mixed phenotypes, with pro-inflammatory macrophages contributing to anti-tumour immune responses, while TAMs are regulatory and promote tumour growth. TAMs secrete IL-10 and TGFβ which can inhibit T cell functions and induce regulatory functions, as well as express ligand receptors for PD-1 which can suppress cytotoxic functions of T cells and NK cells[167]. Fatty acid oxidation in macrophages is required for the maturation of IL-4 induced anti-inflammatory macrophages, and is associated with an immunosuppressive phenotype[167]. Therefore, increased lipid availability and lipid metabolism in macrophages can promote a regulatory phenotype in the TME, promoting immunnosuppression in the tumour. In terms of T cells, lipids can also promote increased levels of Tregs in the TME. Tregs rely heavily on fatty acid oxidation to generate energy, and lipid oxidation promotes the differentiation of Tregs[168]. Interestingly, $CD8^+$ T cells growing in MC38 colorectal adenocarcinoma tumours of obese mice do not demonstrate lipid accumulation compared to $CD8^+$ T cells in tumours of lean mice[169], but instead show reduced activity of amino acid transporters. However, the underlying mechanisms altering $CD8^+$ T cell metabolism within the TME during obesity is unclear.

Obesity-induced IR can also play a role in promoting tumour growth. Hyperinsulinemia and hyperglycemia that result from IR can enhance tumour cell survival, growth, and proliferation. High levels of insulin also exert tumourigenic effects due to its antiapoptotic and proliferative signals[149]. Interestingly, IR can also impact immune cell function. Insulin signalling and glucose availability impact immune cell activity, as immune cell activation and the responses elicited are influenced by their metabolic profile[170]. Evidence suggests that INSR signalling is critical in immune cell function, including T cells. Previously, we have observed an important role of INSR signalling in T cell function, as T cells upregulate their surface expression of INSR upon activation, and impairment of INSR signalling reduces their proliferative capacity and

production of effector molecules[171]. INSR deficiency was also shown to compromise $CD4^+$ and $CD8^+$ T cell populations during influenza infection, and resulted in impaired recovery from weight loss after peak of infection[171]. However, the role of insulin signalling and INSR in the context of T cell anti-tumour immunity is largely unknown.

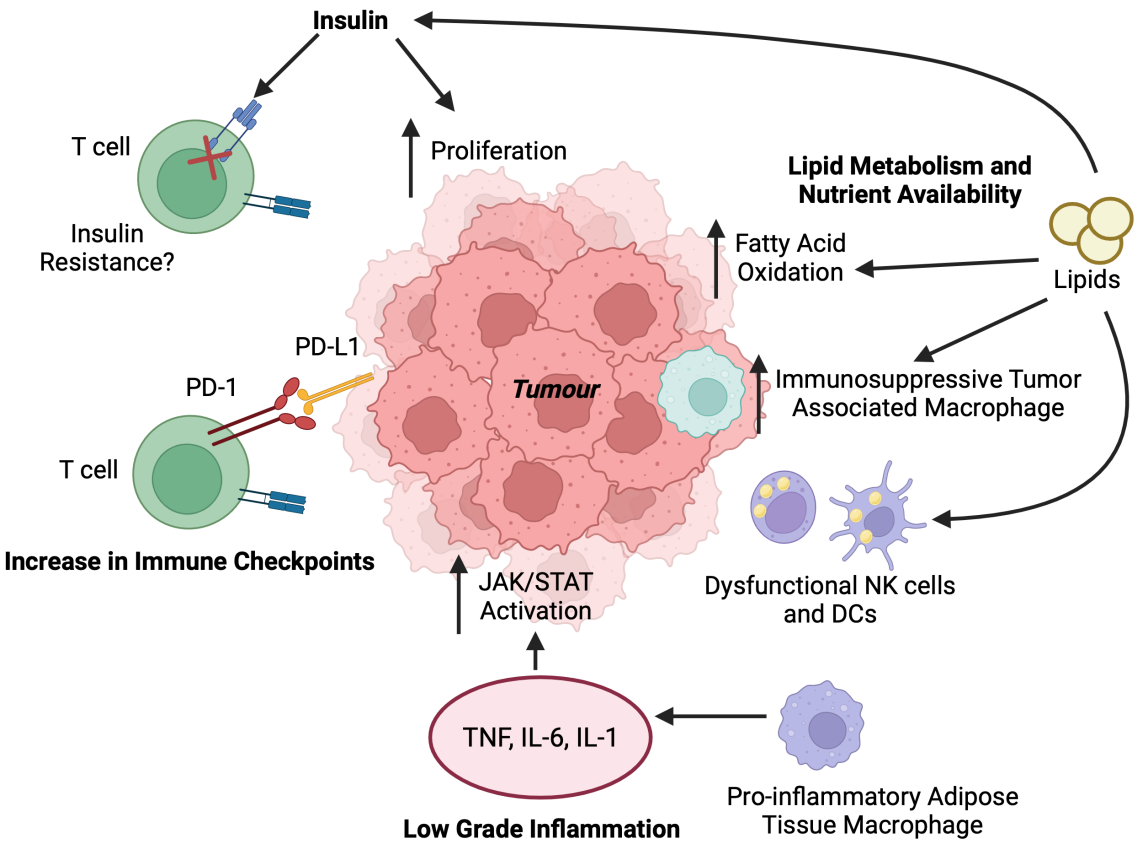

Figure 1.7 Mechanistic links between obesity and cancer. Multiple mechanisms have been proposed linking obesity to cancer risk and progression. Obese adipose tissue is infiltrated with pro-inflammatory macrophages, which produce high levels of TNF, IL-6, and IL-1, which promote JAK/STAT activation in cancer cells to enhance cell growth. There is some evidence that obese environments promote the expression of PD-1 on T cells and PD-L1 on tumour cells, enhancing exhaustion in T cells. Lipids from an obese environment can suppress immunosurveillance, by causing dysfunction in NK cells and DCs, but also promoting the differentiation of anti-inflammatory tumour-associated macrophages. Increased levels of insulin can promote proliferation of cancer cells, and can potentially lead to insulin resistance in T cells. Abbreviations are as follows: PD-1: programmed cell death protein-1; PD-L1: programmed death-ligand 1; NK cell: natural killer cell; DC: dendritic cell; TNF: tumour necrosis factor; IL-6: interleukin-6; IL-1: interleukin-1; JAK: janus kinase; STAT: signal transducer and activator of transcription. Drawn in BioRender.com. Adapted from Dyck & Lynch[149].

1.5 Hypotheses and objectives of study

1.5.1 The role of obesity and INSR signalling on T cell-mediated anti-tumour immunity

It is well established that obesity is linked to various complications. In the context of certain cancers, obese patients have increased risk, as well as worsened prognosis compared to lean patients[155]. Multiple links between obesity and cancer outcomes have been identified, including increased levels of circulating lipids, growth hormones, and adipokines, which can have protumourigenic effects[149]. In addition, recent studies suggest that obesity can contribute to tumourigenesis by impairing anti-tumour immunity. CTLs play critical roles in anti-tumour immunity, through direct tumour cell killing and cytokine production[172]. However, over time in the TME, CTLs become exhausted and display impaired function. T cells express INSR, and insulin signalling in T cells primarily drives pro-inflammatory effects, as the addition of insulin to T cells in vitro promotes IL-2 responsiveness[173] and chemotactic activity[174]. Previously, it has also been observed that INSR signalling plays an important role in T cell function and proliferation[171]. Interestingly, evidence supports the notion that T cells respond poorly to INSR signalling during obesity[175]. Considering the critical role of T cells in anti-tumour immunity, and the importance of INSR for optimal T cell function, it remains to be explored how IR and INSR signalling in T cells impact anti-tumour immunity. Therefore, I aim to examine the impact of obesity and insulin resistance on T cell-mediated anti-tumour immunity and investigate the role of INSR in anti-tumour T cell function. Based on previous studies, I hypothesize that obesity impairs anti-tumour CTL differentiation and/or function through inducing T cell-intrinsic insulin resistance. By using a diet-induced obesity mouse model, and mice with T cell-specific deletion of INSR, we will address the specific aims:

1. Determine the impact of obesity and IR on T cell-mediated anti-tumour immunity.
2. Determine the role of INSR in T cell anti-tumour function.

1.5.2 The role of YAP/TAZ in DC-mediated pathogenesis of IR and NAFLD

Previous studies have also demonstrated that obesity-associated chronic inflammation is linked with the development of IR and NAFLD. DCs have been shown to have a major contribution to obesity-induced inflammation and IR. During obesity, DCs can produce pro-inflammatory cytokines and promote Th1 and Th17 inflammatory responses, worsening the systemic inflammation[176]. Furthermore, depletion of DCs decreases macrophage and T cell

infiltration in adipose tissue and liver and protects mice from obesity-induced IR[61]. One environmental factor that can modulate DC function during obesity is alterations in tissue stiffness. Increases in adipose tissue and liver stiffness can occur during obesity, as obesity increases ECM and collagen fibers formation, causing local fibrosis[64, 65]. In the context of NAFLD, DCs control the activity of many cells known to be critical in fibrogenesis, indirectly controlling fibrosis. DCs are important in promoting $CD4^+$ and $CD8^+$ T cell differentiation, both of which have been implicated in liver fibrosis[177]. The fibrotic processes that occur in the progression of NAFLD increases tissue stiffness[178], potentially activating mechanosensing pathways. Increasing evidence suggests a role for extracellular physical cues coming from tissue stiffness in promoting immune cell recruitment, activation, and inflammatory function[179]. Previously, we have identified TAZ as a potential modulator linking mechanosensing to DC function[66]. Transcriptomic analysis and inhibitor/agonist assays identified TAZ to be important for promoting DC metabolism and function under higher substrate stiffness conditions[66]. In addition to mechanical cues, TAZ and its homologue YAP activity in the HIPPO pathway is regulated by nutrient cues[180]. Under high glucose levels, the AMPK pathway is inhibited, allowing YAP and TAZ to mediate their downstream effects[180]. Given that obesity is associated with alterations in nutrient and mechanical cues, TAZ expression is upregulated in DCs exposed to stiffer substrates, and increased YAP/TAZ activity in innate cells promotes the progression of various inflammatory diseases, I aim to explore the role of YAP/TAZ signalling in DCs in the pathogenesis of obesity-associated IR and NAFLD. Taking into consideration previous studies on YAP/TAZ and the role of DCs in obesity-associated inflammation, I hypothesize that signalling through YAP and TAZ in DCs promotes inflammation and IR in a feed-forward manner, and promotes the development of NAFLD. Using mice with DC-specific deletion of YAP and/or TAZ, we will address the specific aims:

1. Determine whether YAP and/or TAZ in DCs regulates the composition of immune cell populations in the liver at steady-state.
2. Examine the role of YAP and/or TAZ in DCs in the development of obesity-associated IR.
3. Assess the importance of YAP/TAZ in DCs in obesity-associated inflammation and development of NAFLD.

Chapter 2: Methods and Materials

2.1 Mice

All mice used in my studies were generated by intercrossing breeders obtained from Jackson Mice. Genetically manipulated mice were generated as described in respective chapters. 8-12 week old male and female mice were used. All mice were bred and housed in a pathogen-free, temperature-controlled, and 12 hr light and dark cycle environment at the University of Alberta Health Sciences Laboratory Animal Services mouse barrier facility. All mice used in comparative studies were gender and age-matched, and littermates were used as controls if possible. Unless specified, mice were fed a normal chow diet (NCD, 10 kcal% fat). All experimental procedures were approved by the Animal Care committee at the University of Alberta. Mice genotypes were confirmed by PCR and gel electrophoresis.

2.2 Cell Lines and Primary Cell Culture

Mouse Lymphoma Cell Line E.G7-OVA E.G7-OVA cells are T lymphoblasts derived from the C57BL/6 (H-2 b) mouse lymphoma cell line EL4 (ATCC TIB-39)[181]. Cells were maintained in RPMI 1640 medium (Wisent) supplemented with fetal bovine serum (FBS) (10%; Sigma), L-glutamine (2 mM; Gibco), penicillin (100 U/ml; Sigma), streptomycin (100 μg/ml; Sigma), 2-mercaptoethanol (50 μM; Sigma), sodium pyruvate (1 mM; Gibco), and MEM non-essential amino acids (Gibco).

Mouse Colon Adenocarcinoma MC38-OVA Cells were maintained in DMEM medium supplemented with FBS (10%; Sigma), L-glutamine (2 mM; Sigma), penicillin (100 U/ml; Sigma), streptomycin (100 μg/ml; Sigma), 2-mercaptoethanol (50 μM; Sigma), and geneticin 418 (200 ng/mL; ThermoFisher) to select for MC38 cells expressing the OVA-derived CTL epitope SIINFEKL.

2.3 Tissue Isolation and Digestion

Mice were euthanized by CO_2 fixation. Organs, lymph nodes and tumours were dissected from mice after euthanasia for processing.

Spleen Spleens were processed into single cell suspension and filtered through a 40 μm cell strainer prior to hemolysis with Ammonium-Chloride-Potassium (ACK) lysing buffer for 5 min to remove red blood cells.

Lymph Node Inguinal lymph nodes were processed by passing through a 40 μM cell strainer with a PBS wash, without hemolysis.

Tumour Tumour tissue was minced and subjected to collagenase I digestion (2 mg/ml; Sigma) with DNase-I (60 U/ml; Sigma) in 800 μl of DMEM media (Wisent) with gentle shaking for 1 hr at 37ºC, and filtered through a 40 μm cell strainer with a PBS wash.

Liver Liver tissue was minced and subjected to collagenase I digestion (450 U/ml; Sigma) with DNase-I (60 U/ml; Sigma) in 800 μl of DMEM (Wisent) with gentle shaking for 1 hr at 37ºC, and filtered through a 40 μm cell strainer with a HBB (HBSS, 2% bovine serum, 0.2% BSA) wash. After centrifugation at 1500 rpm for 5 min, cell pellets were resuspended in 1 mL of 40% Percoll for density separation. Supernatant was aspirated and single cell suspensions were resuspended in ACK lysing buffer for 5 min.

VAT Epididymal VAT pads were dissected from mice and were mechanically dissociated using a gentleMACS™ Octo Dissociator dissociator in 5 mL of DMEM, and then subjected to collagenase I digestion (2mg/ml; Sigma) with DNase-I (60 U/ml; Sigma) with gentle shaking for 1 hr at 37ºC, and filtered through a 40 μm cell strainer with a PBS wash.

2.4 Flow Cytometry

Immune cells from all mouse tissues were stained with a live/dead exclusion dye (Zombie UV, Biolegend). Fluorophore-conjugated antibodies were diluted 1/200 unless otherwise recommended by the supplier prior to surface and intracellular staining at 4ºC for 30 min. Intracellular staining was done after fixation and permeabilization with a FOXP3 Staining Buffer Set following manufacturer's instructions (eBioscience). For intracellular cytokine staining, cell suspensions were stimulated with phorbol myristate acetate (PMA) and ionomycin in the presence of Brefeldin A (PMA+, Biolegend) for 5 hr. PMA is a diacylglycerol (DAG) mimic and activates protein kinase C[182], while ionomycin is a calcium ionophore which stimulates the release of intracellular free calcium[183]. Therefore, stimulation with PMA and ionomycin bypasses the requirement for TCR complex signalling and leads to the activation of T cells and the production of a variety of cytokines. Brefeldin A inhibits intracellular protein transport by the

Golgi[184], therefore allowing intracellular detection of secreted cytokines and proteins by flow cytometry. Tumour antigen-specific $CD4^+$ and $CD8^+$ T cells from lymphoid organs and tumour infiltrating lymphocytes (TILs) were stained with tetramers (NIH) specific for $OVA_{329-337}$ H-2IA^b (AAHAEINEA) and $OVA_{257-264}$ H-2K^b (SIINFEKL), respectively. Permeabilized/fixed samples were resuspended in permeabilization buffer, while unfixed samples were resuspended in FACS buffer for flow cytometric analysis on a BD LSR Fortessa-SORP or Cytek Aurora at the Flow Cytometry Facility (University of Alberta). FCS plots were generated using FlowJo software (LLC). Gating strategies for FCS plots of liver and VAT for Chapter 4 are found in the Appendix.

2.5 Culturing of Bone Marrow-Derived Dendritic Cells (BMDC)

BMDCs were cultured following a protocol by Inaba et al[185]. Bone marrow progenitor cells were harvested from the femur of C57BL/6 mice and plated at a density of $3x10^6$/3 mL well on 6-well plates with GM-CSF (20 ng/ml, Biolegend) in RPMI 1640 medium (Wisent) supplemented with fetal bovine serum (FBS) (10%; Sigma), L-glutamine (2 mM; Gibco), penicillin (100 U/ml; Sigma), streptomycin (100 μg/ml; Sigma), 2-mercaptoethanol (50 μM; Sigma), sodium pyruvate (1 mM; GIbco), and MEM non-essential amino acids (Gibco). Bone marrow cultures were fed on days 3 and 6 with 1 mL cell culture medium containing fresh GM-CSF.

2.6 Carboxyfluorescein succinimidyl ester (CFSE) proliferation assay

T cell proliferation was examined using a 48-hour CFSE assay, which utilizes a dye that binds covalently to free amines on the surface and inside of cells. CFSE covalently stains cells by crossing the plasma membrane and allows T cell proliferation to be visualized by CFSE dilution after each cycle of division[186]. T cells were harvested from spleens and lymph nodes of OT-I transgenic mice, which have transgenic T cell receptors (TCR) that are designed to recognize ovalbumin residues 257-264 (SIINFEKL) in the context of H-2K^b [187], allowing us to measure the ability of T cells to proliferate. OT-I T cells were purified with an EasySep™ mouse $CD8^+$ T cell negative selection kit (STEMCELL technologies) according to the manufacturer's protocol. Purified $CD8^+$ T cells were labelled with CellTrace™ CFSE Cell Proliferation Kit (ThermoFisher). BMDCs were harvested after 7 days of culture[185], and pulsed for 2 hours with 0 μg/ml, 0.1 μg/ml, 0.01 μg/ml, or 0.001 μg/ml of $OVA_{257-264}$ peptide (GenScript). 10,000 pulsed

DCs were co-cultured with 20,000 CFSE-labeled T cells. Proliferation was measured via flow cytometric analysis for the dilution of CFSE dye.

2.7 In vitro Tumour Killing Assay

Fresh T cells were isolated from the spleen of NCD or HFD-fed OT-I C57BL/6 transgenic mice, or OT-I transgenic LckCre^{+} *Insr*$^{fl/fl}$ or LckCre^{-} *Insr*$^{fl/fl}$ mice with an EasySep™ mouse CD8^{+} T cell negative selection kit (STEMCELL technologies) according to the manufacturer's protocol. MC38-OVA tumour cells (provided by Dr. Kristi Baker, University of Alberta) were harvested after 5 days of culture and co-cultured with the isolated OT-I CD8^{+} T cells at varying ratios (Target:Effector 1:2, 1:4, 1:8) for 24 hrs and 48 hrs. On the day of harvesting the cells, co-cultures were incubated with 1/2000 dilution of CellEvent™ Caspase 3/7 Green Detection Reagent (ThermoFisher Scientific), PMA and ionomycin for 2 hours, followed by the addition of monensin and brefeldin A for another 2 hours before harvesting the cells[188]. Cells were stained with a LIVE/DEAD Near-IR dye (ThermoFisher) and fluorophore-conjugated antibodies for flow cytometry at 4ºC for 30 min. Intracellular staining for IFNγ and GZMB was done after fixation and permeabilization with a FOXP3 staining buffer set (eBioscience).

2.8 Western Blotting

T cells were isolated from the spleen of NCD and HFD-fed mice and cultured with plate-bound antiCD3/CD28 (1µg/mL; Biolegend) for 48 hours, serum starved for 6 hours, followed by stimulation with or without insulin (10 ng/ml; Humalog) for 15 minutes at 37ºC. At the end of stimulation, cells were pelleted and snap-frozen. Cell lysates from purified CD8^{+} T cells were prepared using commercial cell lysis buffer (Cell Signaling) and protease/phosphatase inhibitor (Cell Signaling) according to manufacturer instructions. Protein concentration was determined using a Pierce™ BCA Protein Assay Kit (ThermoFisher). 25-50 µg of protein were loaded with 1x Laemmli Sample Buffer (BIO-RAD) and resolved on 8% Tris-Glycine gel, and transferred onto a polyvinylidene difluoride membrane (Millipore). After transfer using a BioRAD Transblot Turbo, the membrane was blocked with Intercept™ TBS blocking buffer (Li-Cor) for 1 hour. Antibodies used for western blots were diluted in Intercept™ antibody diluent T20 TBS buffer (Li-Cor). Primary antibodies were diluted as follows: phospho-AKT 1/500, total AKT 1/1000. Secondary antibodies were diluted 1/1000. After blocking, primary antibody was incubated

overnight at 4ºC, and then detection antibody (Li-Cor) at room temperature for 1 hr. The membrane was scanned using an Odyssey Fc Imaging System. Protein bands were quantified using the Li-Cor Image Studio Acquisition Software.

2.9 Adoptive Transfer of T cells

$CD8^+$ T cells were purified from the spleen and lymph nodes of NCD or HFD-fed OT-I transgenic mice, or OT-I transgenic $LckCre^+$ $Insr^{fl/fl}$ or $LckCre^-$ $Insr^{fl/fl}$ mice with an EasySep™ mouse $CD8^+$ T cell negative selection kit (STEMCELL technologies) according to the manufacturer's protocol. Purified $CD8^+$ T cells were labelled with CellTrace™ CFSE Cell Proliferation Kit (ThermoFisher) and enumerated. $2x10^6$ CFSE-labelled T cells were intravenously injected into the tail vein of tumour-injected CD45.1 congenic mice 7-9 days post tumour injection once the tumours were palpable. Mice were euthanized 3 days-post injection, and tumour, spleen, and draining and opposite inguinal lymph nodes were collected for processing.

2.10 Real-time qPCR

Total RNA from cultured BMDCs was extracted using a PureLink™ RNA mini kit (ThermoFisher) as per manufacturer's protocol. Reverse-transcription of the RNA was performed using random primers (ThermoFisher). qPCR was performed on a CFX96 Touch Real-Time PCR Detection System (BioRAD) using SUPERGREEN™ Master Mix reagent (Wisent). Each sample was run in triplicate and normalized to housekeeping gene β−actin. Relative fold changes in gene expression were calculated using the ΔΔCT method with the equation $2^{-\Delta\Delta CT}$. The results are shown as fold changes compared to the control group average. For *Yap1* and *Wwtr1* (WW domain containing transcription regulator 1; also known as *Taz*) genetic floxing efficiency, primers specific for detecting exon 2 of the *Yap1* and *Wwtr1* gene were used. Sequences of the mouse forward and reverse primers are as follows: *β−actin* forward: 5'-GACCTCTATGCCAACACAGT-3'; reverse: 5'-AGTACTTGCGCTCAGGAGGA-3'; *Yap1* forward: 5'-TACTGATGCAGGTACTGCGG-3'; reverse: 5'-TCAGGGATCTCAAAGGAGGAC-3'; *Wwtr1* forward: 5'-CAAGTCATCCACGTCACGCA-3'; reverse: 5'-CCGGAATCGGGCTCCTTAAA-3'.

2.11 E.G7-OVA Tumour Model

Mice were subcutaneously injected with E.G7-OVA tumour cell line (ATCC CRL-2113, $2x10^5$ cells/mouse) in the right flank of mice, and euthanized 3-4 weeks post-injection. Tumour growth was monitored every other day starting 6 days post-injection at similar times using a caliper. Tumour volumes were calculated as 3.14 x (width/2) x (length/2) x depth (ellipses formula). The tumour, spleen, and draining inguinal lymph node were obtained from tumour-injected mice for quantification. Tumour-injected mice were housed in a pathogen-free, temperature-controlled, and 12 hr light and dark cycle environment at the University of Alberta Health Sciences Laboratory Animal Services mouse conventional facility.

2.12 Diet-induced obesity (DIO) model

6 week-old male C57BL/6 mice were fed a high fat diet (HFD) consisting of 60 kcal% of fat for 16 weeks[189]. Intraperitoneal glucose tolerance tests and insulin tolerance tests were tested following 16 weeks of feeding to assess for glucose tolerance and insulin tolerance.

2.13 High Fat High Sucrose (HFHS) mouse model

6 week-old mice were put on a HFD consisting of 60 kcal% of fat, supplemented with 42g/L sucrose water for 20 weeks. Intraperitoneal glucose tolerance tests and insulin tolerance tests were conducted following 20 weeks to assess for glucose tolerance and insulin tolerance. Male mice were used for HFHS studies as male mice are more susceptible to diet-induced weight gain and IR[190].

2.14 Intraperitoneal glucose tolerance test (IPGTT) and insulin tolerance test (ITT)

IPGTT Mice were fasted overnight for 16 hours. Body weights were measured to calculate the dosage required to inject 1.5g glucose/kg body weight. In the animal facility in a BSC, the mice were anesthetized with inhalation of isoflurane, and the tail vein was gently punctured with a 25 gauge needle and a baseline blood glucose reading was acquired using a glucometer. Mice were intraperitoneally injected with glucose solution, and blood glucose excursion was measured at 10, 20, 30, 60, 90, and 120 minutes post-injection using a glucose meter (CONTOUR® NEXT).

ITT Mice were fasted for 6 hours. In the animal facility in a BSC, the mice were anesthetized with inhalation of isoflurane, and the tail vein was gently punctured with a 25 gauge needle and a

baseline blood glucose reading was acquired using glucometer. Mice were intraperitoneally injected with insulin (0.75 U insulin/kg body weight; Humalog), and blood glucose levels were measured at 10, 20, 30, 60, 90, and 120 minutes post-injection using a glucose meter (CONTOUR® NEXT).

2.15 Fibrosis Staining

One lobe of the liver was isolated from HFHS treated mice, embedded in paraffin blocks, and longitudinally serially sectioned to 7 µm. Briefly, after deparaffinization (from 100% xylene to decreasing concentrations of EtOH and finally with double distilled H_2O), tissues were stained with Sirius Red/Fast Green Collagen Staining Kit (Catalog #9046, Chondrex Inc) for 45 minutes. Tissues were washed with ddH2O and rehydrated (from ddH20 to EtOH until 100% xylene), and mounted with a toluene mounting medium.

2.16 Statistical Analysis

All statistical analyses were performed using GraphPad Prism 9 software. The number of biological replicates is listed as the n value in figure legends. Statistical significance was assessed using Mann-Whitney U-test, students T-test or Two-Way ANOVA set at $p<0.05$.

2.17 Table of reagents and software

Table 2.1 List of antibodies used for flow cytometry or Western Blotting. All listed antibodies are available commercially.

Reagents	**Clone**	**Source**	**Catalog Number**
Antibodies			
Brilliant Violet 711 anti-mouse CD45 antibody	30-F11	BioLegend	103147
Alexa Fluor 700 anti-mouse CD45 antibody	I3/2.3	BioLegend	147716
Alexa Fluor 488 anti-mouse CD3 antibody	17A2	BioLegend	100210

PE/Dazzle 594 anti-mouse CD4 antibody	GK1.5	BioLegend	100456
PE/Cyanine5 anti-mouse CD8a antibody	53-6.7	BioLegend	100710
Brilliant Violet 605 anti-mouse CD8a antibody	53-6.7	BioLegend	100744
PE/Cyanine7 anti-mouse CD69 antibody	H1.2F3	BioLegend	104512
APC/Cyanine7 anti-mouse CD183 (CXCR3) antibody	CXCR3-173	BioLegend	126552
Brilliant Violet 711 anti-mouse/human CD44 antibody	IM7	BioLegend	103057
Brilliant Violet 510 anti-mouse CD62L antibody	MEL-14	BioLegend	104441
Brilliant Violet 605 anti-mouse CD279 (PD-1) antibody	29F.1A12	BioLegend	135220
Brilliant Violet 650 anti-mouse CD223 (LAG-3) antibody	C9B7W	BioLegend	125227
BUV395 anti-mouse CD366 (TIM-3) antibody	5D12	BD Biosciences	747620
Brilliant Violet 785 anti-mouse/human KLRG1 (MAFA) antibody	2F1/KLRG1	BioLegend	138429
Pacific Blue anti-T-bet antibody	4B10	BioLegend	644808

PerCP-Cy 5.5 anti-mouse FOXP3	R16-715	BD Biosciences	563902
PE anti-mouse IFNγ antibody	XMG1.2	BioLegend	505808
PerCP/Cyanine5.5 anti-human/mouse Granzyme B Recombinant Antibody	QA16A02	BioLegend	372212
Alexa Fluor 647 anti-mouse CD107α (LAMP-1) antibody	1D4B	BioLegend	121610
Brilliant Violet 510 anti-mouse CD45.2 antibody	104	BioLegend	109837
Brilliant Violet 605 anti-mouse CD45.1 antibody	A20	BioLegend	110737
Alexa Fluor 488 anti-GAPDH antibody	W17079A	BioLegend	607906
Alexa Fluor 700 anti-mouse Ly-6G	1A8	BioLegend	127622
PE/Cyanine7 anti-mouse CD64 (FcγRI) antibody	X54-5/7.1	BioLegend	139314
PerCP/Cyanine5.5 anti-mouse/human CD11b antibody	M1/70	BioLegend	101228
APC/Cyanine7 anti-mouse Ly-6C antibody	HK1.4	BioLegend	128026
Brilliant Violet 605 anti-mouse CD11c antibody	N418	BioLegend	117334

FITC anti-mouse I-A^b antibody	AF6-120.1	BioLegend	116406
APC anti-mouse CD103 antibody	2E7	BioLegend	121414
AKT antibody	N/A	Cell Signaling	9272
Phospho-AKT (Ser473) XP Rabbit mAb	D9E	Cell Signaling	4060
IRDye 680RD Goat anti-Rabbit	N/A	Li-Cor	926-68171

Table 2.2 List of reagents used for cell culturing, digestion of tissues, Western Blotting, or histology.

Chemicals and Peptides	**Source**	**Catalog Number**
RPMI 1640 Medium	Wisent	350-002-CL
Fetal Bovine Serum	Sigma	F1051
L-glutamine	Gibco	25030081
Penicillin-Streptomycin	Sigma	P4333
2-Mercaptoethanol	Sigma	60-24-2
Sodium Pyruvate	ThermoFisher	11-360-070
MEM Non-Essential Amino Acids	ThermoFisher	11140-050
DMEM Medium	Wisent	219-010-XK
Geneticin™ Selective Antibiotic (G418 Sulfate)	ThermoFisher	10131-035

Recombinant Mouse GM-CSF (carrier-free)	BioLegend	576304
Collagenase	Sigma	C0130
DNase	Sigma	D5025
Hank's Balanced Salt Solution (HBSS)	Wisent	311-513-CL
Bovine Serum Albumin	Sigma	A8806
Percoll®	Sigma	P1644
$OVA_{257-264}$ peptide	GenScript	RP10611
E.G7-OVA Cell Line	ATCC	CRL-2113
Insulin Lispro U-100	Humalog	N/A
Intercept™ Antibody Diluent T20 TBS	Li-Cor	927-65001
Intercept™ Blocking Buffer TBS	Li-Cor	927-60001
CellTrace™ CFSE	ThermoFisher	C34554
4x Laemmli Sample Buffer	BIO-RAD	1610747
Protease/Phosphatase Inhibitor (100x)	Cell Signaling	5872
Cell Lysis Buffer (10x)	Cell Signaling	9803
Murine OVA/H-$2K^b$ Tetramer	NIH	N/A
Murine OVA/I-A^b Tetramer	NIH	N/A

Zombie UV Fixable Viability Kit	BioLegend	423108
LIVE/DEAD Fixable Near-IR Dead Cell Stain Kit	ThermoFisher	L10119
Sucrose	Millipore-Sigma	1008921003
Xylene	ThermoFisher	95-47-6
Permount™ Mounting Medium	ThermoFisher	SP15-100

Table 2.3 List of commercial assays and kits used.

Commercial Assays/Kits	Source	Catalog Number
EasySep™ Mouse $CD8^+$ T Cell Isolation Kit	STEMCELL	19853A
FOXP3/Transcription Factor Staining Buffer Set	eBioscience	00-5523-00
CellEvent™ Caspase 3/7 Green Detection Reagent	ThermoFisher Scientific	C10423
Pierce™ BCA Protein Assay Kit	ThermoFisher	23227
Immobilon-FL PVDF	Millipore-Sigma	N/A
ELISA MAX™ Deluxe Set Mouse IFN-γ	BioLegend	430804
ELISA MAX™ Deluxe Set Mouse IL-2	BioLegend	431004

PureLink™ RNA mini kit	ThermoFisher	12183018A
Random Primers	ThermoFisher	48190011
Advanced qPCR Mastermix with SUPERGREEN™	Wisent	801-001-AR
Sirius Red/Fast Green Collagen Staining Kit	Chondrex, Inc.	9046

Table 2.4 List of software used for data analysis.

Software	**Source**	Catalog Number
FlowJo	FlowJo, LLC	N/A
GraphPad Prism 9	GraphPad Softwares	N/A
Image Studio Software	Li-Cor	N/A
ImageJ	ImageJ, NIH	N/A

Chapter 3: The role of obesity and INSR signalling on CD8$^+$ T cell-mediated anti-tumour immunity

3.1 Introduction

Obesity and associated IR predispose individuals to increased risk of multiple types of cancers, including breast, liver, pancreatic, and colorectal carcinoma[191]. In addition, obesity and IR worsen several aspects of cancer survivorship including diagnosis, quality of life, cancer recurrence, cancer progression and prognosis[156, 157]. Several mechanisms have been implicated in how obesity promotes tumour burden. Accumulating evidence has demonstrated suppressive effects of obesity on multiple immune cell types and anti-tumour immunity. Lipids in the obese environment can suppress cancer immunosurveillance. For instance, lipids suppress NK cell effector function, causing NK cells to have reduced capacity to kill tumour cells[192]. Lipid accumulation in DCs in tumours prevents them from properly cross-presenting antigens and activating T cells, which can impair CD8$^+$ cytotoxic T lymphocyte (CTL) responses[162]. In addition, lipid uptake in macrophages can drive lipolysis, and skew macrophages towards an immunosuppressive phenotype[167]. Increased lipid metabolism also promotes the differentiation of Tregs[168], which can work to suppress anti-cancer T cell responses. However, the underlying mechanism on how obesity impacts anti-tumour immune responses is unclear. CTLs are critical effectors in anti-cancer responses. CTLs can suppress tumour growth by direct killing of tumour cells through cytolytic mechanisms. Upon recognition of antigen in the context of MHC I, form an immunological synapse. Granzyme B (GZMB) is a serine protease can induce apoptosis in target cells through the activation of caspases[193], while Lysosomal-associated membrane protein-1 (LAMP-1 or CD107α) can be used to identify degranulation activity[194]. CTLs also secrete proinflammatory cytokines, such as IFNγ, IL-2 and TNFα, which can enhance anti-tumour immune responses[172]. However, in the context of a tumour, CTLs are found to become dysfunctional and acquire an exhausted phenotype over time. When exposed to chronic antigen stimulation, T cells enter a dysfunctional state called T cell exhaustion[141], characterized by a decrease in the expression of effector cytokines, but also an increase in expression of co-inhibitory receptors KLRG1, PD-1, LAG-3, and TIM-3[141, 142]. An increase in these co-inhibitory receptors and their interactions with their respective ligands lead to downregulation of TCR signalling, resulting in decreased T cell proliferation, cytokine production, and cytolytic function[143, 144, 145]. Ultimately, this impairs their ability to reduce tumour burden.

Immune cells including T cells express insulin receptors (INSR), and evidence suggests that they respond poorly to INSR signalling during obesity[175]. Previously, an important role of INSR signalling in T cell function has been observed, as T cells upregulate their surface expression of INSR upon activation, and impairment of INSR signalling reduces their proliferative capacity and production of effector molecules[171]. Therefore, this chapter aims to explore how obesity and IR affects $CD8^+$ T-cell mediated anti-tumour immunity, specifically focusing on the hypothesis that obesity impairs anti-tumour CTL differentiation and/or function through inducing T cell-intrinsic insulin resistance. Using an E.G7 subcutaneous tumour model, I demonstrate that obesity is associated with an increase in tumour growth, which is accompanied by impaired $CD8^+$ T cell anti-tumour responses. In addition, I observed similar findings in mice with T cell-specific *Insr* deletion ($LckCre^+$ $Insr^{fl/fl}$).

3.1.1 $LckCre^+$ $Insr^{fl/fl}$ Mouse Model

T cell-specific INSR conditional knockout mice ($LckCre^+$ $Insr^{fl/fl}$) via a Lymphocyte-specific protein tyrosine kinase (Lck) promoter-driven Cre recombinase transgene (LckCre) were generated by crossing C57BL/6 mice with an *Insr* transgene with an exon 4 flanked by *loxP* sites ($Insr^{fl/fl}$) with mice carrying the Cre recombinase transgene driven by the distal promoter of the *Lck* gene. The distal Lck promoter drives Cre-mediated recombination during late stages of T cell development, specifically at or after upregulation of the T cell receptor (TCR) during positive selection, and minimally affects thymocyte development[195].

3.2 Results

3.2.1 Obesity impairs antigen-specific $CD8^+$ T cell-mediated anti-tumour immunity

To explore the impact(s) of obesity on $CD8^+$ T cell anti-tumour immunity, I used a diet-induced obesity (DIO) model[189] in which 6-week old C57BL/6 male mice were fed a 60kcal% fat chow diet (HFD) for 16 weeks, compared to 10kcal% fat in normal chow diet (NCD) controls. First, I validated that the DIO model developed obesity and IR. To assess for IR, I conducted an ITT, which measures the response to exogenous insulin and is indicative of insulin sensitivity, followed by an IPGTT a week apart to measure glucose tolerance and the ability to produce and respond to endogenous insulin. Compared to the NCD-fed mice, HFD-fed mice

developed marked obesity, demonstrated by an increase in body weight **(Figure 3.1 A)**. HFD-fed mice also developed IR, as there was impaired insulin sensitivity shown in the ITT **(Figure 3.1 B, C)** compared to NCD-fed mice. In addition, IPGTT results showed that HFD-fed mice were glucose intolerant with greater glucose excursion, expressed as an integrated area under the curve (AUC) over the 120-minute period, further demonstrating IR **(Figure 3.1 D, E)**.

To assess how obesity impacted $CD8^+$ T cell-mediated anti-tumour immunity, $2x10^5$ OVA-expressing E.G7 tumour cells were subcutaneously injected into the right flank of NCD-fed or HFD-fed mice, and tumour growth was monitored every other day using a caliper. I used the E.G7 cell line, which is a clone of EL4 cells transfected with OVA^{181}, in order to increase tumour immunogenicity and have a way to effectively track tumour antigen-specific T cells. After 3-4 weeks of tumour growth, I examined T cell infiltration into tumours and investigated their functionality. Tumour antigen-specific $CD8^+$ T cells and $CD4^+$ T cells were identified as $OVA_{257-264}$ (SIINFEKL) K^b tetramer positive and $OVA_{329-337}$ (AAHAEINEA) I-A^b tetramer positive, respectively. These tetramers are made up of four MHC class I or class II molecules that are fluorescently conjugated, which present a OVA-derived peptide[196]. T cells that are specific to these antigens are thus detected by the tetramers and can be quantified via flow cytometry.

E.G7 tumours implanted in HFD-fed mice showed accelerated growth compared to tumours in NCD-fed controls **(Figure 3.2 A)**, and a trending increase in endpoint weight **(Figure 3.2 B)**. In addition, when measuring the dimensions after dissection of the tumours, the tumours from HFD-fed mice were also trending towards a larger volume than tumours from NCD-fed mice **(Figure 3.2 C)**. This was associated with a trending decrease in the proportion of $CD45^+$ cells in the tumour **(Figure 3.2 D)**. However, the E.G7 tumour cells also express CD45, and therefore future experiments will assess the proportion of TCR^+ cells instead of $CD45^+$ cells. Tumours of HFD-fed mice also showed a trending decrease in the proportion of $CD8^+$ T cells **(Figure 3.2 E)**, but no clear differences in the proportion of $CD4^+$ T cells **(Figure 3.2 F)**. In addition, there was a reduction in the proportion of OVA-specific $CD8^+$ T cells in the HFD-fed mice **(Figure 3.2 G, H)**. The mean fluorescence intensity (MFI) of $OVA_{257-264}$ K^b tetramer was also decreased on tumour infiltrating HFD $CD8^+$ T cells **(Figure 3.2 I)**, suggesting a decrease in

the expression of OVA-specific TCRs on these T cells, or the TCRs in HFD-fed mice have a lower affinity to the OVA peptide. There were similar proportions of OVA-specific $CD4^+$ T cells as measured by $OVA_{329-337}$ I-A^b tetramer staining within the tumour **(Figure 3.2 J)**, and when exploring the subsets of $CD4^+$ cells, I observed similar frequency of $FOXP3^+$ Tregs in OVA-specific $CD4^+$ T cells **(Figure 3.2 L)** and T-box expressed in T cells (T-bet)-expressing Th1 cells in HFD mice **(Figure 3.2 M)**. This implied that HFD-feeding does not alter the differentiation of T cells into Tregs and Th1 $CD4^+$ subsets within the tumour.

In the draining inguinal lymph node and spleen of the tumour-bearing HFD-fed mice, there was a decrease in the proportion of $CD3^+$ cells compared to NCD-fed mice, indicating a decrease in proportion of total T cells **(Figure 3.3 A, B)**. When looking at the frequencies of $CD4^+$ T cells and $CD8^+$ T cells, there was a small but significant decrease in the proportion of $CD8^+$ T cells only in the draining inguinal lymph nodes of HFD-fed mice **(Figure 3.3 C)**. The proportion of $CD4^+$ T cells in the draining inguinal lymph node and spleens were similar between NCD and HFD-fed mice **(Figure 3.3 E, F)**. There was a trending decrease in the proportion of OVA-specific $CD8^+$ T cells in the lymph node only **(Figure 3.3 G)**, which could be contributing to the decreased levels of OVA-specific $CD8^+$ T cells observed in the tumours. However, OVA-specific $CD4^+$ T cells in the draining lymph node and spleens were similar between NCD and HFD-fed mice **(Figure 3.3 I, J)**. Altogether, these data demonstrate that obesity leads to accelerated tumour growth, which may be in part due to decreases in the proportion of infiltrating OVA-specific $CD8^+$ T cells.

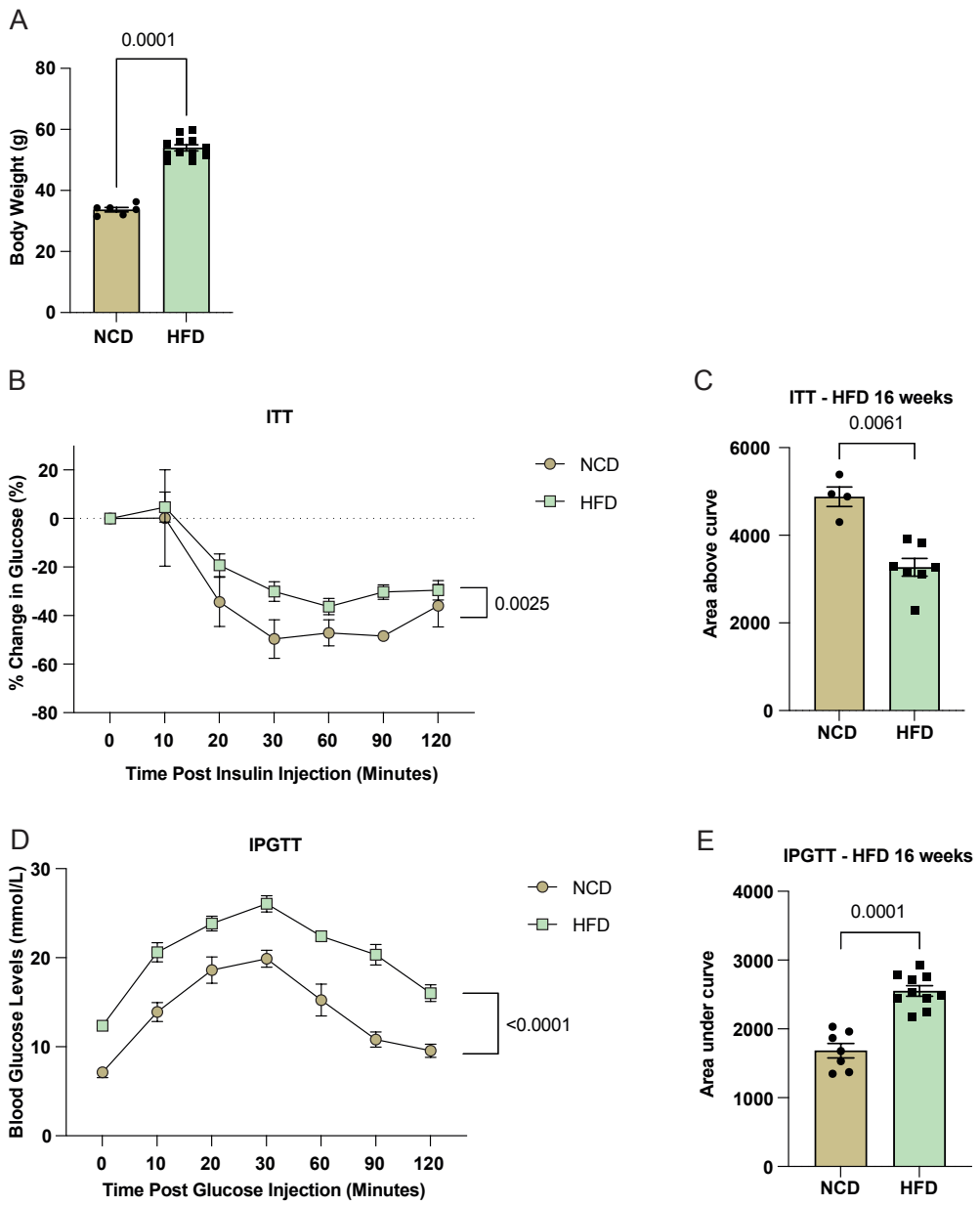

Figure 3.1 Diet induced obesity induces insulin resistance in mice. (A) Body weight of male C57BL/6 mice after 16 weeks of 10kcal% fat chow diet (NCD) or 60kcal% fat chow diet (HFD) (n=6-12). **(B)** Glucose excursion during an ITT. Blood glucose is expressed as a percent change in blood glucose from time point 0. **(C)** Integrated area above the curve (AAC) during an ITT (n=4-7). **(D)** Glucose excursion during an IPGTT. **(E)** Integrated area under the curve (AUC) of glucose excursion during a 120-min IPGTT (n=7-10). P-values are calculated using Mann-Whitney U test. Data are represented as mean ± SEM.

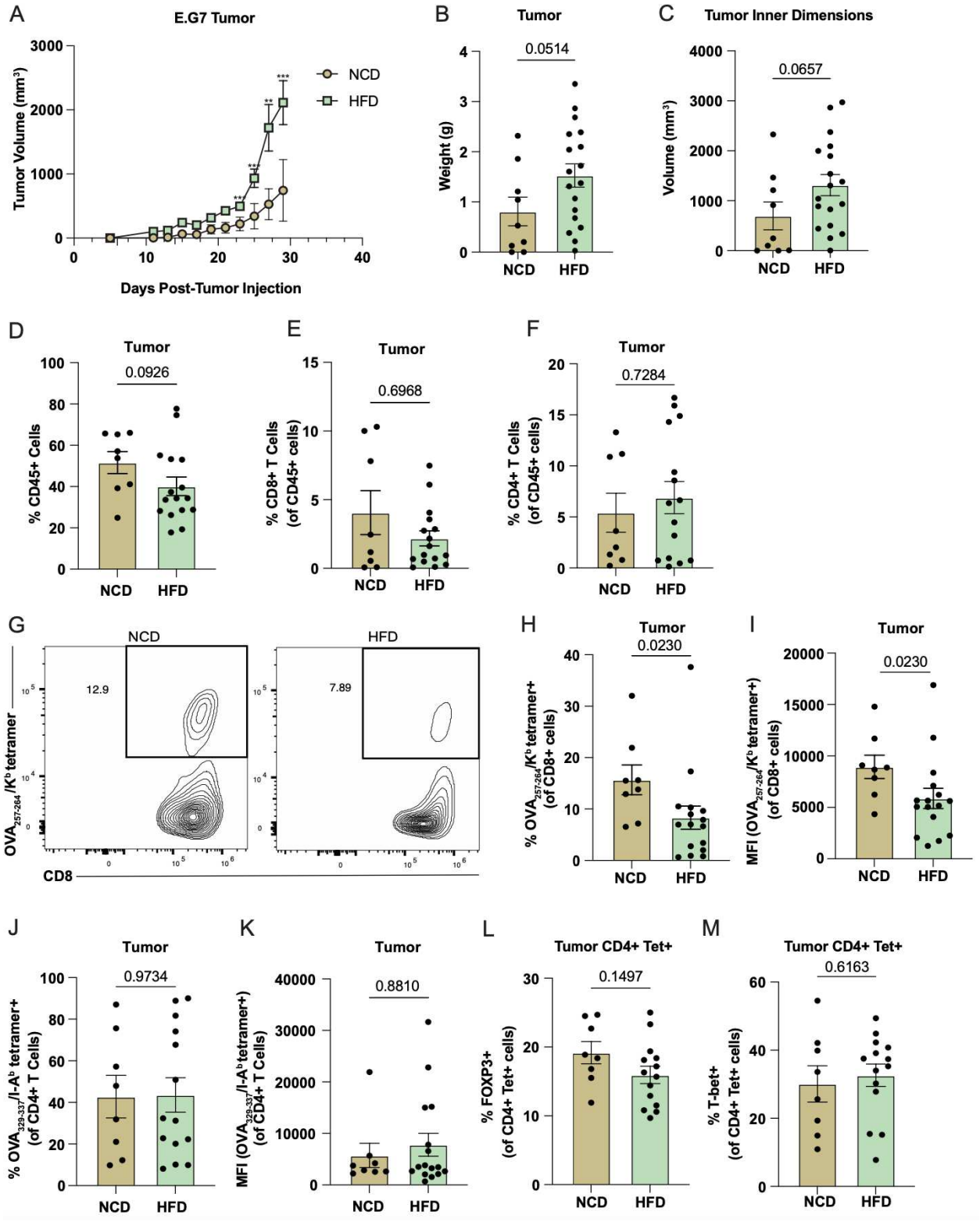
A
E.G7 Tumor
Tumor Volume (mm³)
Days Post-Tumor Injection
NCD
HFD
B
Tumor
0.0514
Weight (g)
C
Tumor Inner Dimensions
0.0657
Volume (mm³)
D
Tumor
0.0926
% CD45+ Cells
E
Tumor
0.6968
% CD8+ T Cells (of CD45+ cells)
F
Tumor
0.7284
% CD4+ T Cells (of CD45+ cells)
G
NCD
HFD
12.9
7.89
OVA257-264/Kb tetramer
CD8
H
Tumor
0.0230
% OVA257-264/Kb tetramer+ (of CD8+ cells)
I
Tumor
0.0230
MFI (OVA257-264/Kb tetramer+) (of CD8+ cells)
J
Tumor
0.9734
% OVA329-337/I-Ab tetramer+ (of CD4+ T Cells)
K
Tumor
0.8810
MFI (OVA329-337/I-Ab tetramer+) (of CD4+ T Cells)
L
Tumor CD4+ Tet+
0.1497
% FOXP3+ (of CD4+ Tet+ cells)
M
Tumor CD4+ Tet+
0.6163
% T-bet+ (of CD4+ Tet+ cells)

Figure 3.2 Diet-induced obesity accelerates tumour growth. C57BL/6 mice were fed a HFD (n=18) or a NCD (n=8) for 16 weeks, and $2x10^5$ E.G7 tumour cells were injected subcutaneously. Graphs show data points from two pooled experiments. **(A)** Tumour growth curves of NCD or HFD-fed C57BL/6 mice. **(B)** Tumour weights after 28 days of growth. **(C)** Tumour volume on day 28 after dissection. (**D-M)** Tumours from NCD (n=8) or HFD (n=16) mice in C were dissected, and immune cell infiltration was analyzed by flow cytometry. Frequency of $CD45^+$ cells **(D),** $CD8^+$ T cells **(E),** and $CD4^+$ T cells **(F)** in tumours. **(G)** Representative flow cytometry plots of $OVA_{257-264}/K^b$ $tetramer^+$ gating on $CD8^+$ T cells. **(H)** Frequency of $OVA_{257-264}/K^b$ $tetramer^+$ $CD8^+$ T cells. **(I)** MFI of $OVA_{257-264}/K^b$ tetramer on $CD8^+$ T cells. **(J)** Frequency of $OVA_{329-337}$/I-A^b $tetramer^+$ $CD4^+$ T cells. **(K)** MFI of $OVA_{329-337}$/I-A^b tetramer on $CD4^+$ T cells. Frequency of $FOXP3^+$ **(L)** and T-bet^+ (**M)** OVA-specific $CD4^+$ T cells. P-values for the tumour growth curve are calculated using two-way ANOVA. P-values for bar graphs are calculated using Mann-Whitney U test. Data are shown as individual mice (dots) and mean ± SEM.

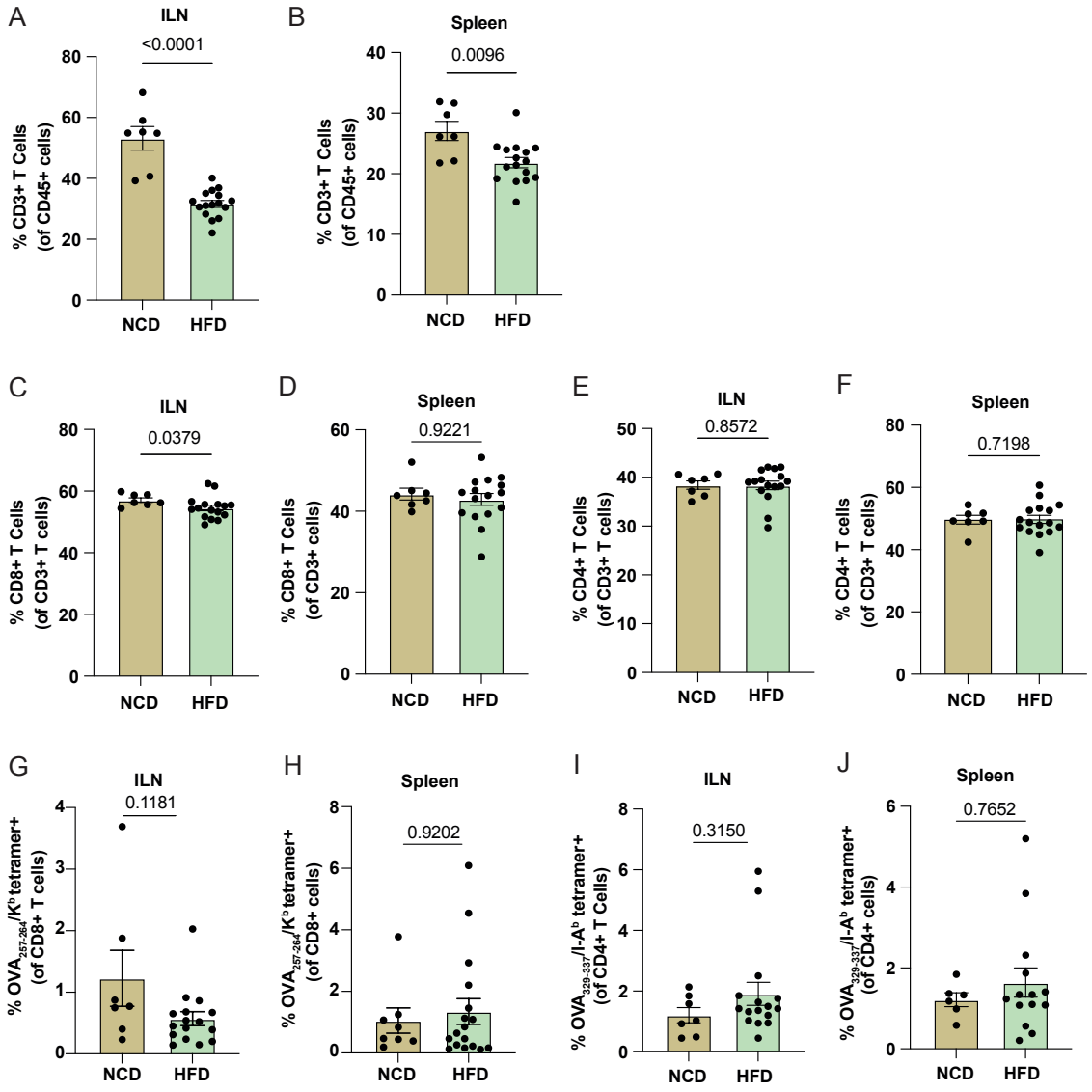

Figure 3.3 Diet-induced obesity decreases the frequency of T cells in the inguinal lymph node and spleen of tumour-bearing mice. Tumour-draining inguinal lymph nodes (ILN) and spleens from tumour-bearing NCD (n=8) or HFD (n=16) mice were dissected, and immune cell infiltration was analyzed by flow cytometry. Graphs show data points from two pooled experiments. Frequency of $CD3^+$ cells in the ILN **(A)** and spleen **(B)**. Frequency of $CD8^+$ T cells in the ILN **(C)** and spleen **(D)**. Frequency of CD4+ T cells in the ILN **(E)** and spleen **(F)**. Frequency of $OVA_{257\text{-}264}/K^b$ tetramer$^+$ (Tet^+) $CD8^+$ T cells in the ILN **(G)** and spleen **(H)**. Frequency of $OVA_{329\text{-}337}$/I-A^b tetramer$^+$ $CD4^+$ T cells in the ILN **(I)** and spleen **(J)**. P-values are calculated using Mann-Whitney U test. Data are shown as individual mice (dots) and mean ± SEM.

3.2.2 Obesity impairs CD8$^+$ T cell-mediated anti-tumour function

Further characterization of tumour infiltrating antigen-specific CD8$^+$ T cells showed that TILs in HFD-fed mice had similar levels of activation as measured by CD69 expression **(Figure 3.4 A)**, which appears on the surface of T cells following stimulation of the TCR[197]. As part of the anti-tumour response, cytokines such as IFNγ are released by CD4$^+$ T cells and CD8$^+$ T cells to mediate inflammatory responses. IFNγ is a pro-inflammatory cytokine produced by CTLs that is important for initiating apoptosis in tumour cells[198]. IFNγ produced by CD4$^+$ T cells and CTLs can also act on neighboring immune cells to enhance anti-tumour responses, such as promoting macrophage polarization to a pro-inflammatory phenotype[199], and can induce expression of MHC class I and class II molecules by APCs for presentation of tumour antigens to T cells[200]. To assess cytokine production and effector function by CD4$^+$ and CD8$^+$ T cells, cells from dissociated tumour were stimulated for 5 hours with PMA and ionomycin with brefeldin A prior to intracellular staining. After PMA and ionomycin stimulation, there was a decrease in the proportion of IFNγ$^+$ CD8$^+$ T cells, and decreased MFI of IFNγ in CD8$^+$ T cells from HFD-fed mice **(Figure 3.4 B-D)**. In addition to cytokine production, CTLs mediate anti-tumour responses through the production of cytolytic molecules. Intratumoural CD8$^+$ T cells from HFD-fed mice also demonstrated a trending decrease in expression of the cytolytic molecule GZMB **(Figure 3.4 E)** and CD107α **(Figure 3.4 F)**. This suggests that HFD feeding reduces CD8$^+$ T cell functionality, and impairs their anti-tumour response. In addition, intratumoural CD4$^+$ T cells showed decreased MFI of IFNγ **(Figure 3.4 G)**, suggesting that HFD also impairs CD4$^+$ T cell responses. This decrease in the expression of IFNγ in CD4$^+$ T cells may be impacting the response of CD8$^+$ T cells, as IFNγ produced by CD4$^+$ Th1 cells can promote the activation and function of CD8$^+$ cytotoxic T cells[201].

To investigate what could be mediating the decrease in effector function, I looked at markers for T cell exhaustion. Tumour infiltrating CD8$^+$ T cells in HFD-fed mice exhibited an increase in the expression of KLRG1 **(Figure 3.4 H)**, a co-inhibitory receptor and marker for senescence in T cells[142]. However, there was no difference in the expression of exhaustion markers PD-1 **(Figure 3.4 I)**, TIM-3 **(Figure 3.4 J)**, and LAG-3 **(Figure 3.4 K)**. Overall, this suggests that HFD does not significantly affect intratumoural CD8$^+$ T cells levels of exhaustion,

and the functional defects observed in $CD8^+$ T cells in the tumours of obese mice are not a result of increased co-inhibitory receptor expression.

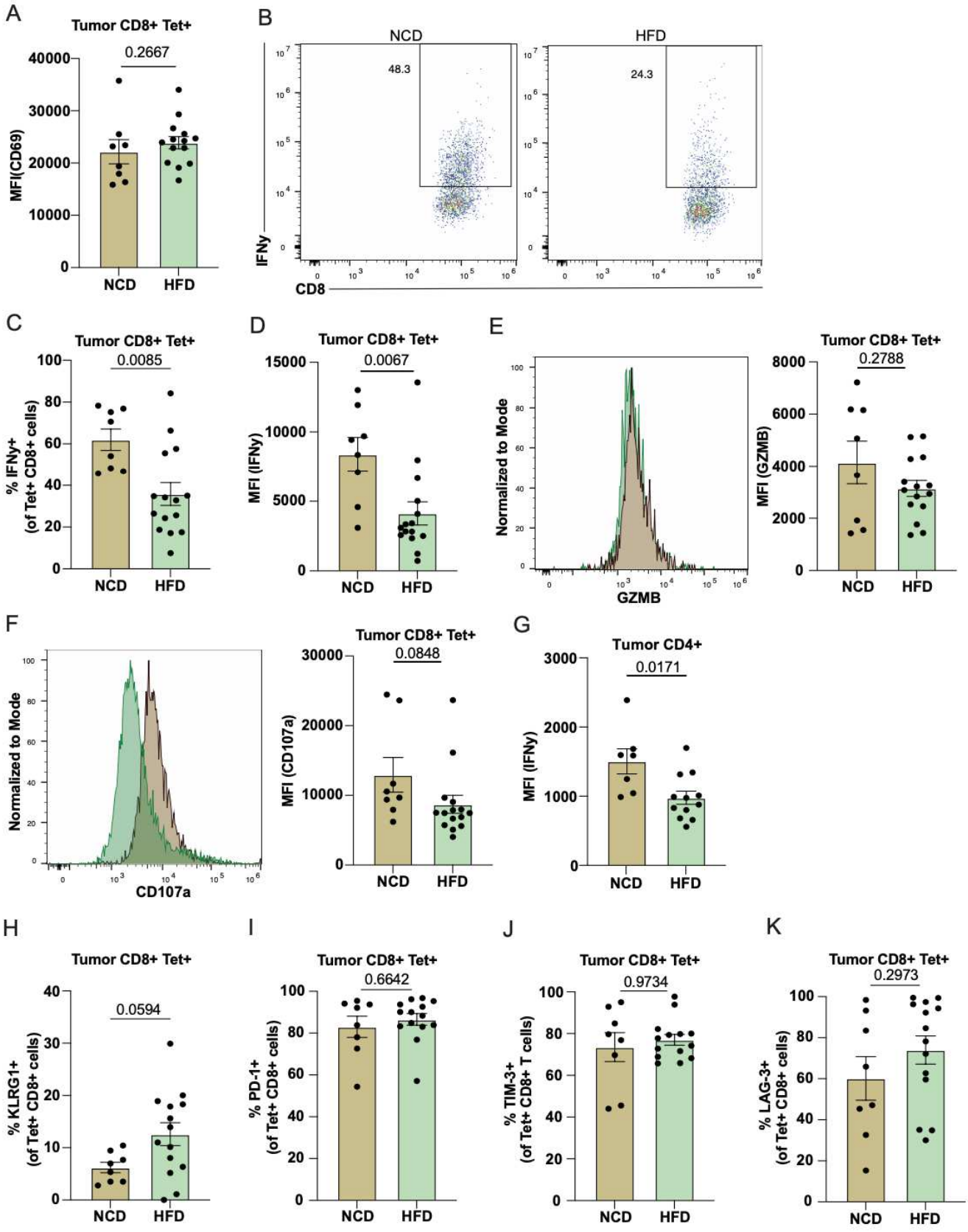
A
Tumor CD8+ Tet+
0.2667
MFI(CD69)
40000
30000
20000
10000
0
NCD
HFD
B
NCD
HFD
48.3
24.3
IFNy
CD8
C
Tumor CD8+ Tet+
0.0085
% IFNy+ (of Tet+ CD8+ cells)
100
80
60
40
20
0
NCD
HFD
D
Tumor CD8+ Tet+
0.0067
MFI (IFNy)
15000
10000
5000
0
NCD
HFD
E
Normalized to Mode
GZMB
Tumor CD8+ Tet+
0.2788
MFI (GZMB)
8000
6000
4000
2000
0
NCD
HFD
F
Normalized to Mode
CD107a
Tumor CD8+ Tet+
0.0848
MFI (CD107a)
30000
20000
10000
0
NCD
HFD
G
Tumor CD4+
0.0171
MFI (IFNy)
3000
2000
1000
0
NCD
HFD
H
Tumor CD8+ Tet+
0.0594
% KLRG1+ (of Tet+ CD8+ cells)
40
30
20
10
0
NCD
HFD
I
Tumor CD8+ Tet+
0.6642
% PD-1+ (of Tet+ CD8+ cells)
100
80
60
40
20
0
NCD
HFD
J
Tumor CD8+ Tet+
0.9734
% TIM-3+ (of Tet+ CD8+ T cells)
100
80
60
40
20
0
NCD
HFD
K
Tumor CD8+ Tet+
0.2973
% LAG-3+ (of Tet+ CD8+ cells)
100
80
60
40
20
0
NCD
HFD

Figure 3.4 Diet-induced obesity impairs $CD8^+$ T cell-mediated anti-tumour function in tumours independent of exhaustion marker expression. (A, H-K) Unstimulated cells from dissociated E.G7 tumours from NCD (n=8) or HFD (n=16) mice 28 days post-implantation (as in Figure 3.2 D-M) were stained with markers of activation or exhaustion markers. Graphs show data points from two pooled experiments. **(B-G)** Cells from dissociated tumours were stimulated with PMA/ionomycin with brefeldin A for 5 hours prior to intracellular staining of IFNγ and GZMB. Fluorescently conjugated anti-CD107α antibodies were added at the beginning of the stimulation. **(A)** MFI of CD69 in $OVA_{257-264}/K^b$ tetramer$^+$ (Tet^+) $CD8^+$ T cells. **(B)** Representative flow cytometry plots of IFNγ staining in $CD8^+$ Tet^+ T cells. **(C)** Frequency of IFNγ+ $CD8^+$ Tet^+ T cells. **(D)** MFI of IFNγ of $CD8^+$ Tet^+ T cells. Representative histogram and MFI of GZMB **(E)** and CD107α **(F)** of $CD8^+$ Tet^+ T cells. **(G)** MFI of IFNγ of $CD4^+$ T cells. Frequency of $CD8^+$ Tet^+ T cells expressing KLRG1 **(H)**, PD-1 **(I)**, TIM-3 **(J)**, and LAG-3 **(K)**. P-values are calculated using Mann-Whitney U test. Data are shown as individual mice (dots) and mean ± SEM.

3.2.3 CD8$^+$ T cells from HFD-fed mice show a trend of increased tumour killing capacity in vitro but decreased ability to eliminate tumours in vivo

To determine whether systemic metabolic, inflammatory and nutrient changes caused by obesity reprogram T cells intrinsically to impair their function and ability to kill tumours, I performed an in vitro killing assay where OT-I T cells from either NCD-fed or HFD-fed transgenic OT-I mice were co-cultured with MC38-OVA tumour cells. I measured the tumour killing capacity of the OT-I CD8$^+$ T cells at 24 hours via LIVE/DEAD (LD) and caspase 3/7 staining. In cells with compromised membranes, the LD dye reacts with free amines in the cell interior and cell surface, indicating dead cells. The caspase 3/7 detection reagent is intrinsically non-fluorescent, but becomes fluorescent upon activation of caspase 3/7 in apoptotic cells[202]. In addition to tumour killing capacity, I assessed levels of activation and IFNγ and GZMB production after 48 hours. Prior to co-culturing, I assessed baseline activation levels. The purified CD8$^+$ T cells from HFD-fed mice showed higher MFI of CD69, indicating increased activation **(Figure 3.5 A)**. Interestingly, the HFD OT-I T cells were more effective at killing tumour cells in vitro **(Figure 3.5 B, C)**, and showed a trending increase in the expression of the activation marker CD69 after 24 hours of co-culture **(Figure 3.5 D).** In accordance with the increased killing capacity, OT-I T cells from HFD-fed mice also had higher MFI of IFNγ and GZMB compared to NCD OT-I T cells after 48 hours of co-culture with tumour cells **(Figure 3.5 E, F)**. This suggested that decreases in CD8$^+$ T cell activation and impaired function may be specific to the HFD tumour microenvironment in vivo compared to NCD tumours. Baseline measurements of activation of purified cells indicated that there were higher levels of CD69 expression prior to co-culture **(Figure 3.5 A)**, which may be contributing to the increased tumour killing in vitro. In addition, I purified bulk CD8$^+$ T cells for this assay, which includes naive, effector and memory T cells. Therefore, there may be differences in the proportion of subsets in NCD and HFD mice, and can impact the amount of tumour killing and IFNγ-producing T cells, but will need to be confirmed in future experiments.

Because in vitro experiments do not reflect physiological conditions, I also assessed whether obesity reprograms T cells intrinsically to impair their function T cells using an adoptive transfer model to compare OT-I CD8$^+$ T cells from NCD and HFD-fed mice. I injected 8-12 week old male CD45.1 congenic mice with 2x10^5 E.G7 tumour cells subcutaneously. After approximately 7-9 days post tumour injection when tumours were palpable, I isolated OT-I CD8$^+$

T cells from the spleen and lymph nodes of OT-I transgenic mice with a CD45.2 background fed either NCD or HFD. I differentiated these cells into CTLs by co-culturing them with $OVA_{257-264}$ peptide and IL-2 for 3 days, and injected $2x10^6$ CTLs intravenously. Tumour growth was monitored for 2 weeks, and the tumours were processed at the end of 2 weeks to assess for T cell infiltration and function.

Mice that were injected with CTLs from NCD-fed mice showed decreased tumour growth compared to mice injected with HFD CTLs **(Figure 3.6 A)**. This was associated with a trending decrease in the proportion of adoptively transferred $CD45.2^+$ T cells within the tumour **(Figure 3.6 B)**. As E.G7 tumour cells can also express CD45.2, future experiments should assess the proportion of TCR^+ $CD45.2^+$ as a marker for adoptively transferred T cells. The intratumoural $CD45.2^+$ $CD8^+$ T cells from HFD-fed mice also showed decreased activation, as measured by CD69 expression **(Figure 3.6 C)**. After stimulation with PMA and ionomycin for 5 hours, there was a trending reduction in the MFI of IFNγ in the intratumoural HFD CTLs compared to the NCD CTLs **(Figure 3.6 D)**, but no difference in GZMB **(Figure 3.6 E)**. There was a similar proportion of adoptively transferred T cells expressing PD-1 which may indicate similar levels of exhaustion **(Figure 3.6 F)**. Altogether, these findings demonstrate that CTLs from HFD-fed mice have impaired tumour killing capacity in vivo, and is associated with decreased production of IFNγ. This is in contrast to the results seen in vitro, where OT-I T cells from HFD-fed mice demonstrated increased ability to kill tumour cells after co-culturing for 24 hours. This suggests that obesity can lead to long-term intrinsic effects on T cells, as the OT-I T cells from HFD-fed mice showed impaired ability to decrease tumour size in vivo.

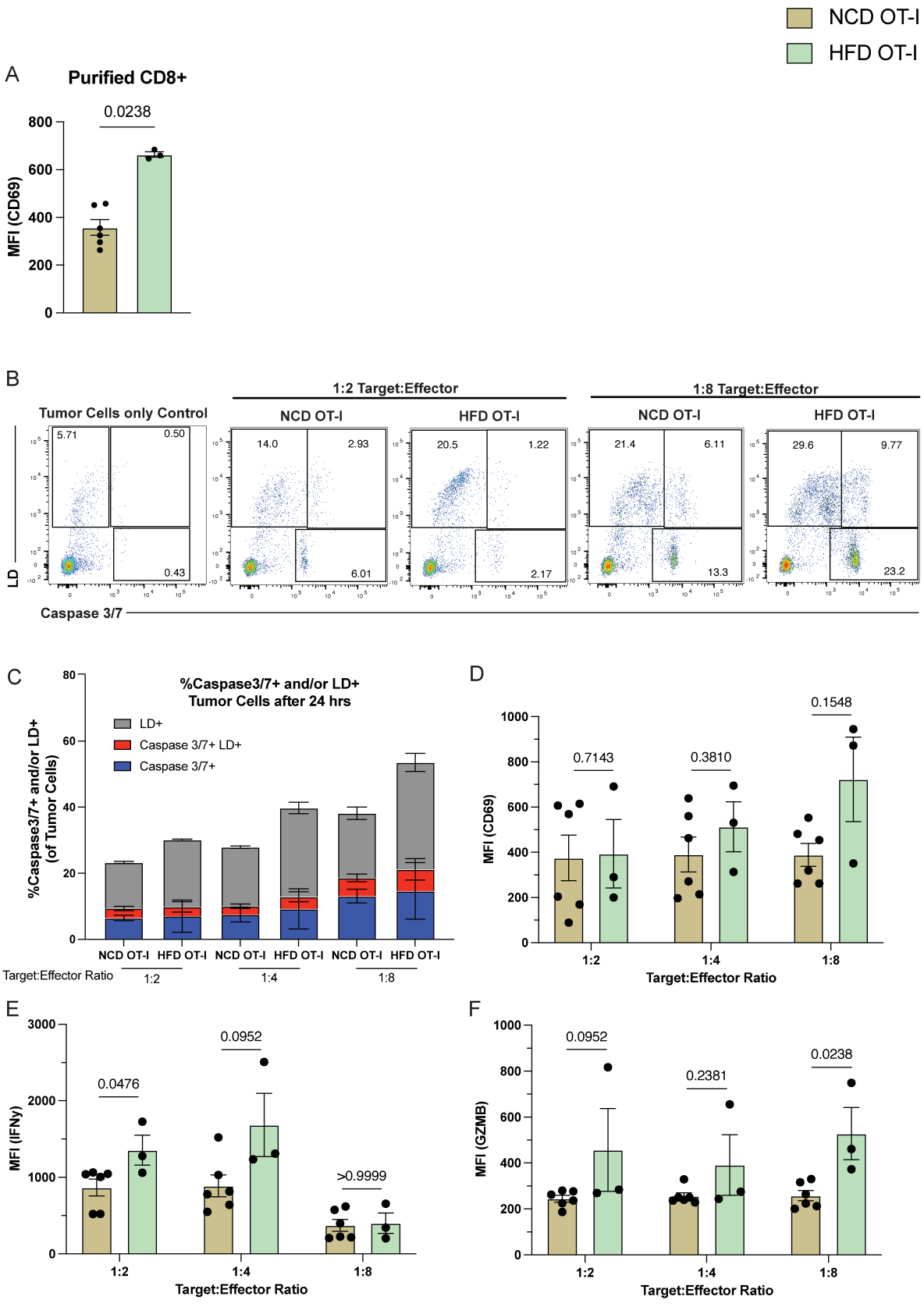
NCD OT-I
HFD OT-I
A
Purified CD8+
0.0238
MFI (CD69)
800
600
400
200
0
B
1:2 Target:Effector
1:8 Target:Effector
Tumor Cells only Control
NCD OT-I
HFD OT-I
NCD OT-I
HFD OT-I
5.71
0.50
0.43
14.0
2.93
6.01
20.5
1.22
2.17
21.4
6.11
13.3
29.6
9.77
23.2
LD
Caspase 3/7
C
%Caspase3/7+ and/or LD+
Tumor Cells after 24 hrs
LD+
Caspase 3/7+ LD+
Caspase 3/7+
%Caspase3/7+ and/or LD+
(of Tumor Cells)
80
60
40
20
0
NCD OT-I
HFD OT-I
NCD OT-I
HFD OT-I
NCD OT-I
HFD OT-I
Target:Effector Ratio
1:2
1:4
1:8
D
0.7143
0.3810
0.1548
MFI (CD69)
1000
800
600
400
200
0
1:2
1:4
1:8
Target:Effector Ratio
E
0.0476
0.0952
>0.9999
MFI (IFNγ)
3000
2000
1000
0
1:2
1:4
1:8
Target:Effector Ratio
F
0.0952
0.2381
0.0238
MFI (GZMB)
1000
800
600
400
200
0
1:2
1:4
1:8
Target:Effector Ratio

Figure 3.5 $CD8^+$ T cells from HFD-fed mice show a trend of increased tumour killing capacity in vitro. OT-I T cells from either NCD-fed (n=6) or HFD-fed (n=3) transgenic OT-I mice were co-cultured with MC38-OVA tumour cells at target:effector ratios of 1:2, 1:4, and 1:8. Tumour killing by the OT-I $CD8^+$ T cells at 24 hours was measured via LIVE/DEAD (LD) and caspase 3/7 staining. Graphs show data points from one experiment. **(A)** MFI of CD69 in purified OT-I T cells prior to co-culturing. **(B)** Representative flow cytometry plots of LD and caspase 3/7 staining gated on tumour cells ($CD8^-$ cells). **(C)** Piled graphs showing frequency of caspase $3/7^+$ (blue), caspase $3/7^+$ LD^+ (red), and LD+ tumour cells after co-culture with OT-I T cells. (D) MFI of CD69 of OT-I T cells after 24 hours of co-culture. MFI of IFNγ **(E)** and GZMB **(F)** of OT-I T cells after 48 hours of co-culture. P-values are calculated using Mann-Whitney U test. Data are shown as individual mice (dots) and mean ± SEM.

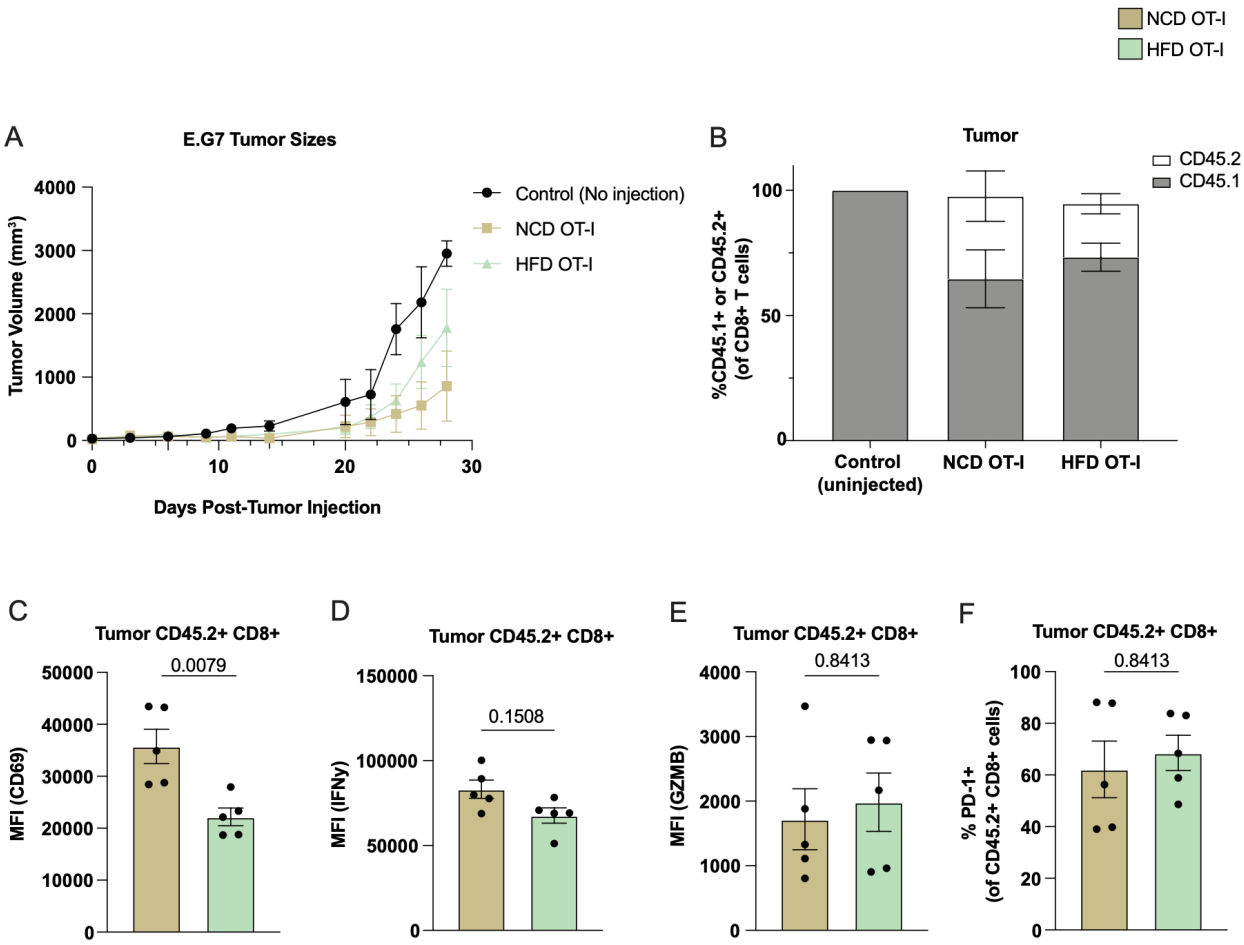

Figure 3.6 Adoptively transferred CTLs from HFD-fed mice have decreased tumour killing capacity in vivo. 8-12 week old male CD45.1 C57BL/6 congenic mice were injected with $2x10^5$ E.G7 tumour cells subcutaneously. After approximately 7-9 days post tumour injection when tumours were palpable, OT-I $CD8^+$ T cells were isolated from the spleen and lymph nodes of NCD or HFD-fed OT-I transgenic mice with a CD45.2 background, and differentiated into CTLs. $2x10^6$ CTLs were injected intravenously into the tumour-bearing mice. Graphs show data points from one experiment. **(A)** Tumour growth curves of CD45.1 C57BL/6 mice injected with no cells (n=3), NCD OT-I T cells (n=5), or HFD OT-I T cells (n=5). **(B)** Frequency of $CD45.2^+$ T cells in tumours from A after 28 days of growth. MFI of CD69 **(C)**, IFNγ **(D)**, and GZMB **(E)** of $CD45.2^+$ $CD8^+$ T cells. (F) Frequency of PD-1^+ $CD45.2^+$ T cells in the tumour. P-values are calculated using Mann-Whitney U test. Data are shown as individual mice (dots) and mean ± SEM.

3.2.4 CD8$^+$ T cells from obese and lean mice show similar levels of proliferation

As I observed a decrease in the proportion of CD8$^+$ T cells within the tumour of HFD-fed mice, I wanted to investigate whether this was due to differences in their proliferation. To measure differences in their ability to proliferate, OT-I T cells from NCD-fed and HFD-fed mice were stained with CFSE and co-cultured with OVA-peptide pulsed DCs at various concentrations, and levels of CFSE staining were measured using flow cytometry after 48 hours. NCD OT-I T cell proliferation was comparable to HFD OT-I T cell proliferation across the different peptide concentrations **(Figure 3.7 A, B)**. Supernatants were also collected from the co-cultures of OVA-pulsed DCs and NCD or HFD OT-I T cells, and levels of IFNγ and IL-2 were measured via enzyme-linked immunosorbent assay (ELISA) to further assess T cell functionality. IFNγ levels in the supernatants were similar **(Figure 3.7 C)**, while levels of IL-2 showed a trending decrease in the supernatants of HFD OT-I T cells at lower OVA concentrations **(Figure 3.7 D)**. Altogether, this suggested that HFD-feeding does not affect proliferation of T cells in vitro, but additional experiments with increased sample size will be required to confirm this.

Prior to tumour infiltration, T cells get primed in draining lymph nodes and undergo clonal expansion in response to recognition of their cognate antigen[203]. To determine whether the differences in frequency of CD8$^+$ T cells within the tumour were due to increased proliferation in a more physiological context**,** I subcutaneously injected 2x10^5 E.G7-OVA tumour cells into 8-12 week old male CD45.1 tumour bearing hosts. Once tumours were palpable approximately 7-9 days post-injection, I isolated and labelled OT-I CD8$^+$ T cells from CD45.2 congenic OT-I transgenic mice fed either NCD or HFD with CFSE. 3 days post-injection with CFSE-labelled T cells, I euthanized the mice and measured levels of proliferation of the adoptively transferred T cells in the draining inguinal lymph node and spleen, and measured infiltration of CD45.2$^+$ cells into the tumours. There were similar levels of proliferation of T cells from HFD-fed mice in the draining inguinal lymph node compared to the NCD OT-I T cells **(Figure 3.7 E, F)**. Also, there was no significant difference in the infiltration of CD45.2$^+$ T cells in the tumour of these mice at this time point **(Figure 3.7 G)**, suggesting that differences in proportion of TILs observed in the previous experiment may require additional time. Overall, obesity does not appear to be altering levels of proliferation in CD8$^+$ T cells in vitro and in vivo.

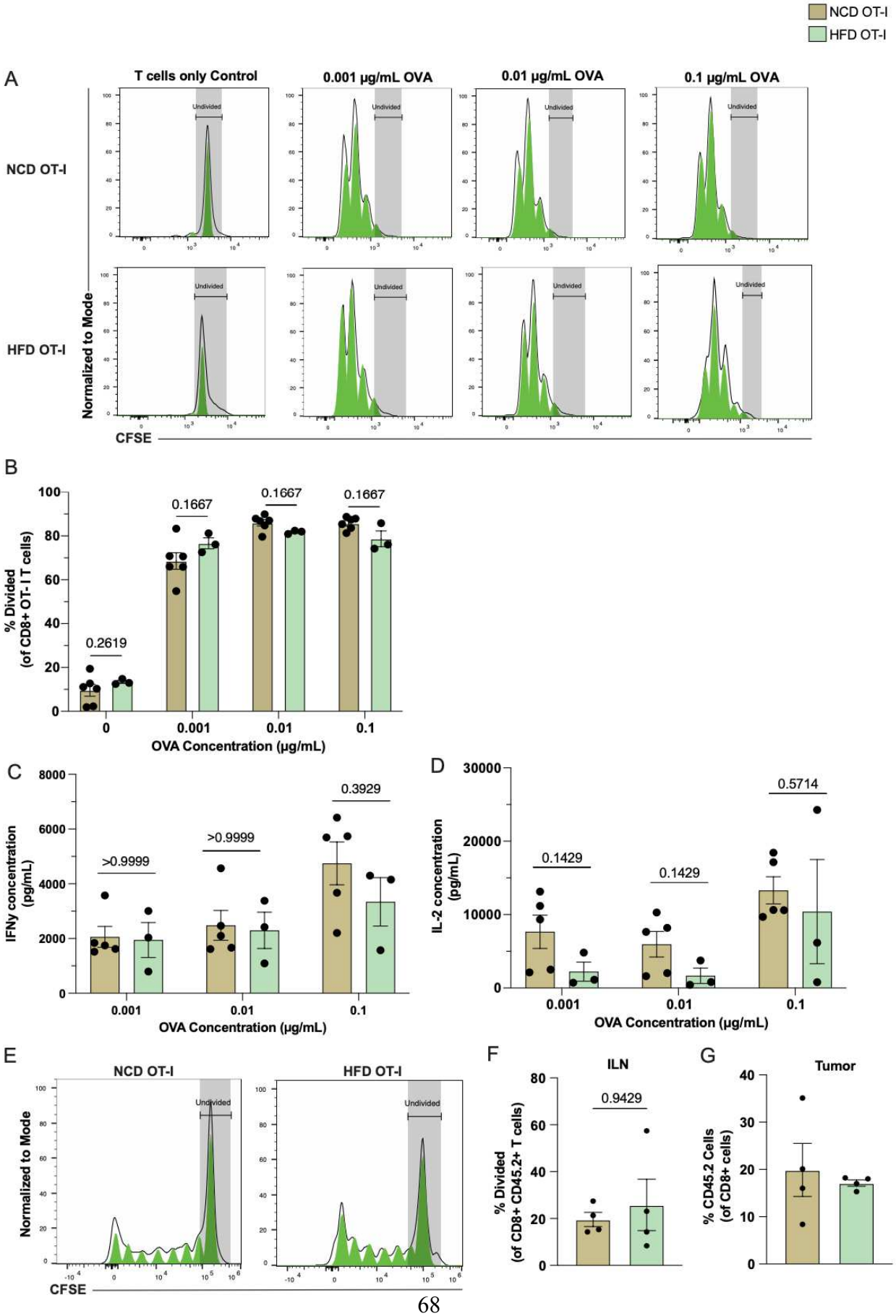
NCD OT-I
HFD OT-I
A
T cells only Control
0.001 µg/mL OVA
0.01 µg/mL OVA
0.1 µg/mL OVA
NCD OT-I
HFD OT-I
Normalized to Mode
CFSE
Undivided
B
% Divided (of CD8+ OT-I T cells)
0.2619
0.1667
0.1667
0.1667
OVA Concentration (µg/mL)
C
IFNγ concentration (pg/mL)
>0.9999
>0.9999
0.3929
OVA Concentration (µg/mL)
D
IL-2 concentration (pg/mL)
0.1429
0.1429
0.5714
OVA Concentration (µg/mL)
E
NCD OT-I
HFD OT-I
Normalized to Mode
CFSE
F
ILN
% Divided (of CD8+ CD45.2+ T cells)
0.9429
G
Tumor
% CD45.2 Cells (of CD8+ cells)

Figure 3.7 $CD8^+$ T cells from obese and lean mice show similar levels of proliferation. (A-D) OT-I T cells from NCD-fed (n=6) and HFD-fed (n=3) mice were stained with CFSE and co-cultured with OVA-peptide pulsed DCs at various concentrations. Levels of CFSE staining were measured via flow cytometry after 48 hours. Supernatants were also collected from the co-cultures of OVA-pulsed DCs and NCD or HFD OT-I T cells. Graphs show data points from one experiment. **(A)** Representative histograms of NCD OT-I T cell proliferation (top row) and HFD OT-I T cell proliferation (bottom row). **(B)** Percentage of OT-I T cells divided. Concentration of IFNγ **(C)** and IL-2 **(D)** in supernatants of co-cultures. **(E-G)** 8-12 week old male CD45.1 C57BL/6 congenic mice were injected with $2x10^5$ E.G7 tumour cells subcutaneously. After 7-9 days post tumour injection, I isolated and labelled OT-I $CD8^+$ T cells from CD45.2 congenic OT-I transgenic mice fed either NCD (n=4) or HFD (n=4) with CFSE. 3 days post-injection with CFSE-labelled T cells, mice were euthanized and levels of proliferation of the adoptively transferred T cells in the draining inguinal lymph node and infiltration of $CD45.2^+$ cells in the tumour were measured. **(E)** Representative histograms of OT-I T cell proliferation. **(F)** Percentage of OT-I T cells divided. **(G)** Frequency of $CD45.2^+$ $CD8^+$ T cells in tumours. P-values are calculated using Mann-Whitney U test. Data are shown as individual mice (dots) and mean ± SEM.

3.2.5 Obesity impairs insulin signalling in T cells

As we demonstrated that HFD impairs anti-tumour immunity, we wanted to explore mechanistically how it could be impairing $CD8^+$ T cells. One notable alteration that occurs during obesity is hyperinsulinemia, which contributes to decreased sensitivity to insulin, and an impairment of insulin signalling[204]. Immune cells, including T cells, express insulin receptors[171], and evidence suggests that obesity induces IR intrinsic to immune cells[175]. Previous work has demonstrated that INSR signalling is important for T cell proliferation, activation, and function[171]. As obesity is strongly associated with insulin resistance, and insulin signalling is critical for optimal T cell function, we wanted to explore the hypothesis that obesity impairs anti-tumour immunity via inducing T cell intrinsic insulin resistance. First, we needed to establish whether obesity would affect insulin signalling in T cells. T cells were isolated from the spleen of NCD and HFD-fed mice and activated with anti-CD3/CD28, as T cells at steady-state do not express insulin receptors, but increase their expression upon activation[171]. In addition, the purified T cells were stimulated with or without the addition of insulin. After 48 hours, levels of Ser473 phosphorylated AKT were measured via western blot to assess insulin signalling, as AKT becomes phosphorylated on Thr308 and Ser473 residues upon activation of the insulin signalling pathway[205]. Without the addition of insulin, there were comparable levels of phosphorylated AKT **(Figure 3.8 A, B)**. However, once insulin was added, T cells from NCD-fed mice showed an increase in phosphorylated levels of AKT relative to total AKT levels, while there was no significant increase in phosphorylated AKT in T cells from HFD-fed mice **(Figure 3.8 A, B)**. This demonstrated that T cells from HFD-fed mice had impaired response to insulin and decreased insulin signalling.

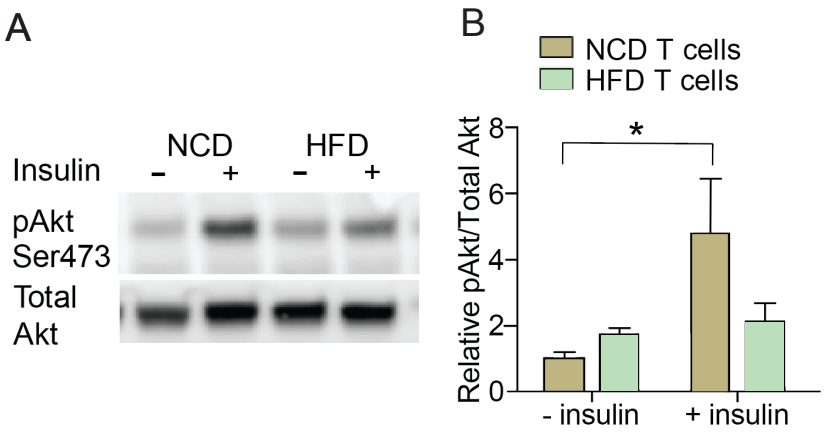

Figure 3.8 Obesity impairs insulin signalling in T cells. Western blotting for Ser473 phosphorylation of AKT in anti-CD3/CD28-activated T cells isolated from HFD or NCD-fed mice. **(A)** Western blot of phospho-AKT1 (Ser473) and total AKT (n=4). **(B)** Quantified phospho-AKT (Ser473) bands from blot normalized to total AKT. 20 μg of proteins were loaded per column for Western blotting. Quantification of protein bands was completed using the Li-Cor Image Studio Acquisition Software. P-values are calculated using Mann-Whitney U test. Data are shown as mean ± SEM.

3.2.6 INSR-deficient T cells have impaired anti-tumour immunity

We observed that obesity impaired insulin signalling in T cells, and previous studies report that INSR signalling is important for T cell activation as well as effector function[171]. However, the importance of INSR in T cells in anti-tumour immune function is unknown. Therefore, we hypothesized that INSR signalling is important in T cell-mediated anti-tumour responses, and deleting INSR would lead to increased tumour growth. To investigate the role of INSR in T-cell mediated anti-tumour immunity, I used a T cell-specific *Insr*-floxed (LckCre^{+} *Insr*$^{fl/fl}$) mouse model. These mice contain a Cre-recombinase gene driven by the distal promoter of the lymphocyte protein tyrosine kinase (*Lck*) gene, which is expressed in the late stages of T cell development[195]. This Cre-recombinase then mediates deletion of loxP sites that flank *Insr* exon 4, leading to a frameshift mutation that destabilizes the mRNA[195], thus efficiently deleting the expression of INSR on T cells. Previous findings with this mouse model demonstrated that at steady-state, thymocytes did not have differences in cellularity and subset frequencies at the CD4 or CD8 single-positive, double-positive, or double-negative stages[171]. LckCre^{-} *Insr*$^{fl/fl}$ mice were used as controls, as previous reports indicated no Cre-associated toxicity when comparing LckCre^{+} *Insr*$^{wt/wt}$ mice with LckCre^{-} *Insr*$^{fl/fl}$ mice[171].

To explore the role of INSR on T cell anti-tumour immunity, 2x10^{5} OVA-expressing E.G7 tumour cells were subcutaneously injected into the right flank of LckCre^{+} *Insr*$^{fl/fl}$ or LckCre^{-} *Insr*$^{fl/fl}$ male and female mice, and tumour growth was monitored every other day using a caliper. Results from male and female mice were pooled together, as analyses showed that there were no significant differences between female and male mice within each group. I examined T cell infiltration into tumours following 3-4 weeks of tumour growth. Tumours implanted in LckCre^{+} *Insr*$^{fl/fl}$ mice showed a trend toward accelerated growth, but similar tumour endpoint weights and inner dimensions compared to tumours in LckCre^{-} *Insr*$^{fl/fl}$ control mice **(Figure 3.9 A-C)**. Although there was no difference in the proportion of CD45^{+} cells, CD4^{+} T cells and CD8^{+} T cells in the tumour **(Figure 3.9 D-F)**, there was a significant reduction in the frequency of OVA-specific CD8^{+} T cells **(Figure 3.9 G, H)**. However, there were no differences in the MFI of $OVA_{257-264}$ K^{b} tetramer **(Figure 3.9 I)**. Additionally, there were no differences in the frequency of OVA-specific CD4^{+} T cells in the tumour **(Figure 3.9 J)**, and no differences in the MFI of $OVA_{329-337}$ I-A^{b} tetramer **(Figure 3.9 K)**. When characterizing the subsets of OVA-

specific $CD4^+$ T cells within the tumour, there was a trending increase in the frequency of Tregs **(Figure 3.9 L)**, but a decrease in the frequency of Th1 cells in $LckCre^+$ $Insr^{fl/fl}$ mice **(Figure 3.9 M)**, suggesting that INSR signalling is important for the differentiation towards Th1 $CD4^+$ T cell subsets. In the draining inguinal lymph node and spleen, there were similar levels of $CD3^+$, $CD4^+$ and $CD8^+$ T cells **(Figure 3.10 A-F)**. However, there was a trending increase in the proportion of $CD8^+$ OVA-specific T cells in the spleen and lymph node of $LckCre^+$ $Insr^{fl/fl}$ mice **(Figure 3.10 G-I)** and $CD4^+$ OVA-specific T cells in the draining lymph node of $LckCre^+$ $Insr^{fl/fl}$ mice **(Figure 3.10 J, K)**. This could suggest that OVA-specific T cells may be accumulating in the peripheral lymphoid organs of $LckCre^+$ $Insr^{fl/fl}$ mice due to impaired migration to the tumour, increased survival in peripheral lymphoid tissue, or increased proliferation.

Further characterization of antigen-specific $CD8^+$ T cells in the tumour showed that INSR deficiency leads to decreased $CD8^+$ T cell activation as measured by CD69 staining **(Figure 3.11 A)**. After 5 hours of stimulation with PMA and ionomycin, there was also a decrease in the proportion of $IFN\gamma^+$ $CD8^+$ T cells, as well as decreased MFI of IFNγ in TILs from $LckCre^+$ $Insr^{fl/fl}$ mice **(Figure 3.11 B-D)**. In addition, the expression of GZMB and CD107α in intratumoural $CD8^+$ T cells from $LckCre^+$ $Insr^{fl/fl}$ mice also showed a trending decrease compared to controls **(Figure 3.11 E, F)**. However, there was a similar level of expression of IFNγ in $CD4^+$ T cells **(Figure 3.11 G)**. This suggests that INSR positively regulates $CD8^+$ T cell anti-tumour effector function in vivo. Of note, there was no difference in the proportion of OVA-specific T cells expressing exhaustion markers KLRG1, PD-1, LAG-3 and TIM-3 **(Figure 3.9 H-K)**, similarly to what was observed in our HFD tumour model. These findings suggested that loss of INSR may not affect $CD8^+$ T cell expression of co-inhibitory receptors within the tumour. Therefore, the functional defects observed in the intratumoural *Insr*-floxed $CD8^+$ T cells is not a consequence of increased co-inhibitory receptor expression.

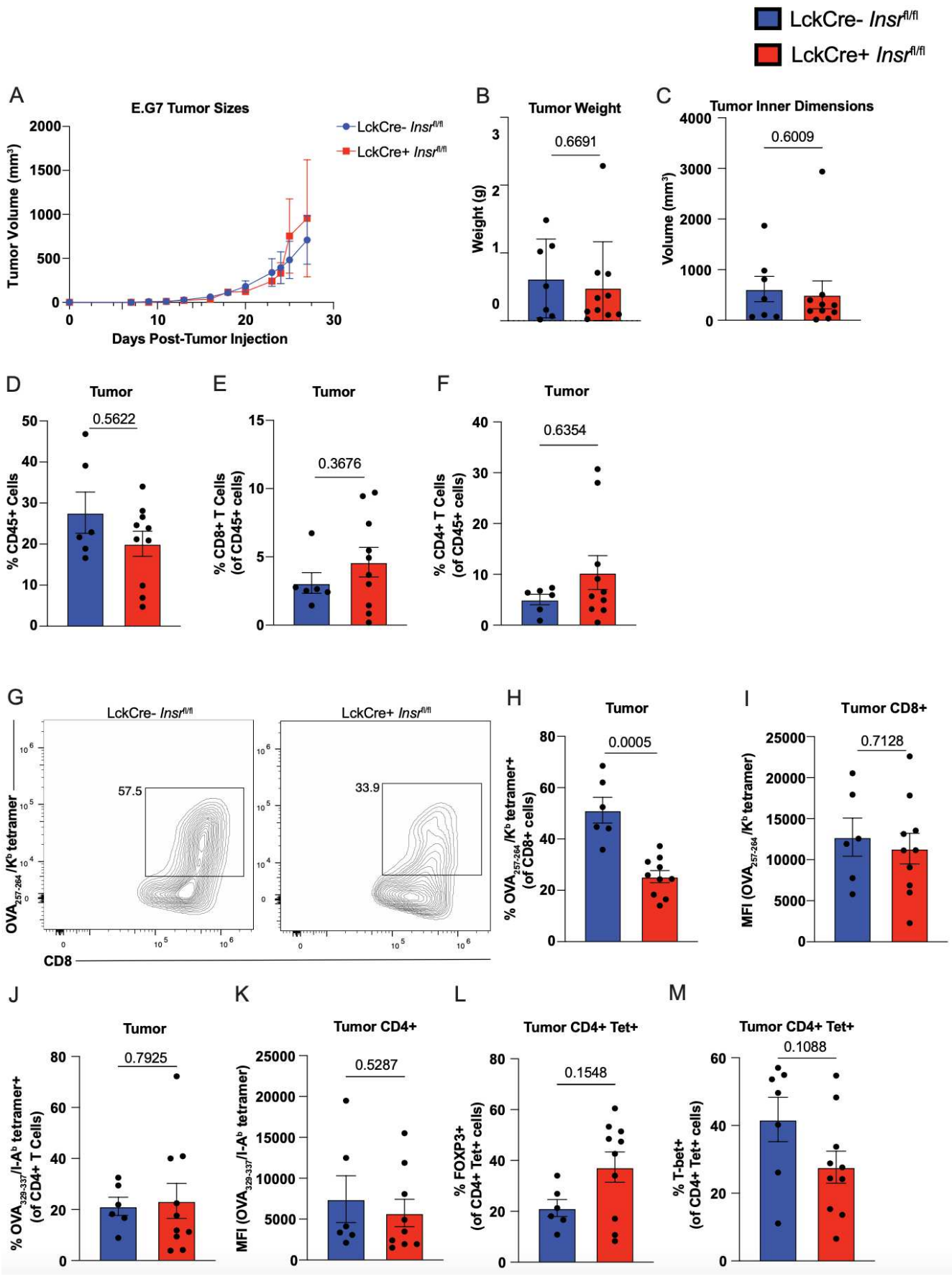
LckCre- Insr fl/fl
LckCre+ Insr fl/fl
A
E.G7 Tumor Sizes
Tumor Volume (mm³)
Days Post-Tumor Injection
B
Tumor Weight
0.6691
Weight (g)
C
Tumor Inner Dimensions
0.6009
Volume (mm³)
D
Tumor
0.5622
% CD45+ Cells
E
Tumor
0.3676
% CD8+ T Cells (of CD45+ cells)
F
Tumor
0.6354
% CD4+ T Cells (of CD45+ cells)
G
LckCre- Insr fl/fl
LckCre+ Insr fl/fl
57.5
33.9
CD8
H
Tumor
0.0005
% OVA257-264/Kb tetramer+ (of CD8+ cells)
I
Tumor CD8+
0.7128
MFI (OVA257-264/Kb tetramer)
J
Tumor
0.7925
% OVA329-337/I-Ab tetramer+ (of CD4+ T Cells)
K
Tumor CD4+
0.5287
MFI (OVA329-337/I-Ab tetramer)
L
Tumor CD4+ Tet+
0.1548
% FOXP3+ (of CD4+ Tet+ cells)
M
Tumor CD4+ Tet+
0.1088
% T-bet+ (of CD4+ Tet+ cells)

Figure 3.9 INSR-deficient T cells have impaired anti-tumour immunity. LckCre^{-} *Insr*$^{fl/fl}$ (n=6) or LckCre^{+} *Insr*$^{fl/fl}$ (n=10) mice were injected subcutaneously with 2x10^{5} E.G7 tumour cells. Graphs show data points from two pooled experiments. **(A)** Tumour growth curves of LckCre^{-} *Insr*$^{fl/fl}$ (n=6) or LckCre^{+} *Insr*$^{fl/fl}$ (n=10) mice. **(B)** Tumour weights after 27 days of growth. **(C)** Tumour volume on day 27 after dissection. (**D-M)** Tumours from LckCre^{-} *Insr*$^{fl/fl}$ (n=6) or LckCre^{+} *Insr*$^{fl/fl}$ (n=10) mice in C were dissected, and immune cell infiltration was analyzed by flow cytometry. Frequency of CD45^{+} cells **(D),** CD8^{+} T cells **(E),** and CD4^{+} T cells **(F)** in tumours. **(G)** Representative flow cytometry plots of OVA$_{257-264}$/K^{b} tetramer^{+} gating on CD8^{+} T cells. **(H)** Frequency of OVA$_{257-264}$/K^{b} tetramer^{+} CD8^{+} T cells. **(I)** MFI of OVA$_{257-264}$/K^{b} tetramer on CD8^{+} T cells. **(J)** Frequency of OVA$_{329-337}$/I-A^{b} tetramer^{+} CD4^{+} T cells. **(K)** MFI of OVA$_{329-337}$/I-A^{b} tetramer on CD4^{+} T cells. Frequency of FOXP3^{+} **(L)** and T-bet^{+} (**M)** CD4^{+} T cells. P-values for the tumour growth curve are calculated using two-way ANOVA. P-values for all bar graphs are calculated using Mann-Whitney U test. Data are shown as individual mice (dots) and mean ± SEM.

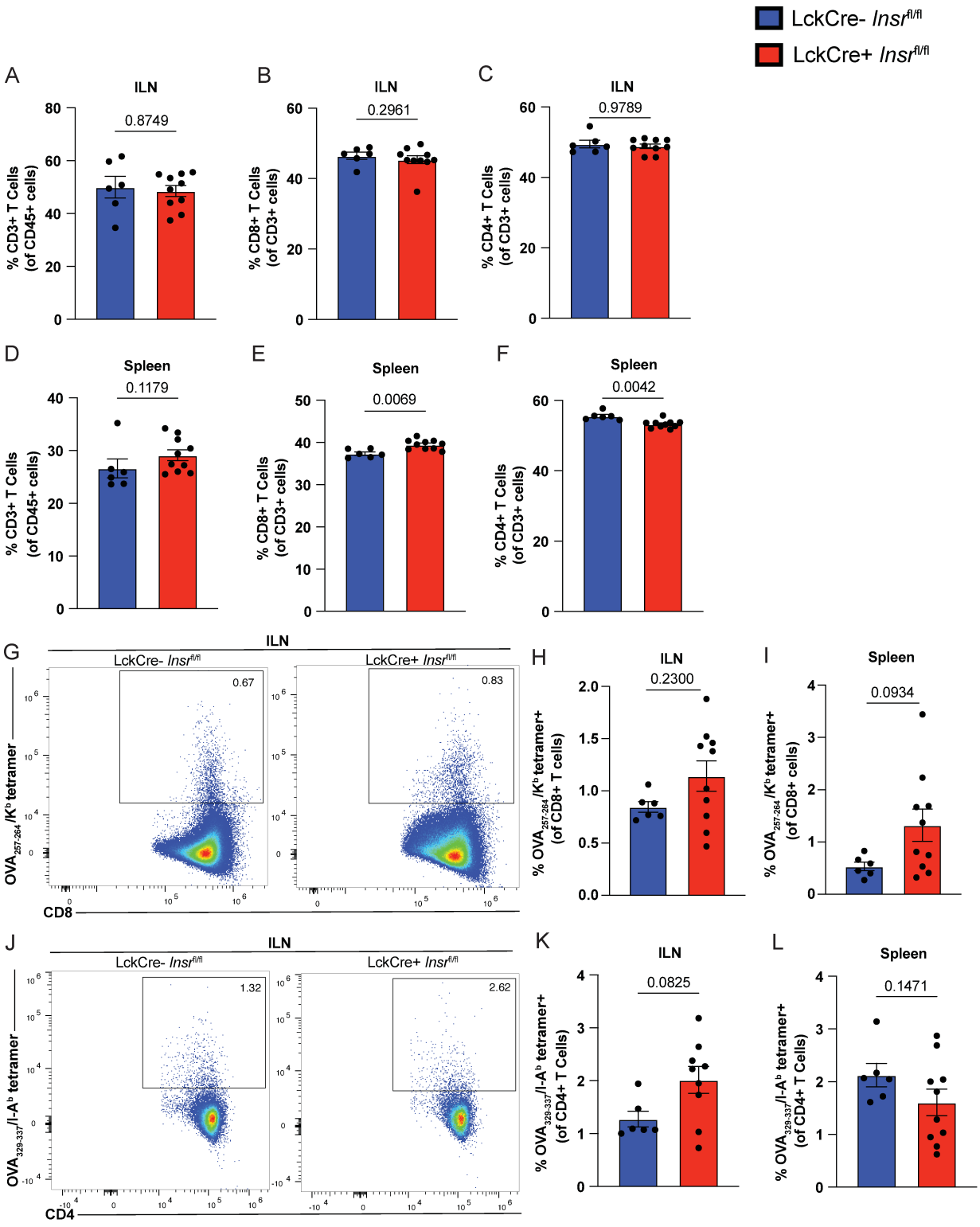
LckCre- Insrfl/fl
LckCre+ Insrfl/fl
A
ILN
0.8749
% CD3+ T Cells (of CD45+ cells)
B
ILN
0.2961
% CD8+ T Cells (of CD3+ cells)
C
ILN
0.9789
% CD4+ T Cells (of CD3+ cells)
D
Spleen
0.1179
% CD3+ T Cells (of CD45+ cells)
E
Spleen
0.0069
% CD8+ T Cells (of CD3+ cells)
F
Spleen
0.0042
% CD4+ T Cells (of CD3+ cells)
G
ILN
LckCre- Insrfl/fl
LckCre+ Insrfl/fl
0.67
0.83
OVA257-264/Kb tetramer
CD8
H
ILN
0.2300
% OVA257-264/Kb tetramer+ (of CD8+ T cells)
I
Spleen
0.0934
% OVA257-264/Kb tetramer+ (of CD8+ cells)
J
ILN
LckCre- Insrfl/fl
LckCre+ Insrfl/fl
1.32
2.62
OVA329-337/I-Ab tetramer
CD4
K
ILN
0.0825
% OVA329-337/I-Ab tetramer+ (of CD4+ T Cells)
L
Spleen
0.1471
% OVA329-337/I-Ab tetramer+ (of CD4+ T Cells)

Figure 3.10 Tumour-bearing LckCre^{+} *Insr*$^{fl/fl}$ mice show trending increase in the proportion of CD8^{+} OVA-specific T cells in the spleen and tumour-draining inguinal lymph node. Tumour-draining inguinal lymph nodes (ILN) and spleens from tumour-bearing LckCre^{-} *Insr*$^{fl/fl}$ (n=6) or LckCre^{+} *Insr*$^{fl/fl}$ (n=10) mice were dissected, and immune cell infiltration was analyzed by flow cytometry. Graphs show data points from two pooled experiments. Frequency of CD3^{+} cells in the ILN **(A)** and spleen **(B)**. Frequency of CD8^{+} T cells in the ILN **(C)** and spleen **(D)**. Frequency of CD4^{+} T cells in the ILN **(E)** and spleen **(F)**. **(G)** Representative flow cytometry plots of $OVA_{257-264}/K^{b}$ tetramer^{+} (Tet^{+}) CD8^{+} T cells in the ILN. Frequency of $OVA_{257-264}/K^{b}$ Tet^{+} CD8^{+} T cells in the ILN **(H)** and spleen **(I)**. **(J)** Representative flow cytometry plots of $OVA_{329-337}$/I-A^{b} Tet^{+} CD4^{+} T cells in the ILN. Frequency of $OVA_{329-337}$/I-A^{b} tetramer^{+} CD4^{+} T cells in the ILN **(K)** and spleen **(L)**. P-values are calculated using Mann-Whitney U test. Data are shown as individual mice (dots) and mean ± SEM.

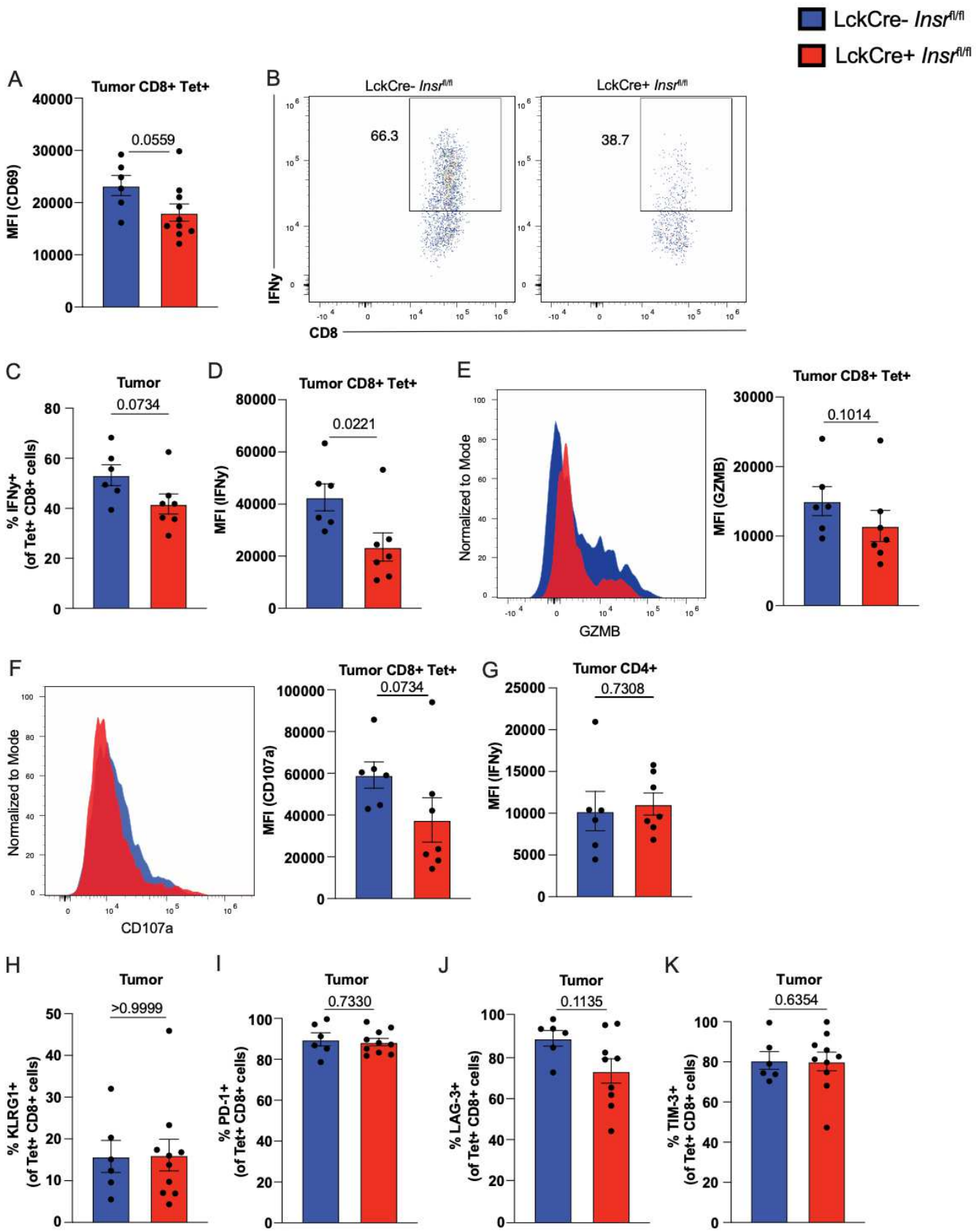
LckCre- Insr fl/fl
LckCre+ Insr fl/fl
A
Tumor CD8+ Tet+
MFI (CD69)
0.0559
B
LckCre- Insr fl/fl
LckCre+ Insr fl/fl
66.3
38.7
IFNy
CD8
C
Tumor
% IFNy+ (of Tet+ CD8+ cells)
0.0734
D
Tumor CD8+ Tet+
MFI (IFNy)
0.0221
E
Normalized to Mode
GZMB
Tumor CD8+ Tet+
MFI (GZMB)
0.1014
F
Normalized to Mode
CD107a
Tumor CD8+ Tet+
MFI (CD107a)
0.0734
G
Tumor CD4+
MFI (IFNy)
0.7308
H
Tumor
% KLRG1+ (of Tet+ CD8+ cells)
>0.9999
I
Tumor
% PD-1+ (of Tet+ CD8+ cells)
0.7330
J
Tumor
% LAG-3+ (of Tet+ CD8+ cells)
0.1135
K
Tumor
% TIM-3+ (of Tet+ CD8+ cells)
0.6354

Figure 3.11 INSR deficiency impairs $CD8^+$ T cell-mediated anti-tumour function in tumours independent of exhaustion marker expression. (A, H-K) Unstimulated cells from dissociated E.G7 tumours from $LckCre^-$ $Insr^{fl/fl}$ (n=6) or $LckCre^+$ $Insr^{fl/fl}$ (n=10) mice were stained with markers of activation or exhaustion markers. Graphs show data points from two pooled experiments. **(B-G)** Cells from dissociated tumours were stimulated with PMA/ionomycin with brefeldin A for 5 hours prior to intracellular staining of IFNγ and GZMB. Fluorescently conjugated anti-CD107α antibodies were added at the beginning of the stimulation. **(A)** MFI of CD69 in $OVA_{257-264}/K^b$ tetramer$^+$ (Tet^+) $CD8^+$ T cells. **(B)** Representative flow cytometry plots of IFNγ staining in $CD8^+$ Tet^+ T cells. **(C)** Frequency of $IFN\gamma^+$ $CD8^+$ Tet^+ T cells. **(D)** MFI of IFNγ of $CD8^+$ Tet^+ T cells. Representative histogram and MFI of GZMB **(E)** and CD107α **(F)** of $CD8^+$ Tet^+ T cells. **(G)** MFI of IFNγ of $CD4^+$ T cells. Frequency of $CD8^+$ Tet^+ T cells expressing KLRG1 **(H)**, PD-1 **(I)**, TIM-3 **(J)**, and LAG-3 **(K)**. P-values are calculated using Mann-Whitney U test. Data are shown as individual mice (dots) and mean ± SEM.

3.2.7 INSR-deficient CD8$^+$ T cells have similar tumour killing capacity in vitro

To further assess effects of INSR deficiency on T cell function, in vitro tumour killing assays were performed. OT-I T cells from either OT-I transgenic LckCre$^-$ *Insr*$^{fl/fl}$ or OT-I transgenic LckCre$^+$ *Insr*$^{fl/fl}$ mice were co-cultured with MC38-OVA tumour cells, and measured for their ability to kill tumours after 24 hours, and assessed for levels of activation and IFNγ production after 48 hours. Prior to co-culture, purified OT-I T cells from both groups showed similar levels of activation **(Figure 3.12 A)**. *Insr*-floxed CD8$^+$ T cells showed similar levels of tumour killing capacity compared to WT controls when comparing LIVE/DEAD (LD) and Caspase 3/7 staining in tumour cells at all target:effector ratios (1:2, 1:4, and 1:8) **(Figure 3.12 B, C)**. In addition, they showed comparable MFI of CD69 after 24 hours of co-culture **(Figure 3.12 D)**, suggesting similar levels of activation. Levels of IFNγ production showed a trending decrease in *Insr*-floxed CD8$^+$ T cells compared to controls, however this difference was not statistically significant **(Figure 3.12 E, F)**. Overall, INSR-deficiency in CD8$^+$ T cells did not appear to affect tumour killing capacity and the proportion of IFNγ-producing cells in vitro, which does not fully mimic a physiological state.

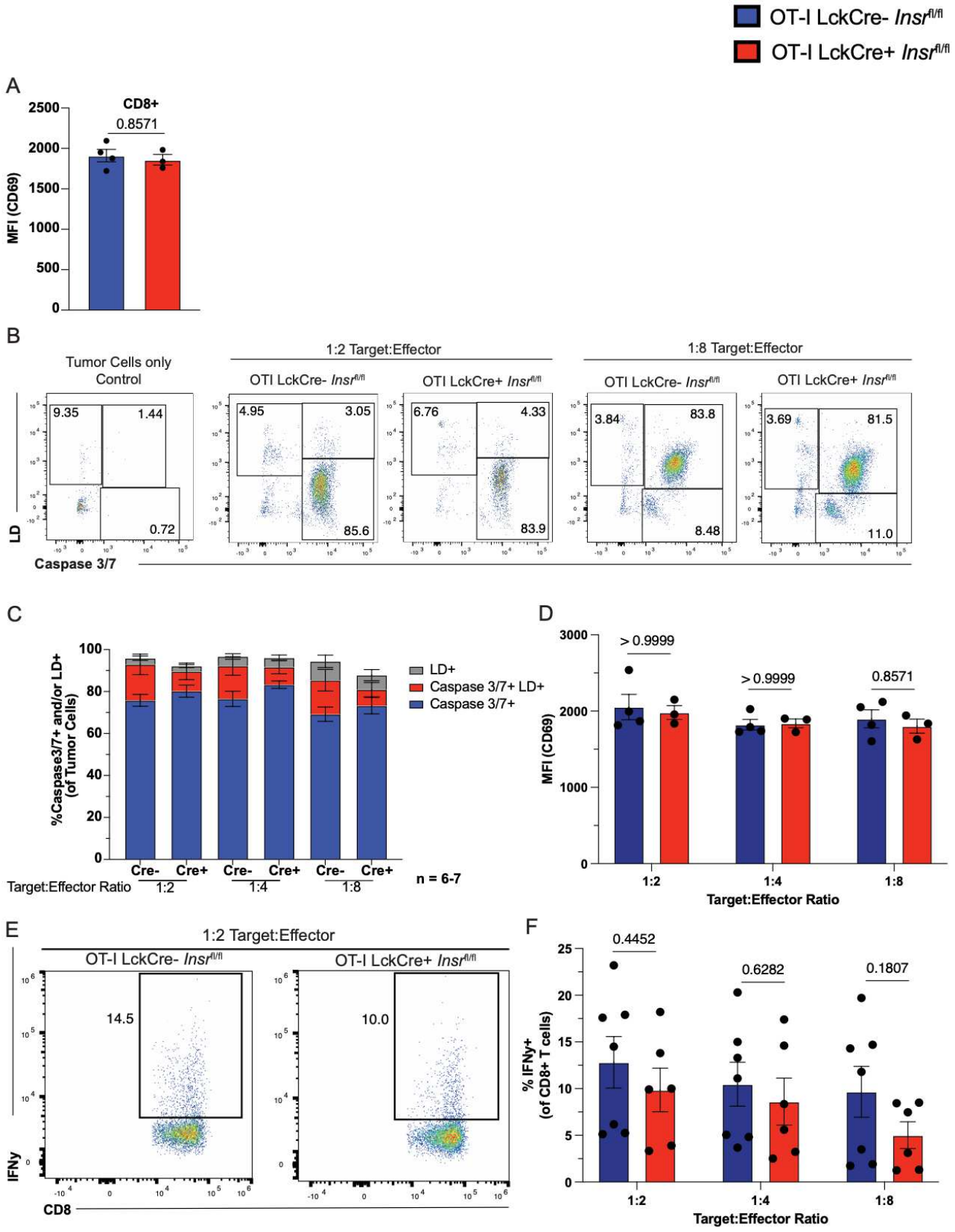
OT-I LckCre- Insr fl/fl
OT-I LckCre+ Insr fl/fl
A
CD8+
0.8571
MFI (CD69)
2500
2000
1500
1000
500
0
B
Tumor Cells only Control
1:2 Target:Effector
1:8 Target:Effector
OTI LckCre- Insr fl/fl
OTI LckCre+ Insr fl/fl
OTI LckCre- Insr fl/fl
OTI LckCre+ Insr fl/fl
9.35
1.44
0.72
4.95
3.05
85.6
6.76
4.33
83.9
3.84
83.8
8.48
3.69
81.5
11.0
LD
Caspase 3/7
C
%Caspase3/7+ and/or LD+ (of Tumor Cells)
100
80
60
40
20
0
LD+
Caspase 3/7+ LD+
Caspase 3/7+
Cre-
Cre+
Cre-
Cre+
Cre-
Cre+
Target:Effector Ratio
1:2
1:4
1:8
n = 6-7
D
MFI (CD69)
3000
2000
1000
0
> 0.9999
> 0.9999
0.8571
1:2
1:4
1:8
Target:Effector Ratio
E
1:2 Target:Effector
OT-I LckCre- Insr fl/fl
OT-I LckCre+ Insr fl/fl
14.5
10.0
IFNy
CD8
F
% IFNy+ (of CD8+ T cells)
25
20
15
10
5
0
0.4452
0.6282
0.1807
1:2
1:4
1:8
Target:Effector Ratio

Figure 3.12 INSR deficient CD8+ T cells have similar tumour killing capacity in vitro. OT-I T cells from either OT-I transgenic LckCre^{-} *Insr*$^{fl/fl}$ (n=4-6) or OT-I transgenic LckCre^{+} *Insr*$^{fl/fl}$ (n=3-6) mice were co-cultured with MC38-OVA tumour cells at target:effector ratios of 1:2, 1:4, and 1:8. Tumour killing by the OT-I CD8^{+} T cells at 24 hours was measured via LIVE/DEAD (LD) and caspase 3/7 staining. Graphs show data points from two pooled experiments. **(A)** MFI of CD69 in purified OT-I T cells prior to co-culturing. **(B)** Representative flow cytometry plots of LD and caspase 3/7 staining gated on tumour cells (CD8^{-} cells). **(C)** Piled graphs showing frequency of caspase 3/7^{+} (blue), caspase 3/7^{+} LD^{+} (red), and LD^{+} tumour cells after co-culture with OT-I T cells. **(D)** MFI of CD69 of OT-I T cells after 24 hours of co-culture. **(E)** Representative flow cytometry plots of IFNγ staining in OT-I T cells after 48 hours of co-culture. **(F)** Frequency of IFNγ^{+} OT-I T cells after 48 hours of co-culture. P-values are calculated using Mann-Whitney U test. Data are shown as individual mice (dots) and mean ± SEM.

3.2.8 INSR-deficient CD8$^+$ T cells have similar proliferative ability but decreased production of pro-inflammatory cytokines in vitro

To assess whether the differences observed in the levels of OVA-specific CD8$^+$ T cells in the tumour were due to differences in proliferation, I used an in vitro CFSE proliferation assay. OT-I CD8$^+$ T cells were isolated from LckCre$^-$ *Insr*$^{fl/fl}$ or LckCre$^+$ *Insr*$^{fl/fl}$ mice and stained with CFSE, and co-cultured with OVA-peptide pulsed DCs at various concentrations. Levels of CFSE staining were measured using flow cytometry after 48 hours. Proliferation was comparable between the OT-I CD8$^+$ T cells deficient and sufficient in INSR at all concentrations of peptide tested **(Figure 3.13 A, B)**. Supernatants were also collected from the co-cultures of OVA-pulsed DCs and INSR-deficient or INSR-sufficient OT-I T cells, and levels of IFNγ and IL-2 were measured via ELISA. Levels of IFNγ were significantly lower in the supernatants of co-cultures with T cells deficient in INSR **(Figure 3.13 C)**, but proliferation and IL-2 levels in the supernatants **(Figure 3.13 D)** were similar, suggesting that INSR is important for CD8$^+$ T cell cytokine secretion.

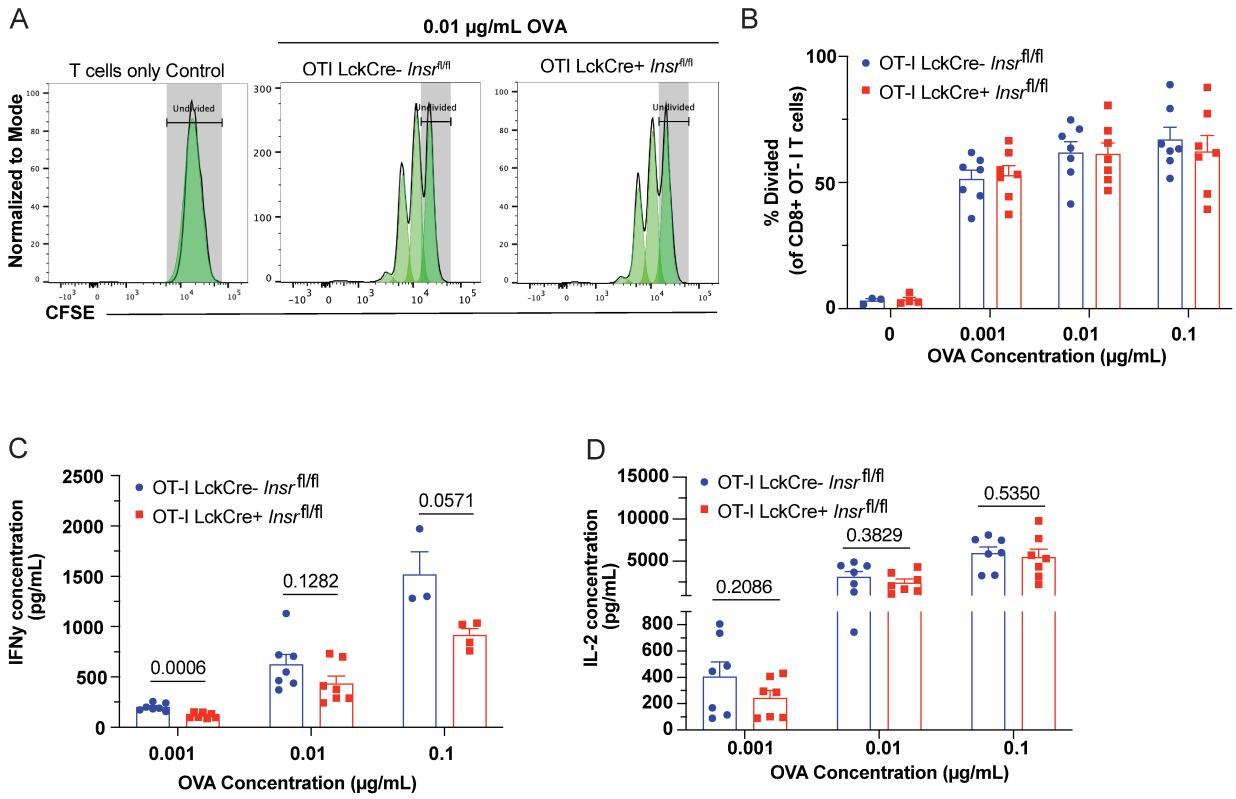

Figure 3.13 INSR-deficient CD8+ T cells have similar proliferative ability but decreased production of pro-inflammatory cytokines in vitro. (A-D) OT-I T cells from OT-I transgenic LckCre^{-} *Insr*$^{fl/fl}$ (n=3-7) or OT-I transgenic LckCre^{+} *Insr*$^{fl/fl}$ (n=4-7) mice were stained with CFSE and co-cultured with OVA-peptide pulsed DCs at various concentrations. Levels of CFSE staining were measured via flow cytometry after 48 hours. Supernatants were also collected from the co-cultures of OVA-pulsed DCs and LckCre^{-} *Insr*$^{fl/fl}$ or LckCre^{+} *Insr*$^{fl/fl}$ OT-I T cells. Graphs show data points from two pooled experiments. **(A)** Representative histograms of OT-I T cell proliferation with DCs pulsed with 0.01 µg/mL of OVA. **(B)** Percentage of OT-I T cells divided. Concentration of IFNγ **(C)** and IL-2 **(D)** in supernatants of co-cultures.

3.2.9 INSR-deficient CD8$^+$ T cells show a trending decrease in proliferation in tumour-bearing mice

To further assess whether the differences observed in the levels of OVA-specific CD8$^+$ T cells in the tumour were due to differences in proliferation, 8-12 week old male CD45.1 tumour bearing hosts were injected with CFSE-labelled OT-I CD8$^+$ T cells from CD45.2 congenic LckCre$^+$ *Insr*$^{fl/fl}$ or LckCre$^-$ *Insr*$^{fl/fl}$ OT-I transgenic mice with CFSE. 3 days post-injection with CFSE-labelled T cells, I euthanized the mice and measured levels of proliferation of the adoptively transferred INSR-deficient CD8$^+$ T cells in the draining inguinal lymph node and spleen, as well as infiltration into the tumours. There was a trending decrease in the percentage of adoptively transferred T cells that were divided in the draining inguinal lymph node **(Figure 3.14 A, B)**, suggesting that INSR may be important for CD8$^+$ T cell proliferation in vivo. However, there was a similar proportion of CD45.2$^+$ T cells within the tumours at this time point, suggesting that more time may be required for T cells in the draining lymph node to migrate into the tumours **(Figure 3.14 C)**.

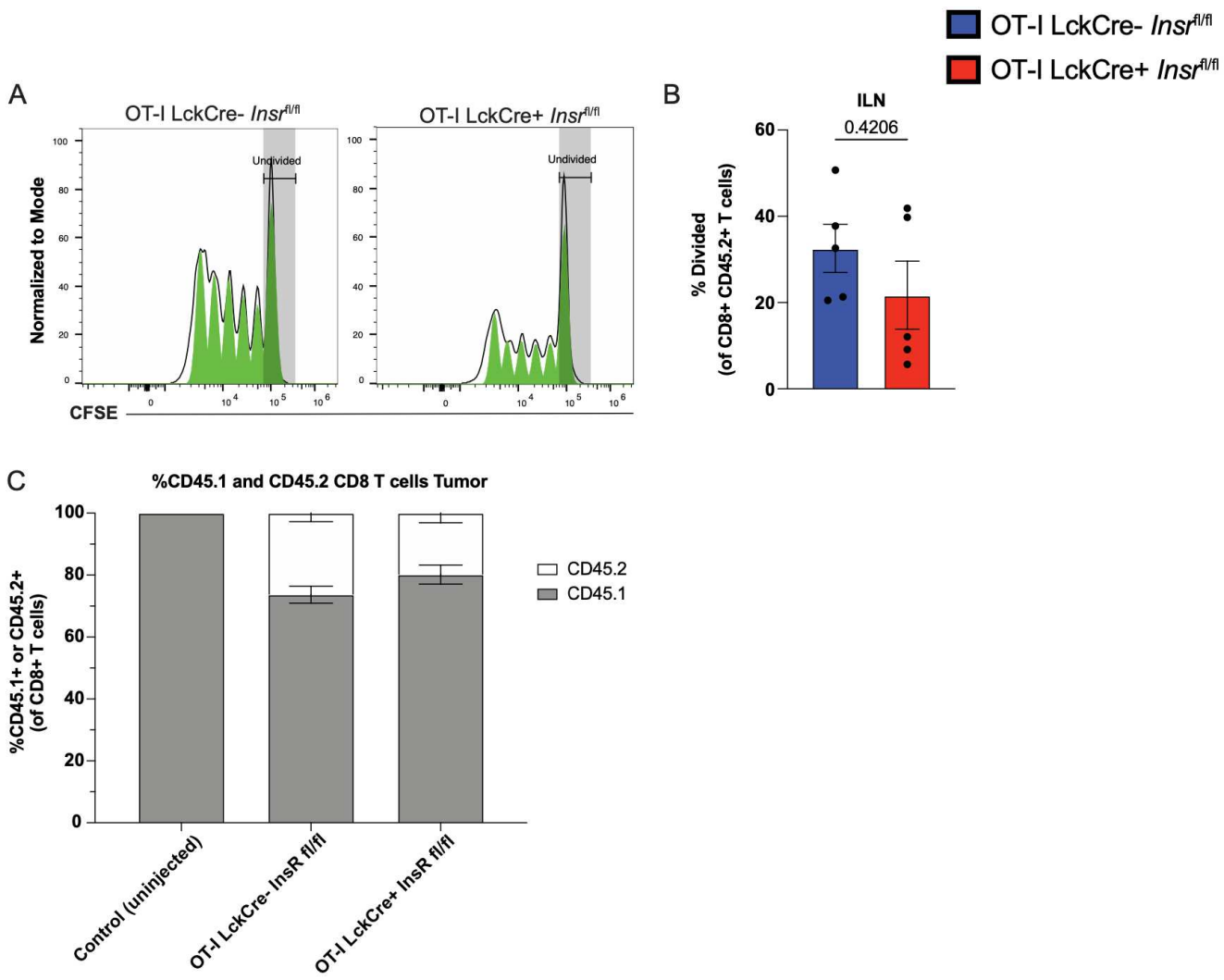

Figure 3.14 INSR-deficient CD8+ T cells show trending decrease in proliferation in tumour-bearing mice. (A-C) 8-12 week old male CD45.1 C57BL/6 congenic mice were injected with $2x10^5$ E.G7 tumour cells subcutaneously. After 7-9 days post tumour injection, I isolated and labelled OT-I $CD8^+$ T cells from CD45.2 congenic OT-I transgenic $LckCre^-$ $Insr^{fl/fl}$ (n=5) or OT-I transgenic $LckCre^+$ $Insr^{fl/fl}$ (n=5) mice with CFSE and injected them intravenously into the tumour-bearing mice. 3 days post-injection with CFSE-labelled T cells, mice were euthanized and levels of proliferation of the adoptively transferred T cells in the draining inguinal lymph node and infiltration of $CD45.2^+$ cells in the tumour were measured. Graphs show data points from one experiment. **(A)** Representative histograms of OT-I T cell proliferation. **(B)** Percentage of OT-I T cells divided. **(C)** Frequency of CD45.2+ CD8+ T cells in tumours. P-values are calculated using Mann-Whitney U test. Data are shown as individual mice (dots) and mean ± SEM.

3.3 Discussion

Obesity is a major risk factor for 13 different types of cancer[155], but the underlying effects of obesity on the anti-tumour immune response is unclear. Using an E.G7 tumour mouse model, I observed an acceleration in tumour growth in HFD-fed mice compared to NCD-fed mice **(Figure 3.2 A-C)**, which is consistent with previous reports of using different tumour models[206, 207, 208]. Obesity also reduced the proportion of intratumoural $CD8^+$ T cells **(Figure 3.2 E)**, which was similarly observed by Ringel et al., where they demonstrated a reduction in the number of intratumoural $CD8^+$ T cells in a MC38 colorectal adenocarcinoma model in HFD-fed mice[206]. The frequency and MFI of OVA-specific $CD8^+$ T cells were decreased in the tumours of HFD-fed mice **(Figure 3.2 G, H)**, which can suggest that there are alterations in binding affinity to the OVA antigen, but also that there could be differences in the repertoire of T cells in the TME of obese mice. The OVA-specific TILs in HFD-fed mice were also functionally impaired, as they had decreased expression of IFNγ, GZMB and CD107α **(Figure 3.4 B-F)**. Intratumoural $CD4^+$ T cells in obese mice also displayed decreased IFNγ production **(Figure 3.4 G)**, which could be augmenting differences seen in the functionality of the intratumoural CTLs. Ringel et al. similarly observed decreased functionality with fewer $CD8^+$ TILs expressing GZMB in HFD-fed mice, but in contrast saw no differences in the production of IFNγ[206]. In addition, there was no difference in expression of multiple exhaustion markers between NCD and HFD-fed mice, which was consistent with observations by Dyck et al. in a HFD MC38 tumour model[169]. Overall, our findings suggest that mechanisms independent of immune checkpoint expression may be contributing to $CD8^+$ T cell dysfunction observed in the tumours of obese mice.

In vitro, I observed contrasting results in tumour killing ability than those observed in vivo. However, I observed increased baseline levels of expression of CD69 in purified $CD8^+$ T cells from obese mice **(Figure 3.5 A)**, which is consistent with reports of increased activation in T cells from obese patients[175]. This discrepancy in baseline activation state may be contributing to the increased tumour killing capacity observed in $CD8^+$ T cells isolated from HFD-fed mice. Also, there may have been differences in proportions of naive, effector and memory T cell subsets that were in the purified cells, as previous reports have indicated that obesity increases memory T cell frequencies in lymphoid tissue[209]. Future experiments will require baseline measurements of these T cell subsets prior to co-culture, and purification of specific subsets (e.g.

naive $CD8^+$ T cells) of T cells from NCD and HFD-fed mice can be used to assess their anti-tumour function in vitro to control for this factor.

Based on the observed decrease in infiltrating $CD8^+$ T cells in the tumour, I next tested the hypothesis that it may be due to differences in their proliferative capacity. Using an in vitro CFSE proliferation assay, I found that OT-I $CD8^+$ T cells from NCD and HFD-fed mice showed similar levels of proliferation **(Figure 3.6 A, B)**, which was consistent with previous reports of comparable Ki67 expression on anti-CD3/anti-CD28 antibody-stimulated splenic $CD8^+$ T cells from NCD and HFD-fed mice[206]. Therefore, differences in the proportion of TILs observed in vivo may be due to differences in migration, as studies have indicated that $CD8^+$ T cells in obese mice express lower levels of receptors involved in transmigration[169]. Additional experiments assessing migratory abilities of T cells from NCD and HFD-fed mice, such as transwell migration assays, can be done to confirm this hypothesis.

In order to assess whether systemic alterations that occur in obesity can lead to long-term reprogramming in T cells that would affect their anti-tumour immune responses, I isolated OT-I $CD8^+$ T cells from NCD and HFD-fed mice expressing CD45.2, differentiated them into CTLs, and adoptively transferred them into tumour-bearing CD45.1 congenic mice. Interestingly, there was accelerated tumour growth in mice that were adoptively transferred with HFD OT-I T cells compared to mice injected with NCD OT-I T cells **(Figure 3.7 A)**, which was associated with a decrease in the proportion of $CD45.2^+$ $CD8^+$ T cells within the tumour **(Figure 3.7 B)**. There was also decreased functionality in the $CD45.2^+$ HFD TILs **(Figure 3.7 D, E)**, suggesting that obesity causes long-lasting alterations in $CD8^+$ T cells. Mechanistically how obesity leads to reprogramming in T cells is unclear, as there are many systemic metabolic, inflammatory and nutrient changes that occur in obesity. Previous findings have indicated that functional defects in $CD8^+$ T cells from obese mice are associated with an impairment in amino acid metabolism, as well as decreased lipid uptake[169]. This warrants future experiments focusing on how HFD-feeding impacts the metabolic program of T cells in the context of cancer.

To explore mechanistically how obesity could be impairing T cell-mediated anti-tumour responses, we decided to focus on the role of insulin signalling, as hyperinsulinemia and insulin

resistance are highly associated with obesity[204]. Furthermore, immune cells including T cells express the INSR[171], and evidence suggests that insulin signalling is important for T cell function, as T cells upregulate their surface expression of INSR upon activation, and impairment of INSR signalling reduces their production of effector molecules[171]. First, we hypothesized that obesity would lead to an impairment in insulin signalling in T cells. After stimulation with anti-CD3/anti-CD28, there was defective insulin-stimulated pAkt signalling **(Figure 3.8 A)**, congruent with previous findings that lymphocytes from obese patients showed reduced insulin-stimulated Akt phosphorylation in vitro[175]. An interesting future experiment would be to isolate T cells from obese and lean tumour-bearing mice to assess whether the presence of a tumour can further impact insulin signalling in T cells.

After observing a decrease in insulin signalling in T cells from HFD-fed mice, we wanted to investigate how INSR-deficiency in T cells would affect their anti-tumour function. As previous studies have shown that INSR in T cells is important for their proliferation, activation, and effector function[171], I hypothesized that INSR-deficiency in T cells would impair their anti-tumour responses. Using LckCre^{+} *Insr*$^{fl/fl}$ mice, which have T cell-specific deletion of *Insr*, I observed a trending decrease in E.G7-OVA tumour growth, but similar endpoint tumour weights and inner dimensions **(Figure 3.9 A-C)**. There were no significant differences in the proportion of CD4^{+} T cells and CD8^{+} T cells within the tumour, but there was a marked reduction in the proportion of OVA-specific CD8^{+} T cells in LckCre^{+} *Insr*$^{fl/fl}$ mice **(Figure 3.9 H, I)**. In addition, there were trending decreases in the expression of effector molecules IFNγ, GZMB, and CD107α **(Figure 3.11 C-G)**. Similarly in an H1N1 influenza model, LckCre^{+} *Insr*$^{fl/fl}$ mice demonstrated impaired anti-viral T cell responses, with decreased expression of flu nucleoprotein (NP) tetramer staining, as well as intracellular cytokine analysis[171]. This finding is in accordance with the notion that INSR is important for maximizing T cell function during acute infection and cancer. However, I observed similar levels of tumour killing capacity in vitro between INSR-sufficient and INSR-deficient T cells **(Figure 3.12 B, C)**. This may be due to differences in levels of insulin in vivo compared to those in vitro, affecting insulin availability for the T cells. Performing in vitro killing assays with the addition of insulin would be an additional experiment to ascertain the importance of insulin signalling in CD8^{+} T cell anti-tumour function.

Similar levels of exhaustion markers in TILs indicated that functional defects observed in the intratumoural *Insr*-floxed $CD8^+$ T cells may not be a consequence of increased immune checkpoint inhibition. Instead, this may be a result of differences in metabolic activity, as INSR signalling reinforces a metabolic program that increases T cell nutrient uptake, and metabolic programs including glycolysis and oxidative phosphorylation (OXPHOS)[171], which is critical for optimal T cell function. Additional studies assessing nutrient uptake, and metabolic programs such as glycolysis and OXPHOS in T cells of $LckCre^+$ $Insr^{fl/fl}$ mice tumour-bearing mice would be required to address this hypothesis.

As I observed differences in proportion of OVA-specific $CD8^+$ T cells in the tumour of LckCre $Insr^{fl/fl}$ mice, I hypothesized that this may be due to differences in proliferation. When conducting an in vitro CFSE proliferation assay, I observed no differences in the proliferation of *Insr*-floxed $CD8^+$ T cells compared to controls **(Figure 3.13 A, B)**. This was surprising, as previous work has demonstrated that *Insr*-floxed $CD4^+$ T cells have decreased proliferative capacity compared to INSR-sufficient $CD4^+$ T cells[171]. This suggests that INSR signalling in $CD8^+$ T cells may not be as important for proliferation as in $CD4^+$ T cells in vitro. However, when assessing proliferation in vivo using an adoptive transfer model, there was a trending decrease in the proportion of adoptively transferred *Insr*-floxed $CD8^+$ T cells that divided in the draining inguinal lymph node **(Figure 3.14 A, B)**, suggesting that INSR signalling may support $CD8^+$ T cell proliferation in vivo. Further studies with increased sample size are required to confirm this.

In summary, this chapter demonstrates that HFD-feeding accelerates tumour growth and impairs $CD8^+$ T cell-mediated immune responses. Specifically, there was a decrease in the proportion of intratumoural $CD8^+$ T cells in HFD-fed mice, and a decrease in the proportion of OVA-specific $CD8^+$ T cells in the tumour. The TILs in HFD-fed mice also displayed impaired effector function without changes in exhaustion status. This is in contrast to observations made in my in vitro experiments, where I observed a trending increase in the killing capacity of HFD $CD8^+$ T cells, which was associated with increased activation levels and production of effector molecules. Thus, I posit that the intratumoural environment renders TILs vulnerable to insulin-resistance-associated functional impairment.

Another notable finding from this chapter is made when I explored the role of altered INSR signalling as a mechanistic basis of obesity-associated T cell defect. Mirroring HFD-fed mice, LckCre^{+} *Insr*$^{fl/fl}$ mice exhibited a reduced proportion of intratumoural OVA-specific CD8^{+} T cells. In addition, the TILs in the LckCre^{+} *Insr*$^{fl/fl}$ mice showed a decrease in their effector function, but no overall differences in expression of exhaustion markers. In vitro, *Insr*-floxed CD8^{+} T cells had similar levels of tumour killing capacity and proliferation. Taken altogether, the impairment of CD8^{+} T cell-mediated anti-tumour immunity observed in HFD-fed mice may be linked to defective insulin signalling in T cells. Understanding the metabolic changes occurring in T cells in HFD-fed mice and LckCre^{+} *Insr*$^{fl/fl}$ mice will provide further insight into their impaired function, and help us establish whether targeting metabolic pathways can be a potential avenue for boosting T cell anti-tumour function.

3.4 Contributions

The ITT and IPGTT characterizing the DIO model were performed with the help of Mengyi Zhu. An undergraduate student, Lucy Lee, aided with all experiments, from preparing tumour cells for injections, measuring tumour sizes, processing of mouse tissues, completion of ELISAs, and analysis of flow cytometry. Western blot analyses for insulin signalling in T cells was completed by Dr. Sue Tsai. For in vitro killing assays, MC38-OVA cells were generously provided by Dr. Kristi Baker. The processing of all mouse tissues was expedited with the help from the members of the Tsai-Clemente lab. Intravenous injections for adoptive transfers were completed with the help of Aklima Akter.

Chapter 4: The role of YAP/TAZ signalling in DC-mediated pathogenesis of insulin resistance and non-alcoholic fatty liver disease

4.1 Introduction

Obesity and associated IR predispose individuals to develop chronic metabolic diseases, such as type 2 diabetes and non-alcoholic fatty liver disease (NAFLD)[210]. These disorders affect a significant proportion of the global population; however, their underlying mechanisms remain incompletely understood. It is known that long-term caloric excess in obesity causes white adipocytes to become hypertrophic and undergo endoplasmic reticulum (ER) stress, resulting in the release of various adipokines and chemoattractants that help activate and/or recruit innate cells, such as macrophages and DCs, as well as pro-inflammatory adaptive immune cells[176]. Signals coming from adipocytes can polarize macrophages to increase the proportion of pro-inflammatory macrophages, which in turn release cytokines systemically such as TNFα, IL-1β, and IL-6 which can impair insulin signalling[176]. DCs also play critical roles in obesity-associated inflammation, as depletion of DCs protected obese mice from adipose tissue inflammation and IR[61, 62]. DCs can produce pro-inflammatory cytokines, and play critical roles in promoting Th1 and Th17 inflammatory responses, worsening the systemic inflammation[176]. These immune cells are important in generating this chronic inflammation and resulting IR, which in turn can predispose individuals to develop NAFLD. In NAFLD, inflammation is often accompanied by fibrotic processes that alter tissue stiffness in the liver[178], potentially activating mechanosensing pathways. Increasing evidence suggests a role for extracellular physical cues coming from tissue stiffness in promoting immune cell recruitment, activation, and inflammatory function[179].

We and others have observed that substrate stiffness is an important determinant of DC function[66, 77]. Particularly, DCs grown under higher stiffness show increased activation and secretion of pro-inflammatory cytokines. Given the accumulating evidence for the importance of mechanical cues in immune function, it is crucial to understand their impact on immune cell activation during disease states, such as NAFLD. We have identified two key molecules involved in the HIPPO pathway, Yes-associated protein (YAP) and Transcriptional co-activator with PDZ-binding motif (TAZ), as potential sensors of mechanical and nutrient cues in DCs. Specifically, transcriptomic analysis and inhibitor/agonist assays identified the Hippo-signalling

molecule, TAZ, to be important for promoting DC metabolism and function under higher substrate stiffness conditions[66]. In addition to mechanical cues, YAP and TAZ activity in the HIPPO pathway is regulated by nutrient cues[180]**.** Under conditions of energy stress, AMPK directly phosphorylates YAP and TAZ, causing inhibition of their activity. However, under high glucose levels, the AMPK pathway is inhibited, allowing YAP and TAZ to mediate their downstream effects[180].

Evidence has shown that YAP/TAZ play a role in inflammatory diseases. In human liver biopsies, immune cells in cirrhotic livers exhibited increased staining for TAZ **(Figure 4.1)**. In the context of myocardial infarction, the genetic deletion of YAP/TAZ leads to impaired pro-inflammatory and enhanced reparative responses to improve infarct healing and cardiac function[118]. Additionally, YAP activity in immune cells has been shown to aggravate inflammatory bowel disease by promoting pro-inflammatory phenotypes in macrophages[119]. Overall, the HIPPO pathway and activity of YAP and TAZ is known to positively regulate inflammatory responses. Therefore, we hypothesized that YAP and TAZ signalling in DCs may perpetuate obesity-linked inflammation in a feed-forward manner and contribute to the pathogenesis of IR and NAFLD.

To investigate the role of YAP and TAZ signalling in DCs, we generated DC-specific YAP/TAZ conditional knockout mice (CD11cCre^{+} *Yap*$^{fl/fl}$ (YAP$^{DC\text{-}KO}$), CD11cCre^{+} *Taz*$^{fl/fl}$ (TAZ$^{DC\text{-}KO}$), CD11cCre^{+} *Yap*$^{fl/fl}$ *Taz*$^{fl/fl}$ (YAP/TAZ$^{DC\text{-}DKO}$)) by crossing CD11c-Cre (008068), *Taz*$^{fl/fl}$ (032669), and *Yap*$^{fl/fl}$ (027929) breeders. The CD11c-Cre transgenic mice express Cre recombinase under the control of the mouse integrin alpha X (CD11c) promoter, which is expressed in DCs, as well as monocyte-derived DCs and macrophages[211]. In *Yap*$^{fl/fl}$ mice , the first two exons of the *Yap1* gene are flanked by loxP sites. In *Taz*$^{fl/fl}$ mice , exon 2 of the *Wwtr1* gene (also known as *Taz*) is flanked by loxP sites. The loxP flanked genes are excised upon Cre recognition, allowing for CD11c cell-specific deletion of *Yap* and/or *Taz*. These DC-specific YAP/TAZ conditional knockout mice were compared with their corresponding CD11cCre^{-} controls (CD11cCre^{-} *Yap*$^{fl/fl}$ (YAP$^{DC\text{-}WT}$), CD11cCre^{-} *Taz*$^{fl/fl}$ (TAZ$^{DC\text{-}WT}$), CD11cCre^{-} *Yap*$^{fl/fl}$ *Taz*$^{fl/fl}$ (YAP/TAZ$^{DC\text{-}WT}$)). In this chapter, I examined whether CD11c-targeted YAP and TAZ deletion causes alterations in immune cell composition in the liver at steady-state compared to

controls. DC-specific ablation of YAP or TAZ led to no significant differences in the number and proportions of myeloid cell populations. Interestingly, there were decreases in a subset of macrophages and DCs in the livers of YAP/TAZ$^{DC\text{-}DKO}$ mice compared to controls. CD11c-targeted YAP and/or TAZ ablation in DCs did not significantly alter the development of IR, demonstrated by comparable insulin sensitivity and glucose tolerance compared to their respective HFHS controls. After HFHS treatment, there were also predominantly no significant differences in immune cell populations in the livers and VAT of YAP$^{DC\text{-}KO}$, TAZ$^{DC\text{-}KO}$, and YAP/TAZ$^{DC\text{-}DKO}$ mice compared to their respective controls. When assessing levels of fibrosis in the liver, YAP/TAZ$^{DC\text{-}DKO}$ and control mice exhibited similar levels of collagen deposition.

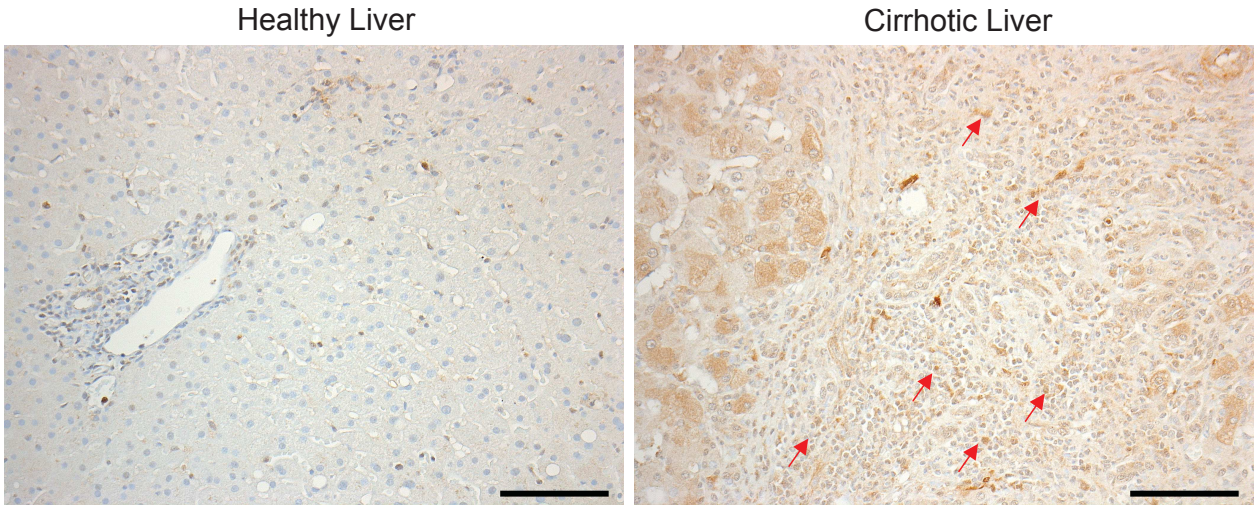

Figure 4.1 Up-regulation of TAZ in immune cells in normal healthy vs cirrhotic livers as visualized by immunohistochemistry. Human liver biopsies of normal healthy or cirrhotic livers stained with anti-human TAZ antibody (1/25 dilution, Sigma HPA039557) and detected using a Biocare MACH4 Universal HRP polymer kit, followed by chromogen exposure. Immunohistochemical stains were performed by the University Health Network (UHN) Pathology Research Program core laboratory. Arrows show immune cells stained with TAZ. Scale bars are 100µm.

4.2 Results

4.2.1 DC-specific YAP and TAZ deletion does not affect proportion and numbers of myeloid cell populations in the liver at steady-state

Previous work has demonstrated that BMDCs under increased mechanical stress upregulate the expression of TAZ[66], and is associated with increased YAP and TAZ nuclear translocation. In addition, at steady-state, our lab has demonstrated there are no significant alterations in DC subsets in the spleens and lungs of mice with CD11c-specific deletion of YAP and/or TAZ[212]. In my project, I examined an additional organ, the liver, as it is one of the key metabolic organs affected by IR and obesity-associated inflammation[60]. I began by investigating the role of YAP/TAZ in liver DCs at steady state, followed by immune characterization of livers in mice with diet-induced NAFLD.

As the $YAP^{DC\text{-}KO}$, $TAZ^{DC\text{-}KO}$, and $YAP/TAZ^{DC\text{-}DKO}$ mice we generated were novel mouse models, I first confirmed the efficiency of *Yap* and *Taz* ablation in DCs. Floxing efficiency was confirmed by RT-qPCR using *Yap1* exon 2 and *Wwtr1* exon 2-specific primers in cultured BMDCs from $YAP^{DC\text{-}KO}$, $TAZ^{DC\text{-}KO}$, and $YAP/TAZ^{DC\text{-}DKO}$ mice vs controls. *Yap1* expression was reduced by 50% and 80% in $YAP^{DC\text{-}KO}$ and $YAP/TAZ^{DC\text{-}DKO}$ mice respectively (**Figure 4.2 A, C),** while *Wwtr1* expression was reduced by 75% both $TAZ^{DC\text{-}KO}$ and $YAP/TAZ^{DC\text{-}DKO}$ mice **(Figure 4.2 B, D).** Thus, I ascertained functional floxing of both *Yap1* and *Wwtr1* genes in DCs, to various extents, in our mouse models.

Previous work in our lab demonstrated no significant differences in the number of cDCs in the spleen and lung of $YAP^{DC\text{-}KO}$, $TAZ^{DC\text{-}KO}$, and $YAP/TAZ^{DC\text{-}DKO}$ mice, suggesting that deletion of YAP and/or TAZ in DCs does not affect DC development in the spleen and lungs. As I aimed to investigate how YAP and TAZ in DCs could contribute to obesity-associated inflammation and the development of NAFLD, I assessed whether YAP and/or TAZ deletion affected the development of DCs and steady state levels of immune cell populations in the liver. Frequencies and numbers of myeloid cell populations (polymorphonuclear leukocytes (PMNs), monocytes, macrophages, and DCs) in the livers of $YAP^{DC\text{-}KO}$, $TAZ^{DC\text{-}KO}$, and $YAP/TAZ^{DC\text{-}DKO}$ mice were quantified and compared with $CD11cCre^{-}$ negative littermate controls. In these experiments, 8-12-week-old female mice were euthanized, and the liver was dissected. The livers

were processed into single cell suspensions, which were stained with fluorescently conjugated antibodies for flow cytometric analysis (summarized in **Table 4.1**).

In mice with DC-specific deficiency of YAP, there were no significant differences in the frequency and number of $CD45^+$ cells, PMNs and monocytes in the liver compared to $CD11cCre^-$ controls **(Figure 4.3 A-F)**. I also assessed the frequency and number of different subsets of macrophages in the liver**.** In the liver, there are two major populations of hepatic macrophages: Kupffer cells (KC) and monocyte-derived macrophages (MdM). KCs are liver resident macrophages important for maintaining homeostasis of the liver, while MdMs can be differentiated from circulating monocytes that rapidly infiltrate the liver in response to injury[213]. They can be distinguished from each other based on differential expression of CD11b[214], an integrin molecule that is involved in cell migration and adhesion. MdMs express high levels of CD11b ($CD11b^{hi}$), while KCs express low levels of CD11b ($CD11b^{lo}$)[214]. Also, a subset of MdMs express CD11c, while KCs do not[215]. In $YAP^{DC\text{-}KO}$ mice, there were no significant differences in the frequency and normalized numbers of both subsets of macrophages in the liver (**Figure 4.3 G, H)** compared to $YAP^{DC\text{-}WT}$ mice. When calculating the ratio of MdMs to KCs, there was also no significant difference between the two groups **(Figure 4.3 I)**. I also examined whether the loss of YAP in $CD11c^+$ cells would impact the number of cDCs in the liver, as this is one of the main cell types in which YAP is ablated. cDCs express high levels of MHC II and CD11c, and are further categorized into two main populations: cDC1 and cDC2[16]. In mice with DC-specific deletion of YAP, there were comparable frequencies and numbers of both cDC1s and cDC2s with control mice **(Figure 4.3 J, K)**. Altogether, these data demonstrate that genetic deletion of YAP in DCs does not affect the proportions and numbers of myeloid cell populations in the liver at steady-state. Similarly, mice with DC-specific deletion of TAZ did not show significant differences in the proportion and number of $CD45^+$ cells, PMNs, monocytes, macrophage subsets and cDCs in the liver compared to controls **(Figure 4.4 A-K)**. Overall, at steady-state, genetic deletion of TAZ in DCs does not affect the composition of myeloid cell populations in the liver of adult mice.

As TAZ is a homologue of YAP with similar functionality, it is plausible that TAZ is compensating for YAP deficiency, and YAP may be compensating for TAZ deficiency. To better

characterize the role of YAP and TAZ in DC function, I characterized myeloid cell populations in the liver of mice with DC-specific knockout of both YAP and TAZ (YAP/TAZ$^{DC\text{-}DKO}$). There was no significant difference in the proportion and number of CD45^{+} cells and PMNs in the liver of YAP/TAZ$^{DC\text{-}DKO}$ mice compared to controls (**Figure 4.5 A-D**). There was a trending increase in the proportion of monocytes in the liver of YAP/TAZ$^{DC\text{-}DKO}$ mice, but no differences in terms of numbers (**Figure 4.5 E, F**). Interestingly, while the proportion and number of KCs were not significantly different between the two groups, there was a significant decrease in the proportion of MdMs in YAP/TAZ$^{DC\text{-}DKO}$ mice compared to CD11cCre^{-} controls **(Figure 4.5 G)**. In addition, there was a trending decrease in the number of MdMs, and a significant reduction in the ratio of MdMs to KCs **(Figure 4.5 I)**. Although there were no differences in the frequency of cDC1s and cDC2s (**Figure 4.5 J)**, there was a decrease in the number of cDC1s and cDC2s in YAP/TAZ$^{DC\text{-}DKO}$ mice (**Figure 4.5 K)**. Altogether, these data suggest that YAP and TAZ deficiency in CD11c^{+} cells does not alter the basal frequencies and numbers of PMNs and monocytes, but decreases in the number of MdMs, and cDCs in the livers of adult mice. As DCs and some MdMs express CD11c, this suggests that YAP and TAZ deficiency may play a role in the development or migration of these populations in the liver.

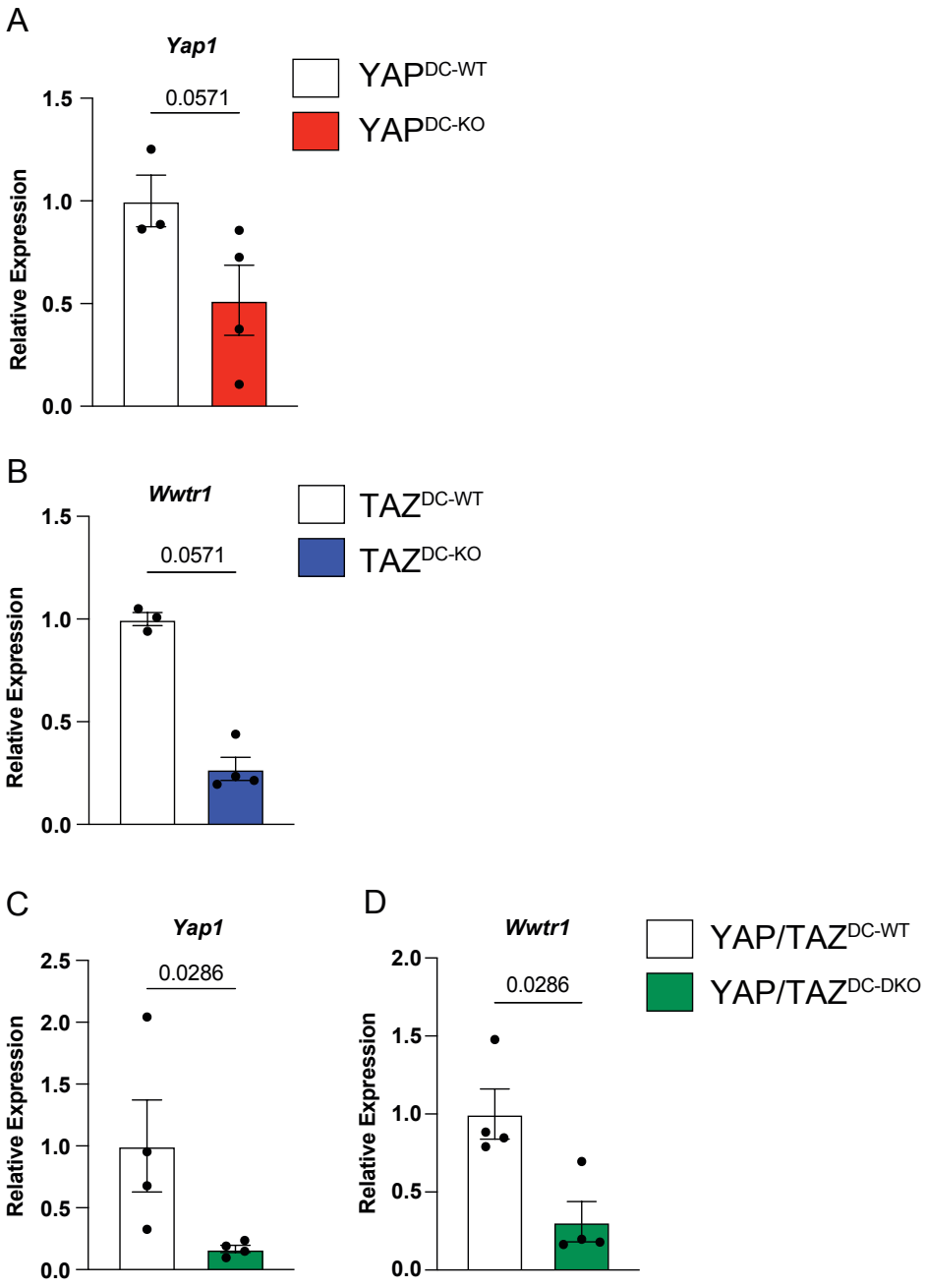

Figure 4.2 Real-time PCR-based assessment of *Yap1* and *Wwtr1* genetic ablation in BMDCs in YAP^{DC-KO}, TAZ^{DC-KO}, and YAP/TAZ^{DC-DKO} mice. (A) Gene expression of *Yap1* in cultured BMDCs from YAP^{DC-KO} mice. **(B)** Gene expression of *Wwtr1* in cultured BMDCs from TAZ^{DC-KO} mice. Gene expression of *Yap1* **(C)** and *Wwtr1* **(D)** in cultured BMDCs from YAP/TAZ^{DC-DKO} mice. P-values are calculated using Mann-Whitney U test. Data are shown as averages of triplicates from individual mice (dots) and mean ± SEM.

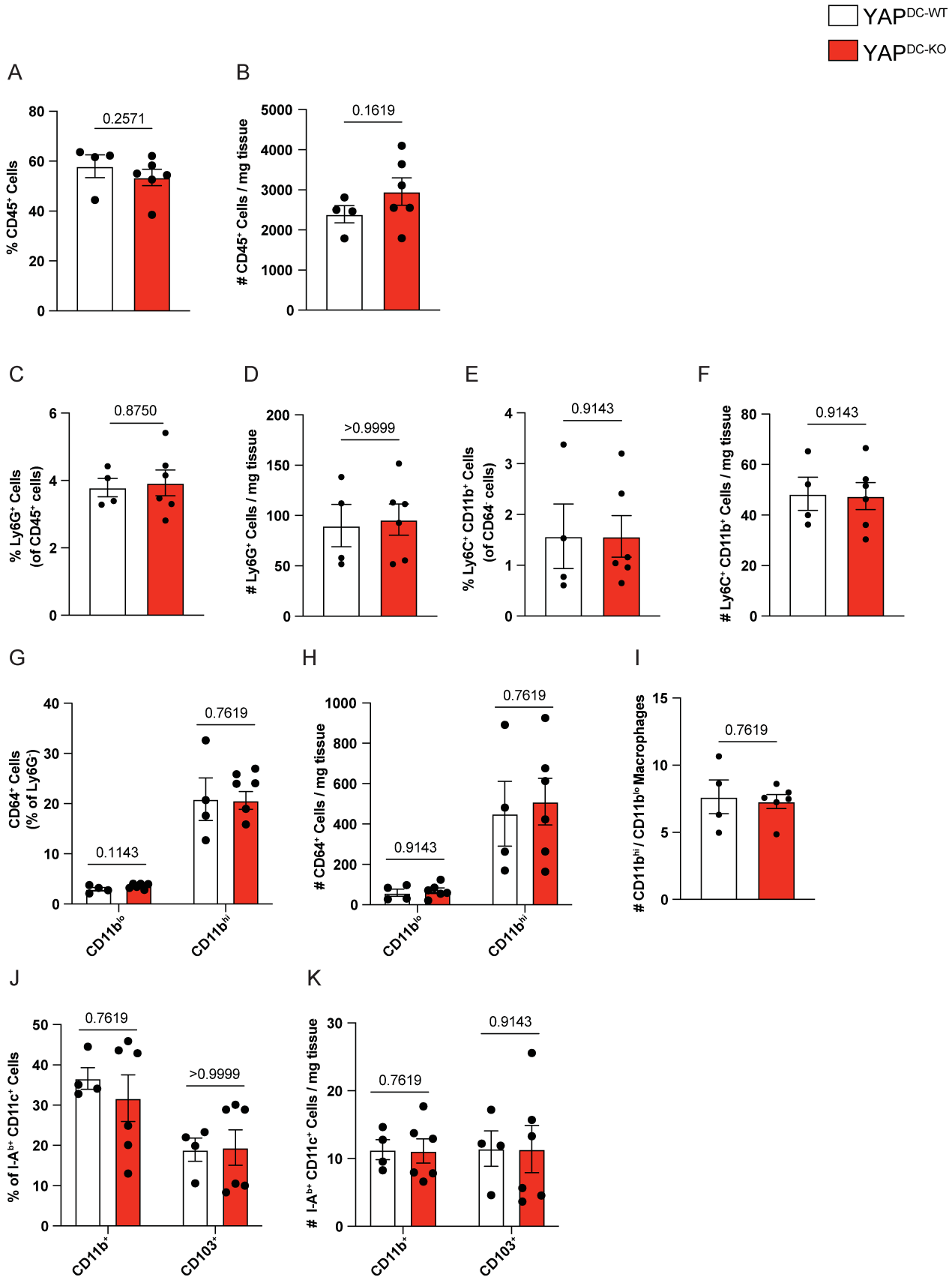
YAP^DC-WT
YAP^DC-KO
A
% CD45⁺ Cells
0.2571
B
CD45⁺ Cells / mg tissue
0.1619
C
% Ly6G⁺ Cells (of CD45⁺ cells)
0.8750
D
Ly6G⁺ Cells / mg tissue
>0.9999
E
% Ly6C⁺ CD11b⁺ Cells (of CD64⁻ cells)
0.9143
F
Ly6C⁺ CD11b⁺ Cells / mg tissue
0.9143
G
CD64⁺ Cells (% of Ly6G⁻)
0.1143
0.7619
CD11b^lo
CD11b^hi
H
CD64⁺ Cells / mg tissue
0.9143
0.7619
CD11b^lo
CD11b^hi
I
CD11b^hi / CD11b^lo Macrophages
0.7619
J
% of I-A^b+ CD11c⁺ Cells
0.7619
>0.9999
CD11b⁺
CD103⁺
K
I-A^b+ CD11c⁺ Cells / mg tissue
0.7619
0.9143
CD11b⁺
CD103⁺

Figure 4.3 DC-specific YAP deletion does not affect proportion and numbers of myeloid cell populations in the liver at steady-state. 8-12-week-old $YAP^{DC\text{-}KO}$ (n=6) or $YAP^{DC\text{-}WT}$ (n=4) female mice were euthanized, and the liver was dissected. The livers were processed into single cell suspensions and stained with fluorescently conjugated antibodies for flow cytometric analysis. Number of cells was quantified and normalized to mg of tissue digested. Graphs show data points from one experiment. **(A-B)** Frequency and number of $CD45^+$ cells. **(C-D)** Frequency and number of PMNs, gated from $Ly6G^+$ cells. **(E-F)** Frequency and number of monocytes, gated from $CD64^-$ $Ly6C^+$ $CD11b^+$ cells. **(G-H)** Frequency and number of KCs ($CD11b^{lo}$) and MdMs ($CD11b^{hi}$), gated from $CD64^+$ $Ly6G^-$ cells. **(I)** Ratio of MdMs : KCs. **(J-K)** Frequency and number of cDC1 ($CD103^+$) and cDC2 ($CD11b^+$), gated from $CD64^-$ $I\text{-}A^{b+}$ $CD11c^+$ cells. P-values are calculated using Mann-Whitney U test. Data are shown as individual mice (dots) and mean ± SEM.

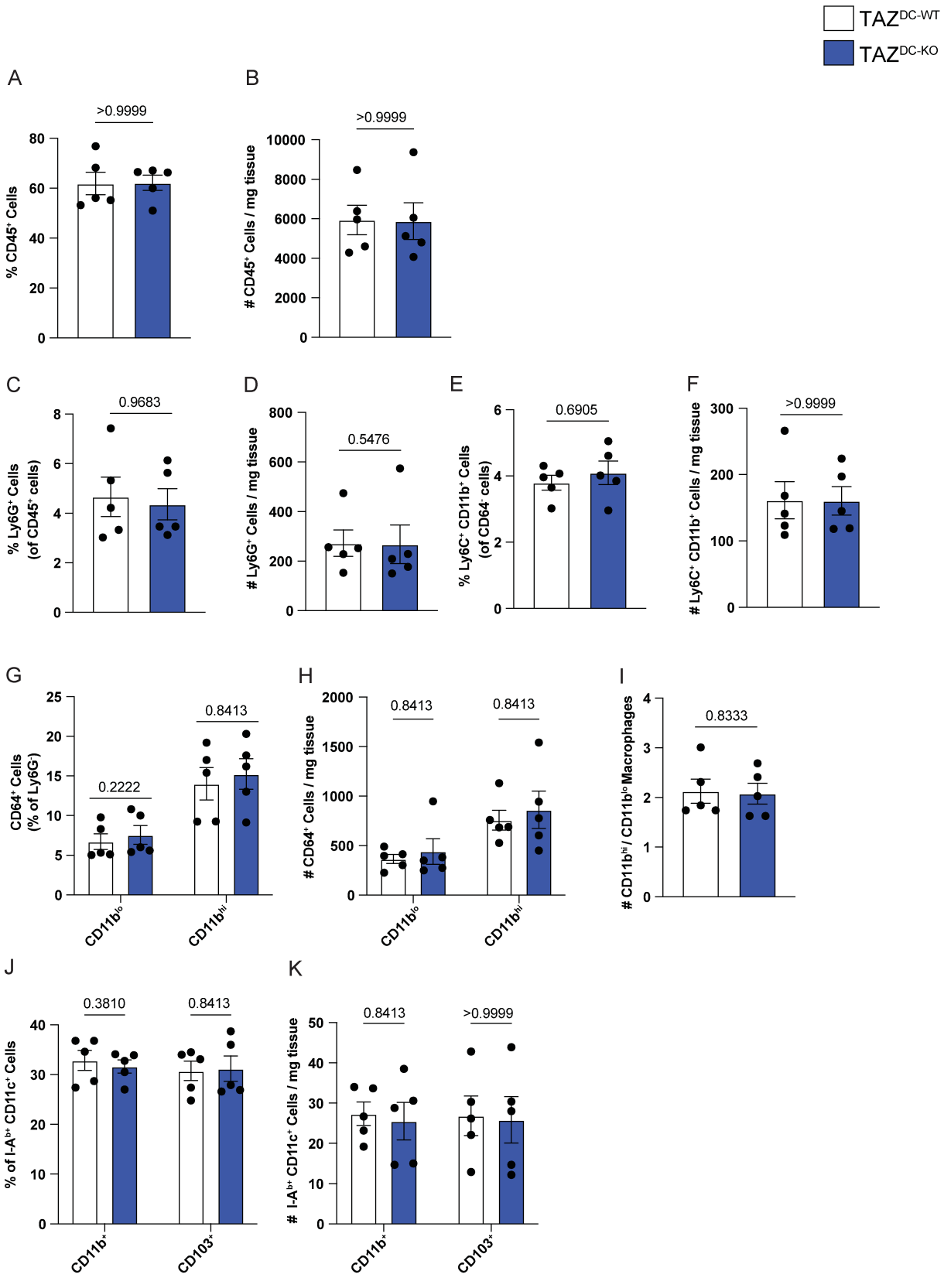
TAZDC-WT
TAZDC-KO
A
>0.9999
% CD45+ Cells
B
>0.9999
CD45+ Cells / mg tissue
C
0.9683
% Ly6G+ Cells (of CD45+ cells)
D
0.5476
Ly6G+ Cells / mg tissue
E
0.6905
% Ly6C+ CD11b+ Cells (of CD64- cells)
F
>0.9999
Ly6C+ CD11b+ Cells / mg tissue
G
0.2222
0.8413
CD64+ Cells (% of Ly6G-)
CD11blo
CD11bhi
H
0.8413
0.8413
CD64+ Cells / mg tissue
CD11blo
CD11bhi
I
0.8333
CD11bhi / CD11blo Macrophages
J
0.3810
0.8413
% of I-Ab+ CD11c+ Cells
CD11b+
CD103+
K
0.8413
>0.9999
I-Ab+ CD11c+ Cells / mg tissue
CD11b+
CD103+

Figure 4.4 DC-specific TAZ deletion does not affect proportion and numbers of myeloid cell populations in the liver at steady-state. 8-12-week-old $TAZ^{DC\text{-}KO}$ (n=5) or $TAZ^{DC\text{-}WT}$ (n=5) female mice were euthanized, and the liver was dissected. The livers were processed into single cell suspensions and stained with fluorescently conjugated antibodies for flow cytometric analysis. Number of cells was quantified and normalized to mg of tissue digested. Graphs show data points from one experiment. **(A-B)** Frequency and number of $CD45^+$ cells. **(C-D)** Frequency and number of PMNs, gated from $Ly6G^+$ cells. **(E-F)** Frequency and number of monocytes, gated from $CD64^-$ $Ly6C^+$ $CD11b^+$ cells. **(G-H)** Frequency and number of KCs ($CD11b^{lo}$) and MdMs ($CD11b^{hi}$), gated from $CD64^+$ $Ly6G^-$ cells. **(I)** Ratio of MdMs : KCs. **(J-K)** Frequency and number of cDC1 ($CD103^+$) and cDC2 ($CD11b^+$), gated from $CD64^-$ $I\text{-}A^{b+}$ $CD11c^+$ cells. P-values are calculated using Mann-Whitney U test. Data are shown as individual mice (dots) and mean ± SEM.

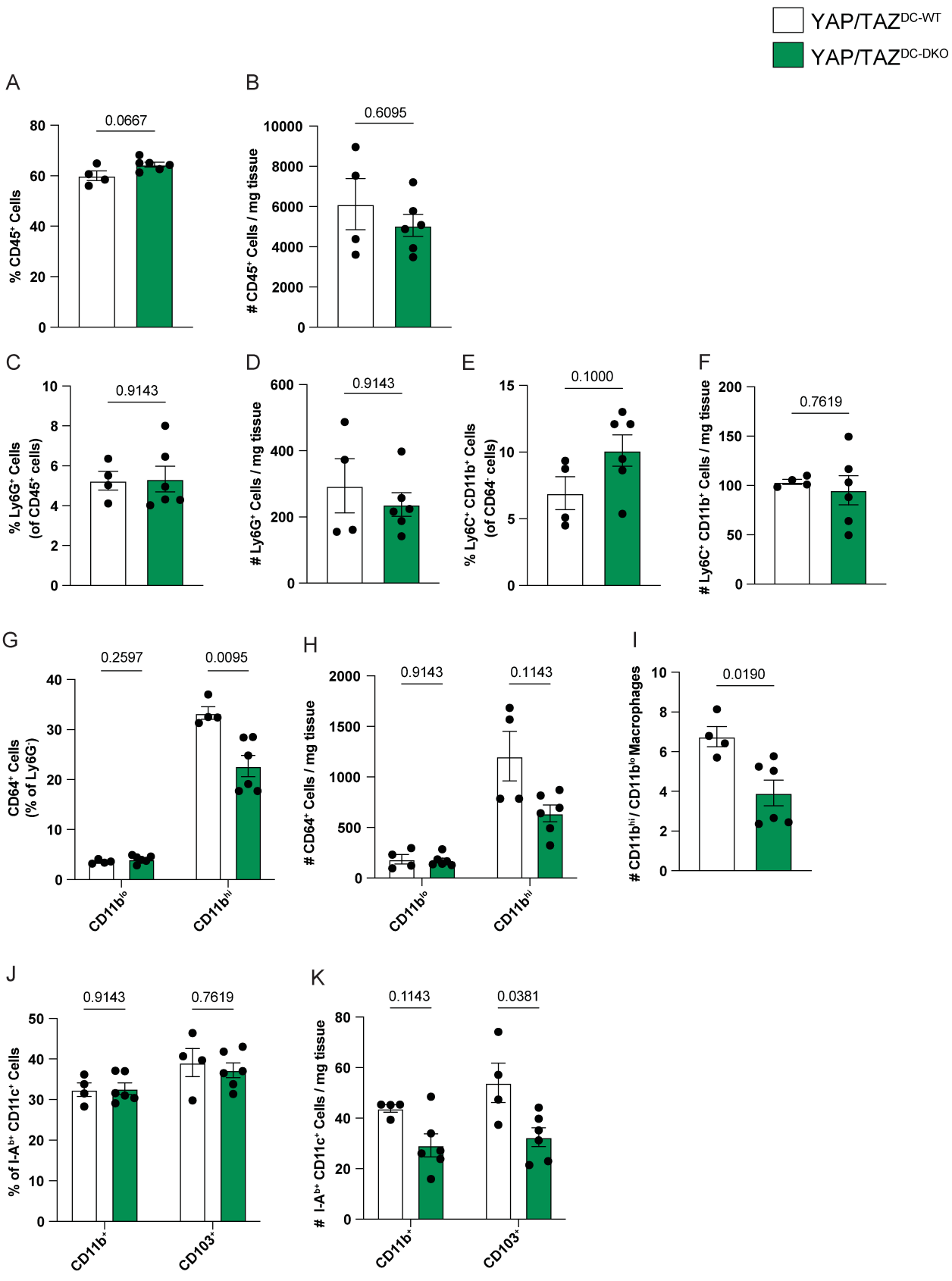
YAP/TAZDC-WT
YAP/TAZDC-DKO
A
% CD45+ Cells
0.0667
B
CD45+ Cells / mg tissue
0.6095
C
% Ly6G+ Cells (of CD45+ cells)
0.9143
D
Ly6G+ Cells / mg tissue
0.9143
E
% Ly6C+ CD11b+ Cells (of CD64- cells)
0.1000
F
Ly6C+ CD11b+ Cells / mg tissue
0.7619
G
CD64+ Cells (% of Ly6G-)
0.2597
0.0095
CD11blo
CD11bhi
H
CD64+ Cells / mg tissue
0.9143
0.1143
CD11blo
CD11bhi
I
CD11bhi / CD11blo Macrophages
0.0190
J
% of I-Ab+ CD11c+ Cells
0.9143
0.7619
CD11b+
CD103+
K
I-Ab+ CD11c+ Cells / mg tissue
0.1143
0.0381
CD11b+
CD103+

Figure 4.5 DC-specific YAP and TAZ decreases the proportion of MdMs and number of cDCs in the liver at steady-state. 8-12-week-old YAP/TAZ$^{DC\text{-}DKO}$ (n=6) or YAP/TAZ$^{DC\text{-}WT}$ (n=4) female mice were euthanized, and the liver was dissected. The livers were processed into single cell suspensions and stained with fluorescently conjugated antibodies for flow cytometric analysis. Number of cells was quantified and normalized to mg of tissue digested. Graphs show data points from one experiment. **(A-B)** Frequency and number of CD45^{+} cells. **(C-D)** Frequency and number of PMNs, gated from Ly6G^{+} cells. **(E-F)** Frequency and number of monocytes, gated from CD64^{-} Ly6C^{+} CD11b^{+} cells. **(G-H)** Frequency and number of KCs (CD11b^{lo}) and MdMs (CD11b^{hi}), gated from CD64^{+} Ly6G^{-} cells. **(I)** Ratio of MdMs : KCs. **(J-K)** Frequency and number of cDC1 (CD103^{+}) and cDC2 (CD11b^{+}), gated from CD64^{-} I-A^{b+} CD11c^{+} cells. P-values are calculated using Mann-Whitney U test. Data are shown as individual mice (dots) and mean ± SEM.

Table 4.1 Changes in frequency and numbers of immune cell populations in the liver of $YAP^{DC\text{-}KO}$, $TAZ^{DC\text{-}KO}$, and $YAP/TAZ^{DC\text{-}DKO}$ mice relative to controls at steady-state. (**ø** = no difference; - = decrease; + = increase) (Trending: º; Significant: *p < 0.05. **p < 0.01.)

Liver	**$YAP^{DC\text{-}KO}$**		**$TAZ^{DC\text{-}KO}$**		**$YAP/TAZ^{DC\text{-}DKO}$**	
Cells	**%**	**#**	**%**	**#**	**%**	**#**
$CD45^+$	**ø**	**ø**	**ø**	**ø**	**ø**	**ø**
PMNs	**ø**	**ø**	**ø**	**ø**	**ø**	**ø**
Monocytes	**ø**	**ø**	**ø**	**ø**	**+º**	**ø**
KCs	**ø**	**ø**	**ø**	**ø**	**ø**	**ø**
MdMs	**ø**	**ø**	**ø**	**ø**	**-****	**-º**
KCs/KC ratio	**N/A**	**ø**	**N/A**	**ø**	**N/A**	**-***
cDC1	**ø**	**ø**	**ø**	**ø**	**ø**	**-***
cDC2	**ø**	**ø**	**ø**	**ø**	**ø**	**-º**

4.2.2 DC-specific YAP and/or TAZ deletion do not affect the development of insulin resistance in HFHS-treated mice

Obesity is linked to the development of IR through various mechanisms, including elevated levels of proinflammatory cytokines. Increased production of TNFα by immune cells such as macrophages and DCs activates serine kinases, which can impair INSR signalling[58]. Interestingly, evidence suggests that DCs cultured on stiffer substrates leads to increased production of TNFα, which is also associated with increased TAZ expression[66]. In addition, inhibition of YAP/TAZ activity abrogates stiffness-mediated increase of pro-inflammatory cytokine production by DCs[66], suggesting that YAP and TAZ signalling in DCs enhances their pro-inflammatory function. During obesity, there is an increase in nutrient signals and alterations in tissue stiffness in various tissues such as the liver[64], which could potentially influence YAP/TAZ signalling in cells. This suggests that obesity can enhance YAP and TAZ activity in cells such as DCs, and augment inflammation. As obesity-associated chronic inflammation is linked to IR, we hypothesized that genetic ablation of YAP and/or TAZ in DCs would hinder the development of IR.

To address whether knockout of YAP and/or TAZ in DCs impacts the development of obesity-linked IR, $YAP^{DC\text{-}KO}$, $TAZ^{DC\text{-}KO}$ and $YAP/TAZ^{DC\text{-}DKO}$ male mice were fed a 60kcal% HFD for 20 weeks starting from 6 weeks of age, supplemented with 42 g/L of sucrose water (High Fat High Sucrose regimen; HFHS). I used this model to induce IR because initial studies using a DIO model did not cause IR in the mice until past 20 weeks of feeding. In addition, I wanted to assess the progression of NAFLD, as supplementation with sucrose water can induce pathology associated with NAFLD[216]. In addition, age-matched $YAP^{DC\text{-}KO}$ and $YAP^{DC\text{-}WT}$, $TAZ^{DC\text{-}KO}$ and $TAZ^{DC\text{-}WT}$, and $YAP/TAZ^{DC\text{-}DKO}$ and $YAP/TAZ^{DC\text{-}WT}$ male mice fed a 10kcal% NCD were used as baseline controls to determine whether YAP and/or TAZ deletion could ameliorate obesity-induced IR. Results from NCD $YAP^{DC\text{-}WT}$ and $YAP^{DC\text{-}KO}$ mice were pooled together and represented as NCD when comparing with HFHS $YAP^{DC\text{-}KO}$ mice, as analyses did not indicate any significant differences between genotypes. Similarly, NCD $TAZ^{DC\text{-}KO}$ and $TAZ^{DC\text{-}WT}$ results were pooled together, and $YAP/TAZ^{DC\text{-}DKO}$ and $YAP/TAZ^{DC\text{-}WT}$ results were pooled as they did not exhibit any differences between genotypes.

To assess responses to exogenous insulin and insulin sensitivity, I conducted an ITT, followed by an IPGTT a week apart to measure glucose tolerance and the ability to produce and respond to endogenous insulin. Compared to NCD-fed mice, the HFHS treated mice exhibited significantly higher body weights **(Figure 4.6, 4.7, 4.8 A)**. Prior to conducting ITT and IPGTT, mice are fasted to provide stable baseline measurements of blood glucose levels[217]. The fasting blood glucose levels prior to the ITT in NCD-fed mice were significantly lower compared to HFHS-treated mice **(Figure 4.6, 4.7, 4.8 B)**. Interestingly, there was a small but significant increase in fasting blood glucose levels in HFHS $YAP^{DC\text{-}KO}$ mice compared to HFHS $YAP^{DC\text{-}WT}$ controls after 6 hours of fasting (**Figure 4.6 B**), but deletion of TAZ, and of both YAP and TAZ in DCs did not lead to any significant differences in fasting blood glucose levels **(Figure 4.7, 4.8 B)**. In response to an insulin challenge, the NCD mice showed a significant reduction in their blood glucose levels compared to all HFHS treated mice, indicating a normal response to insulin **(Figure 4.6, 4.7, 4.8 C, D)**. However, CD11c-targeted deletion of YAP and/or TAZ did not lead to any differences in their sensitivity to insulin compared to controls after a HFHS regimen, which was quantified as an integrated area above the curve (AAC) over the 120 min of the ITT (**Figure 4.6, 4.7, 4.8 D)**. Prior to conducting the IPGTT, NCD-fed mice showed significantly lower fasting blood glucose levels compared to the HFHS mice after 16 hours of fasting (**Figure 4.6, 4.7, 4.8 E**), but comparisons between the HFHS treated mice did not show any differences. After HFHS regimens, CD11c-specific deletion of YAP, and double deletion of YAP and TAZ did not affect tolerance to glucose, which was quantified as integrated area under the curve (AUC) over the 120 min of the IPGTT (**Figure 4.6, 4.8 G)**. There was a trending decrease in glucose excursion in HFHS $TAZ^{DC\text{-}KO}$ mice compared to HFHS $TAZ^{DC\text{-}WT}$ mice during the IPGTT **(Figure 4.7 F**), however not significant. Altogether, these findings suggested that deletion of YAP and/or TAZ in $CD11c^{+}$ cells does not affect the development of obesity-associated IR in HFHS-treated mice.

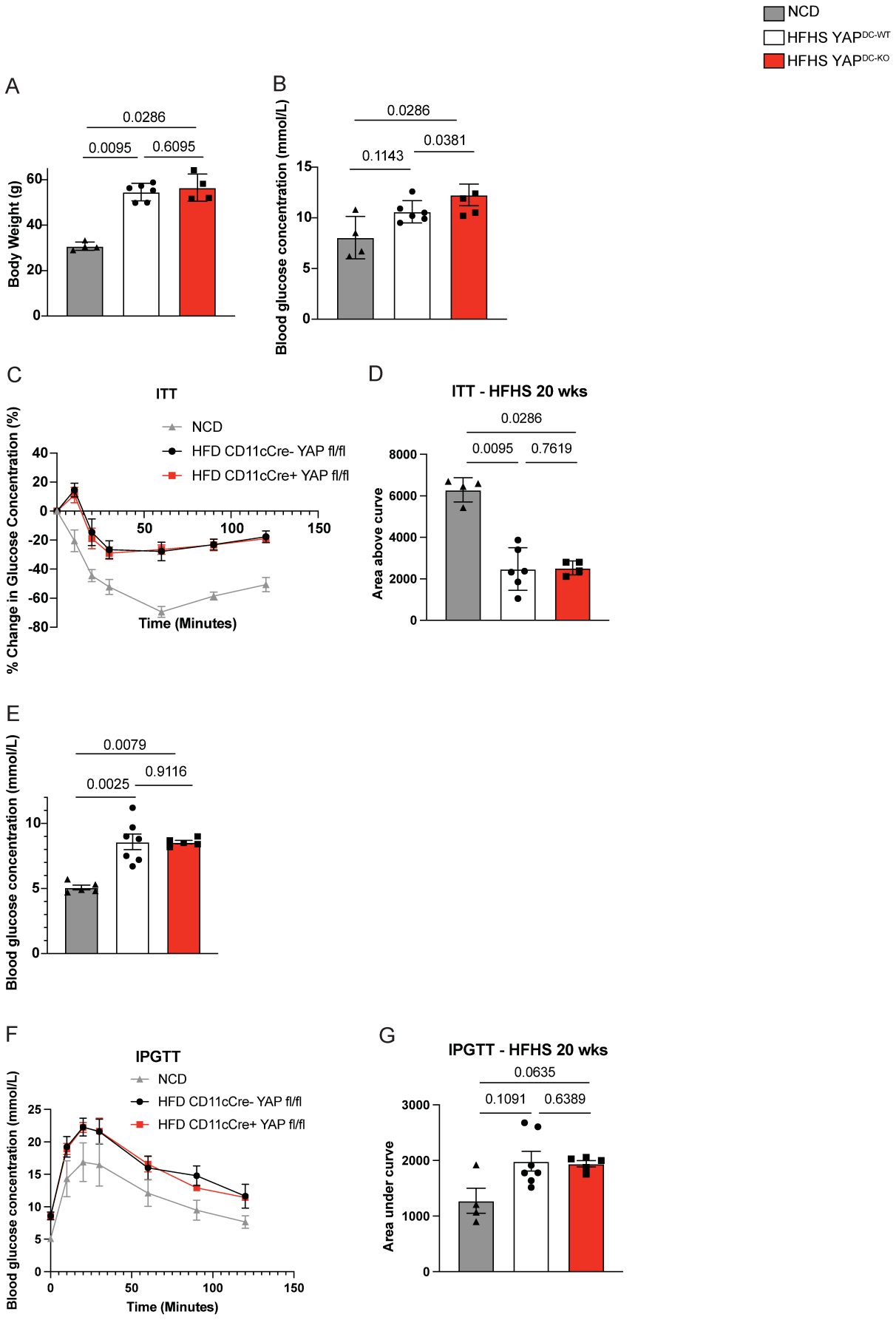
NCD
HFHS YAPDC-WT
HFHS YAPDC-KO
A
0.0286
0.0095
0.6095
Body Weight (g)
B
0.0286
0.1143
0.0381
Blood glucose concentration (mmol/L)
C
ITT
NCD
HFD CD11cCre- YAP fl/fl
HFD CD11cCre+ YAP fl/fl
% Change in Glucose Concentration (%)
Time (Minutes)
D
ITT - HFHS 20 wks
0.0286
0.0095
0.7619
Area above curve
E
0.0079
0.0025
0.9116
Blood glucose concentration (mmol/L)
F
IPGTT
NCD
HFD CD11cCre- YAP fl/fl
HFD CD11cCre+ YAP fl/fl
Blood glucose concentration (mmol/L)
Time (Minutes)
G
IPGTT - HFHS 20 wks
0.0635
0.1091
0.6389
Area under curve

Figure 4.6 DC-specific YAP deletion does not affect the development of insulin resistance in HFHS-treated mice. $YAP^{DC\text{-}KO}$ (n=4-5) or $YAP^{DC\text{-}WT}$ (n=6) male mice were fed a 60kcal% HFD for 20 weeks starting from 6 weeks of age, supplemented with 42 g/L of sucrose water. Age-matched NCD $YAP^{DC\text{-}WT}$ and $YAP^{DC\text{-}KO}$ mice were used as baseline controls, and results were pooled together and represented as NCD (n=4). **(A)** Body weight of NCD or HFHS-treated mice $YAP^{DC\text{-}KO}$ and $YAP^{DC\text{-}WT}$ mice. **(B)** Blood glucose levels after 6 hours of fasting. **(C)** Glucose excursion during an ITT. Blood glucose is expressed as a percent change in blood glucose from time point 0. **(D)** Integrated area above the curve (AAC) during an ITT (n=4-6). **(E)** Blood glucose levels after 16 hours of fasting. **(F)** Glucose excursion during an IPGTT. **(G)** Integrated area under the curve (AUC) of glucose excursion during an 120-min IPGTT (n=4-7). P-values are calculated using Mann-Whitney U test. Data are shown as individual mice (dots) and mean ± SEM.

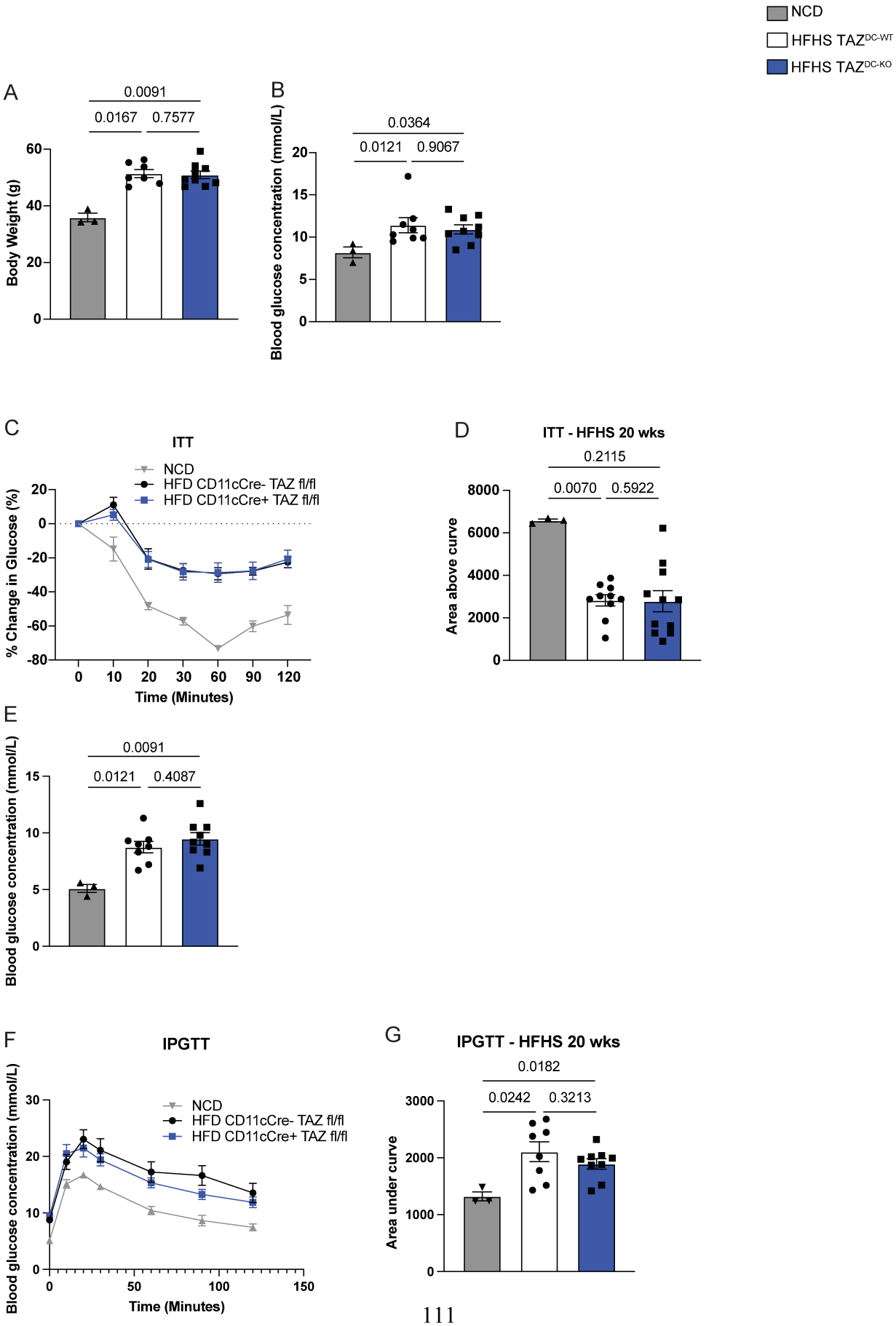
NCD
HFHS TAZDC-WT
HFHS TAZDC-KO
A
0.0091
0.0167
0.7577
Body Weight (g)
60
40
20
0
B
0.0364
0.0121
0.9067
Blood glucose concentration (mmol/L)
20
15
10
5
0
C
ITT
NCD
HFD CD11cCre- TAZ fl/fl
HFD CD11cCre+ TAZ fl/fl
% Change in Glucose (%)
20
0
-20
-40
-60
-80
0
10
20
30
60
90
120
Time (Minutes)
D
ITT - HFHS 20 wks
0.2115
0.0070
0.5922
Area above curve
8000
6000
4000
2000
0
E
0.0091
0.0121
0.4087
Blood glucose concentration (mmol/L)
15
10
5
0
F
IPGTT
NCD
HFD CD11cCre- TAZ fl/fl
HFD CD11cCre+ TAZ fl/fl
Blood glucose concentration (mmol/L)
30
20
10
0
0
50
100
150
Time (Minutes)
G
IPGTT - HFHS 20 wks
0.0182
0.0242
0.3213
Area under curve
3000
2000
1000
0

Figure 4.7 DC-specific TAZ deletion does not affect the development of insulin resistance in HFHS-treated mice. $TAZ^{DC\text{-}KO}$ (n=9-11) or $TAZ^{DC\text{-}WT}$ (n=7-10) male mice were fed a 60kcal% HFD for 20 weeks starting from 6 weeks of age, supplemented with 42 g/L of sucrose water. Age-matched NCD $TAZ^{DC\text{-}WT}$ and $TAZ^{DC\text{-}KO}$ mice were used as baseline controls, and results were pooled together and represented as NCD (n=3). **(A)** Body weight of NCD or HFHS-treated mice $TAZ^{DC\text{-}KO}$ and $TAZ^{DC\text{-}WT}$ mice. **(B)** Blood glucose levels after 6 hours of fasting. **(C)** Glucose excursion during an ITT. Blood glucose is expressed as a percent change in blood glucose from time point 0. **(D)** Integrated area above the curve (AAC) during an ITT (n=3-11). **(E)** Blood glucose levels after 16 hours of fasting. **(F)** Glucose excursion during an IPGTT. **(G)** Integrated area under the curve (AUC) of glucose excursion during an 120-min IPGTT (n=3-9). P-values are calculated using Mann-Whitney U test. Data are shown as individual mice (dots) and mean ± SEM.

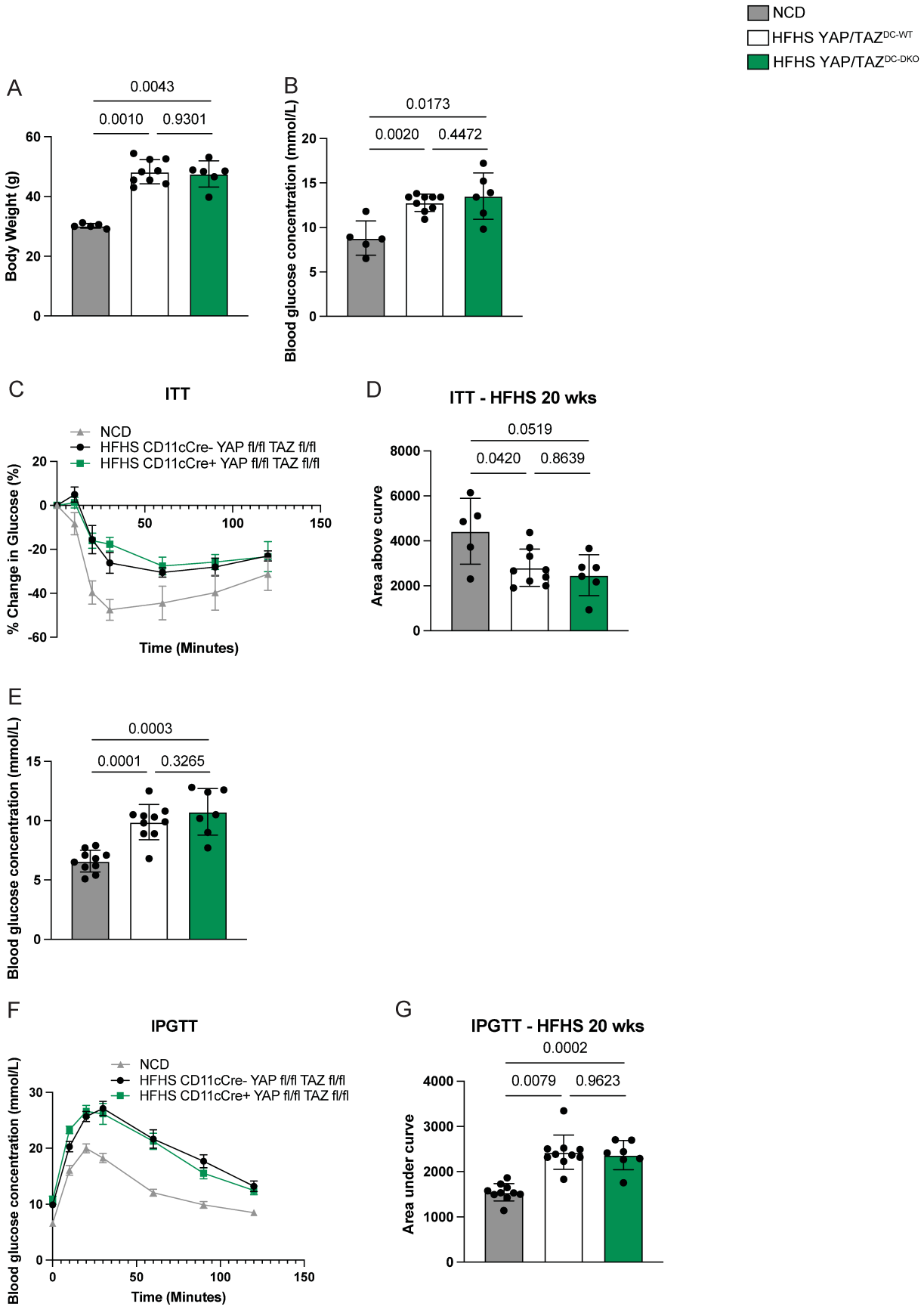
NCD
HFHS YAP/TAZDC-WT
HFHS YAP/TAZDC-DKO
A
0.0043
0.0010
0.9301
Body Weight (g)
B
0.0173
0.0020
0.4472
Blood glucose concentration (mmol/L)
C
ITT
NCD
HFHS CD11cCre- YAP fl/fl TAZ fl/fl
HFHS CD11cCre+ YAP fl/fl TAZ fl/fl
% Change in Glucose (%)
Time (Minutes)
D
ITT - HFHS 20 wks
0.0519
0.0420
0.8639
Area above curve
E
0.0003
0.0001
0.3265
Blood glucose concentration (mmol/L)
F
IPGTT
NCD
HFHS CD11cCre- YAP fl/fl TAZ fl/fl
HFHS CD11cCre+ YAP fl/fl TAZ fl/fl
Blood glucose concentration (mmol/L)
Time (Minutes)
G
IPGTT - HFHS 20 wks
0.0002
0.0079
0.9623
Area under curve

Figure 4.8 DC-specific YAP and TAZ deletion does not affect the development of insulin resistance in HFHS-treated mice. YAP/TAZ$^{DC\text{-}DKO}$ (n=6-7) or YAP/TAZ$^{DC\text{-}WT}$ (n=9-10) male mice were fed a 60kcal% HFD for 20 weeks starting from 6 weeks of age, supplemented with 42 g/L of sucrose water. Age-matched NCD YAP/TAZ$^{DC\text{-}WT}$ and YAP/TAZ$^{DC\text{-}DKO}$ mice were used as baseline controls, and results were pooled together and represented as NCD (n=5-10). **(A)** Body weight of NCD or HFHS-treated mice YAP/TAZ$^{DC\text{-}KO}$ and YAP/TAZ$^{DC\text{-}WT}$ mice. **(B)** Blood glucose levels after 6 hours of fasting. **(C)** Glucose excursion during an ITT. Blood glucose is expressed as a percent change in blood glucose from time point 0. **(D)** Integrated area above the curve (AAC) during an ITT (n=5-9). **(E)** Blood glucose levels after 16 hours of fasting. **(F)** Glucose excursion during an IPGTT. **(G)** Integrated area under the curve (AUC) of glucose excursion during an 120-min IPGTT (n=7-10). P-values are calculated using Mann-Whitney U test. Data are shown as individual mice (dots) and mean ± SEM.

4.2.3 Deletion of YAP and/or TAZ in CD11c$^+$ cells do not affect levels of myeloid cells in the liver of HFHS-treated mice

In my investigation of the development of obesity-related IR, I observed that CD11c-targeted deletion of YAP and/or TAZ did not lead to any significant differences in insulin sensitivity and glucose tolerance compared to controls. Although there were no differences in insulin and glucose tolerance, I wanted to determine whether deletion of YAP and TAZ in CD11c$^+$ cells affects inflammation in the liver and VAT that is observed during obesity, as inflammation in the VAT is a main driver for systemic inflammation observed in obese conditions, and hepatic inflammation is an indication for the progression of NAFLD[218]. Increased inflammation in the liver can aggravate the process of fibrosis, and thus facilitate the progression of simple steatosis to nonalcoholic steatohepatitis and fibrosis[219]. As previous studies have suggested that YAP and TAZ signalling in DCs enhances their production of pro-inflammatory cytokines[66], I hypothesized that the knockout of YAP and/or TAZ in DCs would decrease levels of pro-inflammatory immune cell infiltrates in the liver and VAT.

Following the ITT and IPGTT, HFHS YAP$^{DC\text{-}KO}$, TAZ$^{DC\text{-}KO}$, and YAP/TAZ$^{DC\text{-}DKO}$ mice and their appropriate controls were euthanized, and liver and VAT were collected. To characterize the levels of inflammation under HFHS conditions, I quantified levels of immune cell infiltration in the liver and VAT, as well as T cell production of IFNγ, TNFα, and IL-17 via flow cytometry (summarized in Table 4.2 and Table 4.3). In addition, I compared the HFHS-treated groups to NCD YAP$^{DC\text{-}WT}$ and YAP$^{DC\text{-}KO}$, TAZ$^{DC\text{-}WT}$ and TAZ$^{DC\text{-}KO}$, YAP/TAZ$^{DC\text{-}WT}$ and YAP/TAZ$^{DC\text{-}DKO}$ mice respectively as controls. Results from NCD YAP$^{DC\text{-}WT}$ and YAP$^{DC\text{-}KO}$ mice were pooled together, and NCD TAZ$^{DC\text{-}WT}$ and TAZ$^{DC\text{-}KO}$ mice were pooled together, as analyses did not indicate any significant differences between genotypes. Although I observed differences in MdMs and DCs between lean YAP/TAZ$^{DC\text{-}WT}$ and YAP/TAZ$^{DC\text{-}DKO}$ female mice at 8-12 weeks of age **(Figure 4.5),** at 25 weeks of age there were no significant differences between NCD YAP/TAZ$^{DC\text{-}WT}$ and YAP/TAZ$^{DC\text{-}DKO}$ mice when assessing immune cell populations in the liver. However, I used male mice for HFHS studies, while baseline data was collected using female mice. This suggests that there may be potential sex-dependent differences, or YAP/TAZ signalling in DCs in older mice do not play a significant role in the development of DCs in the liver. Therefore, I pooled results from both YAP/TAZ$^{DC\text{-}WT}$ and YAP/TAZ$^{DC\text{-}DKO}$ NCD controls as well when comparing to HFHS-treated YAP/TAZ$^{DC\text{-}WT}$ and YAP/TAZ$^{DC\text{-}DKO}$ mice.

Compared to NCD-fed controls, HFHS-treated groups tended to exhibit increased hepatic inflammation, as demonstrated by a trending increase in the number of $CD45^+$ cells and cDC2s in HFHS $YAP^{DC\text{-}WT}$ and $YAP^{DC\text{-}KO}$ mice (**Figure 4.9 B, K)**, increased number of $CD45^+$ cells and monocytes in HFHS $TAZ^{DC\text{-}WT}$ and $TAZ^{DC\text{-}KO}$ mice (**Figure 4.10 B, F)**, and increased frequency of monocytes and ratio of MdMs to KCs in HFHS YAP/$TAZ^{DC\text{-}WT}$ and YAP/$TAZ^{DC\text{-}DKO}$ mice (**Figure 4.11 E, I)**. When comparing HFHS-treated groups with CD11c-specific deletion of YAP and/or TAZ to their respective HFHS YAP and/or TAZ sufficient controls, it did not reveal any appreciable differences in frequencies and numbers of PMNs, monocytes, KCs, MdMs, and cDCs in the liver (**Figure 4.9, 4.10, 4.11)**. Overall, these data suggest that YAP and/or TAZ deficiency in DCs does not significantly alter infiltration of myeloid cell populations in the liver during obesity.

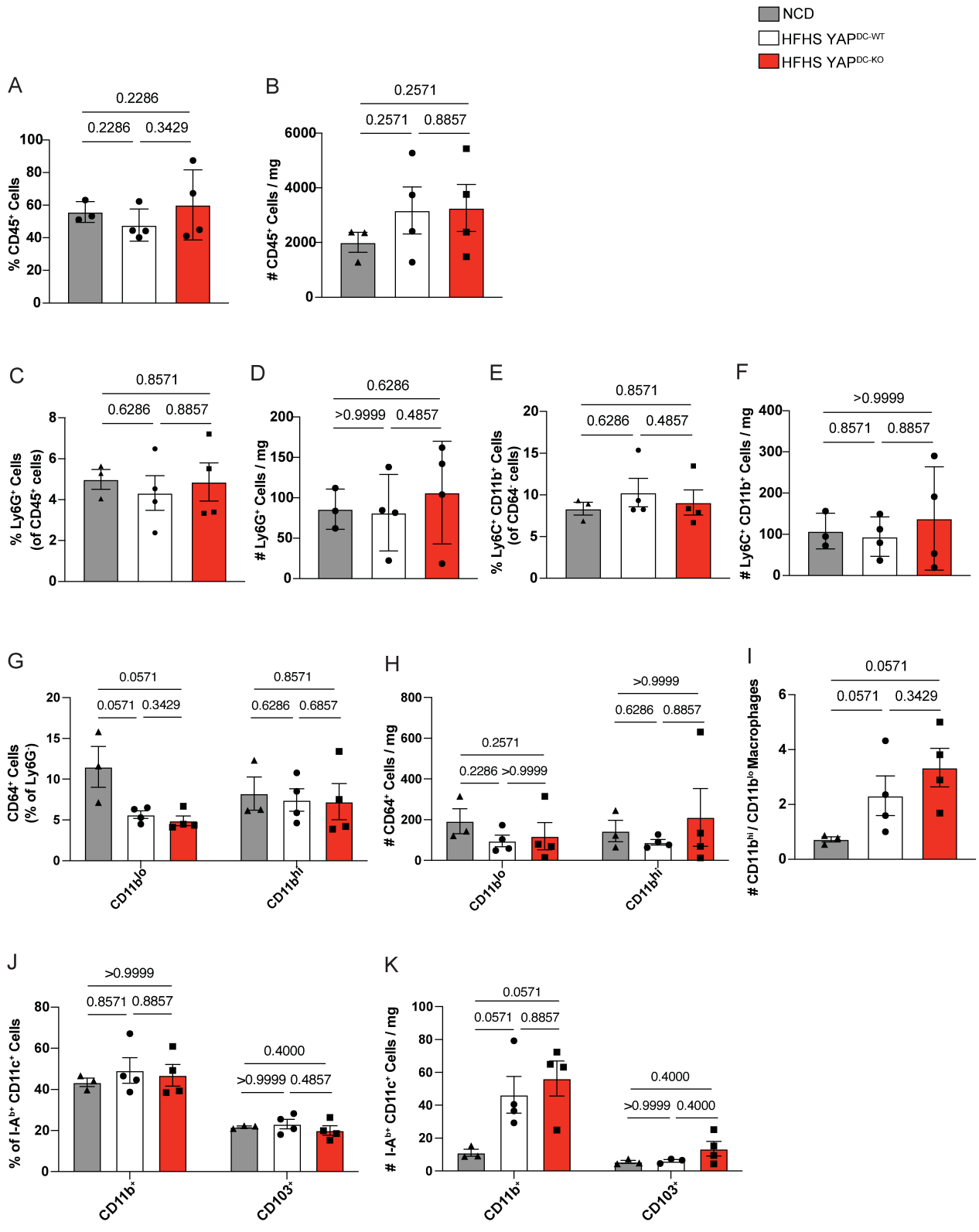
NCD
HFHS YAP^DC-WT
HFHS YAP^DC-KO
A
% CD45+ Cells
0.2286
0.2286 0.3429
B
CD45+ Cells / mg
0.2571
0.2571 0.8857
C
% Ly6G+ Cells (of CD45+ cells)
0.8571
0.6286 0.8857
D
Ly6G+ Cells / mg
0.6286
>0.9999 0.4857
E
% Ly6C+ CD11b+ Cells (of CD64- cells)
0.8571
0.6286 0.4857
F
Ly6C+ CD11b+ Cells / mg
>0.9999
0.8571 0.8857
G
CD64+ Cells (% of Ly6G-)
0.0571
0.0571 0.3429
0.8571
0.6286 0.6857
CD11b^lo
CD11b^hi
H
CD64+ Cells / mg
0.2571
0.2286 >0.9999
>0.9999
0.6286 0.8857
CD11b^lo
CD11b^hi
I
CD11b^hi / CD11b^lo Macrophages
0.0571
0.0571 0.3429
J
% of I-A^b+ CD11c+ Cells
>0.9999
0.8571 0.8857
0.4000
>0.9999 0.4857
CD11b+
CD103+
K
I-A^b+ CD11c+ Cells / mg
0.0571
0.0571 0.8857
0.4000
>0.9999 0.4000
CD11b+
CD103+

Figure 4.9 Deletion of YAP in $CD11c^+$ cells does not affect levels of myeloid cell infiltration into the liver of HFHS-treated mice. Myeloid cell populations were quantified by flow cytometry from dissociated livers of HFHS $YAP^{DC\text{-}KO}$ (n=4) or $YAP^{DC\text{-}WT}$ (n=4) mice. Age-matched NCD $YAP^{DC\text{-}WT}$ and $YAP^{DC\text{-}KO}$ mice were used as baseline controls, and results were pooled together and represented as NCD (n=3). Number of cells was quantified and normalized to mg of tissue digested. Graphs show data points from one experiment. **(A-B)** Frequency and number of $CD45^+$ cells. **(C-D)** Frequency and number of PMNs, gated from $Ly6G^+$ cells. **(E-F)** Frequency and number of monocytes, gated from $CD64^-$ $Ly6C^+$ $CD11b^+$ cells. **(G-H)** Frequency and number of KCs ($CD11b^{lo}$) and MdMs ($CD11b^{hi}$), gated from $CD64^+$ $Ly6G^-$ cells. **(I)** Ratio of MdMs : KCs. **(J-K)** Frequency and number of cDC1 ($CD103^+$) and cDC2 ($CD11b^+$), gated from $CD64^-$ $I\text{-}A^{b+}$ $CD11c^+$ cells. P-values are calculated using Mann-Whitney U test. Data are shown as individual mice (dots) and mean ± SEM.

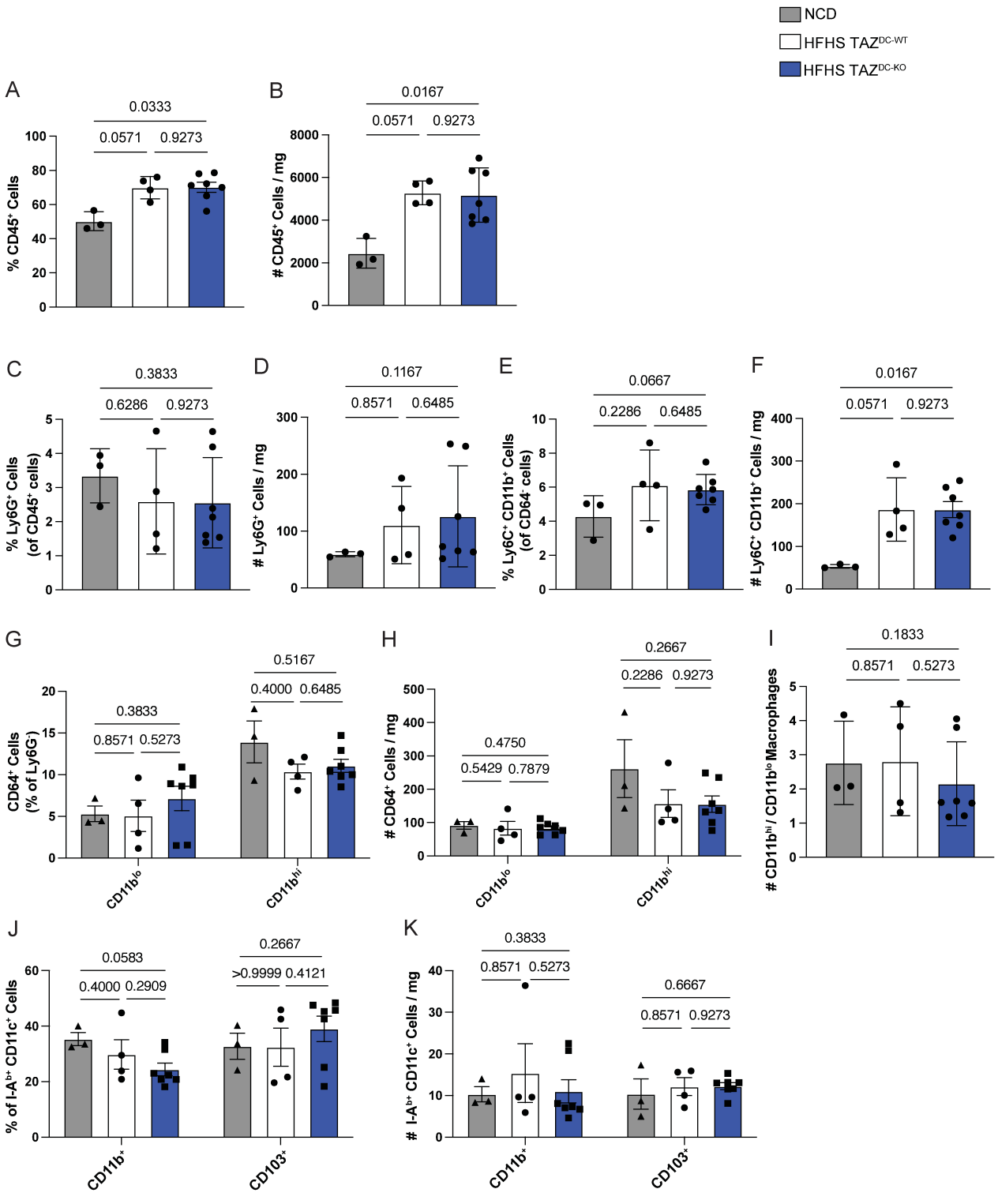
NCD
HFHS TAZDC-WT
HFHS TAZDC-KO
A
% CD45+ Cells
0.0333
0.0571
0.9273
B
CD45+ Cells / mg
0.0167
0.0571
0.9273
C
% Ly6G+ Cells (of CD45+ cells)
0.3833
0.6286
0.9273
D
Ly6G+ Cells / mg
0.1167
0.8571
0.6485
E
% Ly6C+ CD11b+ Cells (of CD64- cells)
0.0667
0.2286
0.6485
F
Ly6C+ CD11b+ Cells / mg
0.0167
0.0571
0.9273
G
CD64+ Cells (% of Ly6G-)
0.3833
0.8571
0.5273
0.5167
0.4000
0.6485
CD11blo
CD11bhi
H
CD64+ Cells / mg
0.4750
0.5429
0.7879
0.2667
0.2286
0.9273
CD11blo
CD11bhi
I
CD11bhi / CD11blo Macrophages
0.1833
0.8571
0.5273
J
% of I-Ab+ CD11c+ Cells
0.0583
0.4000
0.2909
0.2667
>0.9999
0.4121
CD11b+
CD103+
K
I-Ab+ CD11c+ Cells / mg
0.3833
0.8571
0.5273
0.6667
0.8571
0.9273
CD11b+
CD103+

Figure 4.10 Deletion of TAZ in $CD11c^+$ cells does not affect levels of myeloid cell infiltration into the liver of HFHS-treated mice. Myeloid cell populations were quantified by flow cytometry from dissociated livers of HFHS $TAZ^{DC\text{-}KO}$ (n=7) or $TAZ^{DC\text{-}WT}$ (n=4) mice. Age-matched NCD $TAZ^{DC\text{-}WT}$ and $TAZ^{DC\text{-}KO}$ mice were used as baseline controls, and results were pooled together and represented as NCD (n=3). Number of cells was quantified and normalized to mg of tissue digested. Graphs show data points from one experiment. **(A-B)** Frequency and number of $CD45^+$ cells. **(C-D)** Frequency and number of PMNs, gated from $Ly6G^+$ cells. **(E-F)** Frequency and number of monocytes, gated from $CD64^-$ $Ly6C^+$ $CD11b^+$ cells. **(G-H)** Frequency and number of KCs ($CD11b^{lo}$) and MdMs ($CD11b^{hi}$), gated from $CD64^+$ $Ly6G^-$ cells. **(I)** Ratio of MdMs : KCs. **(J-K)** Frequency and number of cDC1 ($CD103^+$) and cDC2 ($CD11b^+$), gated from $CD64^-$ $I\text{-}A^{b+}$ $CD11c^+$ cells. P-values are calculated using Mann-Whitney U test. Data are shown as individual mice (dots) and mean ± SEM.

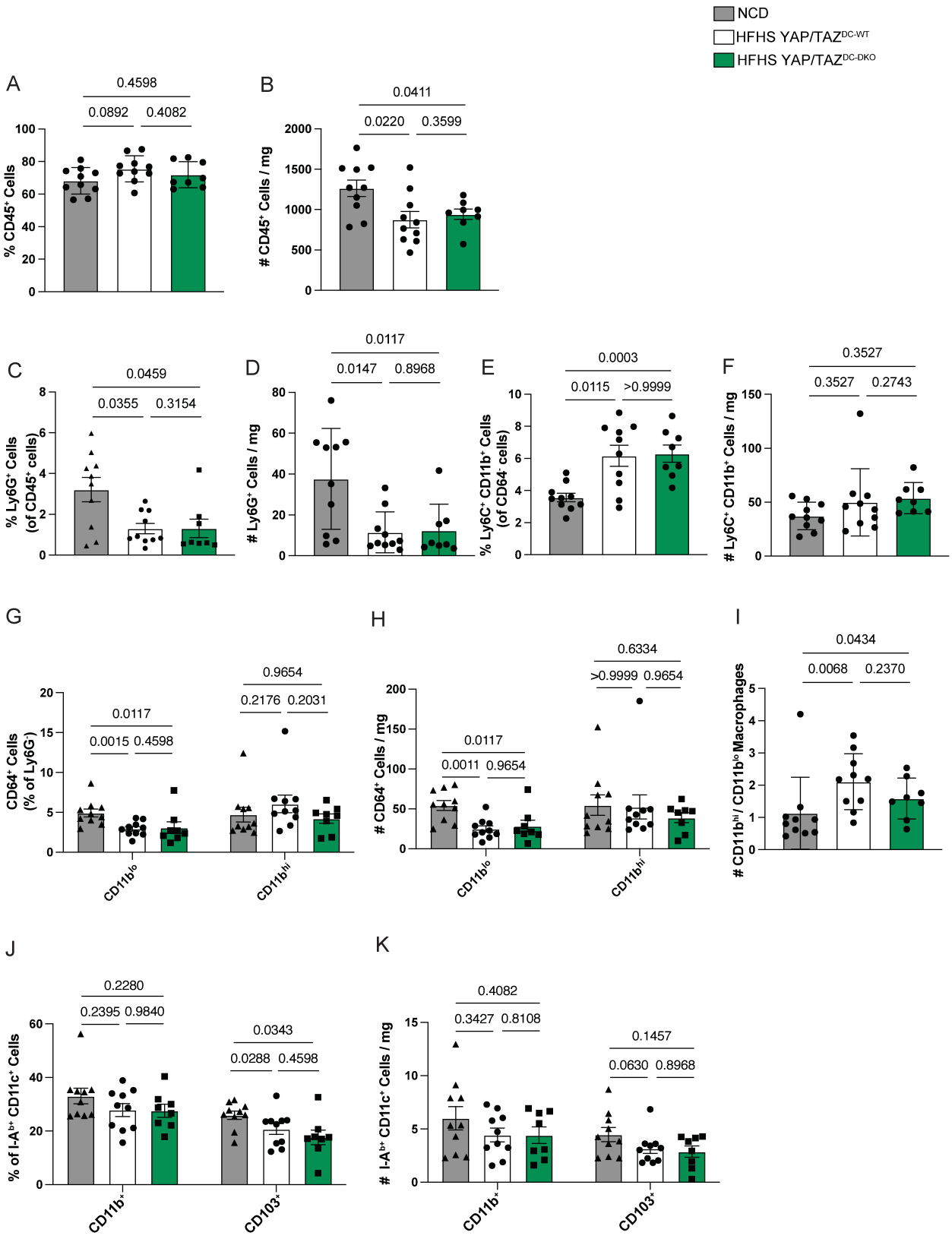
NCD
HFHS YAP/TAZDC-WT
HFHS YAP/TAZDC-DKO
A
0.4598
0.0892
0.4082
% CD45+ Cells
B
0.0411
0.0220
0.3599
CD45+ Cells / mg
C
0.0459
0.0355
0.3154
% Ly6G+ Cells (of CD45+ cells)
D
0.0117
0.0147
0.8968
Ly6G+ Cells / mg
E
0.0003
0.0115
>0.9999
% Ly6C+ CD11b+ Cells (of CD64- cells)
F
0.3527
0.3527
0.2743
Ly6C+ CD11b+ Cells / mg
G
0.0117
0.0015
0.4598
0.9654
0.2176
0.2031
CD64+ Cells (% of Ly6G-)
CD11blo
CD11bhi
H
0.6334
>0.9999
0.9654
0.0117
0.0011
0.9654
CD64+ Cells / mg
CD11blo
CD11bhi
I
0.0434
0.0068
0.2370
CD11bhi / CD11blo Macrophages
J
0.2280
0.2395
0.9840
0.0343
0.0288
0.4598
% of I-Ab+ CD11c+ Cells
CD11b+
CD103+
K
0.4082
0.3427
0.8108
0.1457
0.0630
0.8968
I-Ab+ CD11c+ Cells / mg
CD11b+
CD103+

Figure 4.11 Deletion of YAP and TAZ in CD11c^{+} cells does not affect levels of myeloid cell infiltration into the liver of HFHS-treated mice. Myeloid cell populations were quantified by flow cytometry from dissociated livers of HFHS YAP/TAZ$^{DC\text{-}DKO}$ (n=8) or YAP/TAZ$^{DC\text{-}WT}$ (n=10) mice. Age-matched NCD YAP/TAZ$^{DC\text{-}WT}$ and YAP/TAZ$^{DC\text{-}DKO}$ mice were used as baseline controls, and results were pooled together and represented as NCD (n=10). Number of cells was quantified and normalized to mg of tissue digested. Graphs show data points from two pooled experiments. **(A-B)** Frequency and number of CD45^{+} cells. **(C-D)** Frequency and number of PMNs, gated from Ly6G^{+} cells. **(E-F)** Frequency and number of monocytes, gated from CD64^{-} Ly6C^{+} CD11b^{+} cells. **(G-H)** Frequency and number of KCs (CD11b^{lo}) and MdMs (CD11b^{hi}), gated from CD64^{+} Ly6G^{-} cells. **(I)** Ratio of MdMs : KCs. **(J-K)** Frequency and number of cDC1 (CD103^{+}) and cDC2 (CD11b^{+}), gated from CD64^{-} I-A^{b+} CD11c^{+} cells. P-values are calculated using Mann-Whitney U test. Data are shown as individual mice (dots) and mean ± SEM.

4.2.4 Deletion of YAP and/or TAZ in CD11c$^+$ cells do not affect levels of T cell infiltration into the liver of HFHS-treated mice

In an obese state, there is an increase in T cell infiltration and skewing towards pro-inflammatory phenotypes in the liver[220]. DCs are critical players in activation of T cells, as they present antigens on MHC I and II molecules that can be recognized by T cells, and express co-stimulatory molecules necessary for full activation of T cells. In addition, DCs secrete cytokines that can further activate T cells and direct their differentiation[221]. To determine whether YAP and/or TAZ deficiency in DCs impairs recruitment and activation of T cells in the liver during obesity, I quantified the frequencies and numbers of $CD4^+$ and $CD8^+$ T cells**.** In the HFHS-treated mice, there was a trending increase in the proportion **(Figure 4.14 A)** or number **(Figure 4.12 B, 4.13 B)** of total T cells in the liver compared to NCD-fed controls. HFHS-treated YAP^{DC-WT} and YAP^{DC-KO} mice showed a trending decrease in the proportion of $CD4^+$ T cells with a concomitant increase in the proportion of $CD8^+$ T cells in the liver compared to NCD-fed controls (**Figure 4.12 C, E)**, which is consistent with observations made in mouse models of NASH[215]. Under HFHS conditions, CD11c-specific ablation of YAP and/or TAZ did not alter total T cell, $CD4^+$ and $CD8^+$ T cell proportions and numbers in the liver (**Figure 4.12, 4.13, 4.14 A-F**). Different subsets of T cells can be identified through expression of L-selectin (CD62L) and CD44. CD62L is a cell adhesion molecule that mediates T cell trafficking to lymphoid tissues[222], while CD44 is also a cell adhesion molecule that is also a marker for activation of T cells[223]. Naive T cells have high proliferative capacity and can access lymphoid tissue, and are identified as $CD62L^{hi}$ $CD44^{lo}$ [222]. Central memory T cells are $CD62L^{hi}$ $CD44^{hi}$ and can circulate between lymphoid organs, and exhibit rapid effector function. Effector memory T cells traffic to non-lymphoid tissues and can provide immediate protection against pathogens, and are $CD44^{hi}$ $CD62L^{lo}$ [222]. In the HFHS-treated mice, there was a trending increase in the proportion or number of $CD4^+$ and $CD8^+$ effector memory T cells in the liver compared to NCD controls (**Figure 4.12, 4.13, 4.14 G-J)**, but no differences were observed between HFHS-treated mice with CD11c-targeted deletion of YAP and/or TAZ and HFHS controls (**Figure 4.12, 4.13, 4.14 G-J)**. This suggests that YAP and/or TAZ activity in DCs does not alter the differentiation of naive and memory T cell populations in the liver during obesity.

Although there were no differences in naive and memory subsets of T cells in the liver, I wanted to assess whether YAP and/or TAZ deletion in DCs could affect T cell functionality.

DCs play critical roles in mediating T cell responses, as cDC1s are important for initiation of $CD8^+$ cytotoxic immune responses, while cDC2s can induce Th17 immune responses[17]. Previous studies have demonstrated a noticeable shift to more pro-inflammatory Th1 and Th17 $CD4^+$ T cells, as well as increased $CD8^+$ T cells during obesity, which is associated with increased production of cytokines such as IFNγ, TNFα, and IL-17[27]. To determine whether YAP and/or deficiency in DCs affects the proportion and number of TNFα and IFNγ-producing $CD8^+$ T cells, as well as IFNγ and IL-17-producing $CD4^+$ T cells, I quantified these populations following stimulation with PMA and ionomycin and intracellular cytokine staining. The livers of HFHS-treated mice exhibited a trending increase in the proportion and number of $IFN\gamma^+$ $CD4^+$ T cells, IL-17^+ $CD4^+$ T cells, and IFNγ-producing $CD8^+$ T cells compared to NCD controls (**Figure 4.15, 4.16, 4.17 A-F)**. In HFHS-treated mice, CD11c-specific ablation of YAP and/or TAZ predominantly did not lead to any differences in the frequency and number of $IFN\gamma^+$ $CD4^+$ T cells, IL-17^+ $CD4^+$ T cells, and IFNγ-producing $CD8^+$ T cells (**Figure 4.15, 4.16, 4.17 A-F)**. Interestingly, HFHS $YAP^{DC\text{-}KO}$ mice exhibited a trending decrease in the frequency of IFNγ-producing $CD4^+$ T cells in the liver compared to HFHS $YAP^{DC\text{-}WT}$ controls **(Figure 4.15 A, B)**. This suggested that YAP activity in DCs may play a role in aiding in the differentiation of Th subsets to induce Th1 responses. In addition, there was a trending decrease in the frequency of $IFN\gamma^+$ $CD8^+$ T cells in HFHS $YAP^{DC\text{-}KO}$ mice compared to HFHS $YAP^{DC\text{-}WT}$ controls (**Figure 4.15 E, F)**. This may be a result of a decrease in IFNγ-producing $CD4^+$ T cells, as IFNγ produced by Th1 cells can promote the activation and function of $CD8^+$ cytotoxic T cells[29]. Altogether, these data suggest that YAP in DCs has moderate involvement in T cell differentiation, as indicated by decreasing proportions of IFNγ-producing $CD4^+$ and $CD8^+$ T cells. As IL-12 and IFNγ are main drivers of Th1 differentiation[224], YAP activity in DCs could potentially be involved in the regulation of these cytokines. However, further characterization of DCs and their ability to produce IL-12 and IFNγ in the liver is required to confirm this.

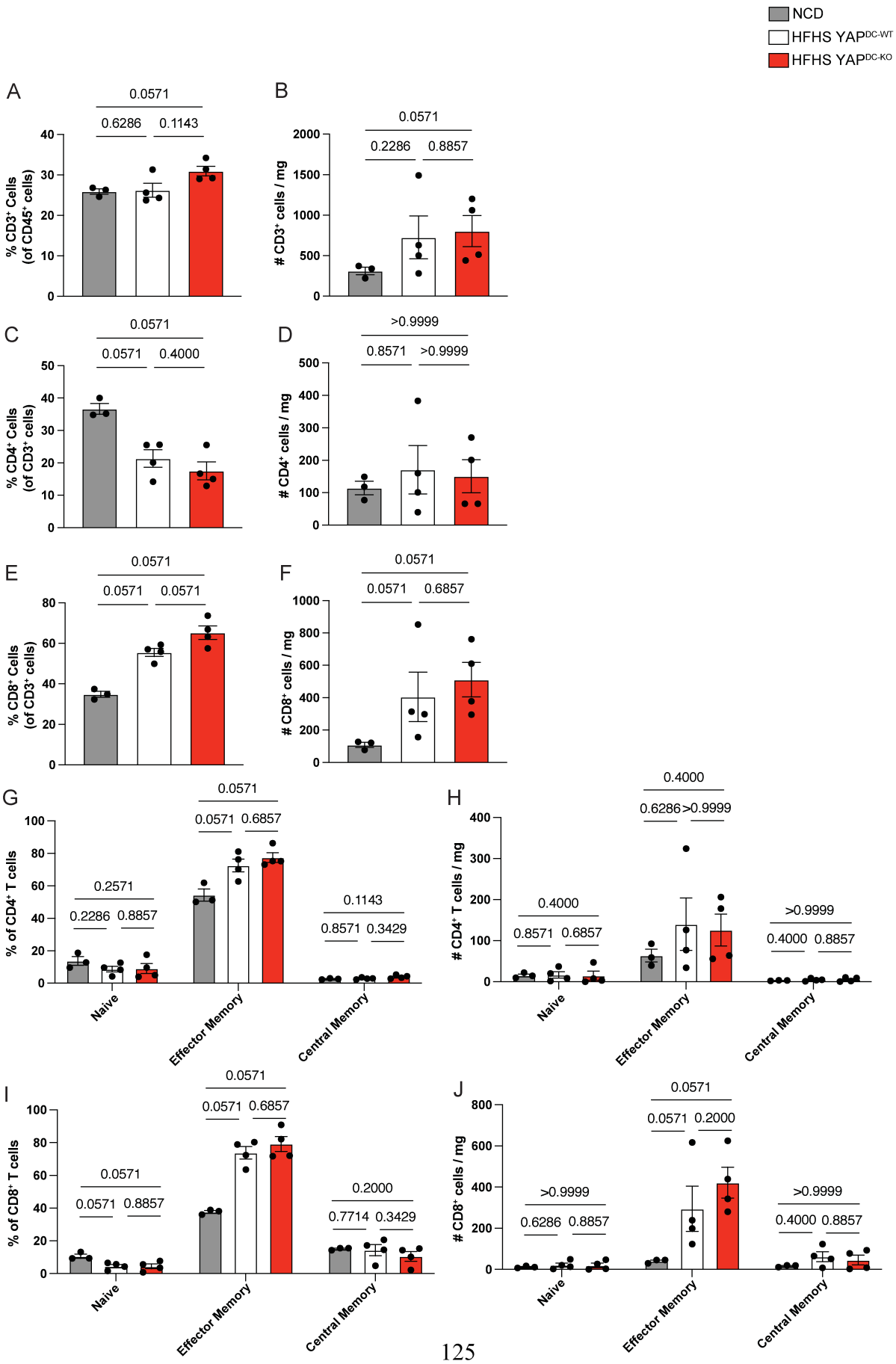
NCD
HFHS YAP DC-WT
HFHS YAP DC-KO
A
% CD3+ Cells (of CD45+ cells)
0.0571
0.6286
0.1143
B
CD3+ cells / mg
0.0571
0.2286
0.8857
C
% CD4+ Cells (of CD3+ cells)
0.0571
0.0571
0.4000
D
CD4+ cells / mg
>0.9999
0.8571
>0.9999
E
% CD8+ Cells (of CD3+ cells)
0.0571
0.0571
0.0571
F
CD8+ cells / mg
0.0571
0.0571
0.6857
G
% of CD4+ T cells
0.0571
0.0571
0.6857
0.2571
0.2286
0.8857
0.1143
0.8571
0.3429
Naive
Effector Memory
Central Memory
H
CD4+ T cells / mg
0.4000
0.6286
>0.9999
0.4000
0.8571
0.6857
>0.9999
0.4000
0.8857
Naive
Effector Memory
Central Memory
I
% of CD8+ T cells
0.0571
0.0571
0.6857
0.0571
0.0571
0.8857
0.2000
0.7714
0.3429
Naive
Effector Memory
Central Memory
J
CD8+ cells / mg
0.0571
0.0571
0.2000
>0.9999
0.6286
0.8857
>0.9999
0.4000
0.8857
Naive
Effector Memory
Central Memory

Figure 4.12 Deletion of YAP in CD11c^{+} cells does not affect levels of T cell infiltration into the liver of HFHS-treated mice. T cell populations were quantified by flow cytometry from dissociated livers of HFHS YAP$^{DC\text{-}KO}$ (n=4) or YAP$^{DC\text{-}WT}$ (n=4) mice. Age-matched NCD YAP$^{DC\text{-}WT}$ and YAP$^{DC\text{-}KO}$ mice were used as baseline controls, and results were pooled together and represented as NCD (n=3). Number of cells was quantified and normalized to mg of tissue digested. Graphs show data points from one experiment. **(A-B)** Frequency and number of CD3^{+} cells. **(C-D)** Frequency and number of CD4^{+} T cells, gated from CD3^{+} cells. **(E-F)** Frequency and number of CD8^{+} T cells, gated from CD3^{+} cells. **(G-H)** Frequency and number of naive (CD62L^{hi} CD44^{lo}), effector memory (CD62L^{lo} CD44^{hi}) and central memory (CD62L^{hi} CD44^{hi}) CD4^{+} T cells. **(I-J)** Frequency and number of naive, effector memory, and central memory CD8^{+} T cells. P-values are calculated using Mann-Whitney U test. Data are shown as individual mice (dots) and mean ± SEM.

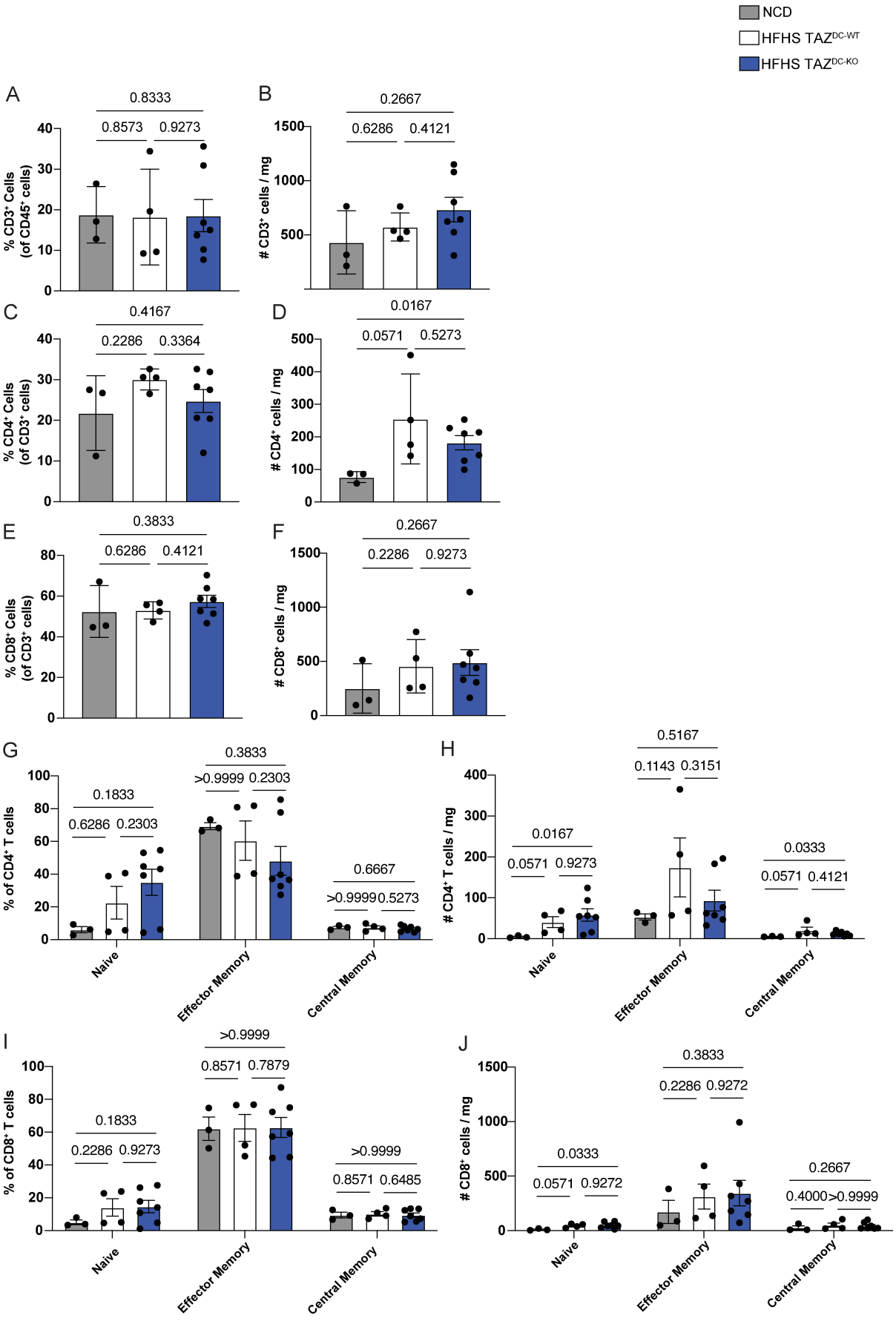
NCD
HFHS TAZDC-WT
HFHS TAZDC-KO
A
0.8333
0.8573
0.9273
% CD3+ Cells (of CD45+ cells)
B
0.2667
0.6286
0.4121
CD3+ cells / mg
C
0.4167
0.2286
0.3364
% CD4+ Cells (of CD3+ cells)
D
0.0167
0.0571
0.5273
CD4+ cells / mg
E
0.3833
0.6286
0.4121
% CD8+ Cells (of CD3+ cells)
F
0.2667
0.2286
0.9273
CD8+ cells / mg
G
0.3833
>0.9999
0.2303
0.1833
0.6286
0.2303
0.6667
>0.9999
0.5273
% of CD4+ T cells
Naive
Effector Memory
Central Memory
H
0.5167
0.1143
0.3151
0.0167
0.0571
0.9273
0.0333
0.0571
0.4121
CD4+ T cells / mg
Naive
Effector Memory
Central Memory
I
>0.9999
0.8571
0.7879
0.1833
0.2286
0.9273
>0.9999
0.8571
0.6485
% of CD8+ T cells
Naive
Effector Memory
Central Memory
J
0.3833
0.2286
0.9272
0.0333
0.0571
0.9272
0.2667
0.4000
>0.9999
CD8+ cells / mg
Naive
Effector Memory
Central Memory

Figure 4.13 Deletion of TAZ in CD11c^{+} cells does not affect levels of T cell infiltration into the liver of HFHS-treated mice. T cell populations were quantified by flow cytometry from dissociated livers of HFHS TAZ$^{DC\text{-}KO}$ (n=7) or TAZ$^{DC\text{-}WT}$ (n=4) mice. Age-matched NCD TAZ$^{DC\text{-}WT}$ and TAZ$^{DC\text{-}KO}$ mice were used as baseline controls, and results were pooled together and represented as NCD (n=3). Number of cells was quantified and normalized to mg of tissue digested. Graphs show data points from one experiment. **(A-B)** Frequency and number of CD3^{+} cells. **(C-D)** Frequency and number of CD4^{+} T cells, gated from CD3^{+} cells. **(E-F)** Frequency and number of CD8^{+} T cells, gated from CD3^{+} cells. **(G-H)** Frequency and number of naive (CD62L^{hi} CD44^{lo}), effector memory (CD62L^{lo} CD44^{hi}) and central memory (CD62L^{hi} CD44^{hi}) CD4^{+} T cells. **(I-J)** Frequency and number of naive, effector memory, and central memory CD8^{+} T cells. P-values are calculated using Mann-Whitney U test. Data are shown as individual mice (dots) and mean ± SEM.

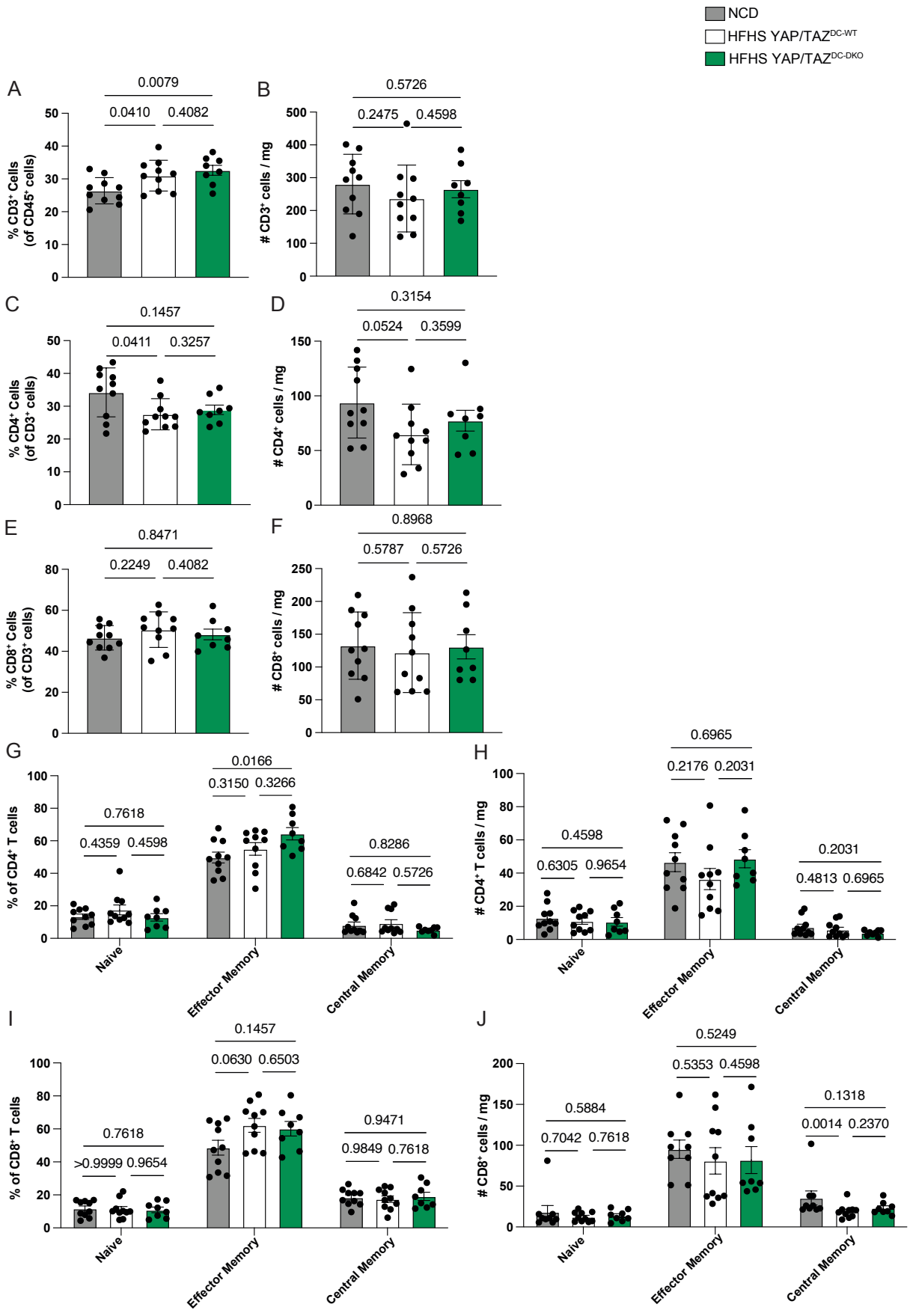
NCD
HFHS YAP/TAZDC-WT
HFHS YAP/TAZDC-DKO
A
0.0079
0.0410
0.4082
% CD3+ Cells (of CD45+ cells)
B
0.5726
0.2475
0.4598
CD3+ cells / mg
C
0.1457
0.0411
0.3257
% CD4+ Cells (of CD3+ cells)
D
0.3154
0.0524
0.3599
CD4+ cells / mg
E
0.8471
0.2249
0.4082
% CD8+ Cells (of CD3+ cells)
F
0.8968
0.5787
0.5726
CD8+ cells / mg
G
0.0166
0.3150
0.3266
0.7618
0.4359
0.4598
0.8286
0.6842
0.5726
% of CD4+ T cells
Naive
Effector Memory
Central Memory
H
0.6965
0.2176
0.2031
0.4598
0.6305
0.9654
0.2031
0.4813
0.6965
CD4+ T cells / mg
Naive
Effector Memory
Central Memory
I
0.1457
0.0630
0.6503
0.7618
>0.9999
0.9654
0.9471
0.9849
0.7618
% of CD8+ T cells
Naive
Effector Memory
Central Memory
J
0.5249
0.5353
0.4598
0.5884
0.7042
0.7618
0.1318
0.0014
0.2370
CD8+ cells / mg
Naive
Effector Memory
Central Memory

Figure 4.14 Deletion of YAP and TAZ in CD11c^{+} cells does not affect levels of T cell infiltration into the liver of HFHS-treated mice. T cell populations were quantified by flow cytometry from dissociated livers of HFHS YAP/TAZ$^{DC\text{-}DKO}$ (n=8) or YAP/TAZ$^{DC\text{-}WT}$ (n=10) mice. Age-matched NCD YAP/TAZ$^{DC\text{-}WT}$ and YAP/TAZ$^{DC\text{-}DKO}$ mice were used as baseline controls, and results were pooled together and represented as NCD (n=10). Number of cells was quantified and normalized to mg of tissue digested. Graphs show data points from two pooled experiments. **(A-B)** Frequency and number of CD3^{+} cells. **(C-D)** Frequency and number of CD4^{+} T cells, gated from CD3^{+} cells. **(E-F)** Frequency and number of CD8^{+} T cells, gated from CD3^{+} cells. **(G-H)** Frequency and number of naive (CD62L^{hi} CD44^{lo}), effector memory (CD62L^{lo} CD44^{hi}) and central memory (CD62L^{hi} CD44^{hi}) CD4^{+} T cells. **(I-J)** Frequency and number of naive, effector memory, and central memory CD8^{+} T cells. P-values are calculated using Mann-Whitney U test. Data are shown as individual mice (dots) and mean ± SEM.

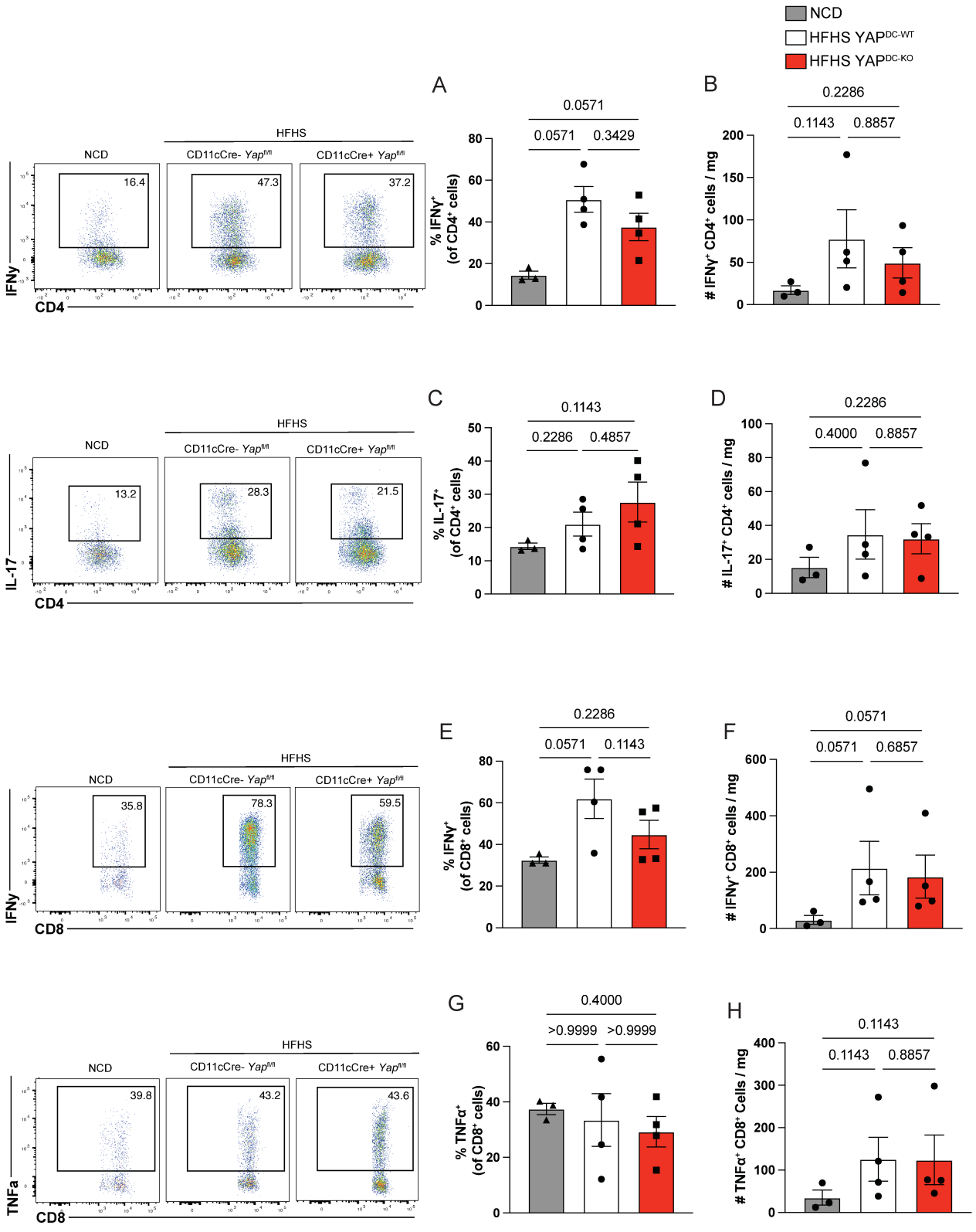
NCD
HFHS YAP^DC-WT
HFHS YAP^DC-KO
HFHS
NCD
CD11cCre- Yap^fl/fl
CD11cCre+ Yap^fl/fl
16.4
47.3
37.2
IFNγ
CD4
A
0.0571
0.0571
0.3429
% IFNγ+ (of CD4+ cells)
B
0.2286
0.1143
0.8857
IFNγ+ CD4+ cells / mg
13.2
28.3
21.5
IL-17
C
0.1143
0.2286
0.4857
% IL-17+ (of CD4+ cells)
D
0.2286
0.4000
0.8857
IL-17+ CD4+ cells / mg
35.8
78.3
59.5
CD8
E
0.2286
0.0571
0.1143
% IFNγ+ (of CD8+ cells)
F
0.0571
0.0571
0.6857
IFNγ+ CD8+ cells / mg
39.8
43.2
43.6
TNFa
G
0.4000
>0.9999
>0.9999
% TNFα+ (of CD8+ cells)
H
0.1143
0.1143
0.8857
TNFα+ CD8+ Cells / mg

Figure 4.15 Deletion of YAP in CD11c^{+} cells leads to a trending decrease in IFNγ production by T cells in the liver of HFHS-treated mice. Cells from dissociated livers of HFHS YAP$^{DC\text{-}KO}$ (n=4) or YAP$^{DC\text{-}WT}$ (n=4) mice were stimulated with PMA/ionomycin with brefeldin A for 5 hours prior to intracellular staining of IFNγ, TNFα, and IL-17. Age-matched NCD YAP$^{DC\text{-}WT}$ and YAP$^{DC\text{-}KO}$ mice were used as baseline controls, and results were pooled together and represented as NCD (n=3). Number of cells was quantified and normalized to mg of tissue digested. Graphs show data points from one experiment. **(A-B)** Frequency and number of IFNγ^{+} CD4^{+} T cells. **(C-D)** Frequency and number of IL-17^{+} CD4^{+} T cells. **(E-F)** Frequency and number of IFNγ^{+} CD8^{+} T cells. **(G-H)** Frequency and number of TNFα^{+} CD8^{+} T cells. P-values are calculated using Mann-Whitney U test. Data are shown as individual mice (dots) and mean ± SEM.

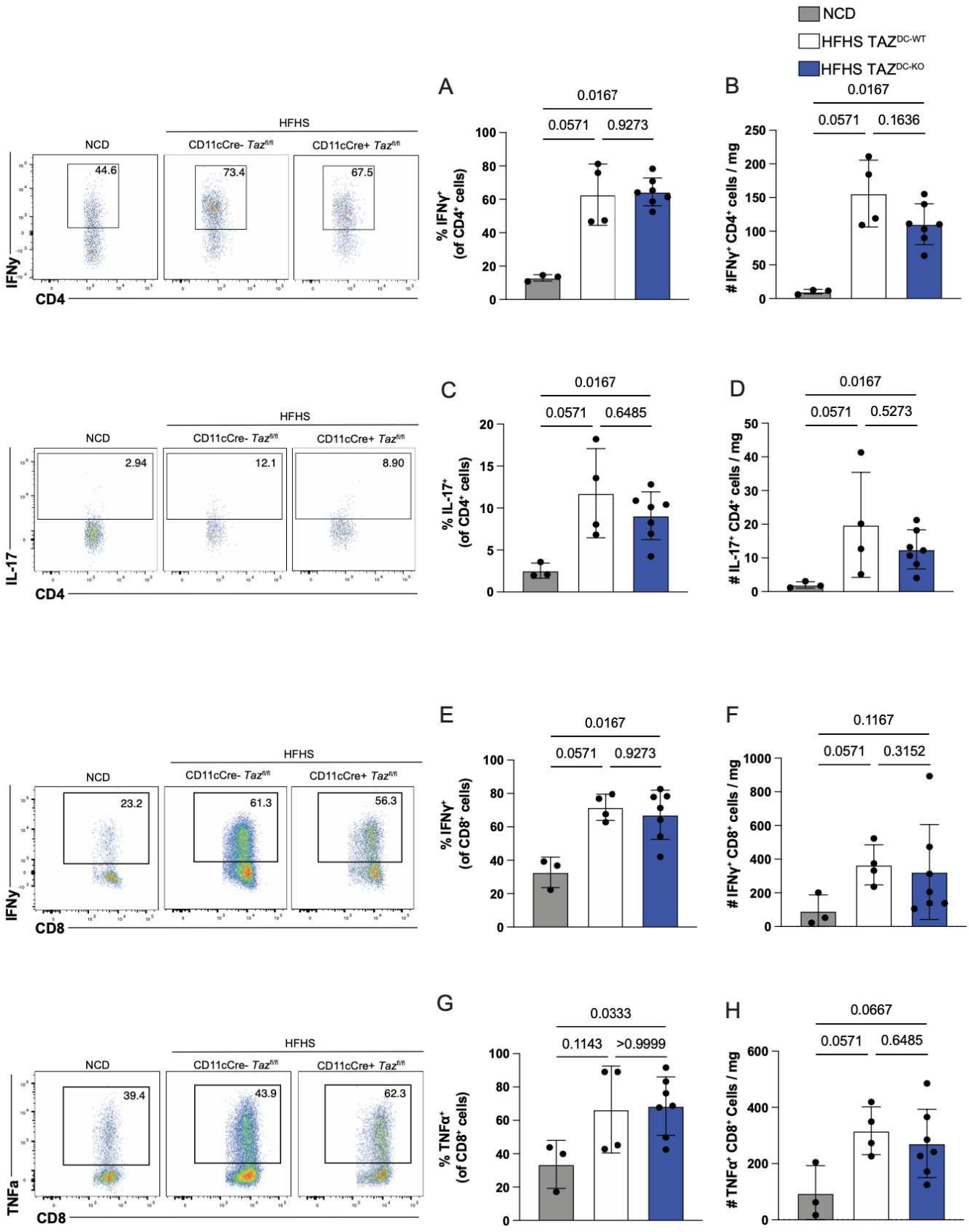
NCD
HFHS TAZDC-WT
HFHS TAZDC-KO
HFHS
NCD
CD11cCre- Taz fl/fl
CD11cCre+ Taz fl/fl
44.6
73.4
67.5
IFNγ
CD4
A
0.0167
0.0571
0.9273
% IFNγ+ (of CD4+ cells)
B
0.0167
0.0571
0.1636
IFNγ+ CD4+ cells / mg
2.94
12.1
8.90
IL-17
C
0.0167
0.0571
0.6485
% IL-17+ (of CD4+ cells)
D
0.0167
0.0571
0.5273
IL-17+ CD4+ cells / mg
23.2
61.3
56.3
CD8
E
0.0167
0.0571
0.9273
% IFNγ+ (of CD8+ cells)
F
0.1167
0.0571
0.3152
IFNγ+ CD8+ cells / mg
39.4
43.9
62.3
TNFa
G
0.0333
0.1143
>0.9999
% TNFα+ (of CD8+ cells)
H
0.0667
0.0571
0.6485
TNFα+ CD8+ Cells / mg

Figure 4.16 Deletion of TAZ in CD11c^{+} cells does not affect pro-inflammatory cytokine production by T cells in the liver of HFHS-treated mice. Cells from dissociated livers of HFHS TAZ$^{DC\text{-}KO}$ (n=7) or TAZ$^{DC\text{-}WT}$ (n=4) mice were stimulated with PMA/ionomycin with brefeldin A for 5 hours prior to intracellular staining of IFNγ, TNFα, and IL-17. Age-matched NCD TAZ$^{DC\text{-}WT}$ and TAZ$^{DC\text{-}KO}$ mice were used as baseline controls, and results were pooled together and represented as NCD (n=3). Number of cells was quantified and normalized to mg of tissue digested. Graphs show data points from one experiment. **(A-B)** Frequency and number of IFNγ^{+} CD4^{+} T cells. **(C-D)** Frequency and number of IL-17^{+} CD4^{+} T cells. **(E-F)** Frequency and number of IFNγ^{+} CD8^{+} T cells. **(G-H)** Frequency and number of TNFα^{+} CD8^{+} T cells. P-values are calculated using Mann-Whitney U test. Data are shown as individual mice (dots) and mean ± SEM.

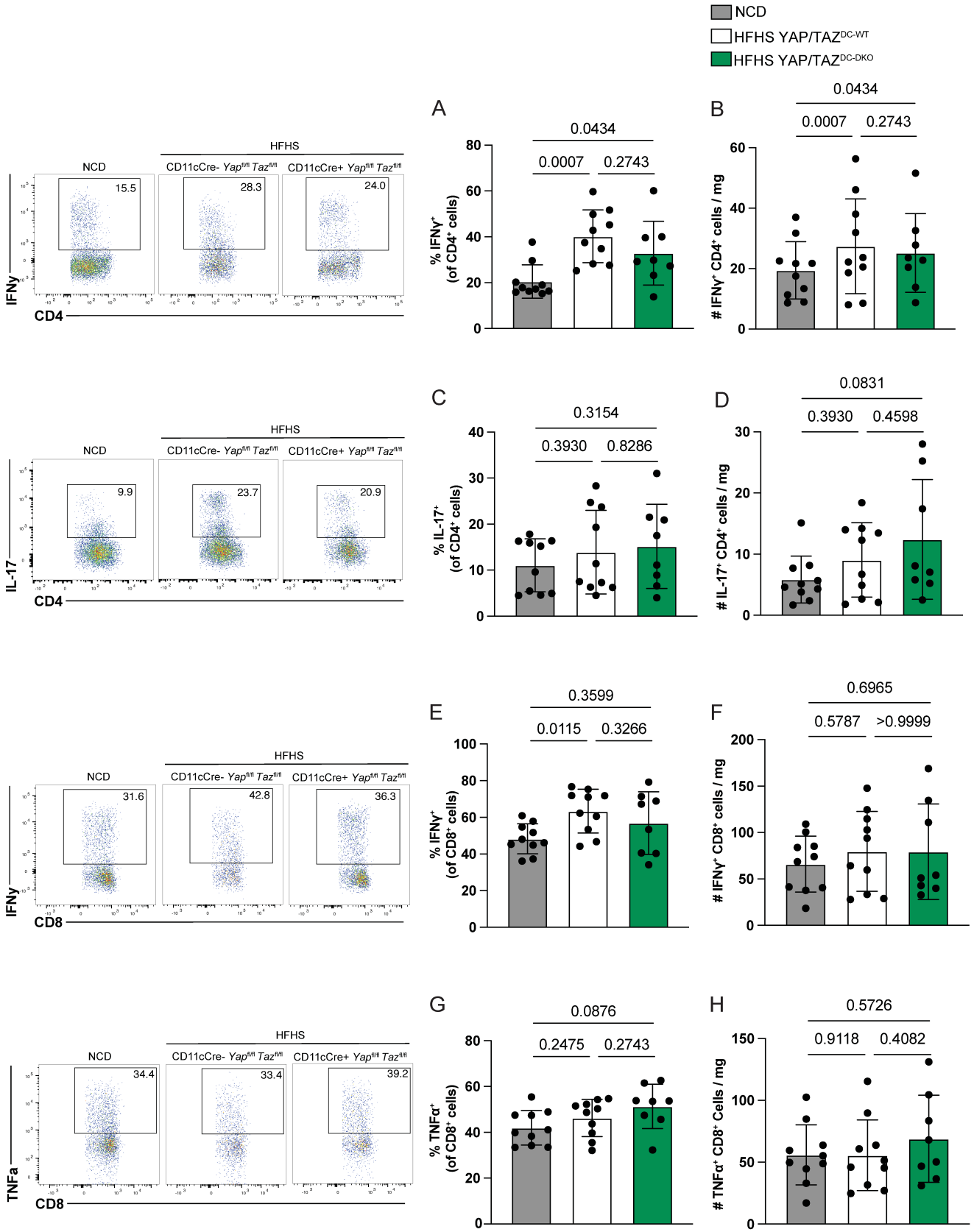
NCD
HFHS YAP/TAZDC-WT
HFHS YAP/TAZDC-DKO
HFHS
NCD
CD11cCre- Yapfl/fl Tazfl/fl
CD11cCre+ Yapfl/fl Tazfl/fl
15.5
28.3
24.0
IFNγ
CD4
A
0.0434
0.0007
0.2743
% IFNγ+ (of CD4+ cells)
B
0.0434
0.0007
0.2743
IFNγ+ CD4+ cells / mg
9.9
23.7
20.9
IL-17
C
0.3154
0.3930
0.8286
% IL-17+ (of CD4+ cells)
D
0.0831
0.3930
0.4598
IL-17+ CD4+ cells / mg
31.6
42.8
36.3
CD8
E
0.3599
0.0115
0.3266
% IFNγ+ (of CD8+ cells)
F
0.6965
0.5787
>0.9999
IFNγ+ CD8+ cells / mg
TNFa
34.4
33.4
39.2
G
0.0876
0.2475
0.2743
% TNFα+ (of CD8+ cells)
H
0.5726
0.9118
0.4082
TNFα+ CD8+ Cells / mg

Figure 4.17 Deletion of YAP and TAZ in CD11c$^+$ cells does not affect pro-inflammatory cytokine production by T cells in the liver of HFHS-treated mice. Cells from dissociated livers of HFHS YAP/TAZ$^{DC\text{-}DKO}$ (n=8) or YAP/TAZ$^{DC\text{-}WT}$ (n=10) mice were stimulated with PMA/ionomycin with brefeldin A for 5 hours prior to intracellular staining of IFNγ, TNFα, and IL-17. Age-matched NCD YAP/TAZ$^{DC\text{-}WT}$ and YAP/TAZ$^{DC\text{-}DKO}$ mice were used as baseline controls, and results were pooled together and represented as NCD (n=10). Number of cells was quantified and normalized to mg of tissue digested. Graphs show data points from two pooled experiments. **(A-B)** Frequency and number of IFNγ$^+$ CD4$^+$ T cells. **(C-D)** Frequency and number of IL-17$^+$ CD4$^+$ T cells. **(E-F)** Frequency and number of IFNγ$^+$ CD8$^+$ T cells. **(G-H)** Frequency and number of TNFα$^+$ CD8$^+$ T cells. P-values are calculated using Mann-Whitney U test. Data are shown as individual mice (dots) and mean ± SEM.

Table 4.2 Changes in frequency and numbers of immune cell populations in the liver of HFHS-treated $YAP^{DC\text{-}KO}$, $TAZ^{DC\text{-}KO}$, and $YAP/TAZ^{DC\text{-}DKO}$ mice relative to HFHS controls. (**ø** = no difference; - = decrease; + = increase) (Trending: º; Significant: *p < 0.05. **p < 0.01.)

Liver	**HFHS $YAP^{DC\text{-}KO}$**		**HFHS $TAZ^{DC\text{-}KO}$**		**HFHS $YAP/TAZ^{DC\text{-}DKO}$**	
Cells	**%**	#	**%**	#	**%**	#
$CD45^+$	**ø**	**ø**	**ø**	**ø**	**ø**	**ø**
PMNs	**ø**	**ø**	**ø**	**ø**	**ø**	**ø**
Monocytes	**ø**	**ø**	**ø**	**ø**	**ø**	**ø**
KCs	**ø**	**ø**	**ø**	**ø**	**ø**	**ø**
MdMs	**ø**	**ø**	**ø**	**ø**	**ø**	**ø**
cDC1	**ø**	**ø**	**ø**	**ø**	**ø**	**ø**
cDC2	**ø**	**ø**	**ø**	**ø**	**ø**	**ø**
$CD3^+$	**ø**	**ø**	**ø**	**ø**	**ø**	**ø**
$CD4^+$ T cells	**ø**	**ø**	**ø**	**ø**	**ø**	**ø**
$CD8^+$ T cells	+º	**ø**	**ø**	**ø**	**ø**	**ø**
$CD4^+$ Naive T cells	**ø**	**ø**	**ø**	**ø**	**ø**	**ø**
$CD4^+$ Central Memory T cells	**ø**	**ø**	**ø**	**ø**	**ø**	**ø**
$CD4^+$ Effector Memory T cells	**ø**	**ø**	**ø**	**ø**	**ø**	**ø**

$CD8^+$ Naive T cells	**ø**	**ø**	**ø**	**ø**	**ø**	**ø**
$CD8^+$ Central Memory T cells	**ø**	**ø**	**ø**	**ø**	**ø**	**ø**
$CD8^+$ Effector Memory T cells	**ø**	**ø**	**ø**	**ø**	**ø**	**ø**
$IFN\gamma^+$ $CD4^+$ T cells	**-º**	**ø**	**ø**	**ø**	**ø**	**ø**
$IL\text{-}17^+$ $CD4^+$ T cells	**ø**	**ø**	**ø**	**ø**	**ø**	**ø**
$IFN\gamma^+$ $CD8^+$ T cells	**-º**	**ø**	**ø**	**ø**	**ø**	**ø**
$TNF\alpha^+$ $CD8^+$ T cells	**ø**	**ø**	**ø**	**ø**	**ø**	**ø**

4.2.5 Deletion of YAP and/or TAZ in CD11c$^+$ cells do not affect levels of immune infiltration into the VAT of HFHS-treated mice

In addition to the liver, I assessed the composition of immune cells in the VAT of HFHS-treated mice, as VAT is a key site of inflammation during obesity. Therefore, I wanted to determine whether YAP and/or TAZ in DCs is important for modulating VAT inflammation. I was unable to isolate sufficient amounts of VAT from NCD-fed mice for analysis, and only compared HFHS-treated mice. When examining the immune cell compartment of the VAT, CD11c-specific deletion of YAP and/or TAZ did not affect the frequency of CD45$^+$ cells, PMNs, and monocytes **(Figure 4.18, 4.19, 4.20 A-C)**. In obese AT, macrophage subsets can be categorized into two major groups based on expression of CD11c and mannose receptor (CD206), which is a C-type lectin that is important for endocytosis and phagocytosis[29]. CD11c$^-$ resident macrophages are described to be more anti-inflammatory, with increased expression of IL-10 and arginase[14]. Although CD206 has been predominantly described as a marker for more homeostatic and anti-inflammatory macrophages, CD11c$^+$ CD206$^+$ macrophages are found in obese VAT and express pro-inflammatory cytokines, and are associated with IR[32]. When comparing VAT in mice with CD11c-specific deletion of YAP and/or TAZ to controls, there were similar proportions of CD11c$^-$ and CD11c$^+$ 206$^+$ macrophages, with majority of the macrophages expressing CD11c$^+$ 206$^+$ (**Figure 4.18, 4.19, 4.20 D)**. In addition, the proportion of cDC1 and cDC2s were not significantly different between the HFHS-treated mice (**Figure 4.18, 4.19, 4.20 E)**. When assessing T cell subsets in the VAT, HFHS-treated mice with CD11c-targeted deletion of YAP and/or TAZ mostly showed similar proportions of T cells (**Figure 4.21, 4.22, 4.23 A)**, proportions of CD4$^+$ and CD8$^+$ T cells (**Figure 4.21, 4.22, 4.23 B, C)**, as well as frequencies of naive, effector memory, and central memory in both CD4$^+$ and CD8$^+$ populations (**Figure 4.21, 4.22, 4.23 D, E)**. There were trending decreases in the frequency of total T cells in HFHS YAP/TAZ$^{DC\text{-}DKO}$ mice (**Figure 4.23 A)**, and trending decreases in the proportion of CD8$^+$ effector memory T cells in HFHS TAZ$^{DC\text{-}KO}$ mice compared to controls (**Figure 4.22 E)**, but not significant. Altogether, these data suggest that YAP and TAZ deletion in DCs does not alter the frequency of immune cell populations infiltrating VAT during obesity.

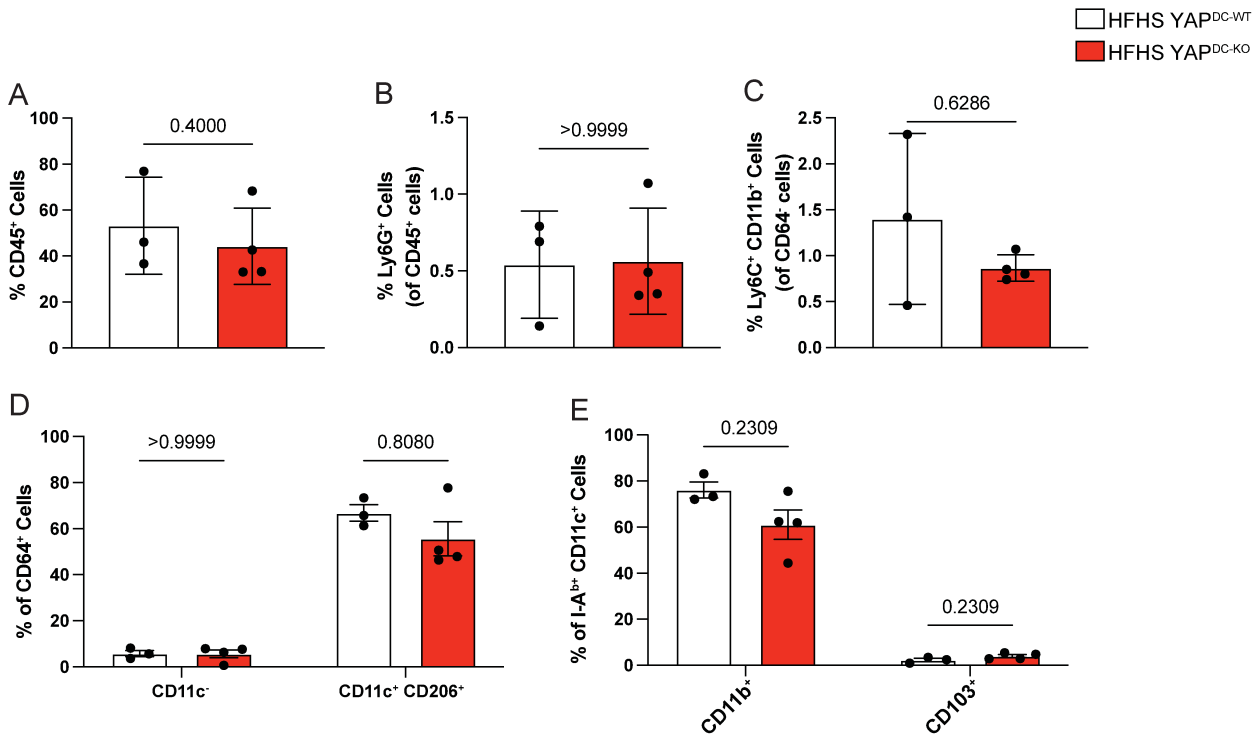

Figure 4.18 Deletion of YAP in CD11c$^+$ cells does not affect frequencies of myeloid cell populations in the VAT of HFHS-treated mice. Myeloid cell populations were quantified by flow cytometry from dissociated VAT of HFHS YAP$^{DC\text{-}KO}$ (n=4) or YAP$^{DC\text{-}WT}$ (n=3) mice. Graphs show data points from one experiment. **(A)** Frequency of CD45$^+$ cells. **(B)** Frequency of PMNs, gated from Ly6G$^+$ cells. **(C)** Frequency of monocytes, gated from CD64$^-$ Ly6C$^+$ CD11b$^+$ cells. **(D)** Frequency of CD11c$^-$ and CD11c$^+$ CD206$^+$ macrophages, gated from CD64$^+$ Ly6G$^-$ cells. **(E)** Frequency of cDC1 (CD103$^+$) and cDC2 (CD11b$^+$), gated from CD64$^-$ I-A^{b+} CD11c$^+$ cells. P-values are calculated using Mann-Whitney U test. Data are shown as individual mice (dots) and mean ± SEM.

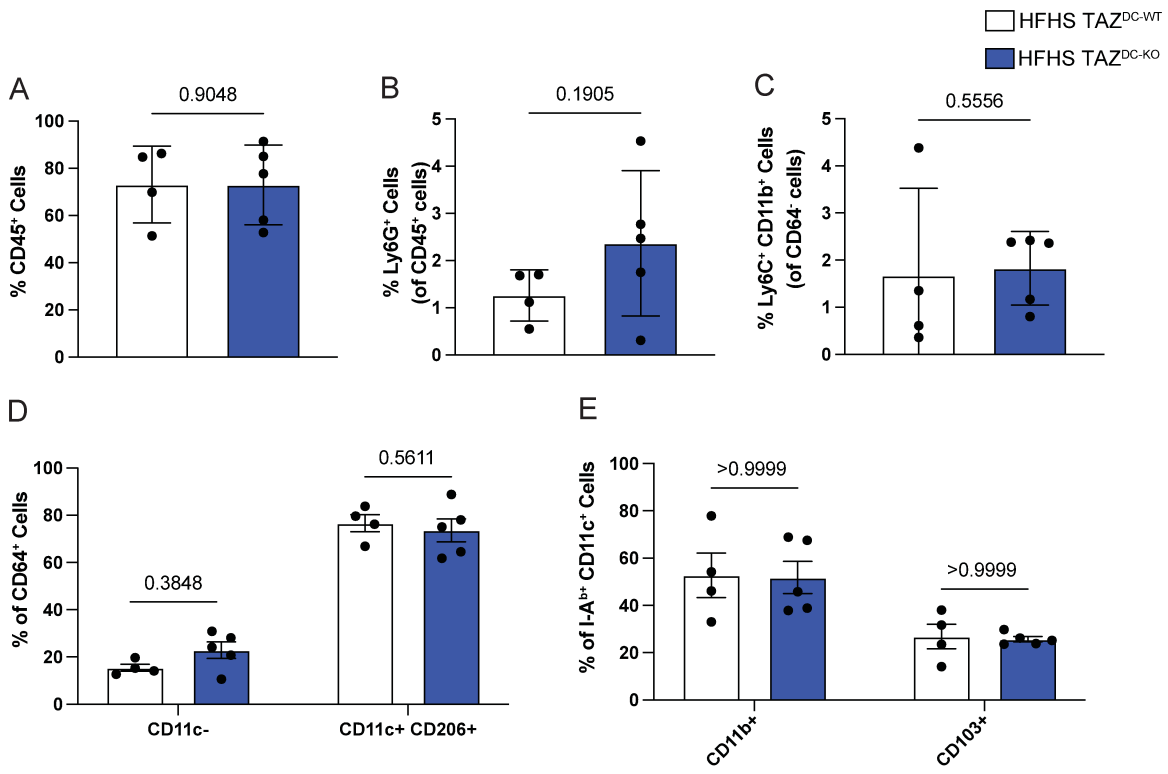

Figure 4.19 Deletion of TAZ in CD11c$^+$ cells does not affect frequencies of myeloid cell populations in the VAT of HFHS-treated mice. Myeloid cell populations were quantified by flow cytometry from dissociated VAT of HFHS TAZ$^{DC\text{-}KO}$ (n=5) or TAZ$^{DC\text{-}WT}$ (n=4) mice. Graphs show data points from one experiment. **(A)** Frequency of CD45$^+$ cells. **(B)** Frequency of PMNs, gated from Ly6G$^+$ cells. **(C)** Frequency of monocytes, gated from CD64$^-$ Ly6C$^+$ CD11b$^+$ cells. **(D)** Frequency of CD11c$^-$ and CD11c$^+$ CD206$^+$ macrophages, gated from CD64$^+$ Ly6G$^-$ cells. **(E)** Frequency of cDC1 (CD103$^+$) and cDC2 (CD11b$^+$), gated from CD64$^-$ I-A^{b+} CD11c$^+$ cells. P-values are calculated using Mann-Whitney U test. Data are shown as individual mice (dots) and mean ± SEM.

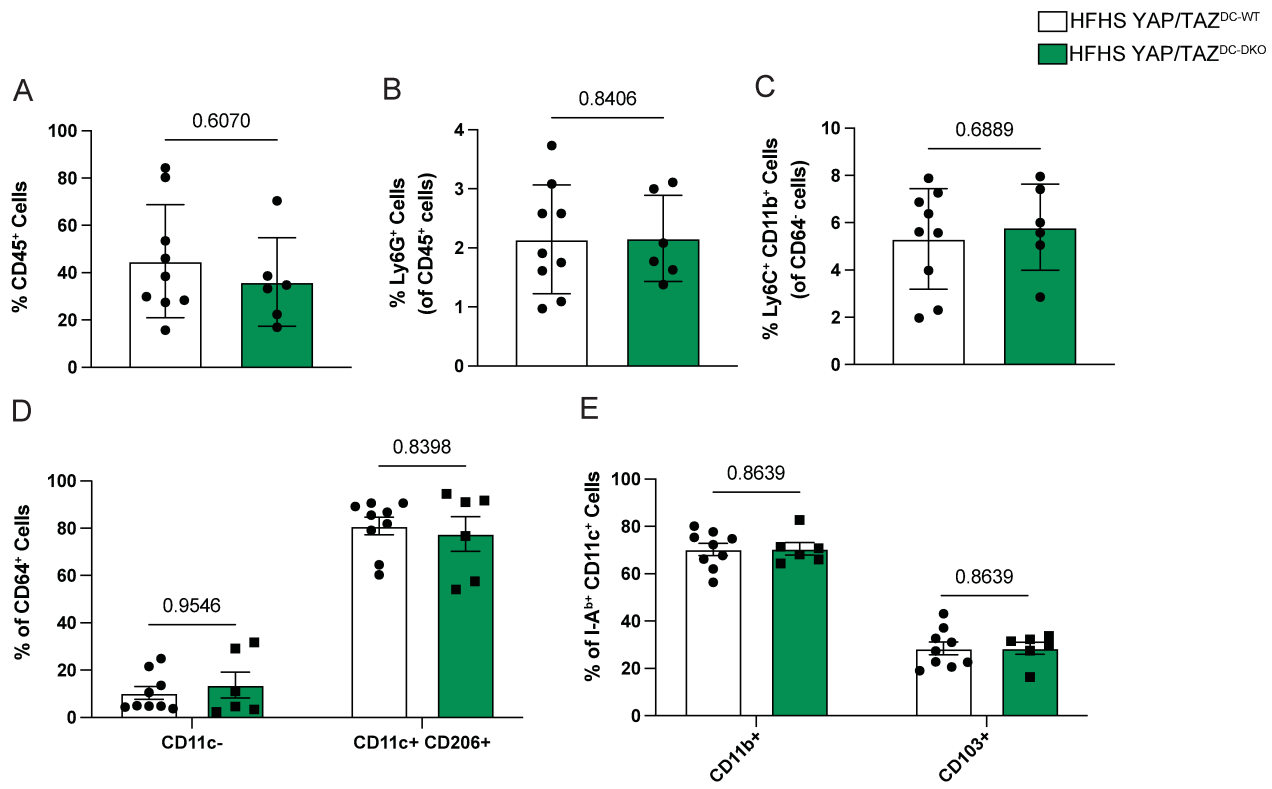

Figure 4.20 Deletion of YAP and TAZ in CD11c+ cells does not affect frequencies of myeloid cell populations in the VAT of HFHS-treated mice. Myeloid cell populations were quantified by flow cytometry from dissociated VAT of HFHS YAP/TAZ$^{DC\text{-}DKO}$ (n=6) or YAP/TAZ$^{DC\text{-}WT}$ (n=9) mice. Graphs show data points from two pooled experiments. **(A)** Frequency of CD45^{+} cells. **(B)** Frequency of PMNs, gated from Ly6G^{+} cells. **(C)** Frequency of monocytes, gated from CD64^{-} Ly6C^{+} CD11b^{+} cells. **(D)** Frequency of CD11c^{-} and CD11c^{+} CD206^{+} macrophages, gated from CD64^{+} Ly6G^{-} cells. **(E)** Frequency of cDC1 (CD103^{+}) and cDC2 (CD11b^{+}), gated from CD64^{-} I-A^{b+} CD11c^{+} cells. P-values are calculated using Mann-Whitney U test. Data are shown as individual mice (dots) and mean ± SEM.

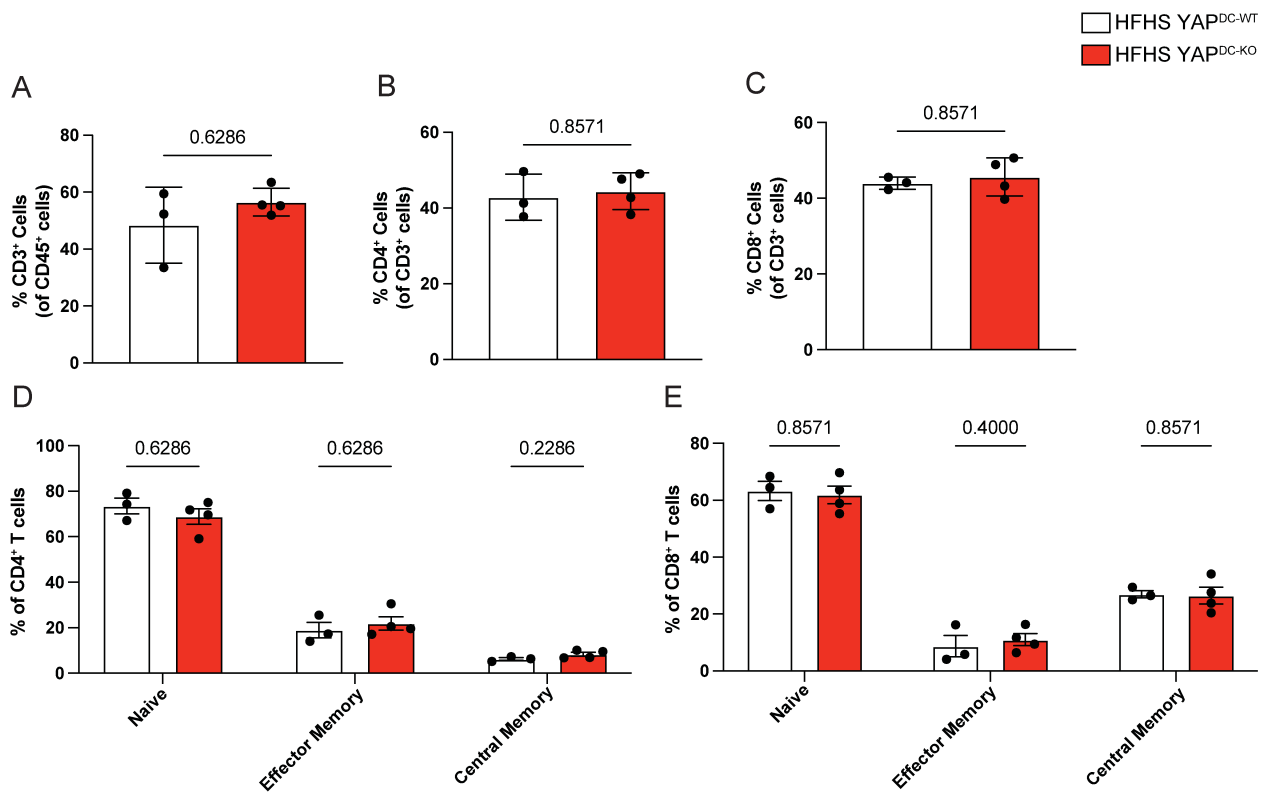

Figure 4.21 Deletion of YAP in CD11c^{+} cells does not affect frequencies of T cell populations in the VAT of HFHS-treated mice. T cell populations were quantified by flow cytometry from dissociated VAT of HFHS YAP$^{DC\text{-}KO}$ (n=4) or YAP$^{DC\text{-}WT}$ (n=3) mice. (A) Frequency of CD3^{+} cells. (B) Frequency of CD4^{+} T cells, gated from CD3^{+} cells. (C) Frequency of CD8^{+} T cells, gated from CD3^{+} cells. (D) Frequency of naive (CD62L^{hi} CD44^{lo}), effector memory (CD62L^{lo} CD44^{hi}) and central memory (CD62L^{hi} CD44^{hi}) CD4^{+} T cells. (E) Frequency and number of naive, effector memory, and central memory CD8^{+} T cells. P-values are calculated using Mann-Whitney U test. Data are shown as individual mice (dots) and mean ± SEM.

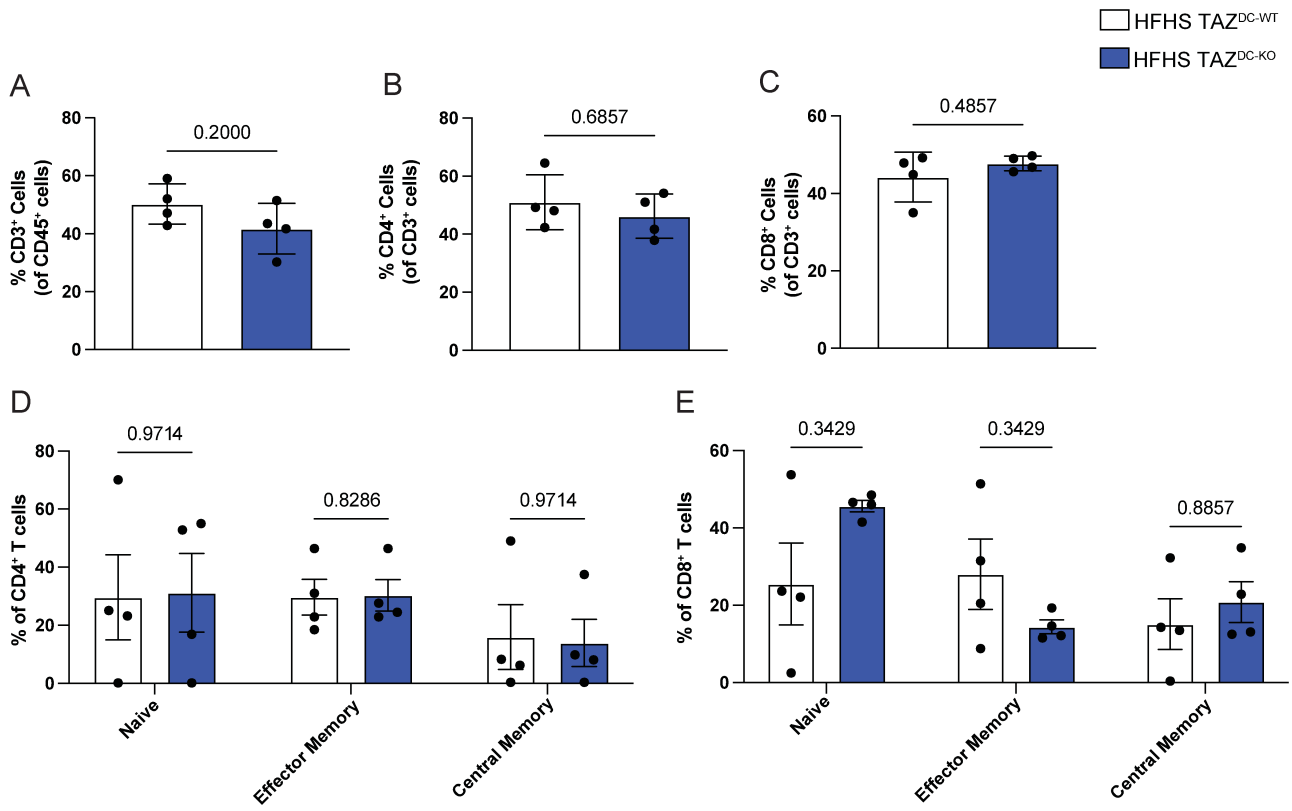

Figure 4.22 Deletion of TAZ in CD11c^{+} cells does not affect frequencies of T cell populations in the VAT of HFHS-treated mice. T cell populations were quantified by flow cytometry from dissociated VAT of HFHS TAZ$^{DC\text{-}KO}$ (n=4) or TAZ$^{DC\text{-}WT}$ (n=4) mice. (A) Frequency of CD3^{+} cells. (B) Frequency of CD4^{+} T cells, gated from CD3^{+} cells. (C) Frequency of CD8^{+} T cells, gated from CD3^{+} cells. (D) Frequency of naive (CD62L^{hi} CD44^{lo}), effector memory (CD62L^{lo} CD44^{hi}) and central memory (CD62L^{hi} CD44^{hi}) CD4^{+} T cells. (E) Frequency and number of naive, effector memory, and central memory CD8^{+} T cells. P-values are calculated using Mann-Whitney U test. Data are shown as individual mice (dots) and mean ± SEM.

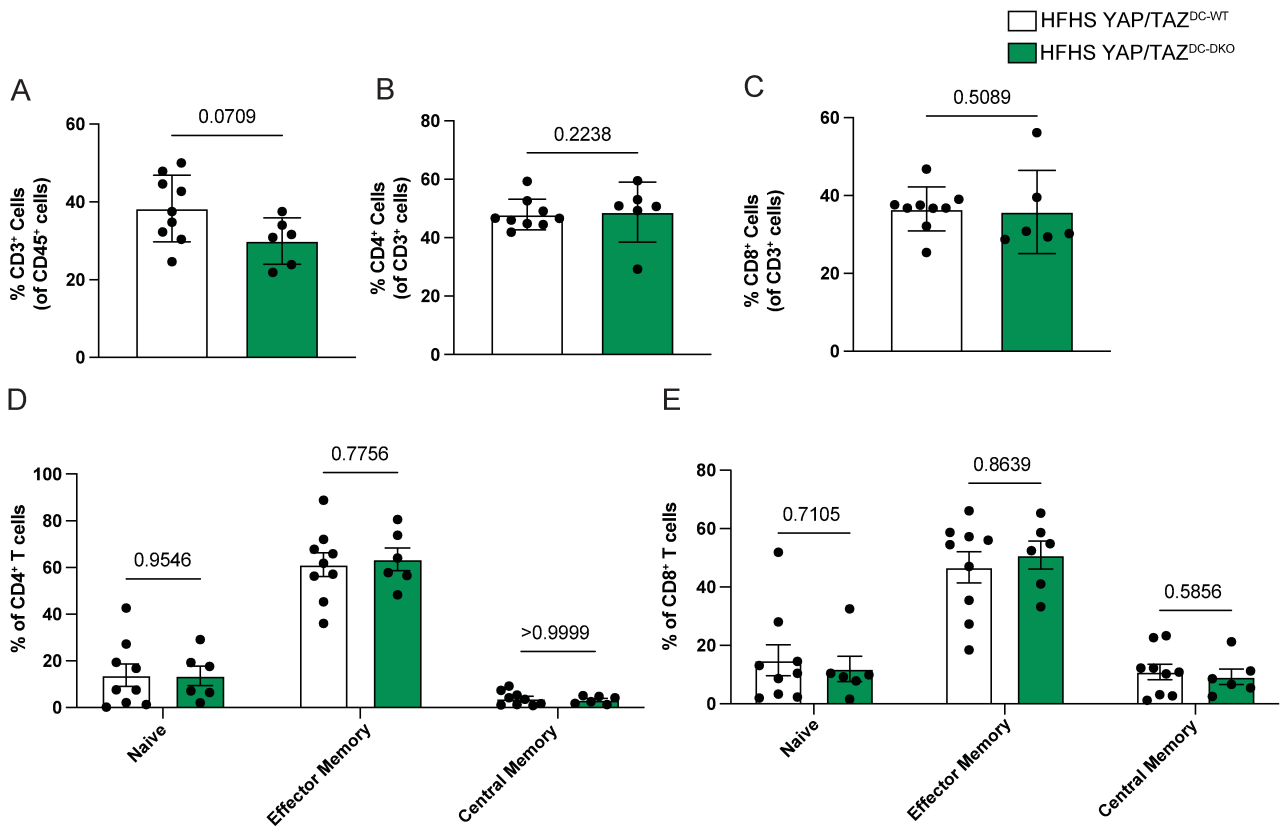

Figure 4.23 Deletion of YAP and TAZ in CD11c^{+} cells does not affect frequencies of T cell populations in the VAT of HFHS-treated mice. T cell populations were quantified by flow cytometry from dissociated VAT of HFHS YAP/TAZ$^{DC\text{-}DKO}$ (n=6) or YAP/TAZ$^{DC\text{-}WT}$ (n=9) mice. (A) Frequency of CD3^{+} cells. (B) Frequency of CD4^{+} T cells, gated from CD3^{+} cells. (C) Frequency of CD8^{+} T cells, gated from CD3^{+} cells. (D) Frequency of naive (CD62L^{hi} CD44^{lo}), effector memory (CD62L^{lo} CD44^{hi}) and central memory (CD62L^{hi} CD44^{hi}) CD4^{+} T cells. (E) Frequency and number of naive, effector memory, and central memory CD8^{+} T cells. P-values are calculated using Mann-Whitney U test. Data are shown as individual mice (dots) and mean ± SEM.

Table 4.3 Changes in frequency of immune cell populations in the VAT of HFHS-treated $YAP^{DC\text{-}KO}$, $TAZ^{DC\text{-}KO}$, and $YAP/TAZ^{DC\text{-}DKO}$ mice relative to HFHS controls. (**ø** = no difference; - = decrease; + = increase) (Trending: º; Significant: *p < 0.05. **p < 0.01.)

VAT	**$YAP^{DC\text{-}KO}$**	**$TAZ^{DC\text{-}KO}$**	**$YAP/TAZ^{DC\text{-}DKO}$**
Cells			
$CD45^+$	**ø**	**ø**	**ø**
PMNs	**ø**	**ø**	**ø**
Monocytes	**ø**	**ø**	**ø**
$CD11c^-$ Macrophages	**ø**	**ø**	**ø**
$CD11c^+$ $CD206^+$ Macrophages	**ø**	**ø**	**ø**
cDC1	**ø**	**ø**	**ø**
cDC2	**ø**	**ø**	**ø**
$CD3^+$	**ø**	**ø**	**-º**
$CD4^+$ T cells	**ø**	**ø**	**ø**
$CD8^+$ T cells	**ø**	**ø**	**ø**
$CD4^+$ Naive T cells	**ø**	**ø**	**ø**
$CD4^+$ Central Memory T cells	**ø**	**ø**	**ø**
$CD4^+$ Effector Memory T cells	**ø**	**ø**	**ø**
$CD8^+$ Naive T cells	**ø**	**+º**	**ø**
$CD8^+$ Central Memory T cells	**ø**	**-º**	**ø**
$CD8^+$ Effector Memory T cells	**ø**	**ø**	**ø**

4.2.6 Deletion of YAP and TAZ in CD11c^{+} cells does not affect liver fibrosis in HFHS-treated mice

In addition to increased inflammation in the liver, one of the parameters that indicates progression of NAFLD is fibrosis. Liver fibrosis is a consequence of the wound-healing response of the liver to repeated injury[225]. Under normal conditions, hepatic stellate cells (HSCs) in the liver act as major storage sites for vitamin A. However, chronic inflammation leads to the activation of HSCs and causes them to adopt a proinflammatory and fibrogenic phenotype[226]. This results in excessive accumulation of extracellular matrix proteins in the liver, including collagen[225]. To characterize levels of fibrosis in the livers of HFHS-treated CD11cCre *Yap*$^{fl/fl}$ *Taz*$^{fl/fl}$ mice, I used Sirius Red and Fast Green staining[227]. Sirius Red stains collagen fibers, while Fast Green binds to non-collagenous proteins. I quantified the proportion of the liver positive for Sirius Red staining. Histological analysis of livers of HFHS YAP/TAZ$^{DC\text{-}DKO}$ mice demonstrated a similar proportion of collagen staining compared to HFHS YAP/TAZ$^{DC\text{-}WT}$ mice (**Figure 4.22 A)**. Therefore, this suggests that YAP and TAZ deletion in DCs does not significantly affect the progression of fibrosis in the liver.

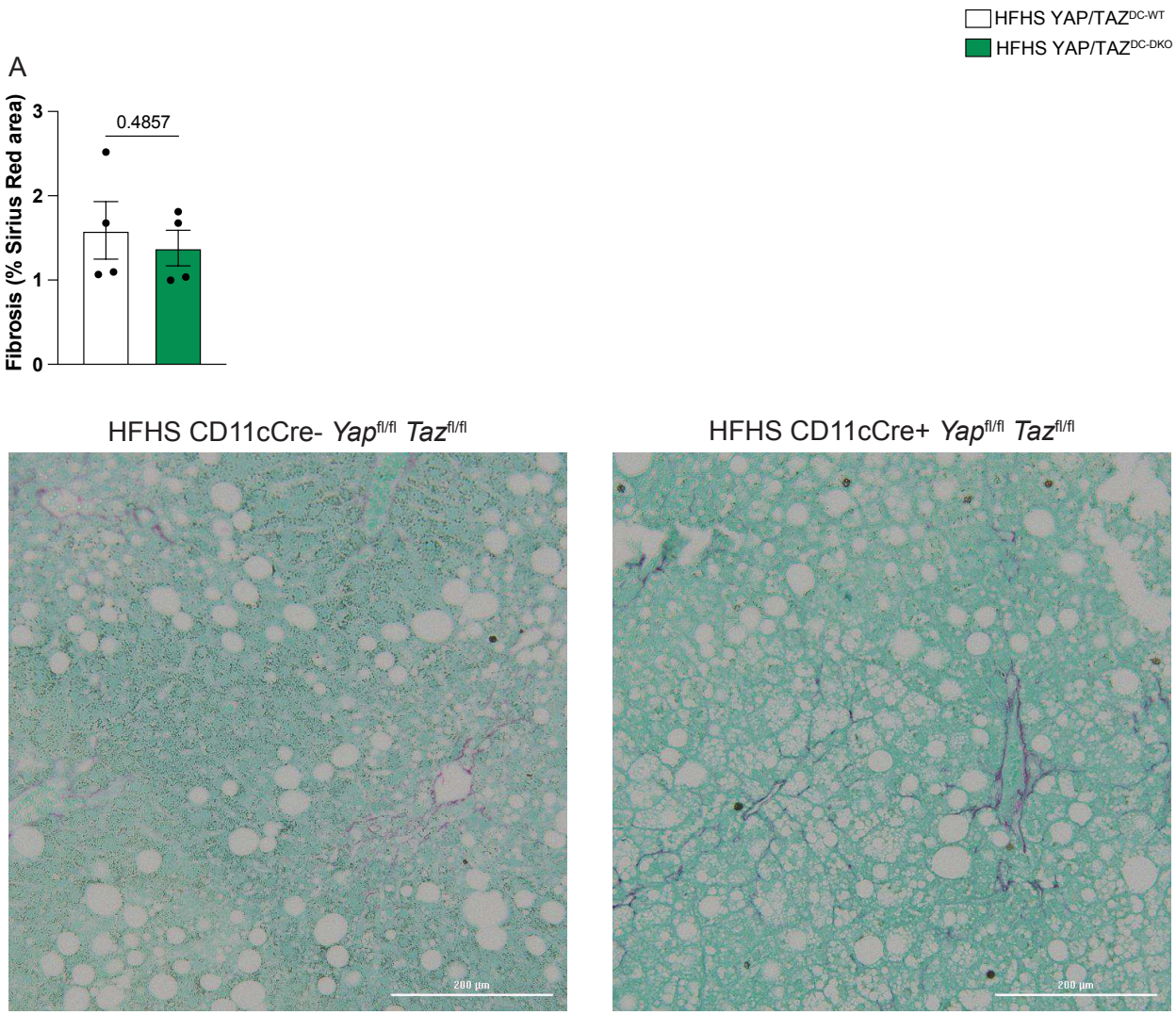

Figure 4.24 Deletion of YAP and TAZ in CD11c+ cells does not affect liver fibrosis in HFHS-treated mice. Histological analysis of liver sections from HFHS YAP/TAZ$^{DC\text{-}DKO}$ (n=4) or YAP/TAZ$^{DC\text{-}WT}$ (n=4) mice using Sirius Red/Fast Green staining to stain for collagen fibers. **(A)** Fibrosis in livers, quantified as the proportion of the liver positive for Sirius Red staining. Representative images of liver sections (bar = 200 µm). P-values are calculated using Mann-Whitney U test. Data are shown as individual mice (dots) and mean ± SEM.

4.3 Discussion

In this chapter, I explored the role of YAP and TAZ in DCs using a CD11cCre model. As YAP and TAZ signalling is typically involved in regulation of the cell cycle and cell proliferation (ref), I hypothesized that YAP and TAZ may play a role in the development of DCs. At steady-state, I observed that myeloid cell populations in the liver of $YAP^{DC\text{-}KO}$ and $TAZ^{DC\text{-}KO}$ mice were not significantly different from their control littermates (**Figure 4.3 and 4.4**). Interestingly, double knockout of YAP and TAZ in $CD11c^{+}$ cells led to a decrease in the proportion and number of MdMs, as well as cDC1s in the liver **(Figure 4.5)**. In cDC development, precursors of cDCs leave the BM and enter circulation to reach peripheral tissues to terminally differentiate into cDCs. As YAP and TAZ activity in the Hippo signalling pathway is typically involved in regulation of the cell cycle and cellular proliferation[228], these findings may suggest that YAP and TAZ may be important in the development of DCs. However, additional studies would be required to assess the role of YAP and TAZ in DC development, including examination of precursors of DCs. The differences observed may also be due to other factors such as survival and migration. Further studies using transwell migration assays can be performed to investigate the role of YAP and/or TAZ in DC migration. Interestingly, the NCD $YAP/TAZ^{DC\text{-}DKO}$ and $YAP/TAZ^{DC\text{-}WT}$ controls at 25 weeks of age did not exhibit significant differences in immune cell composition in the liver, while there were differences in MdMs and DCs at 8-12 weeks of age. However, I also only used females for baseline measurements, while males were used as NCD controls to compare with the HFHS-treated mice. It is possible that there are sex-dependent differences in YAP and TAZ activity, but there are no studies currently that indicate sex differences in YAP and TAZ signalling. In addition, mice used for baseline measurements were 8-12 weeks of age, while the mice used as NCD controls were 25 weeks of age. Therefore, the discrepancy in these NCD data could be due to a combination of age/sex effects on YAP/TAZ signalling in liver DCs.

Previous studies have indicated that signalling through YAP/TAZ in DCs is associated with increased production of pro-inflammatory cytokines[66]. As obesity-associated inflammation is linked to the development of IR, I hypothesized that YAP and TAZ signalling in DCs would enhance the development of IR. However, HFHS-treated $YAP^{DC\text{-}KO}$, $TAZ^{DC\text{-}KO}$, and $YAP/TAZ^{DC\text{-}DKO}$ mice demonstrated significantly higher fasting blood glucose levels compared

to NCD controls, indicative of IR. In addition, HFHS-treated $YAP^{DC\text{-}KO}$, $TAZ^{DC\text{-}KO}$, and $YAP/TAZ^{DC\text{-}DKO}$ mice exhibited similar levels of insulin sensitivity and glucose tolerance compared to their HFHS-treated $CD11cCre^-$ controls (**Section 4.3.2)**, demonstrating that deletion of YAP and/or TAZ in DCs does not impair development of IR. This may be due to the contribution of other mechanisms involved in obesity-associated IR. Specifically, increased levels of FFAs in circulation can lead to activation of JNK and IKK[50], which phosphorylate serine residues on IRS. Furthermore, increases in other immune cells seen during obesity, such as pro-inflammatory macrophages, can produce high levels of TNFα, which can signal through TNFR and activate JNK and IKK, resulting in inhibitory serine phosphorylation of IRS[16]. In addition, there are other factors in an obese environment that could bypass YAP/TAZ signalling, and lead to enhanced activation of DCs. For example, the uptake of FFAs by adipose tissue DCs can induce the activation of the MAPK pathway, leading to increased maturation and higher levels of MHC II expression[229]. Furthermore, FFA uptake in adipose tissue DCs leads to the formation of lipid droplets, which can promote DC activation and antigen cross-presentation, ultimately enhancing $CD4^+$ and $CD8^+$ T cell activity[230].

In general, the VAT and livers of HFHS $YAP^{DC\text{-}KO}$, $TAZ^{DC\text{-}KO}$, and $YAP/TAZ^{DC\text{-}DKO}$ mice showed similar levels of immune cell infiltration compared to their respective HFHS controls **(Section 4.3.3)**. Interestingly, the livers of HFHS-treated $YAP^{DC\text{-}KO}$ mice showed a trending decrease in the proportion of $IFN\gamma^+$ $CD4^+$ T cells and $IFN\gamma^+$ $CD8^+$ T cells compared to HFHS $YAP^{DC\text{-}WT}$ mice (**Figure 4.15)**. This suggests that YAP signalling in DCs may be involved in the regulation of DC IL-12 and IFNγ production, key cytokines involved in Th1 differentiation[224]. Functional comparison of YAP-deficient DCs with YAP-sufficient DCs by assessing their cytokine production would be a future experiment to explore this hypothesis. I also examined levels of fibrosis in the livers of HFHS $YAP/TAZ^{DC\text{-}WT}$ and $YAP/TAZ^{DC\text{-}DKO}$ mice as a readout for NAFLD disease progression. There were no significant differences in the levels of fibrosis in HFHS $YAP/TAZ^{DC\text{-}WT}$ and HFHS $YAP/TAZ^{DC\text{-}DKO}$ mice (**Figure 4.23)**. This was unsurprising, as flow cytometric analyses on the livers indicated similar levels of inflammation and inflammatory cell populations in both groups. These findings further support the notion that YAP and TAZ in DCs do not play a significant role in the pathogenesis of NAFLD.

A potential caveat in our mouse model is that I have not fully verified the efficiency of YAP/TAZ deletion. Although I have assessed levels of mRNA via RT-qPCR, it is important to also assess the protein levels of YAP and TAZ present in $CD11c^+$ cells. Inefficient deletion of YAP and TAZ in DCs could lead to the differences observed. Therefore, confirmation of floxing efficiency via quantification of YAP and TAZ proteins in DCs should be conducted. Although liver stiffness is reported to be altered during the progression of NAFLD[231], the degree to which the liver tissues stiffen in our mice compared to controls is unknown. Therefore, it may be possible that there is limited activation of YAP/TAZ signalling due to insufficient changes in tissue stiffness. For future experiments, liver stiffness after HFHS-treatment needs to be assessed to determine whether mechanical cues could be enhancing YAP/TAZ signalling. In addition, due to technical difficulties, I was unable to determine whether YAP and TAZ expression or nuclear translocation is upregulated under HFD conditions. Although multiple factors could influence YAP/TAZ signalling during obesity such as nutrient and mechanical cues, it is unclear whether obese conditions upregulate YAP and TAZ signalling in DCs. Therefore, further investigation of YAP/TAZ expression in hepatic and adipose tissue DCs between NCD and HFD-fed mice via flow cytometry or western blotting is warranted. Overall, this chapter demonstrates that deletion of YAP and/or TAZ deletion in DCs does not significantly alter the development of IR and levels of obesity-associated inflammation in the liver and VAT in a NAFLD model, unlike other reports describing a proinflammatory role of YAP in macrophages in the context of IBD[119], NASH[131], and myocardial infarction[118].

4.4 Contributions

The work characterizing our mouse models at steady-state was completed by me. The characterization of IR using ITT and IPGTT was completed with the help of Dr. Masoud Akbari and Kasia Dzierlega. The processing of all mouse tissues was expedited with the help from the members of the Tsai-Clemente lab. Paraffin-embedding and slide preparation of liver sections for histological analysis were completed with the help of Erin Strachan and Dr. Kacie Norton (University of Alberta). Access to the gentleMACS™ Octo Dissociator was kindly provided by Dr. Harissios Vliagoftis (University of Alberta) for processing of visceral adipose tissue samples. Access to the CFX96 Touch Real-Time PCR Detection System was kindly provided by Dr. Amit Bhavsar (University of Alberta).

Chapter 5: Discussion

5.1 Conclusions

5.1.1 The role of YAP and TAZ in DC-mediated pathogenesis of IR and NAFLD

Previously, we and others have described substrate stiffness as an important factor for modulating the response of DCs[66, 77]. DCs grown on higher stiffness conditions show increased activation and secretion of pro-inflammatory cytokines. Using transcriptomic analysis, we have found that TAZ is upregulated in BMDCs grown on higher stiffness substrates[66]. Furthermore, inhibition of TAZ and its homolog YAP abrogated the effects of stiffer substrates in the production of cytokines, suggesting that mechanotransduction through YAP/TAZ in DCs is associated with increased production of pro-inflammatory cytokines[66]. The contribution of DCs in obesity-associated inflammation is linked to the development of IR, as DC depletion models have shown protection from obesity-induced IR[61, 62]. Therefore, I set out to test the hypothesis that YAP and TAZ activity in DCs would enhance the development of IR.

Using a HFHS diet model, I compared CD11c-specific YAP and/or TAZ deletion in the development of IR and observed similar fasting glucose levels and tolerance to insulin and glucose **(Figure 4.6, 4.7, 4.8)**. This observation contrasts with our previous findings that exposure to stiff substrates induces a pro-inflammatory phenotype. To reconcile these differences, I envision a number of alternative scenarios. Firstly, although the participation of DCs in HFD-associated inflammation has been previously documented[61, 62], YAP/TAZ-mediated mechanosensing in DCs may not be a major pathway contributing to DC activation in this setting. Our previous findings were conducted in vitro with artificial stiffnesses, which does not capture the complexity and conditions of DCs within an organism. In vivo, the obese environment is complex, and although we expected increased tissue stiffness and nutrient signals that would activate YAP/TAZ, there are other factors that could bypass YAP/TAZ signalling, and lead to enhanced activation of DCs. For example, the uptake of FFAs by adipose tissue DCs leads to the activation of the MAPK pathway, leading to increased maturation and higher levels of MHC II expression[229]. In addition, one of the main ways that DCs can contribute to obesity-mediated inflammation is through interactions with T cells. T cells are major participants in obesity-associated inflammation, as $CD8^+$ T cells and Th1 cells produce IFNγ, and Th17 $CD4^+$ T

cells, contributing to the development of IR[35, 63]. As CD11c-specific deletion of YAP and/or TAZ did not alter T cell infiltration in the VAT and livers of HFHS-treated mice, it suggests that YAP/TAZ deletion in DCs may not be impairing their antigen presentation capabilities, which can be confirmed in future work using CFSE assays.

In addition, the lack of differences in IR may be due to additional mechanisms involved in the development of obesity-associated IR. For instance, increased levels of FFAs in circulation can lead to activation of JNK and IKK in adipocytes and hepatocytes[50], which phosphorylate serine residues on IRS. Furthermore, increases in other immune cells seen during obesity, such as pro-inflammatory macrophages, can produce high levels of TNFα, which can signal through TNFR and activate JNK and IKK, resulting in inhibitory serine phosphorylation of IRS[58].

To assess for increased progression of NAFLD, I investigated whether deletion of YAP and/or TAZ in DCs affects inflammation in the liver and VAT. Inflammation is an indication for progression from simple steatosis to NASH, and can facilitate the process of fibrosis. As our previous studies suggested that YAP and TAZ signalling in DCs enhances their production of pro-inflammatory cytokines[66], I hypothesized that the knockout of YAP and/or TAZ in DCs would decrease levels of pro-inflammatory immune cells in the liver and VAT. In general, deletion of YAP and/or TAZ in DCs did not alter the frequency and numbers of myeloid cells and T cells in the livers and VAT of obese mice, as well as T cell functionality. There are other mechanotransduction pathways that could be compensating for a deficiency in YAP and TAZ, such as through integrins and mechanosensitive ion channels. Integrin signalling in DCs leads to cytoskeletal rearrangements which are critical for formation of immune synapses between DCs and T cells[96], while Piezo1 has been shown to regulate IL-12 and TGFβ1 production by DCs to Th1 and Treg differentiation[100]. In addition to mechanotransduction pathways, there may be other signalling pathways in DCs that are enhancing DC function that do not require YAP/TAZ. As mentioned previously, elevated levels of FFAs can lead to increased DC effector function. In the liver, lipid content in DCs is positively correlated with immunogenicity and leads to greater activation of T cells and NK cells[232], while adipose tissue DCs show increased maturation and expression of MHC II with uptake of FFAs[229]. Therefore, there are other signalling pathways modulating DC function that may be compensating for the loss of YAP/TAZ. In addition, the

contribution of other cell types that are expanded during obesity, such as pro-inflammatory macrophages, can also compensate if there is a defect in DCs with YAP/TAZ deletion.

Taken altogether, this study suggests that YAP and TAZ in DCs do not play a significant role in the pathogenesis of IR and NAFLD. However, it remains to be explored whether YAP and TAZ affect DC function at steady-state, and whether it could play a functional role in other diseases. As we have previously identified that increased stiffness leads to increased pro-inflammatory function in DCs, it would be important to determine what is regulating this phenomenon for therapeutic applications. In addition to liver disease, many chronic diseases are associated with increasing inflammation, and subsequent tissue stiffness which impairs organ function, such as pulmonary fibrosis. Therefore, deepening our understanding of the signalling pathways involved in DC mechanotransduction and its impact on their effector function could help ameliorate the progression of these diseases. Manipulation of DC mechanosensing pathways could potentially be used to inhibit overactive immune responses to limit damage, or to improve immunogenicity where DC function may be impaired.

5.1.2 The role of obesity and INSR signalling in T cell-mediated anti-tumour immunity

The underlying mechanism of obesity causing cancer and inferior outcomes is complex and incompletely understood. Multiple links between obesity and cancer have been proposed, including increased levels of circulating lipids, growth hormones, and adipokines, which can have protumourigenic effects[149]. Increased lipid availability during obesity can also promote tumour growth, as cancer cells can utilize lipids to create energy by fatty acid oxidation for their proliferation[161]. In addition, recent studies suggest that obesity can contribute to tumourigenesis by impairing anti-tumour immunity. To determine how obesity mechanistically impairs anti-tumour immunity, I used a subcutaneous E.G7 lymphoma tumour cell model and assessed tumour growth and immune cell infiltration. I observed an acceleration in tumour growth in HFD-fed mice compared to NCD-fed mice **(Figure 3.2 A-C)**, which is consistent with previous reports of using different tumour models[206, 207, 208]. This is also similar to what has been observed clinically, as obese cancer patients demonstrate worsened cancer progression in several types of cancers[157].

One proposed mechanism for how obesity increases tumour burden is through impairment of immune surveillance through metabolic dysfunction. In obesity, there is an increase in lipid availability, which can impact the efficacy of various immune cells and their anti-tumour responses. Lipid uptake in macrophages is associated with polarization to immunoregulatory phenotype. Accumulation of oxidized lipids in DCs in the tumour environment is associated with impaired cross presentation by inhibiting MHC translocation to the cell surface[162], impairing their ability to activate T cells. Increased lipid availability also causes metabolic programming in NK cells that results in defects in cytokine secretion, cytotoxicity, and failure to form an immune synapse[165]. Notably, a study by Ringel et al. highlighted the importance of $CD8^+$ T cells mediating differences in tumour burden between lean and obese mice. MC38 tumour growth was accelerated in HFD-fed mice compared to NCD-fed mice, similarly to our findings. Interestingly, when they implanted MC38 tumours in TCRα chain knock-out (TCRα-KO) mice, which lack conventional αβ T cells, there was no difference in the growth rate between mice fed a NCD compared to HFD[206]. In addition, when implanting tumours in mice depleted of $CD8^+$ T cells by using an anti-CD8 antibody, there were no diet-dependent changes in tumour growth rates. This suggested that HFD induced alterations increase tumour growth by limiting $CD8^+$ T cell responses, and prompted our investigation on how HFD could be impacting T cell-mediated anti-tumour responses.

When assessing TILs in obese and lean mice, obesity reduced the proportion of intratumoural $CD8^+$ T cells **(Figure 3.2 E)**, which was similarly observed by Ringel et al., where they demonstrated a reduction in the number of intratumoural $CD8^+$ T cells in a MC38 model in HFD-fed mice[206]. The frequency of OVA-specific $CD8^+$ T cells were also decreased in the tumours of HFD-fed mice **(Figure 3.2 G, H)**, which exhibited impaired functionality, with decreased expression of IFNγ, GZMB and CD107α. Intratumoural $CD4^+$ T cells in obese mice also displayed decreased IFNγ production **(Figure 3.4 G)**, which could be augmenting differences seen in the functionality of the intratumoural CTLs. Similarly, Dyck et al. observed a reduction in $IFN\gamma^+$ and $GZMB^+$ $CD8^+$ T cells in the tumours of obese mice[169], while Ringel et al. found only a reduction in $IFN\gamma^+$ $CD8^+$ T cells[206].

To determine whether the defects observed were due to exhaustion in T cells, we assessed the expression of co-inhibitory markers on the surface of $CD8^+$ T cells, including PD-1, LAG-3, TIM-3 and KLRG1. Interestingly, there was an increase in the frequency of $KLRG1^+$ $CD8^+$ T cells. However, we did not observe differences in PD-1, LAG-3, and TIM-3 expression in TILs of obese and lean mice as previously reported[169]. However, other studies have indicated that obesity increases PD-1 expression on $CD8^+$ T cells in a B16-F0 mouse melanoma tumour model[233]. This discrepancy may be due to the different tumour models utilized, as each tumour can have distinct tumour microenvironments that alter immune cell phenotype and function. In addition, the proportion of PD-1^+ TILs in NCD-fed mice was high, with approximately 90% of TILs expressing PD-1 **(Figure 3.4 I)**. Therefore, this left minimal room to increase under HFD conditions. Inhibition of T cells through exhaustion markers is also dependent on availability of ligands. There is the possibility that tumour cells or immune cells such as macrophages and DCs are expressing higher levels of ligands for inhibitory receptors within the obese TME, which may be causing functional defects. Although we did not examine the expression of these ligands, Dyck et al. observed similar levels of PD-L1 in intratumoural leukocytes of obese and lean mice[169]. It would be worthwhile to also explore expression of other ligands, such as galectin-9 which binds to TIM-3, and MHC II and galectin-3 which interact with LAG-3[145], as these may be differentially expressed and inhibit T cell responses. Overall, our findings suggest that mechanisms independent of immune checkpoint expression may be contributing to $CD8^+$ T cell dysfunction observed in the tumours of obese mice.

To explore mechanistically how obesity could be impairing T cell-mediated anti-tumour responses, we focused on the role of insulin signalling, as hyperinsulinemia and IR are highly associated with obesity[204]. Furthermore, immune cells including T cells express the INSR[171], and evidence suggests that insulin signalling is important for T cell function, as T cells upregulate their surface expression of INSR upon activation, and impairment of INSR signalling reduces their production of effector molecules[171]. First, we hypothesized that obesity would lead to an impairment in insulin signalling in T cells. After stimulation with anti-CD3/anti-CD28, there was defective insulin-stimulated pAkt signalling **(Figure 3.8 A)**, congruent with previous findings that lymphocytes from obese patients showed reduced insulin-stimulated AKT phosphorylation in vitro[175]. An interesting future experiment would be to isolate T cells from obese and lean

tumour-bearing mice to assess whether the presence of a tumour can further impact insulin signalling in T cells.

After observing a reduction in insulin signalling in T cells from HFD-fed mice, we wanted to investigate how INSR-deficiency in T cells would impact their anti-tumour function. Using a mouse model with T cell-specific deletion of INSR, I observed a trending decrease in E.G7-OVA tumour growth, but no differences in endpoint tumour weights and dimensions **(Figure 3.9 A-C)**. Mice with T cell-targeted ablation of INSR also exhibited a decreased proportion of intratumoural OVA-specific $CD8^+$ T cells. This may be due to alterations in proliferation, as I observed a trending decrease in the frequency of adoptively transferred *Insr*-floxed $CD8^+$ T cells that divided in the draining inguinal lymph node **(Figure 3.14 A, B)**, suggesting that INSR signalling may support $CD8^+$ T cell proliferation in vivo. The differences in frequency may also be due to defects in migration in the T cells. However, this would need to be confirmed in future experiments that assess migratory abilities of INSR-deficient T cells, such as transwell assays. I also observed impaired effector functions in INSR-deficient TILs, with trending decreases in the expression of effector molecules IFNγ, GZMB, and CD107α **(Figure 3.11 C-G)**. Similar to HFD-fed mice, I did not observe any significant differences in the frequency of TILs expressing exhaustion markers **(Figure 3.11 H-K)**. Therefore, it suggests that mechanisms independent of immune checkpoint expression leads to INSR-deficient $CD8^+$ T cell dysfunction in tumours.

A potential mechanism for impaired anti-tumour T cell responses under HFD conditions and in INSR-deficient T cells is due to metabolic dysfunction **(Figure 5.1)**. During obesity, there are alterations in metabolic homeostasis, including increases in circulating FFAs and insulin, which can in turn affect immunometabolism. This is critical, as T cell metabolism is tightly linked to their differentiation, activation, and function. The ability of a T cell to mount an effective anti-tumour response is determined by its metabolic state and the availability of nutrients. Importantly, activated $CD8^+$ T cells increase their metabolic rate, which is dependent on amino acid uptake[234]. Specifically, it has been shown that CD8 T cell activation requires the activity of the amino acid transporter Solute carrier family 7 member 5 (SLC7A5)[235], which transports large neutral amino acids including leucine, phenylalanine, and tryptophan in

exchange with intracellular glutamine. Dyck et al. observed that intratumoural $CD8^+$ T cells in obese mice showed a reduction in SLC7A5 activity, and expression of CD98, which forms a complex with SLC7A5, was reduced[169]. These findings suggest that obesity leads to systemic metabolic remodeling, which potentially contributes to $CD8^+$ T cell functional defects. These alterations in amino acid metabolism could potentially be attributed to impaired INSR signalling. Upon stimulation by insulin, the activity and recruitment of amino acid transporters is enhanced. Insulin has been shown to increase mRNA abundance of the amino acid transporter SLC7A5 via an mTORC1-dependent mechanism in skeletal muscle cells[236]. Insulin also increases the expression of activating transcription factor 4 (ATF4), a transcription factor that induces amino acid synthesis and uptake[237]. In addition, we have previously found that INSR-deficient $CD4^+$ T cells have lower mRNA levels of SLC7A5 relative to INSR-sufficient T cells, which is also associated with decreased CD98 expression[171]. Therefore, defects in INSR signalling may impair uptake of amino acids, thus impairing T cell activation and function. Future work should assess the uptake of amino acids and expression of amino acid transporters in TILs of HFD vs NCD mice and INSR-deficient vs INSR-sufficient TILs.

In addition to alterations in amino acid metabolism, defects in glucose uptake and glycolytic activity in T cells can be impacted by impaired INSR signalling, resulting in T cell dysfunction. Glycolysis is a multi-step process that converts glucose into two molecules of pyruvate, and generates ATP and other metabolic intermediates. Upon T cell activation, T cells increase glucose uptake by upregulation of glucose transporters, and upregulate a glycolytic program which helps T cells generate metabolic precursors for the biosynthesis of proteins and nucleic acids to fuel clonal expansion and differentiation into effector cells[238]. Insulin stimulates glycolysis, as INSR signalling promotes glucose uptake and the activities of glycolytic enzymes such as hexokinase 2 and phosphofructokinase[239]. Notably, INSR-deficient T cells demonstrate deficient glycolytic reprogramming following activation, as demonstrated by decreased expression of glycolytic enzymes including hexokinase 2 and phosphofructokinase, and decreased glycolytic flux compared to INSR-sufficient T cells[171]. Therefore, diminished glycolytic activity in INSR-deficient T cells can reduce ATP and metabolic intermediates required for protein synthesis, proliferation, and migration, ultimately impairing their anti-tumour responses. Although there are reports of no differences in glycolytic activity between

splenic $CD8^+$ T cells from lean and obese mice[169] and no differences in glycolytic gene expression between TILs in lean and obese mice[206], it still remains to be assessed whether there are differences in glycolytic activity within the TME.

In addition to decreased levels of ATP and metabolite intermediates, a reduction in glycolytic activity and levels of glycolytic enzymes can also impact T cell function by regulating effector molecule production. Specifically, reduced glycolytic rates have been implicated as a mechanism for attenuated production of cytokines through post-transcriptional modifications. Glyceraldehyde 3-phosphate dehydrogenase (GAPDH) is a moonlighting protein that functions as a glycolytic enzyme, but is also involved in regulating mRNA stability. GAPDH has a well-established role in glycolysis where it catalyzes the conversion of glyceraldehyde-3-phosphate to 1,3,-bisphospho-d-glycerate[240]. However, recent studies have begun to appreciate its role in post-transcriptional regulation. GAPDH has been shown to bind to adenylate-uridylate (AU)-rich elements in the 3′ UTRs of IFNγ and IL-2 mRNAs[241]. When glucose is present, GAPDH engages in its enzymatic function; when cells are glucose-restricted, GAPDH becomes available to bind the 3′UTR of IFN-γ mRNA, preventing its efficient translation. In addition to GADPH, other RNA binding proteins have recently been identified that regulate cytokine production in T cells[242]. Of note, ZFP36 Ring Finger Protein Like 1 (ZFP36L1) is known to regulate cellular function by enhancing the decay of target mRNAs, and has been shown to bind to the 3'UTR of IFNγ, IL-2, and TNF mRNAs, leading to their degradation[242]. Interestingly, it has been reported that after insulin stimulation, there is an inhibition in the mRNA decay activity of ZFP36L1[243]. Activation of AKT downstream of insulin signalling led to phosphorylation of ZFP36L1 and stabilization of reporter mRNAs in fibroblasts[243]. Therefore, it would be interesting to explore how INSR signalling in T cells can regulate RNA binding proteins such as GAPDH and ZFP36L1 and their interactions with IL-2, TNF, and IFNγ mRNA. These hypotheses can be tested using electrophoretic mobility shift assays (EMSA) experiments to assess protein-mRNA interactions.

Through my study, I expanded on how obesity can impair T cell-mediated anti-tumour responses. I demonstrated that obesity accelerates tumour growth, which is associated with decreased frequencies of intratumoural $CD8^+$ T cells. The TILs in HFD-fed mice also exhibited

impaired effector functions, but no alterations in expression of exhaustion markers. To explore mechanistically how T cells were impaired in HFD-fed mice, I found that T cells from HFD-fed mice had diminished responses to insulin stimulation. Building from this, I found that INSR-deficiency in T cells may be impairing T cell functionality and in mounting an effective anti-tumour response. LckCre^{+} *Insr*$^{fl/fl}$ mice demonstrated reduced intratumoural OVA-specific CD8^{+} T cells, along with decreased effector function. INSR-deficient CD8^{+} T cells also showed no alterations in exhaustion state, mirroring what I observed in HFD-fed mice. Collectively, these findings suggest that the impaired CD8^{+} T cell-mediated anti-tumour immunity observed in HFD-fed mice may be linked to defective insulin signalling in T cells.

Given that multiple arms of the INSR signalling pathway converge with those downstream of antigen and costimulatory receptors, PRRs, cytokines and nutrient sensing pathways, future efforts are needed to elucidate the signalling networks insulin uses in immune cells and how this is regulated in the face of different stimuli. There are many therapeutic applications as our understanding of how INSR plays a role in mediating T cell-mediated responses increases. By determining the pathway alterations responsible for the IR-associated phenotype, we could potentially manipulate these pathways to boost CTL function. Interestingly, patients with various types of cancers were markedly insulin-resistant compared to age-matched healthy controls[244]. Future studies should address whether immune cells in these patients also demonstrate an insulin-resistant phenotype, and whether ameliorating IR in these patients can improve cancer outcomes. Insulin sensitizing agents such as AMPK agonists, including metformin, are potential candidates for therapeutics as they already are commonly prescribed medications in patients with type 2 diabetes, and mediate improved insulin sensitivity by increasing INSR activity, while also increasing recruitment and activity of the glucose transporters[245]. In immune cells, this effect is expected to reactivate cell intrinsic insulin response. A greater understanding of how obesity affects the TME and anti-tumour immunity can aid in the design of metabolic and immunotherapies against cancer.

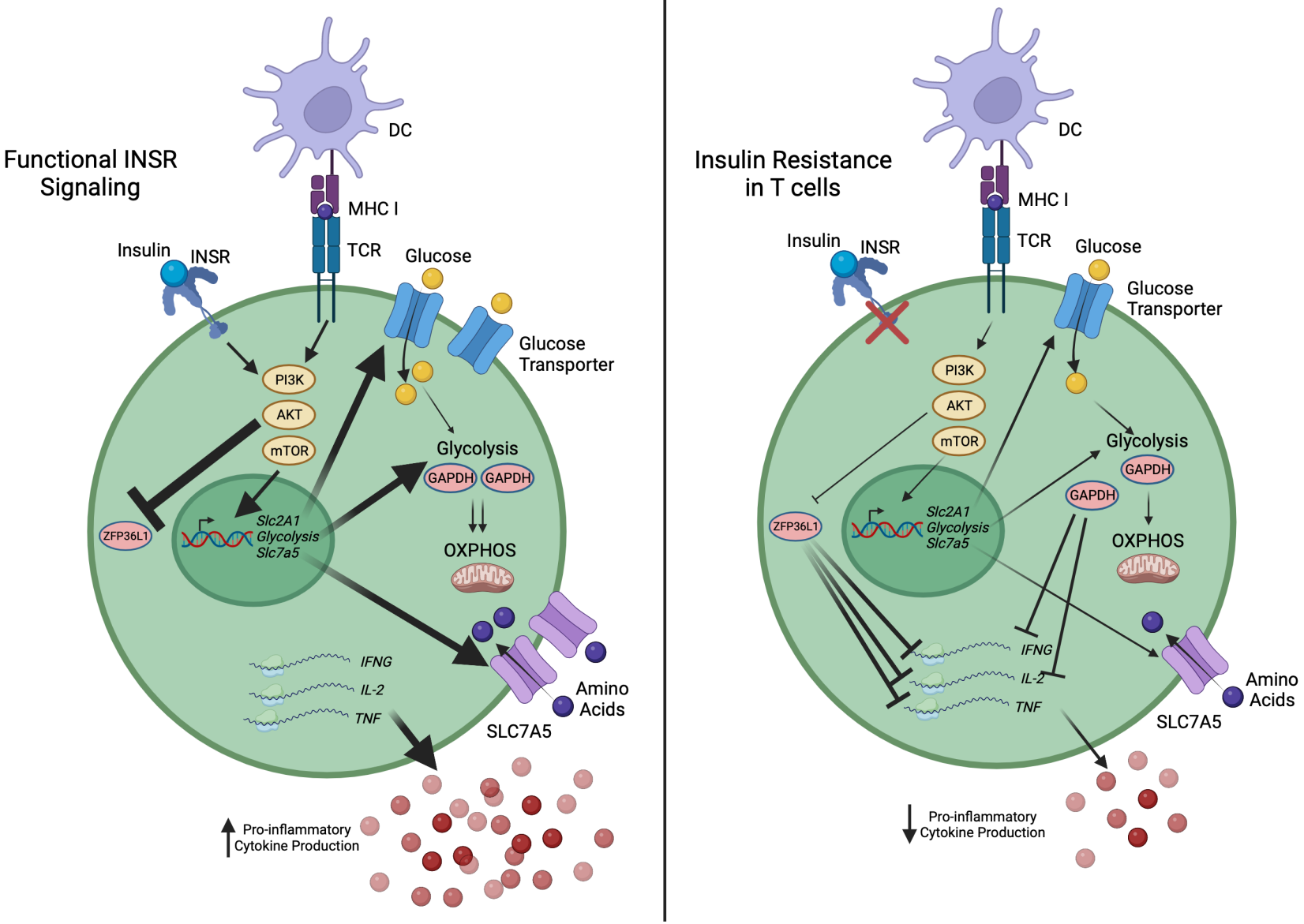
Functional INSR Signaling
DC
MHC I
TCR
Insulin
INSR
Glucose
Glucose Transporter
PI3K
AKT
mTOR
Glycolysis
GAPDH
GAPDH
ZFP36L1
Slc2A1
Glycolysis
Slc7a5
OXPHOS
IFNG
IL-2
TNF
Amino Acids
SLC7A5
Pro-inflammatory Cytokine Production
Insulin Resistance in T cells
DC
MHC I
TCR
Insulin
INSR
Glucose
Glucose Transporter
PI3K
AKT
mTOR
Glycolysis
GAPDH
GAPDH
ZFP36L1
Slc2A1
Glycolysis
Slc7a5
OXPHOS
IFNG
IL-2
TNF
Amino Acids
SLC7A5
Pro-inflammatory Cytokine Production

Figure 5.1 Proposed mechanism linking obesity and insulin resistance in T cells to decreased effector function. Obesity leads to widespread metabolic dysfunction in the body. Hypertrophic adipocytes during obesity become stressed and produce pro-inflammatory cytokines which can signal through receptors to dampen insulin receptor signalling, and lead to a state of hyperinsulinemia which can induce insulin resistance in T cells. With functional INSR signalling (left), there is a synergistic effect with TCR signalling, promoting activation of the PI3K/AKT/mTOR pathway. This promotes the upregulation of genes for glucose transport (*Slc2A1*), glycolysis, and amino acid transport (*Slc7a5*), enhancing glycolysis, OXPHOS, and amino acid metabolism essential for T cell function and differentiation. In addition, activation of AKT leads to the phosphorylation and inhibition of ZFP36L1, preventing its mRNA decay activity on *IFNG, IL-2, and TNF* mRNA transcripts. Increased glycolytic activity also sequesters GAPDH from binding to the 3' UTR regions of *IFNG* and *IL-2*, allowing for increased production of these cytokines. When T cells are insulin resistant (right), either induced by obesity-associated factors or by genetic ablation of INSR, decreased INSR signalling reduces signalling through the PI3K/AKT/mTOR pathway. Reduction of PI3K/AKT/mTOR signalling inhibits transcription of genes involved in glucose uptake, amino acid uptake, and glycolysis. This reduces the amount of available nutrients to generate energy and substrates critical for T cell function and activation. Impaired INSR signalling also increases ZFP36L1 activity, and decreases the amount of GAPDH being utilized for glyoclysis. ZFP36L1 and GAPDH can bind to 3' UTR regions of IFNγ, IL-2, and TNFα mRNA, preventing their translation. Consequently, there are decreases in the production of pro-inflammatory cytokines. Abbreviations are as follows: IL-6: interleukin-6; TNFα: tumour necrosis factor alpha; INSR: insulin receptor; MHC I: major histocompatibility complex class I; TCR: T cell receptor; PI3K: phosphatidylinositol 3-kinase; AKT: Ak strain transforming; mTOR: mammalian target of rapamycin; *Slc2A1*: solute carrier family 2 member 1; *Slc7a5*: solute carrier family 7 member 5; ZFP36L1: ZFP36 ring finger protein like 1; GAPDH: glyceraldehyde 3-phosphate dehydrogenase; OXPHOS: oxidative phosphorylation. Drawn in BioRender.com.

References

1. Organization, W.H. Obesity and overweight. 2021 [cited March 1, 2023]Available from: https://www.who.int/news-room/fact-sheets/detail/obesity-and-overweight

2. Ellulu, M.S., Patimah, I., Khaza'ai, H., Rahmat, A. & Abed, Y. Obesity and inflammation: the linking mechanism and the complications. *Arch Med Sci* **13**, 851-863 (2017).

3. Hruby, A. & Hu, F.B. The Epidemiology of Obesity: A Big Picture. *Pharmacoeconomics* **33**, 673-689 (2015).

4. Jung, U.J. & Choi, M.S. Obesity and its metabolic complications: the role of adipokines and the relationship between obesity, inflammation, insulin resistance, dyslipidemia and nonalcoholic fatty liver disease. *Int J Mol Sci* **15**, 6184-6223 (2014).

5. Ahima, R.S. & Flier, J.S. Adipose tissue as an endocrine organ. *Trends Endocrinol Metab* **11**, 327-332 (2000).

6. Cannon, B. & Nedergaard, J. Brown adipose tissue: function and physiological significance. *Physiol Rev* **84**, 277-359 (2004).

7. Vijgen, G.H. *et al.* Brown adipose tissue in morbidly obese subjects. *PLoS One* **6**, e17247 (2011).

8. Rosen, E.D. & Spiegelman, B.M. What we talk about when we talk about fat. *Cell* **156**, 20-44 (2014).

9. Shuster, A., Patlas, M., Pinthus, J.H. & Mourtzakis, M. The clinical importance of visceral adiposity: a critical review of methods for visceral adipose tissue analysis. *Br J Radiol* **85**, 1-10 (2012).

10. Khan, S., Chan, Y.T., Revelo, X.S. & Winer, D.A. The Immune Landscape of Visceral Adipose Tissue During Obesity and Aging. *Front Endocrinol (Lausanne)* **11**, 267 (2020).

11. Karastergiou, K. & Mohamed-Ali, V. The autocrine and paracrine roles of adipokines. *Mol Cell Endocrinol* **318**, 69-78 (2010).

12. Wynn, T.A. & Vannella, K.M. Macrophages in Tissue Repair, Regeneration, and Fibrosis. *Immunity* **44**, 450-462 (2016).

13. Catrysse, L. & van Loo, G. Adipose tissue macrophages and their polarization in health and obesity. *Cell Immunol* **330**, 114-119 (2018).

14. Wentworth, J.M. *et al.* Pro-inflammatory CD11c+CD206+ adipose tissue macrophages are associated with insulin resistance in human obesity. *Diabetes* **59**, 1648-1656 (2010).

15. Banchereau, J. *et al.* Immunobiology of dendritic cells. *Annu Rev Immunol* **18**, 767-811 (2000).

16. Watowich, S.S. & Liu, Y.J. Mechanisms regulating dendritic cell specification and development. *Immunol Rev* **238**, 76-92 (2010).

17. Schlitzer, A. *et al.* Identification of cDC1- and cDC2-committed DC progenitors reveals early lineage priming at the common DC progenitor stage in the bone marrow. *Nature Immunology* **16**, 718-728 (2015).

18. Macdougall, C.E. *et al.* Visceral Adipose Tissue Immune Homeostasis Is Regulated by the Crosstalk between Adipocytes and Dendritic Cell Subsets. *Cell Metab* **27**, 588-601.e584 (2018).

19. Wu, D. *et al.* Eosinophils sustain adipose alternatively activated macrophages associated with glucose homeostasis. *Science* **332**, 243-247 (2011).

20. Wencker, M. *et al.* Innate-like T cells straddle innate and adaptive immunity by altering antigen-receptor responsiveness. *Nat Immunol* **15**, 80-87 (2014).

21. Lynch, L. *et al.* Adipose tissue invariant NKT cells protect against diet-induced obesity and metabolic disorder through regulatory cytokine production. *Immunity* **37**, 574-587 (2012).

22. Winer, D.A., Winer, S., Chng, M.H., Shen, L. & Engleman, E.G. B Lymphocytes in obesity-related adipose tissue inflammation and insulin resistance. *Cell Mol Life Sci* **71**, 1033-1043 (2014).

23. Nishimura, S. *et al.* Adipose Natural Regulatory B Cells Negatively Control Adipose Tissue Inflammation. *Cell Metab* **18**, 759-766 (2013).

24. van den Broek, T., Borghans, J.A.M. & van Wijk, F. The full spectrum of human naive T cells. *Nat Rev Immunol* **18**, 363-373 (2018).

25. Saravia, J., Chapman, N.M. & Chi, H. Helper T cell differentiation. *Cellular & Molecular Immunology* **16**, 634-643 (2019).

26. Feuerer, M. *et al.* Lean, but not obese, fat is enriched for a unique population of regulatory T cells that affect metabolic parameters. *Nat Med* **15**, 930-939 (2009).

27. Han, J.M. & Levings, M.K. Immune regulation in obesity-associated adipose inflammation. *J Immunol* **191**, 527-532 (2013).

28. Cinti, S. *et al.* Adipocyte death defines macrophage localization and function in adipose tissue of obese mice and humans. *J Lipid Res* **46**, 2347-2355 (2005).

29. Taylor, P.R. *et al.* Macrophage receptors and immune recognition. *Annu Rev Immunol* **23**, 901-944 (2005).

30. Elgazar-Carmon, V., Rudich, A., Hadad, N. & Levy, R. Neutrophils transiently infiltrate intra-abdominal fat early in the course of high-fat feeding. *J Lipid Res* **49**, 1894-1903 (2008).

31. Bertola, A. *et al.* Identification of adipose tissue dendritic cells correlated with obesity-associated insulin-resistance and inducing Th17 responses in mice and patients. *Diabetes* **61**, 2238-2247 (2012).

32. DeFuria, J. *et al.* B cells promote inflammation in obesity and type 2 diabetes through regulation of T-cell function and an inflammatory cytokine profile. *Proc Natl Acad Sci U S A* **110**, 5133-5138 (2013).

33. Strissel, K.J. *et al.* T-cell recruitment and Th1 polarization in adipose tissue during diet-induced obesity in C57BL/6 mice. *Obesity (Silver Spring)* **18**, 1918-1925 (2010).

34. Gaffen, S.L., Kramer, J.M., Yu, J.J. & Shen, F. The IL-17 cytokine family. *Vitam Horm* **74**, 255-282 (2006).

35. Nishimura, S. *et al.* CD8+ effector T cells contribute to macrophage recruitment and adipose tissue inflammation in obesity. *Nat Med* **15**, 914-920 (2009).

36. Wilcox, G. Insulin and insulin resistance. *Clin Biochem Rev* **26**, 19-39 (2005).

37. Dimitriadis, G., Mitrou, P., Lambadiari, V., Maratou, E. & Raptis, S.A. Insulin effects in muscle and adipose tissue. *Diabetes Res Clin Pract* **93 Suppl 1**, S52-59 (2011).

38. Boucher, J., Kleinridders, A. & Kahn, C.R. Insulin receptor signaling in normal and insulin-resistant states. *Cold Spring Harb Perspect Biol* **6** (2014).

39. Haeusler, R.A., McGraw, T.E. & Accili, D. Biochemical and cellular properties of insulin receptor signalling. *Nature Reviews Molecular Cell Biology* **19**, 31-44 (2018).

40. Kadowaki, T., Ueki, K., Yamauchi, T. & Kubota, N. SnapShot: Insulin signaling pathways. *Cell* **148**, 624, 624.e621 (2012).

41. Taniguchi, C.M., Emanuelli, B. & Kahn, C.R. Critical nodes in signalling pathways: insights into insulin action. *Nature Reviews Molecular Cell Biology* **7**, 85-96 (2006).

42. Goldstein, B.J., Ahmad, F., Ding, W., Li, P.M. & Zhang, W.R. Regulation of the insulin signalling pathway by cellular protein-tyrosine phosphatases. *Mol Cell Biochem* **182**, 91-99 (1998).

43. Millward, T.A., Zolnierowicz, S. & Hemmings, B.A. Regulation of protein kinase cascades by protein phosphatase 2A. *Trends Biochem Sci* **24**, 186-191 (1999).

44. Carracedo, A. & Pandolfi, P.P. The PTEN–PI3K pathway: of feedbacks and cross-talks. *Oncogene* **27**, 5527-5541 (2008).

45. Emanuelli, B. *et al.* SOCS-3 is an insulin-induced negative regulator of insulin signaling. *J Biol Chem* **275**, 15985-15991 (2000).

46. Aguirre, V., Uchida, T., Yenush, L., Davis, R. & White, M.F. The c-Jun NH(2)-terminal kinase promotes insulin resistance during association with insulin receptor substrate-1 and phosphorylation of Ser(307). *J Biol Chem* **275**, 9047-9054 (2000).

47. Gao, Z. *et al.* Serine phosphorylation of insulin receptor substrate 1 by inhibitor kappa B kinase complex. *J Biol Chem* **277**, 48115-48121 (2002).

48. Li, Y. *et al.* Protein kinase C Theta inhibits insulin signaling by phosphorylating IRS1 at Ser(1101). *J Biol Chem* **279**, 45304-45307 (2004).

49. Zhang, J., Gao, Z., Yin, J., Quon, M.J. & Ye, J. S6K directly phosphorylates IRS-1 on Ser-270 to promote insulin resistance in response to TNF-(alpha) signaling through IKK2. *J Biol Chem* **283**, 35375-35382 (2008).

50. Schenk, S., Saberi, M. & Olefsky, J.M. Insulin sensitivity: modulation by nutrients and inflammation. *J Clin Invest* **118**, 2992-3002 (2008).

51. Ali, O. Genetics of type 2 diabetes. *World J Diabetes* **4**, 114-123 (2013).

52. Shi, H. *et al.* TLR4 links innate immunity and fatty acid-induced insulin resistance. *J Clin Invest* **116**, 3015-3025 (2006).

53. Westwick, J.K., Bielawska, A.E., Dbaibo, G., Hannun, Y.A. & Brenner, D.A. Ceramide activates the stress-activated protein kinases. *J Biol Chem* **270**, 22689-22692 (1995).

54. Teruel, T., Hernandez, R. & Lorenzo, M. Ceramide mediates insulin resistance by tumor necrosis factor-alpha in brown adipocytes by maintaining Akt in an inactive dephosphorylated state. *Diabetes* **50**, 2563-2571 (2001).

55. Ye, J. Mechanisms of insulin resistance in obesity. *Front Med* **7**, 14-24 (2013).

56. Ye, J. Role of insulin in the pathogenesis of free fatty acid-induced insulin resistance in skeletal muscle. *Endocr Metab Immune Disord Drug Targets* **7**, 65-74 (2007).

57. DeFronzo, R.A. *et al.* Type 2 diabetes mellitus. *Nature Reviews Disease Primers* **1**, 15019 (2015).

58. Peraldi, P., Hotamisligil, G.S., Buurman, W.A., White, M.F. & Spiegelman, B.M. Tumor necrosis factor (TNF)-alpha inhibits insulin signaling through stimulation of the p55 TNF receptor and activation of sphingomyelinase. *J Biol Chem* **271**, 13018-13022 (1996).

59. Hirosumi, J. *et al.* A central role for JNK in obesity and insulin resistance. *Nature* **420**, 333-336 (2002).

60. Wu, H. & Ballantyne, C.M. Metabolic Inflammation and Insulin Resistance in Obesity. *Circ Res* **126**, 1549-1564 (2020).

61. Stefanovic-Racic, M. *et al.* Dendritic cells promote macrophage infiltration and comprise a substantial proportion of obesity-associated increases in CD11c+ cells in adipose tissue and liver. *Diabetes* **61**, 2330-2339 (2012).

62. Cho, K.W. *et al.* Adipose Tissue Dendritic Cells Are Independent Contributors to Obesity-Induced Inflammation and Insulin Resistance. *J Immunol* **197**, 3650-3661 (2016).

63. Winer, S. *et al.* Normalization of obesity-associated insulin resistance through immunotherapy. *Nat Med* **15**, 921-929 (2009).

64. Sun, J. *et al.* Association between abdominal obesity and liver steatosis and fibrosis among patients with chronic hepatitis B measured by Fibroscan. *Exp Ther Med* **18**, 1891-1898 (2019).

65. Sun, K., Kusminski, C.M. & Scherer, P.E. Adipose tissue remodeling and obesity. *J Clin Invest* **121**, 2094-2101 (2011).

66. Chakraborty, M. *et al.* Mechanical Stiffness Controls Dendritic Cell Metabolism and Function. *Cell Rep* **34**, 108609 (2021).

67. Lee, M., Du, H., Winer, D.A., Clemente-Casares, X. & Tsai, S. Mechanosensing in macrophages and dendritic cells in steady-state and disease. *Frontiers in Cell and Developmental Biology* **10** (2022).

68. Banchereau, J. & Steinman, R.M. Dendritic cells and the control of immunity. *Nature* **392**, 245-252 (1998).

69. Steinman, R.M. & Idoyaga, J. Features of the dendritic cell lineage. *Immunol Rev* **234**, 5-17 (2010).

70. Marzaioli, V. *et al.* Monocyte-Derived Dendritic Cell Differentiation in Inflammatory Arthritis Is Regulated by the JAK/STAT Axis via NADPH Oxidase Regulation. *Front Immunol* **11**, 1406 (2020).

71. Swiecki, M. & Colonna, M. The multifaceted biology of plasmacytoid dendritic cells. *Nat Rev Immunol* **15**, 471-485 (2015).

72. Liu, K. *et al.* In vivo analysis of dendritic cell development and homeostasis. *Science* **324**, 392-397 (2009).

73. Jonuleit, H. *et al.* Pro-inflammatory cytokines and prostaglandins induce maturation of potent immunostimulatory dendritic cells under fetal calf serum-free conditions. *Eur J Immunol* **27**, 3135-3142 (1997).

74. Waskow, C. *et al.* The receptor tyrosine kinase Flt3 is required for dendritic cell development in peripheral lymphoid tissues. *Nat Immunol* **9**, 676-683 (2008).

75. Schaupp, L. *et al.* Microbiota-Induced Type I Interferons Instruct a Poised Basal State of Dendritic Cells. *Cell* **181**, 1080-1096.e1019 (2020).

76. Craig, D.H., Schaubert, K.L., Shiratsuchi, H., Kan-Mitchell, J. & Basson, M.D. Increased pressure stimulates aberrant dendritic cell maturation. *Cell Mol Biol Lett* **13**, 260-270 (2008).

77. Mennens, S.F.B. *et al.* Substrate stiffness influences phenotype and function of human antigen-presenting dendritic cells. *Sci Rep* **7**, 17511 (2017).

78. Kang, J.H. *et al.* Biomechanical forces enhance directed migration and activation of bone marrow-derived dendritic cells. *Sci Rep* **11**, 12106 (2021).

79. Lewis, J.S. *et al.* The effect of cyclic mechanical strain on activation of dendritic cells cultured on adhesive substrates. *Biomaterials* **34**, 9063-9070 (2013).

80. Pearce, E.J. & Everts, B. Dendritic cell metabolism. *Nat Rev Immunol* **15**, 18-29 (2015).

81. Cabeza-Cabrerizo, M., Cardoso, A., Minutti, C.M., Pereira da Costa, M. & Reis e Sousa, C. Dendritic Cells Revisited. *Annu Rev Immunol* **39**, 131-166 (2021).

82. Vanepps, J.S. & Vorp, D.A. Mechano-pathobiology of atherogenesis: a review. *J Surg Res* **142**, 202-217 (2007).

83. Hampton, H.R. & Chtanova, T. Lymphatic Migration of Immune Cells. *Front Immunol* **10**, 1168 (2019).

84. Förster, R. *et al.* CCR7 coordinates the primary immune response by establishing functional microenvironments in secondary lymphoid organs. *Cell* **99**, 23-33 (1999).

85. Craig, D.H., Shiratsuchi, H. & Basson, M.D. Increased extracellular pressure provides a novel adjuvant stimulus for enhancement of conventional dendritic cell maturation strategies. *Biochem Biophys Res Commun* **387**, 174-179 (2009).

86. Cerboni, S., Gentili, M. & Manel, N. Diversity of pathogen sensors in dendritic cells. *Adv Immunol* **120**, 211-237 (2013).

87. Blumenthal, D., Chandra, V., Avery, L. & Burkhardt, J.K. Mouse T cell priming is enhanced by maturation-dependent stiffening of the dendritic cell cortex. *Elife* **9** (2020).

88. Tamkun, J.W. *et al.* Structure of integrin, a glycoprotein involved in the transmembrane linkage between fibronectin and actin. *Cell* **46**, 271-282 (1986).

89. Hynes, R.O. Integrins: bidirectional, allosteric signaling machines. *Cell* **110**, 673-687 (2002).

90. Aglialoro, F., Hofsink, N., Hofman, M., Brandhorst, N. & van den Akker, E. Inside Out Integrin Activation Mediated by PIEZO1 Signaling in Erythroblasts. *Front Physiol* **11**, 958 (2020).

91. Liu, D., Wu, J., An, J. & Cyster, J.G. Requirements for cDC2 positioning in blood-exposed regions of the neonatal and adult spleen. *J Exp Med* **217** (2020).

92. Li, S., Dislich, B., Brakebusch, C.H., Lichtenthaler, S.F. & Brocker, T. Control of Homeostasis and Dendritic Cell Survival by the GTPase RhoA. *J Immunol* **195**, 4244-4256 (2015).

93. Lessey, E.C., Guilluy, C. & Burridge, K. From mechanical force to RhoA activation. *Biochemistry* **51**, 7420-7432 (2012).

94. Laudanna, C., Campbell, J.J. & Butcher, E.C. Role of Rho in chemoattractant-activated leukocyte adhesion through integrins. *Science* **271**, 981-983 (1996).

95. Xu, Y. *et al.* Dendritic cell motility and T cell activation requires regulation of Rho-cofilin signaling by the Rho-GTPase activating protein myosin IXb. *J Immunol* **192**, 3559-3568 (2014).

96. Rodríguez-Fernández, J.L. & Criado-García, O. The Actin Cytoskeleton at the Immunological Synapse of Dendritic Cells. *Front Cell Dev Biol* **9**, 679500 (2021).

97. Parpaite, T. & Coste, B. Piezo channels. *Current biology : CB* **27**, R250-r252 (2017).

98. Solis, A.G. *et al.* Mechanosensation of cyclical force by PIEZO1 is essential for innate immunity. *Nature* **573**, 69-74 (2019).

99. Wang, Y. *et al.* Dendritic cell Piezo1 integrating mechanical stiffness and inflammatory signals directs the differentiation of T_H1 and T_{reg} cells in cancer. *bioRxiv*, 2022.2005.2017.492270 (2022).

100. Wang, Y. *et al.* Dendritic cell Piezo1 directs the differentiation of T(H)1 and T(reg) cells in cancer. *Elife* **11** (2022).

101. Misra, J.R. & Irvine, K.D. The Hippo Signaling Network and Its Biological Functions. *Annu Rev Genet* **52**, 65-87 (2018).

102. Chan, E.H. *et al.* The Ste20-like kinase Mst2 activates the human large tumor suppressor kinase Lats1. *Oncogene* **24**, 2076-2086 (2005).

103. Hergovich, A., Schmitz, D. & Hemmings, B.A. The human tumour suppressor LATS1 is activated by human MOB1 at the membrane. *Biochem Biophys Res Commun* **345**, 50-58 (2006).

104. Zhao, B. *et al.* Inactivation of YAP oncoprotein by the Hippo pathway is involved in cell contact inhibition and tissue growth control. *Genes Dev* **21**, 2747-2761 (2007).

105. Lei, Q.Y. *et al.* TAZ promotes cell proliferation and epithelial-mesenchymal transition and is inhibited by the hippo pathway. *Mol Cell Biol* **28**, 2426-2436 (2008).

106. Vassilev, A., Kaneko, K.J., Shu, H., Zhao, Y. & DePamphilis, M.L. TEAD/TEF transcription factors utilize the activation domain of YAP65, a Src/Yes-associated protein localized in the cytoplasm. *Genes Dev* **15**, 1229-1241 (2001).

107. Mahoney, W.M., Jr., Hong, J.H., Yaffe, M.B. & Farrance, I.K. The transcriptional co-activator TAZ interacts differentially with transcriptional enhancer factor-1 (TEF-1) family members. *Biochem J* **388**, 217-225 (2005).

108. Sabra, H. *et al.* β1 integrin-dependent Rac/group I PAK signaling mediates YAP activation of Yes-associated protein 1 (YAP1) via NF2/merlin. *J Biol Chem* **292**, 19179-19197 (2017).

109. Aragona, M. *et al.* A mechanical checkpoint controls multicellular growth through YAP/TAZ regulation by actin-processing factors. *Cell* **154**, 1047-1059 (2013).

110. Driscoll, T.P., Cosgrove, B.D., Heo, S.J., Shurden, Z.E. & Mauck, R.L. Cytoskeletal to Nuclear Strain Transfer Regulates YAP Signaling in Mesenchymal Stem Cells. *Biophys J* **108**, 2783-2793 (2015).

111. Wang, W. *et al.* AMPK modulates Hippo pathway activity to regulate energy homeostasis. *Nat Cell Biol* **17**, 490-499 (2015).

112. Yang, C.S. *et al.* Glutamine-utilizing transaminases are a metabolic vulnerability of TAZ/YAP-activated cancer cells. *EMBO Rep* **19** (2018).

113. Koo, J.H. *et al.* Induction of AP-1 by YAP/TAZ contributes to cell proliferation and organ growth. *Genes Dev* **34**, 72-86 (2020).

114. Pavel, M. *et al.* Contact inhibition controls cell survival and proliferation via YAP/TAZ-autophagy axis. *Nat Commun* **9**, 2961 (2018).

115. Huang, Y.J. *et al.* Ovatodiolide suppresses colon tumorigenesis and prevents polarization of M2 tumor-associated macrophages through YAP oncogenic pathways. *J Hematol Oncol* **10**, 60 (2017).

116. Yang, W. *et al.* Influence of the Hippo-YAP signalling pathway on tumor associated macrophages (TAMs) and its implications on cancer immunosuppressive microenvironment. *Ann Transl Med* **8**, 399 (2020).

117. Feng, Y. *et al.* The signaling protein Wnt5a promotes TGFβ1-mediated macrophage polarization and kidney fibrosis by inducing the transcriptional regulators Yap/Taz. *J Biol Chem* **293**, 19290-19302 (2018).

118. Mia, M.M. *et al.* YAP/TAZ deficiency reprograms macrophage phenotype and improves infarct healing and cardiac function after myocardial infarction. *PLoS Biol* **18**, e3000941 (2020).

119. Zhou, X. *et al.* YAP Aggravates Inflammatory Bowel Disease by Regulating M1/M2 Macrophage Polarization and Gut Microbial Homeostasis. *Cell Rep* **27**, 1176-1189.e1175 (2019).

120. Meli, V.S. *et al.* YAP-mediated mechanotransduction tunes the macrophage inflammatory response. *Sci Adv* **6** (2020).

121. Liu, M. *et al.* Macrophage MST1/2 Disruption Impairs Post-Infarction Cardiac Repair via LTB4. *Circ Res* **129**, 909-926 (2021).

122. Totaro, A., Panciera, T. & Piccolo, S. YAP/TAZ upstream signals and downstream responses. *Nat Cell Biol* **20**, 888-899 (2018).

123. Du, X. *et al.* Hippo/Mst signalling couples metabolic state and immune function of CD8α(+) dendritic cells. *Nature* **558**, 141-145 (2018).

124. Ingber, D.E. Mechanobiology and diseases of mechanotransduction. *Ann Med* **35**, 564-577 (2003).

125. Gotschy, A. *et al.* Local arterial stiffening assessed by MRI precedes atherosclerotic plaque formation. *Circ Cardiovasc Imaging* **6**, 916-923 (2013).

126. Palombo, C. & Kozakova, M. Arterial stiffness, atherosclerosis and cardiovascular risk: Pathophysiologic mechanisms and emerging clinical indications. *Vascul Pharmacol* **77**, 1-7 (2016).

127. Blacher, J. *et al.* Carotid arterial stiffness as a predictor of cardiovascular and all-cause mortality in end-stage renal disease. *Hypertension* **32**, 570-574 (1998).

128. Stewart, D.C. *et al.* Quantitative assessment of intestinal stiffness and associations with fibrosis in human inflammatory bowel disease. *PLoS One* **13**, e0200377 (2018).

129. Nahon, P. *et al.* Liver stiffness measurement versus clinicians' prediction or both for the assessment of liver fibrosis in patients with chronic hepatitis C. *Am J Gastroenterol* **101**, 2744-2751 (2006).

130. Krausgruber, T. *et al.* IRF5 promotes inflammatory macrophage polarization and TH1-TH17 responses. *Nature Immunology* **12**, 231-238 (2011).

131. Song, K. *et al.* Yes-Associated Protein in Kupffer Cells Enhances the Production of Proinflammatory Cytokines and Promotes the Development of Nonalcoholic Steatohepatitis. *Hepatology* **72**, 72-87 (2020).

132. Wang, C. *et al.* Verteporfin inhibits YAP function through up-regulating 14-3-3σ sequestering YAP in the cytoplasm. *Am J Cancer Res* **6**, 27-37 (2016).

133. Sung, H. *et al.* Global Cancer Statistics 2020: GLOBOCAN Estimates of Incidence and Mortality Worldwide for 36 Cancers in 185 Countries. *CA Cancer J Clin* **71**, 209-249 (2021).

134. Tian, T., Olson, S., Whitacre, J.M. & Harding, A. The origins of cancer robustness and evolvability. *Integr Biol (Camb)* **3**, 17-30 (2011).

135. Chen, D.S. & Mellman, I. Oncology meets immunology: the cancer-immunity cycle. *Immunity* **39**, 1-10 (2013).

136. Keefe, D. *et al.* Perforin triggers a plasma membrane-repair response that facilitates CTL induction of apoptosis. *Immunity* **23**, 249-262 (2005).

137. Aqbi, H.F., Wallace, M., Sappal, S., Payne, K.K. & Manjili, M.H. IFN-γ orchestrates tumor elimination, tumor dormancy, tumor escape, and progression. *J Leukoc Biol* (2018).

138. Pardoll, D.M. & Topalian, S.L. The role of CD4+ T cell responses in antitumor immunity. *Curr Opin Immunol* **10**, 588-594 (1998).

139. Mumberg, D. *et al.* CD4(+) T cells eliminate MHC class II-negative cancer cells in vivo by indirect effects of IFN-gamma. *Proc Natl Acad Sci U S A* **96**, 8633-8638 (1999).

140. Fridman, W.H., Pagès, F., Sautès-Fridman, C. & Galon, J. The immune contexture in human tumours: impact on clinical outcome. *Nat Rev Cancer* **12**, 298-306 (2012).

141. Wherry, E.J. T cell exhaustion. *Nat Immunol* **12**, 492-499 (2011).

142. Greenberg, S.A., Kong, S.W., Thompson, E. & Gulla, S.V. Co-inhibitory T cell receptor KLRG1: human cancer expression and efficacy of neutralization in murine cancer models. *Oncotarget* **10**, 1399-1406 (2019).

143. Riley, J.L. PD-1 signaling in primary T cells. *Immunol Rev* **229**, 114-125 (2009).

144. Du, W. *et al.* TIM-3 as a Target for Cancer Immunotherapy and Mechanisms of Action. *Int J Mol Sci* **18** (2017).

145. Anderson, A.C., Joller, N. & Kuchroo, V.K. Lag-3, Tim-3, and TIGIT: Co-inhibitory Receptors with Specialized Functions in Immune Regulation. *Immunity* **44**, 989-1004 (2016).

146. Iwai, Y. *et al.* Involvement of PD-L1 on tumor cells in the escape from host immune system and tumor immunotherapy by PD-L1 blockade. *Proc Natl Acad Sci U S A* **99**, 12293-12297 (2002).

147. Cham, C.M., Driessens, G., O'Keefe, J.P. & Gajewski, T.F. Glucose deprivation inhibits multiple key gene expression events and effector functions in CD8+ T cells. *Eur J Immunol* **38**, 2438-2450 (2008).

148. Wang, W. & Zou, W. Amino Acids and Their Transporters in T Cell Immunity and Cancer Therapy. *Mol Cell* **80**, 384-395 (2020).

149. Dyck, L. & Lynch, L. Cancer, obesity and immunometabolism - Connecting the dots. *Cancer Lett* **417**, 11-20 (2018).

150. Chang, C.H. *et al.* Posttranscriptional control of T cell effector function by aerobic glycolysis. *Cell* **153**, 1239-1251 (2013).

151. Buck, M.D., Sowell, R.T., Kaech, S.M. & Pearce, E.L. Metabolic Instruction of Immunity. *Cell* **169**, 570-586 (2017).

152. Vinay, D.S. *et al.* Immune evasion in cancer: Mechanistic basis and therapeutic strategies. *Semin Cancer Biol* **35 Suppl**, S185-s198 (2015).

153. Curiel, T.J. *et al.* Specific recruitment of regulatory T cells in ovarian carcinoma fosters immune privilege and predicts reduced survival. *Nat Med* **10**, 942-949 (2004).

154. Zou, W. Regulatory T cells, tumour immunity and immunotherapy. *Nat Rev Immunol* **6**, 295-307 (2006).

155. Avgerinos, K.I., Spyrou, N., Mantzoros, C.S. & Dalamaga, M. Obesity and cancer risk: Emerging biological mechanisms and perspectives. *Metabolism* **92**, 121-135 (2019).

156. Calle, E.E., Rodriguez, C., Walker-Thurmond, K. & Thun, M.J. Overweight, obesity, and mortality from cancer in a prospectively studied cohort of U.S. adults. *N Engl J Med* **348**, 1625-1638 (2003).

157. Schmitz, K.H. *et al.* Impact of obesity on cancer survivorship and the potential relevance of race and ethnicity. *J Natl Cancer Inst* **105**, 1344-1354 (2013).

158. Font-Burgada, J., Sun, B. & Karin, M. Obesity and Cancer: The Oil that Feeds the Flame. *Cell Metab* **23**, 48-62 (2016).

159. Uddin, S. *et al.* Role of leptin and its receptors in the pathogenesis of thyroid cancer. *Int J Clin Exp Pathol* **4**, 637-643 (2011).

160. Beloribi-Djefaflia, S., Vasseur, S. & Guillaumond, F. Lipid metabolic reprogramming in cancer cells. *Oncogenesis* **5**, e189 (2016).

161. Carracedo, A., Cantley, L.C. & Pandolfi, P.P. Cancer metabolism: fatty acid oxidation in the limelight. *Nat Rev Cancer* **13**, 227-232 (2013).

162. Herber, D.L. *et al.* Lipid accumulation and dendritic cell dysfunction in cancer. *Nat Med* **16**, 880-886 (2010).

163. Lynch, L.A. *et al.* Are natural killer cells protecting the metabolically healthy obese patient? *Obesity (Silver Spring)* **17**, 601-605 (2009).

164. Woo, S.R., Corrales, L. & Gajewski, T.F. Innate immune recognition of cancer. *Annu Rev Immunol* **33**, 445-474 (2015).

165. O'Shea, D., Cawood, T.J., O'Farrelly, C. & Lynch, L. Natural killer cells in obesity: impaired function and increased susceptibility to the effects of cigarette smoke. *PLoS One* **5**, e8660 (2010).

166. Butt, A.Q. & Mills, K.H. Immunosuppressive networks and checkpoints controlling antitumor immunity and their blockade in the development of cancer immunotherapeutics and vaccines. *Oncogene* **33**, 4623-4631 (2014).

167. Noy, R. & Pollard, J.W. Tumor-associated macrophages: from mechanisms to therapy. *Immunity* **41**, 49-61 (2014).

168. Michalek, R.D. *et al.* Cutting edge: distinct glycolytic and lipid oxidative metabolic programs are essential for effector and regulatory CD4+ T cell subsets. *J Immunol* **186**, 3299-3303 (2011).

169. Dyck, L. *et al.* Correction: Suppressive effects of the obese tumor microenvironment on CD8 T cell infiltration and effector function. *J Exp Med* **219** (2022).

170. Ganeshan, K. & Chawla, A. Metabolic regulation of immune responses. *Annu Rev Immunol* **32**, 609-634 (2014).

171. Tsai, S. *et al.* Insulin Receptor-Mediated Stimulation Boosts T Cell Immunity during Inflammation and Infection. *Cell Metab* **28**, 922-934.e924 (2018).

172. Yue, S., Luo, M., Liu, H. & Wei, S. Recent Advances of Gold Compounds in Anticancer Immunity. *Front Chem* **8**, 543 (2020).

173. Berman, J.S. & Center, D.M. Chemotactic activity of porcine insulin for human T lymphocytes in vitro. *The Journal of Immunology* **138**, 2100-2103 (1987).

174. Fischer, H.J. *et al.* The Insulin Receptor Plays a Critical Role in T Cell Function and Adaptive Immunity. *J Immunol* **198**, 1910-1920 (2017).

175. Viardot, A. *et al.* Obesity is associated with activated and insulin resistant immune cells. *Diabetes Metab Res Rev* **28**, 447-454 (2012).

176. McArdle, M.A., Finucane, O.M., Connaughton, R.M., McMorrow, A.M. & Roche, H.M. Mechanisms of obesity-induced inflammation and insulin resistance: insights into the emerging role of nutritional strategies. *Front Endocrinol (Lausanne)* **4**, 52 (2013).

177. Rahman, A.H. & Aloman, C. Dendritic cells and liver fibrosis. *Biochim Biophys Acta* **1832**, 998-1004 (2013).

178. Cassinotto, C. *et al.* Liver stiffness in nonalcoholic fatty liver disease: A comparison of supersonic shear imaging, FibroScan, and ARFI with liver biopsy. *Hepatology* **63**, 1817-1827 (2016).

179. Lo, C.M., Wang, H.B., Dembo, M. & Wang, Y.L. Cell movement is guided by the rigidity of the substrate. *Biophys J* **79**, 144-152 (2000).

180. Koo, J.H. & Guan, K.L. Interplay between YAP/TAZ and Metabolism. *Cell Metab* **28**, 196-206 (2018).

181. Moore, M.W., Carbone, F.R. & Bevan, M.J. Introduction of soluble protein into the class I pathway of antigen processing and presentation. *Cell* **54**, 777-785 (1988).

182. Frey, M.R., Leontieva, O., Watters, D.J. & Black, J.D. Stimulation of protein kinase C-dependent and -independent signaling pathways by bistratene A in intestinal epithelial cells. *Biochem Pharmacol* **61**, 1093-1100 (2001).

183. Morgan, A.J. & Jacob, R. Ionomycin enhances Ca2+ influx by stimulating store-regulated cation entry and not by a direct action at the plasma membrane. *Biochem J* **300 (Pt 3)**, 665-672 (1994).

184. Chardin, P. & McCormick, F. Brefeldin A: the advantage of being uncompetitive. *Cell* **97**, 153-155 (1999).

185. Inaba, K. *et al.* Generation of large numbers of dendritic cells from mouse bone marrow cultures supplemented with granulocyte/macrophage colony-stimulating factor. *J Exp Med* **176**, 1693-1702 (1992).

186. Quah, B.J. & Parish, C.R. The use of carboxyfluorescein diacetate succinimidyl ester (CFSE) to monitor lymphocyte proliferation. *J Vis Exp* (2010).

187. Hogquist, K.A. *et al.* T cell receptor antagonist peptides induce positive selection. *Cell* **76**, 17-27 (1994).

188. Mowat, C., Mosley, S.R., Namdar, A., Schiller, D. & Baker, K. Anti-tumor immunity in mismatch repair-deficient colorectal cancers requires type I IFN-driven CCL5 and CXCL10. *J Exp Med* **218** (2021).

189. Wang, C.Y. & Liao, J.K. A mouse model of diet-induced obesity and insulin resistance. *Methods Mol Biol* **821**, 421-433 (2012).

190. Casimiro, I., Stull, N.D., Tersey, S.A. & Mirmira, R.G. Phenotypic sexual dimorphism in response to dietary fat manipulation in C57BL/6J mice. *J Diabetes Complications* **35**, 107795 (2021).

191. Lauby-Secretan, B. *et al.* Body Fatness and Cancer--Viewpoint of the IARC Working Group. *N Engl J Med* **375**, 794-798 (2016).

192. Michelet, X. *et al.* Metabolic reprogramming of natural killer cells in obesity limits antitumor responses. *Nat Immunol* **19**, 1330-1340 (2018).

193. Trapani, J.A. & Smyth, M.J. Functional significance of the perforin/granzyme cell death pathway. *Nature Reviews Immunology* **2**, 735-747 (2002).

194. Aktas, E., Kucuksezer, U.C., Bilgic, S., Erten, G. & Deniz, G. Relationship between CD107a expression and cytotoxic activity. *Cell Immunol* **254**, 149-154 (2009).

195. Zhang, D.J. *et al.* Selective expression of the Cre recombinase in late-stage thymocytes using the distal promoter of the Lck gene. *J Immunol* **174**, 6725-6731 (2005).

196. Landais, E. *et al.* New design of MHC class II tetramers to accommodate fundamental principles of antigen presentation. *J Immunol* **183**, 7949-7957 (2009).

197. Ziegler, S.F., Ramsdell, F. & Alderson, M.R. The activation antigen CD69. *Stem Cells* **12**, 456-465 (1996).

198. Tau, G.Z., Cowan, S.N., Weisburg, J., Braunstein, N.S. & Rothman, P.B. Regulation of IFN-gamma signaling is essential for the cytotoxic activity of CD8(+) T cells. *J Immunol* **167**, 5574-5582 (2001).

199. Wu, C. *et al.* IFN-γ primes macrophage activation by increasing phosphatase and tensin homolog via downregulation of miR-3473b. *J Immunol* **193**, 3036-3044 (2014).

200. Früh, K. & Yang, Y. Antigen presentation by MHC class I and its regulation by interferon gamma. *Curr Opin Immunol* **11**, 76-81 (1999).

201. Bhat, P., Leggatt, G., Waterhouse, N. & Frazer, I.H. Interferon-γ derived from cytotoxic lymphocytes directly enhances their motility and cytotoxicity. *Cell Death & Disease* **8**, e2836-e2836 (2017).

202. Lakhani, S.A. *et al.* Caspases 3 and 7: key mediators of mitochondrial events of apoptosis. *Science* **311**, 847-851 (2006).

203. Kanda, Y., Okazaki, T. & Katakai, T. Motility Dynamics of T Cells in Tumor-Draining Lymph Nodes: A Rational Indicator of Antitumor Response and Immune Checkpoint Blockade. *Cancers (Basel)* **13** (2021).

204. Draznin, B. Molecular mechanisms of insulin resistance: serine phosphorylation of insulin receptor substrate-1 and increased expression of p85alpha: the two sides of a coin. *Diabetes* **55**, 2392-2397 (2006).

205. Tsuchiya, A., Kanno, T. & Nishizaki, T. PI3 kinase directly phosphorylates Akt1/2 at Ser473/474 in the insulin signal transduction pathway. *J Endocrinol* **220**, 49-59 (2014).

206. Ringel, A.E. *et al.* Obesity Shapes Metabolism in the Tumor Microenvironment to Suppress Anti-Tumor Immunity. *Cell* **183**, 1848-1866.e1826 (2020).

207. Algire, C. *et al.* Diet and tumor LKB1 expression interact to determine sensitivity to anti-neoplastic effects of metformin in vivo. *Oncogene* **30**, 1174-1182 (2011).

208. Nimri, L., Saadi, J., Peri, I., Yehuda-Shnaidman, E. & Schwartz, B. Mechanisms linking obesity to altered metabolism in mice colon carcinogenesis. *Oncotarget* **6**, 38195-38209 (2015).

209. Misumi, I. *et al.* Obesity Expands a Distinct Population of T Cells in Adipose Tissue and Increases Vulnerability to Infection. *Cell Rep* **27**, 514-524.e515 (2019).

210. Tsai, S., Clemente-Casares, X., Revelo, X.S., Winer, S. & Winer, D.A. Are obesity-related insulin resistance and type 2 diabetes autoimmune diseases? *Diabetes* **64**, 1886-1897 (2015).

211. Caton, M.L., Smith-Raska, M.R. & Reizis, B. Notch-RBP-J signaling controls the homeostasis of CD8- dendritic cells in the spleen. *J Exp Med* **204**, 1653-1664 (2007).

212. Chu, K. Mechanosensing modulates dendritic cell function and metabolism. Master of Science thesis, University of Alberta, 2022.

213. Shan, Z. & Ju, C. Hepatic Macrophages in Liver Injury. *Front Immunol* **11**, 322 (2020).

214. Krenkel, O. & Tacke, F. Liver macrophages in tissue homeostasis and disease. *Nature Reviews Immunology* **17**, 306-321 (2017).

215. Wen, Y., Lambrecht, J., Ju, C. & Tacke, F. Hepatic macrophages in liver homeostasis and diseases-diversity, plasticity and therapeutic opportunities. *Cell Mol Immunol* **18**, 45-56 (2021).

216. Kohli, R. *et al.* High-fructose, medium chain trans fat diet induces liver fibrosis and elevates plasma coenzyme Q9 in a novel murine model of obesity and nonalcoholic steatohepatitis. *Hepatology* **52**, 934-944 (2010).

217. Benedé-Ubieto, R., Estévez-Vázquez, O., Ramadori, P., Cubero, F.J. & Nevzorova, Y.A. Guidelines and Considerations for Metabolic Tolerance Tests in Mice. *Diabetes Metab Syndr Obes* **13**, 439-450 (2020).

218. Pierantonelli, I. & Svegliati-Baroni, G. Nonalcoholic Fatty Liver Disease: Basic Pathogenetic Mechanisms in the Progression From NAFLD to NASH. *Transplantation* **103**, e1-e13 (2019).

219. Del Campo, J.A., Gallego, P. & Grande, L. Role of inflammatory response in liver diseases: Therapeutic strategies. *World J Hepatol* **10**, 1-7 (2018).

220. Breuer, D.A. *et al.* CD8(+) T cells regulate liver injury in obesity-related nonalcoholic fatty liver disease. *Am J Physiol Gastrointest Liver Physiol* **318**, G211-g224 (2020).

221. Clark, G.J. *et al.* The role of dendritic cells in the innate immune system. *Microbes Infect* **2**, 257-272 (2000).

222. Sallusto, F., Geginat, J. & Lanzavecchia, A. Central memory and effector memory T cell subsets: function, generation, and maintenance. *Annu Rev Immunol* **22**, 745-763 (2004).

223. Ponta, H., Sherman, L. & Herrlich, P.A. CD44: from adhesion molecules to signalling regulators. *Nat Rev Mol Cell Biol* **4**, 33-45 (2003).

224. Zhang, Y., Zhang, Y., Gu, W. & Sun, B. TH1/TH2 cell differentiation and molecular signals. *Adv Exp Med Biol* **841**, 15-44 (2014).

225. Bataller, R. & Brenner, D.A. Liver fibrosis. *J Clin Invest* **115**, 209-218 (2005).

226. Marra, F. Hepatic stellate cells and the regulation of liver inflammation. *J Hepatol* **31**, 1120-1130 (1999).

227. López-De León, A. & Rojkind, M. A simple micromethod for collagen and total protein determination in formalin-fixed paraffin-embedded sections. *J Histochem Cytochem* **33**, 737-743 (1985).

228. Yu, F.X., Zhao, B. & Guan, K.L. Hippo Pathway in Organ Size Control, Tissue Homeostasis, and Cancer. *Cell* **163**, 811-828 (2015).

229. Soedono, S. & Cho, K.W. Adipose Tissue Dendritic Cells: Critical Regulators of Obesity-Induced Inflammation and Insulin Resistance. *Int J Mol Sci* **22** (2021).

230. den Brok, M.H., Raaijmakers, T.K., Collado-Camps, E. & Adema, G.J. Lipid Droplets as Immune Modulators in Myeloid Cells. *Trends Immunol* **39**, 380-392 (2018).

231. Yoneda, M. *et al.* Transient elastography in patients with non-alcoholic fatty liver disease (NAFLD). *Gut* **56**, 1330-1331 (2007).

232. Ibrahim, J. *et al.* Dendritic cell populations with different concentrations of lipid regulate tolerance and immunity in mouse and human liver. *Gastroenterology* **143**, 1061-1072 (2012).

233. Wang, Z. *et al.* Paradoxical effects of obesity on T cell function during tumor progression and PD-1 checkpoint blockade. *Nature Medicine* **25**, 141-151 (2019).

234. Loftus, R.M. & Finlay, D.K. Immunometabolism: Cellular Metabolism Turns Immune Regulator. *J Biol Chem* **291**, 1-10 (2016).

235. Sinclair, L.V. *et al.* Control of amino-acid transport by antigen receptors coordinates the metabolic reprogramming essential for T cell differentiation. *Nat Immunol* **14**, 500-508 (2013).

236. Walker, D.K. *et al.* Insulin increases mRNA abundance of the amino acid transporter SLC7A5/LAT1 via an mTORC1-dependent mechanism in skeletal muscle cells. *Physiol Rep* **2**, e00238 (2014).

237. Malmberg, S.E. & Adams, C.M. Insulin signaling and the general amino acid control response. Two distinct pathways to amino acid synthesis and uptake. *J Biol Chem* **283**, 19229-19234 (2008).

238. Palmer, C.S., Ostrowski, M., Balderson, B., Christian, N. & Crowe, S.M. Glucose metabolism regulates T cell activation, differentiation, and functions. *Front Immunol* **6**, 1 (2015).

239. Qaid, M.M. & Abdelrahman, M.M. Role of insulin and other related hormones in energy metabolism—A review. *Cogent Food & Agriculture* **2**, 1267691 (2016).

240. White, M.R. & Garcin, E.D. D-Glyceraldehyde-3-Phosphate Dehydrogenase Structure and Function. *Subcell Biochem* **83**, 413-453 (2017).

241. Nagy, E. & Rigby, W.F. Glyceraldehyde-3-phosphate dehydrogenase selectively binds AU-rich RNA in the NAD(+)-binding region (Rossmann fold). *J Biol Chem* **270**, 2755-2763 (1995).

242. Popović, B. *et al.* Time-dependent regulation of cytokine production by RNA binding proteins defines T cell effector function. *Cell Rep* **42**, 112419 (2023).

243. Schmidlin, M. *et al.* The ARE-dependent mRNA-destabilizing activity of BRF1 is regulated by protein kinase B. *Embo j* **23**, 4760-4769 (2004).

244. Màrmol, J.M. *et al.* Insulin resistance in patients with cancer: a systematic review and meta-analysis. *Acta Oncol*, 1-8 (2023).

245. Drzewoski, J. & Hanefeld, M. The Current and Potential Therapeutic Use of Metformin-The Good Old Drug. *Pharmaceuticals (Basel)* **14** (2021).

Appendix

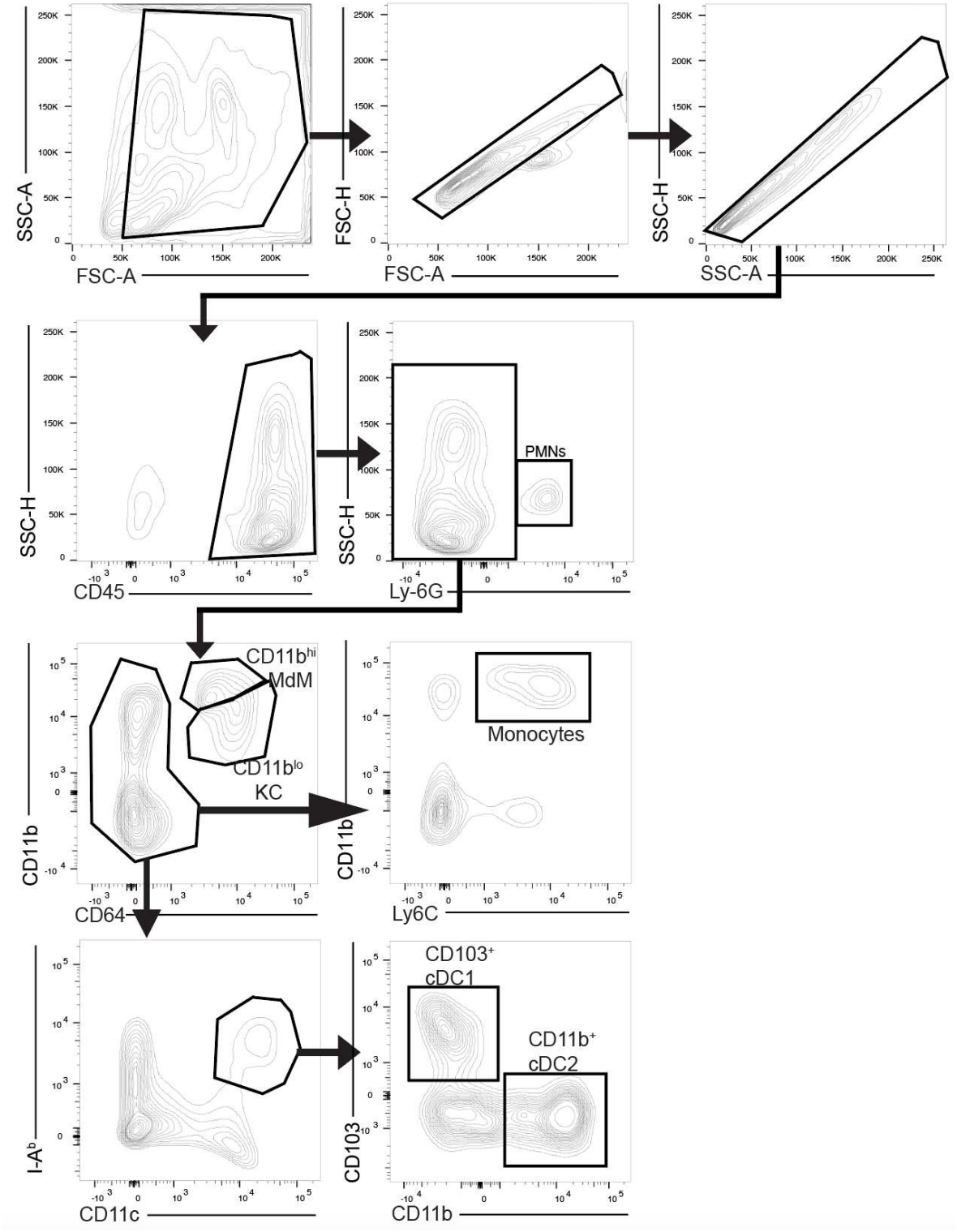

Figure A.1 Gating strategy of myeloid cells in the liver. Gating strategies for flow cytometry analysis of myeloid cells in the liver in Figures 4.3, 4.4, 4.5, 4.9, 4.10, and 4.11.

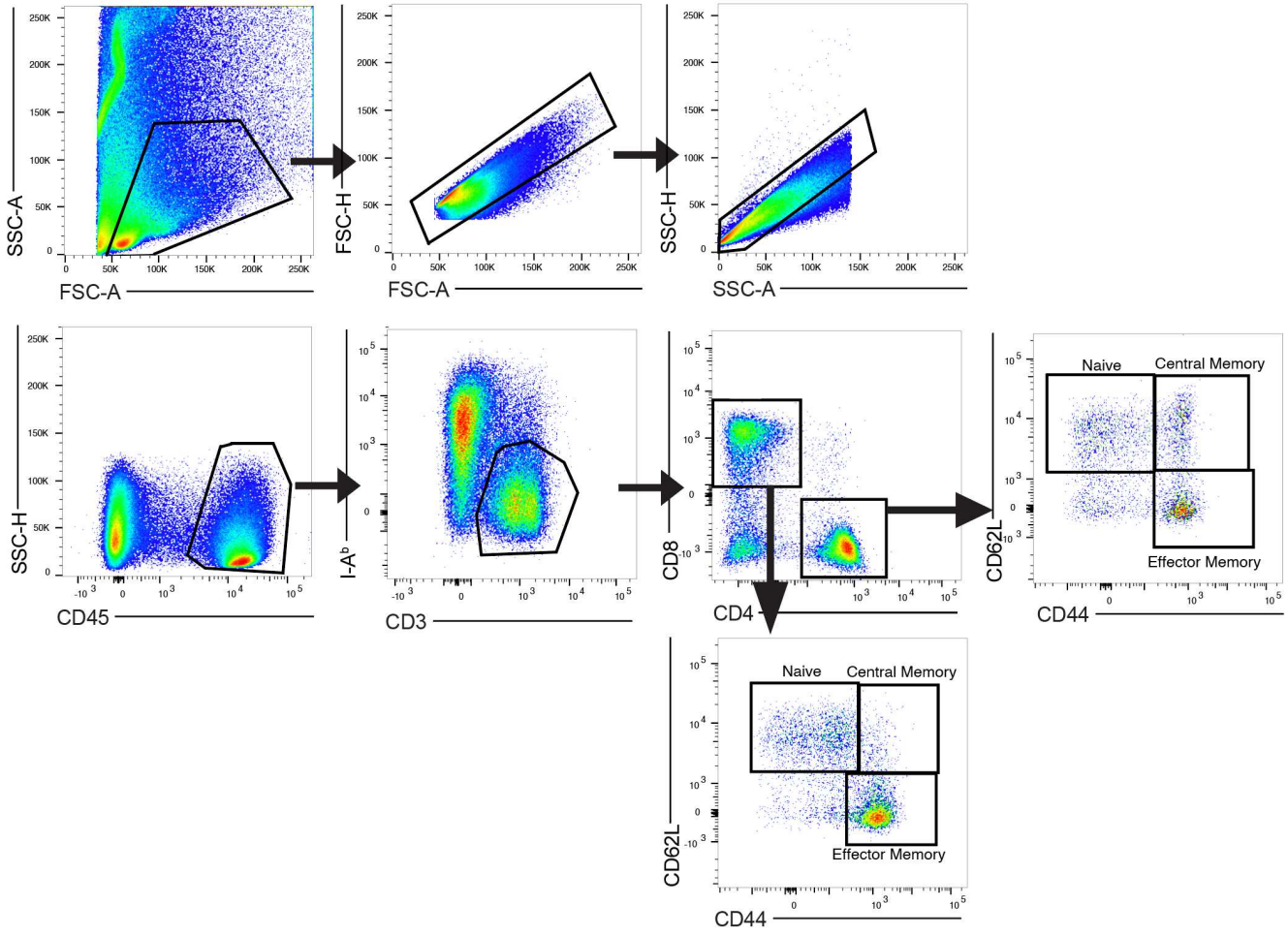

Figure A.2 Gating strategy of T cells in the liver and VAT. Gating strategies for flow cytometry analysis of T cell populations in the liver and VAT in Figures 4.12, 4.13, 4.14, 4.21, 4.22, and 4.23.

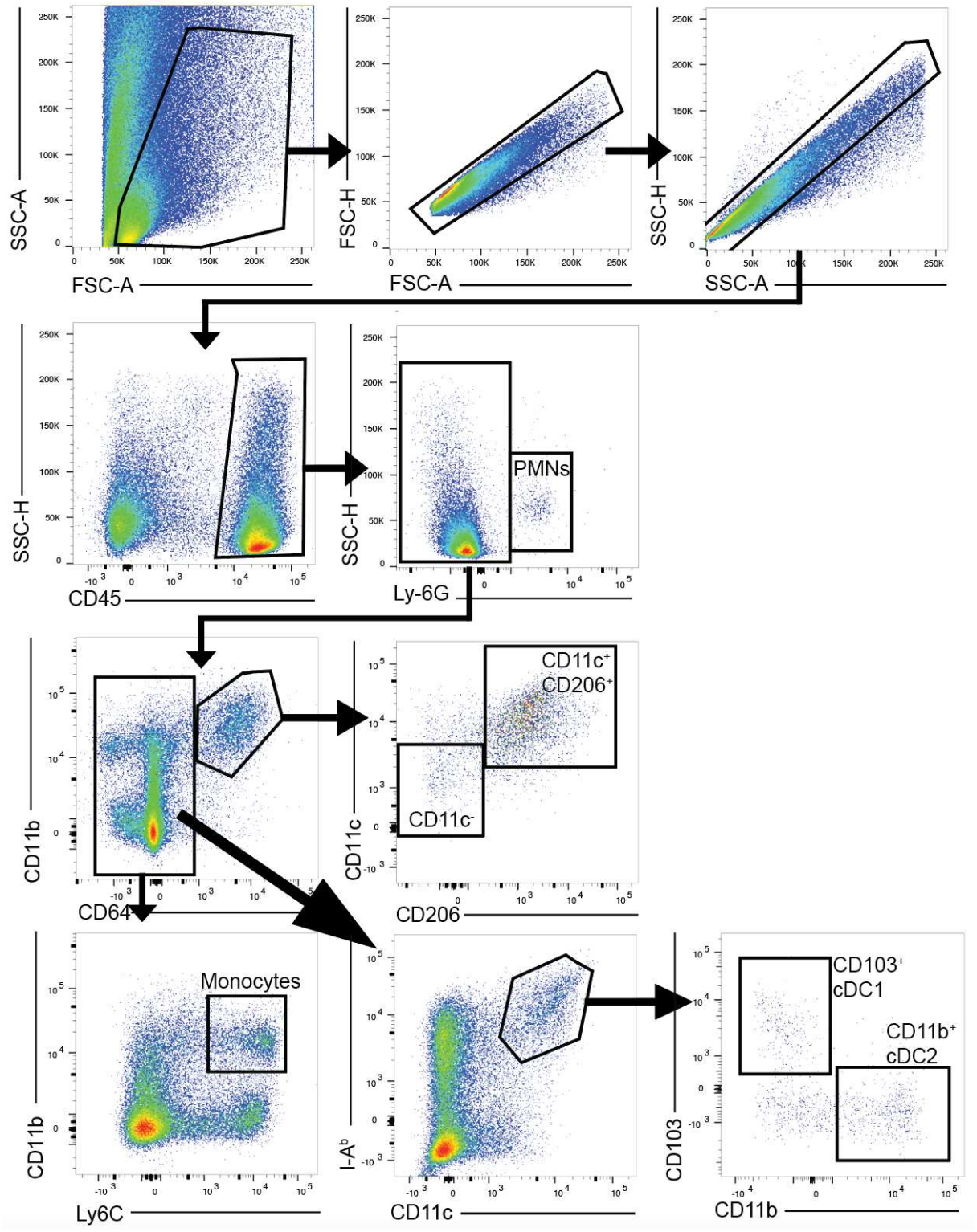

Figure A.3 Gating strategy of myeloid cells in the VAT. Gating strategies for flow cytometry analysis of myeloid cells in the VAT in Figures 4.18, 4.19, and 4.20.